

OPTICAL AND THERMAL PROPERTIES OF SELECTED TERNARY AMORPHOUS SEMICONDUCTORS

THESIS SUBMITTED TO THE
COCHIN UNIVERSITY OF SCIENCE AND TECHNOLOGY
FOR THE DEGREE OF
DOCTOR OF PHILOSOPHY

K. NANDAKUMAR

**DEPARTMENT OF PHYSICS
COCHIN UNIVERSITY OF SCIENCE & TECHNOLOGY
COCHIN - 682 022
INDIA**

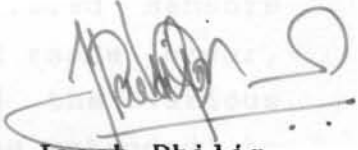
JULY 1992

CERTIFICATE

Certified that the work presented in this thesis is based on the bona fide work done by Mr. K. Nandakumar under my guidance in the Department of Physics, Cochin University of Science and Technology, and has not been included in any other thesis submitted previously for the award of any degree.

Cochin 682 022
July 14, 1992

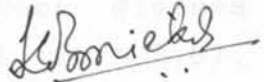



Dr. Jacob Philip
Supervising Guide

DECLARATION

Certified that the work presented in this thesis is based on the original work done by me under the guidance of Dr. Jacob Philip, Professor, Department of Physics, Cochin University of Science and Technology, and has not been included in any other thesis submitted previously for the award of any degree.

Cochin 682 022
July 14, 1992


K. Nandakumar

PREFACE

Chalcogenide glasses form an important class of materials among amorphous semiconductors and have attracted much attention in recent years. One of the main reasons for this is the technological importance of these materials. They find potential applications in xerography, optical memory cores, photovoltaic solar cells, switching devices, infrared sensors etc. Since amorphous materials do not possess long range order, the simple correlation with atomic structure and the various physical properties of crystalline solids cannot be extended to them. Chalcogenide glasses can be prepared over a wide composition range and hence the composition dependence of various physical properties of these glasses have become a matter of considerable interest. Since the physical properties of chalcogenide glasses do change with composition, this provides composition dependent tunability of the physical properties which will help in the selection of desired materials for specific technological applications.

Our aim has been to investigate systematically the effect of the replacement of elements on various properties of binary chalcogenide semiconducting glass systems by elements of the same group of the periodic table. Recently a physical model based on changes in network topology with composition has been proposed. This model makes use of short range interactions and predicts rigidity to percolate maximum in the network at the average coordination number $\langle r \rangle = 2.4$. Lately arguments based on medium range interactions existing in covalent network glasses suggests the occurrence of a mechanical threshold at $\langle r \rangle = 2.67$. So a systematic investigation of the composition dependence of various properties of chalcogenide glasses having a large glass forming region is necessary to resolve this controversy. Glasses

belonging to IV-V-VI group are good candidates to clarify this controversy because of their large glass forming region.

We have concentrated our investigations on three families of glasses viz., As-Sb-Se, As-Te-Se and Ge-As-Se systems. Two experimental techniques; the photoacoustic (PA) technique and differential scanning calorimetry (DSC) have been employed for systematic investigations of the optical and thermal properties of these glassy systems. The PA technique has been used to study the optical band gap and thermal diffusivity of these three systems whereas DSC has been employed to study the glass transition temperature and heat capacity in As-Te-Se and Ge-As-Se systems. The composition dependence of these properties has also been investigated in detail. Apart from PA technique, the UV-Vis-NIR spectrophotometry has also been used to measure the optical band gap of these glasses.

The thesis is presented in eight chapters. The first chapter of the thesis, written in two parts, is an introductory one; Part-A being devoted to a review of the status of amorphous semiconductor research and Part-B reviews principle of photoacoustic spectroscopy of condensed matter. Part-A includes an introduction to chalcogenide glasses followed by a brief discussion on the important structural models proposed for chalcogenide glasses and their optical and thermal properties. The principle of the photoacoustic effect, its use as an analytical tool and its various applications are presented in part-B. Necessary theory of the photoacoustic effect, with particular reference to signal generation from condensed matter, is briefly outlined.

Chapter II deals with the description of the experimental techniques used in the present investigations. A brief description of photoacoustic spectrometer and its different

modules are given in this chapter. A detailed description of the room temperature and high temperature PA cells used in the present investigations and their calibration procedures are discussed in this chapter. Descriptions of the differential scanning calorimeter (Perkin-Elmer Delta series) and UV-Vis-NIR spectrophotometer (Hitachi model U-3400) are also discussed in this chapter.

Chapter III deals with energy gap studies on As-Sb-Se glass systems using PA technique. The glasses studied can be classified into four groups depending on the Sb concentration as $As_xSb_5Se_{95-x}$ with $25 \leq x \leq 45$, $As_xSb_{10}Se_{90-x}$ with $20 \leq x \leq 40$, $As_xSb_{15}Se_{85-x}$ with $15 \leq x \leq 35$ and $As_xSb_{20}Se_{80-x}$ with $10 \leq x \leq 30$. The PA spectra, which is essentially the variation of PA amplitude with incident wavelength, give the optical absorption characteristics of the samples. The variation of the optical energy gap, determined from the PA spectra, with the composition parameter x is presented for all the systems. In all the compositions studied, the optical band gap shows a marked change at the stoichiometric compositions of the As-Sb-Se system which corresponds to an average coordination number of $\langle r \rangle = 2.4$. The observed behaviour has been explained on the basis of chemical bonding and the changes in the short range order in the glass network. A comparison of the optical band gap values obtained using the PA technique with that obtained using the UV-Vis-NIR spectrophotometer is also presented in this chapter.

Chapter IV deals with thermal diffusivity measurements on As-Sb-Se glasses. The PA technique has proved to be a very effective method for determining the thermal transport properties of solid samples. The details of thermal diffusivity measurements and the determination of glass transition temperature T_g , using PA technique, of these glasses are

described in detail. The composition dependence of α and T_g of As-Sb-Se systems are discussed in this chapter. The features of the temperature dependent variations of α of these glasses are also discussed in detail.

Chapter V describes the optical energy gap and thermal diffusivity measurements in As-Te-Se glasses using PA technique. The compositions studied can be categorized into three groups depending on the Te concentration as $As_xTe_5Se_{95-x}$, $As_xTe_{10}Se_{90-x}$ with $x = 30, 35, 40, 45$ and 50 at.% and $As_{40}(Te,Se)_{60}$ with Te concentration equals $0, 5, 10, 15$ and 20 at.%, which are the stoichiometric compositions of the As-Te-Se system. The results show the evidence for the existence of critical composition at which the average coordination number $\langle r \rangle = 2.4$.

Chapter VI is devoted to studies of the optical band gap and thermal diffusivity in Ge-As-Se glasses using PA technique. The compositions studied can be categorized into two groups as $Ge_xAs_{10}Se_{90-x}$ with $x = 5, 10, 15, 20, 25, 30, 35$ and 40 such that average coordination number varies from 2.2 to 2.9 and $(Ge_{0.5}As_{0.5})_xSe_{100-x}$ with $x = 10, 20, 26.7, 30, 40, 44, 50$ and 60 covering average coordination numbers between 2.15 and 2.9 . The composition dependence of optical band gap and thermal diffusivity of these two sets are investigated. The results support the existence of medium range order and the formation of layered structure in network systems as the average coordination number is varied as has been proposed recently.

Calorimetric investigations on As-Te-Se and Ge-As-Se glasses are given in detail in chapter VII. The measurement of glass transition temperature and its composition dependence are described in this chapter. The variation of specific heat of these systems with temperature and the coordination dependence

of the change in heat capacity during glass transition are also discussed in this chapter.

Chapter VIII is the concluding chapter incorporating overall conclusion of the work presented in the earlier chapters. Emphasis has been given to the importance of the study of various physical properties of chalcogenide glasses using PA technique and differential scanning calorimetry. The importance and relevance of the study of composition dependent variation of such properties is highlighted on the basis of the content of the thesis. Further scope of the work in this direction on other chalcogenide systems are also discussed.

Most of the results presented in the thesis have already been published/ accepted for publication/ communicated in the form of following papers:

1. Energy gap studies on As-Sb-Se glasses
Bull.Mater.Sci., 11, No.4, 297 (1988)
2. Composition and temperature dependence of thermal diffusivity in As-Sb-Se glasses
Jour.Acoust.Soc.India., XVII(3&4), 351 (1989)
3. Photoacoustic investigation of optical energy gap in As-Se-Te glasses
in Physical Acoustics (Plenum press), 545 (1991)
4. Studies of glass transition and thermal diffusivity in As-Sb-Se glasses
Phil.Mag B, 63, No.2, 493 (1991)
5. Composition dependence of optical bandgap and thermal diffusivity in As-Te-Se glasses

Jour.Non-Cryst.solids - (in press)

6. Photoacoustic investigation of thermal diffusivity in As-Te-Se glasses
J. Acoust.Soc.India - (in press)
7. Thermal diffusivity threshold in Ge-As-Se glasses
Proceedings of the Seventh International Conference on Phonon Scattering In Condensed Matter (Springer-Verlag, 1992) - to be published
8. Calorimetric Investigations on As-Te-Se and Ge-As-Se glasses
Pramana-J. Phys., (communicated 1992)
9. Composition dependence of the optical band gap and thermal diffusivity in Ge-As-Se glasses
Phys. Rev. B (Communicated 1992)

The following papers have also been published during the course of this work as a co-author.

1. Photoacoustic investigation of glass transition in As_xTe_{1-x} glasses
Phys. Stat. Solidi (a), **114**, 525 (1989)
2. On the imaging application of photoacoustic technique
Jour. Acoust. Soc. Ind., Vol XVIII(3&4), 28 (1990)
3. Photoacoustic study of the compositional dependence of the optical band gap in Ge-As-Te glasses
Ind. Jour. Phys., **65(A)**, 306 (1991)

CONTENTS

PREFACE		i
ACKNOWLEDGEMENTS		vii
Chapter I	INTRODUCTION	
	PART A: A GLIMPSE AT THE PHYSICS OF AMORPHOUS SEMICONDUCTORS	
1.1	Opening Remarks	1
1.2	Classification and preparation of amorphous semiconductors	2
1.3	Chalcogenide glasses: Structure and properties	4
1.4	Band models	21
1.5	Optical properties of amorphous semiconductors	26
1.6	Thermal properties of amorphous semiconductors	33
	PART B: PHOTOACOUSTICS AND PHOTOACOUSTIC SPECTROSCOPY	
1.7	Introduction	35
1.8	Theory of photoacoustic effect in solids	38
1.9	Applications of the photoacoustic effect	51
1.10	Work presented in the thesis	54
	References	55
Chapter II	EXPERIMENTAL TECHNIQUES USED IN THE PRESENT INVESTIGATIONS	
2.1	General considerations of a photoacoustic spectrometer	67
2.2	The present experimental setup	74
2.3	Differential scanning calorimetry	83
2.4	UV-Vis-NIR spectrophotometer	94
	References	96

Chapter III	ENERGY GAP STUDIES ON As-Sb-Se GLASSES	
3.1	Introduction	99
3.2	Experimental details	100
3.3	Photoacoustic spectra of As-Sb-Se glasses	103
3.4	Composition dependence of optical band gap	108
	References	114
Chapter IV	THERMAL DIFFUSIVITY MEASUREMENTS ON As-Sb-Se GLASSES	
4.1	Introduction	116
4.2	RG theory of thermal diffusivity measurement	117
4.3	Thermal diffusivity measurements on As-Sb-Se glasses	120
4.4	composition dependence of thermal diffusivity in As-Sb-Se glasses	123
4.5	Composition dependence of glass transition temperature using PA technique	130
4.6	Temperature dependence of thermal diffusivity of $As_xSb_{15}Se_{85-x}$ glasses	145
	References	150
Chapter V	OPTICAL ENERGY GAP AND THERMAL DIFFUSIVITY IN As-Te-Se GLASSES	
5.1	Introduction	152
5.2	Experimental details	154
5.3	Composition dependence of optical band gap in As-Te-Se system	163
5.4	Composition dependence of thermal diffusivity in As-Te-Se system	167
	References	172

Chapter VI	OPTICAL BAND GAP AND THERMAL DIFFUSIVITY IN Ge-As-Se GLASSES	
6.1	Introduction	173
6.2	Composition dependence of optical band gap in Ge-As-Se glasses	177
6.3	Composition dependence of thermal diffusivity in Ge-As-Se glasses	185
	References	191
Chapter VII	CALORIMETRIC MEASUREMENTS ON As-Te-Se AND Ge-As-Se GLASSES	
7.1	Introduction	193
7.2	Experimental details	195
7.3	Composition dependence of glass transition temperature in As-Te-Se and Ge-As-Se glasses	199
7.4	Variation of C_p during glass transition in As-Te-Se and Ge-As-Se glasses	205
	References	219
Chapter VIII	SUMMARY AND CONCLUSIONS	221

CHAPTER I

INTRODUCTION

PART A : A GLIMPSE AT THE PHYSICS OF AMORPHOUS SEMICONDUCTORS

1.1 Opening Remarks

The study of non-crystalline materials has become one of the frontier areas of research in solid state physics in recent years. The impact of amorphous materials on the world of science and technology has been enormous, covering such diverse applications as electrophotography, memory and switching elements, energy conversion devices such as solar cells etc. and the interest in both fundamental and applied aspects of these materials has grown rapidly during the last 3-4 decades. Research in the fascinating areas of amorphous semiconductors started gaining momentum in the 1950's with the discovery by Kolomiets that chalcogenide glasses behave like intrinsic semiconductors and that their electrical conductivity cannot be increased by adding dopants [1] and later the studies by Spear [2] and Tauc [3] have made important contributions to this field. The switching and memory effects in chalcogenids glasses reported by Ovshinsky [4] was a turning point which attracted many researchers to the world of amorphous materials. The important discoveries made on optical memory effects, imaging, reversible photostructural changes, photodoping etc. have shown possibilities for new technological applications for non-crystalline semiconductors.

Our understanding of the physics of crystalline solids has shown remarkable progress during the past 65 years. This was achieved mostly by the application of quantum mechanics and

subsequently by the development of band theory which turned out to be very successful in explaining most of the properties of crystalline materials because of the mathematical simplicity resulting from the periodicity of the lattice [5,6]. But proper theoretical understanding of disordered systems was largely undeveloped mainly because of the mathematical complexity in dealing with non-periodic systems. An important theoretical contribution on this topic was made by Anderson [7] and the concept of Anderson localization has played a significant role in interpreting the transport properties of amorphous semiconductors. Several numerical and analytical works have been reported based on this concept [8-14]. Scaling theories and the ideas of localization and percolation have been exploited by several workers to solve many problems associated with disordered systems [15,16,17]. Pioneering work done by Mott [18] on the various theoretical aspects of the problem made significant contributions to our understanding of the amorphous state. Much progress has been made recently in our understanding of the structure of amorphous semiconductors, particularly of covalently bonded materials where "superstructural units" such as regular rings or clusters are prevalent. But much remains still unclear and a lot more remain to be understood. It seems further substantial progress in this area will come only from further advances in experimental techniques and theoretical descriptions of the disordered state of matter.

1.2 Classification and preparation of amorphous semiconductors

Amorphous semiconductors can be divided into two groups as tetrahedrally coordinated silicon like materials and chalcogenide glasses which contain one or more of the chalcogen elements of the sixth column of the periodic table: Sulphur, Selenium and Tellurium [19]. The distinction between these two classes can be well accounted for on the basis of chemical

considerations. The four-fold coordination in Si leads to symmetrical bonding and the formation of rigid structures. In this case a continuous random network with tetrahedral bonds can be constructed with negligible density deficit and very little possibility for local reorganisation of atoms. On the other hand two-fold coordination in Se is very asymmetrical and the structure gives rise to greater degree of flexibility. A major distinction comes from the fact that in Se, not in Si, the uppermost valence band is formed from nonbonding lone pair p electrons and is very important when we consider the defect chemistry and various properties that differentiate it from Si like materials.

Amorphous solids are generally prepared by two different methods viz., vapour condensation technique and melt-quenching technique. Vapour condensation technique is employed to prepare thin films while bulk glasses, having a well defined glass transition temperature, are prepared by the melt-quenching technique.

Out of the two classes of materials described, chalcogenide glasses can be prepared in the form of bulk as well as thin film forms; but a direct comparison of the properties of thin films and bulk glasses may not be possible. Stable glasses may undergo a second order phase transition at the glass transition temperature T_g which marks the onset of softening of the network. Less stable glasses may undergo phase separation and crystallization on heating. To prepare such glasses rather fast quenching rate is needed to avoid crystallization. Therefore quenching rate is an important parameter in the preparation of glasses by melt-quenching [19].

The Si type materials cannot often be prepared in the glassy form by melt-quenching. These materials are usually

prepared in thin film form by deposition on a substrate. Several techniques such as vacuum evaporation, sputtering, electrolytic deposition, glow discharge deposition, chemical vapour deposition etc. are employed for preparing the material in the thin film form.

The reason why some of the materials can be prepared in thin film as well as bulk forms whereas others can only be prepared in the thin film form can be explained by the nature of chemical bonds present in these materials. This difference has its origin in the mismatch between constraints and the number of degrees of freedom in three dimensions and the flexibility required to accommodate the mismatch. The flexibility of covalent bond angles is largest for the two-fold coordinated Se-type materials and least for the tetrahedrally coordinated Si-type materials. The reason for this is the greater variety of admixture from other atomic orbitals to the covalent bond when the coordination number is less than the number of valence electrons. Therefore based on chemical considerations and average coordination number $\langle r \rangle$, a classification of amorphous solids can be made as shown in Fig.1.1. According to this, glasses are restricted to $3 \geq \langle r \rangle \geq 2$ and materials with higher connectivity viz., $4 \geq \langle r \rangle \geq 3$ are over constrained amorphous while those with $\langle r \rangle < 2$ are underconstrained amorphous. The average coordination $\langle r \rangle = 4$ separates non-crystalline metals from semiconductors or insulators.

1.3 Chalcogenide glasses : Structure and properties

Chalcogenide glasses form an important class of amorphous semiconductors. These materials have a disordered structure and lack long-range periodicity of constituent atoms. However, the disorder is not complete on the atomic scale.

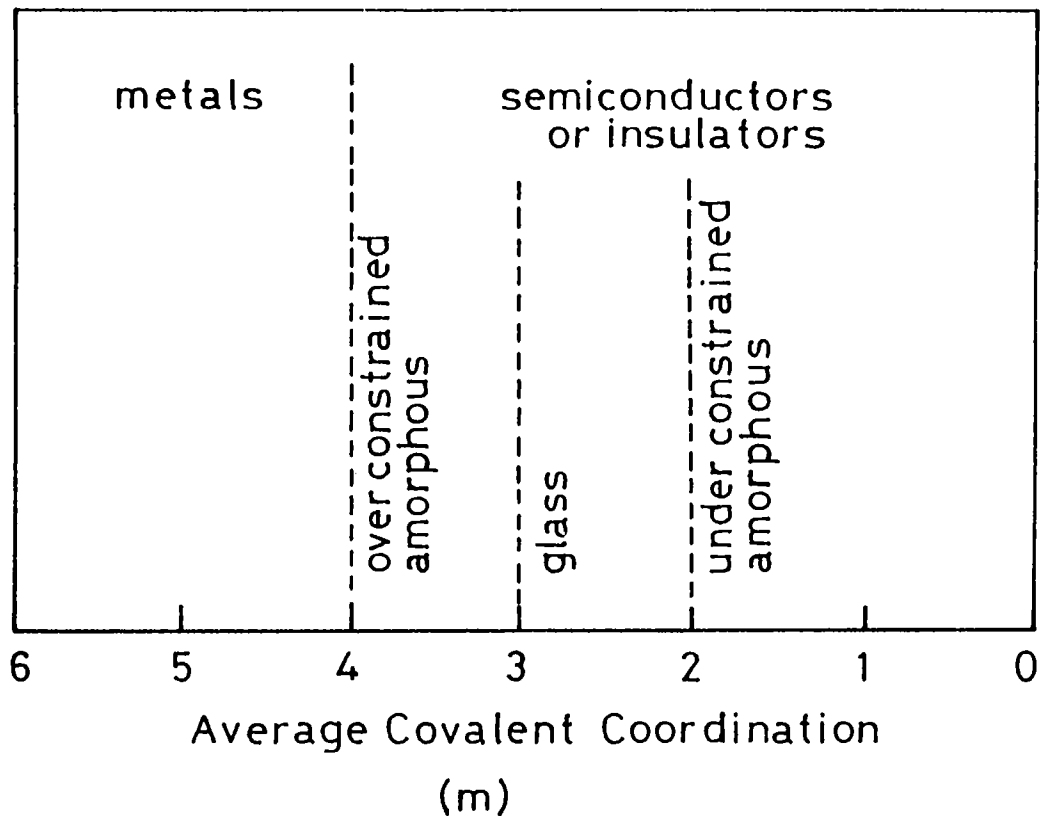


Fig.1.1 Classification scheme for amorphous solids based on average coordination number

Short-range order similar to that present in crystalline materials is also present in these disordered materials. In chalcogenide glasses, the covalently bonded atoms are arranged in an open network with order extending upto third or fourth nearest neighbours and they are also referred to as network glasses [19]. The semiconducting property of chalcogenide glasses is, however, a direct consequence of the covalent bonding that exists in these materials.

How disordered is the atomic structure of an amorphous solid? Although it is indisputable that such structures are devoid of long-range translational periodicity, the question of the degree of residual structural order present in a non-crystalline material at shorter length scales remains controversial. Disorder in materials can be manifested in many ways as vibrational, spin and orientational disorder (all referred to a periodic lattice) and topological disorder, which is the type of disorder associated with the structure of glassy and amorphous solids in which the structure cannot be defined in terms of a periodic lattice.

Determination of the atomic structure of amorphous materials is unfortunately a non-trivial task. Because the structure can be defined essentially only in terms of a 'unit cell' containing an infinitely large number of atoms as there is no long-range periodic symmetry, a statistical description is unavoidable. The structure of a particular amorphous solid can therefore never be determined unambiguously, and this uncertainty is compounded by the fact that the structure of a non-crystalline material, at both microscopic and macroscopic levels, often depends on details of the method of preparation. Furthermore, in general, more than one experimental structural probe must be used to obtain as full a picture as possible of the structural arrangement in an amorphous solid.

In discussing the structure of amorphous materials, it is useful to consider the types of structural order that can exist in such materials at various length scales. Such categorization is convenient in two regards : the classification is hierarchical, so that a particular type of order at one length scale can be dictated by order at a smaller scale (but not necessarily the converse); and the various experimental probes are generally sensitive to structural correlations at different length scales. One can consider three contiguous length scales [20], short-range order (SRO) in the range 2-5 Å⁰; medium-range order (MRO) in the range 5-20 Å⁰; and long range structure (LRS) at distances ≥ 20 Å⁰. By definition there is no long range order, in the form of translational periodicity, in the structure of a glass.

Since there is no unique structure for an amorphous material, structural modelling is very useful in determining the structure of amorphous solids. The structure of amorphous semiconductors is developed by the repetition of one or more basic molecular units in a way that cannot be identified topologically with any known crystalline structure or with any periodic array. But the atomic order within a molecular unit might be similar within small bond angle distortions in both crystalline and amorphous phases. This reveals the importance of short-range in describing structural behaviour of a non-periodic network. The major point in describing the amorphous structure is the specification of the short-range order and the topological rules which determine it. The most important aspects of the short-range order are the number and type of immediate neighbours, and their spatial arrangement about a given reference atom. Given the short-range order, with three parameters viz., the number of bonds, the bond length and the bond angle having well defined values in a narrow range, it is possible to construct a model for the amorphous structure. Such

models are known as random networks. Zachariassen was the first to model an amorphous solid by a random network of atoms with near perfect short-range order [21], with particular reference to oxide glasses. Several models have been proposed for the local structure of chalcogenide glasses which are mainly modifications of the covalent random network (CRN) model [22-27].

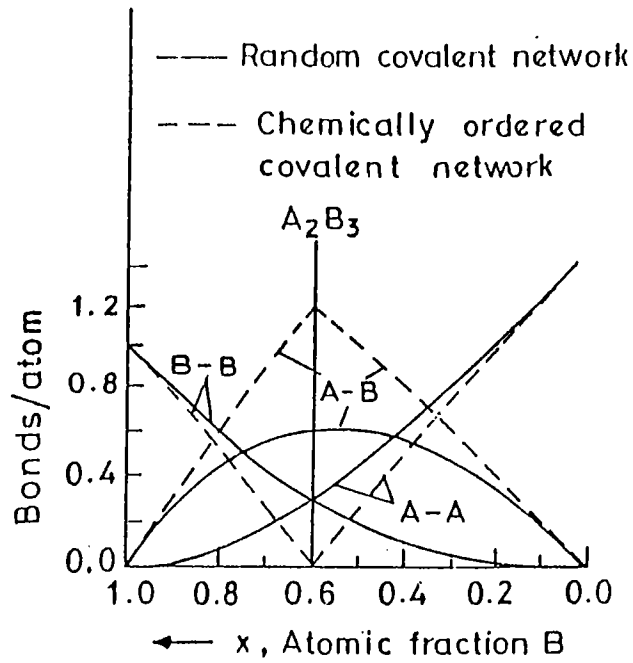
Locally the network topology is fully three dimensional for a random network of four-fold coordinated atoms while for twofold- and threefold- coordinated atoms, the local topologies are respectively one and two dimensional. The lower coordination also allows the real solid to deviate from a completely interconnected network through the incorporation of discrete molecular species. The resultant solid can then be described in terms of a mixture of molecular and polymeric species. Discrete molecular species have been identified in a-Se as Se_8 ring molecules [28-30], in a-As as As_4 pyramidal molecules [31], and in 'S-rich' glasses in the As-S and Ge-S binary alloys as S_8 ring molecules [32 -35]. It has to be noted that CRNs are idealistic models in the sense that they generate amorphous state in a dense state without taking into account structural defects such as voids and they are often inadequate in accounting for features observed in medium range order and growth morphology.

The network structure for a binary alloy system $A_{1-x}B_x$, where A and B are two different atomic species and x is a normalized concentration variable, can be specified in four stages (i) the local coordination of each atomic species; (ii) the distribution of bond types A-A, A-B and B-B; (iii) the specification of characteristic local molecular environments; and (iv) the topological rules for the interconnection of the molecular building units [33, 35]. It is assumed that the binary

covalent alloy system obeys the 8-n rule, where n is the valency so that the coordinations of A and B are Z_A and Z_B respectively. This type of coordination dominates in bulk-quenched glasses and well-annealed films. Recently, there has been considerable interest in "wrong atomic coordinations" or so-called valence alteration in chalcogenide glasses [20]. A small number of these wrong-coordination sites, e.g., either one-fold or three-fold coordinated Se atoms or both appear to be present in chalcogenide glasses with characteristic densities of 10^{16} - 10^{18} cm^{-3} . These centres are electronically active and give rise to interesting photoelectronic and spin resonance properties [36-39].

The 'random covalent network' (RCN) and the 'chemically ordered network' (CON) are the two distinct models [33,40] which describe the distribution of the three bond types, A-A, A-B and B-B, that are consistent with the assumed idealized 8-n coordination. The RCN model treats the bond distribution as purely statistical and completely determined by the respective coordinations Z_A and Z_B , and the fractional coordinations of A and B atoms, $1-x$ and x , respectively. This approach to the bonding neglects factors such as the relative bond energies and admits A-A, A-B and B-B bonds at all compositions other than $x = 0$ and $x = 1$. On the other hand the CON model emphasizes the relative bond energies and is based on the assumption that heteropolar or A-B bonds are favoured at all compositions. A completely chemically ordered phase thus occurs at a composition $X_c = Z_A/(Z_A+Z_B)$ and the compound is $A_{Z_A}B_{Z_B}$ containing A-B bonds only. For compositions defined by $1 > x > x_c$, the alloys contain A-B and B-B bonds; whereas for $X_c > x > 0$, the alloys contain A-B and A-A bonds. The bond counting statistics for (3:2) and (4:2) alloys as per both the models are shown in Fig.1.2. The existence of compound phases at a- As_2S_3 , a- As_2Se_3 , a- GeS_2 , and a- GeSe_2 , suggests that chemical ordering prevails in the four

(a) $A_{1-x}B_x$ 3:2



(b) $A_{1-x}B_x$ 4:2

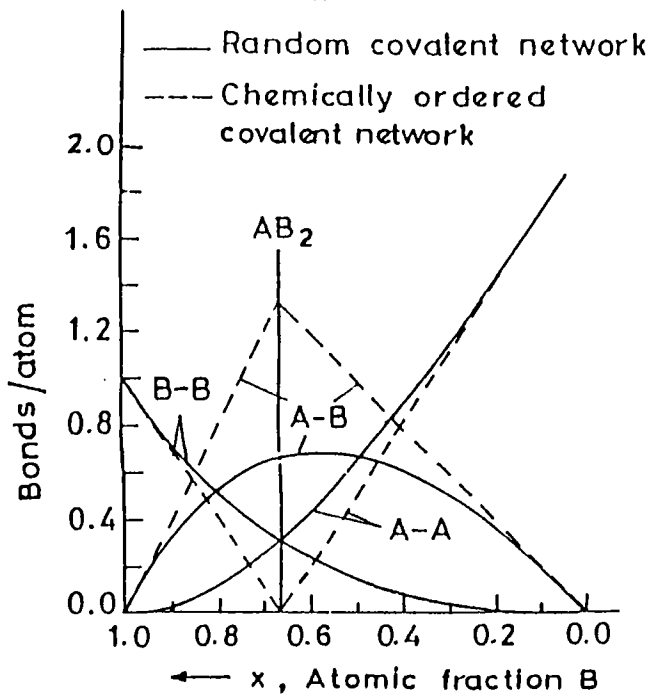


Fig.1.2 Bond counting statistics for a (3:2) and (4:2) network alloys

alloy systems A-S, As-Se, Ge-S, and Ge-Se, at least over the bulk-glass forming range. This is supported by other structural measurements, for example, RDF's obtained by X-ray diffraction [41-44], and by the structural interpretations of IR and Raman vibrational spectroscopy [32,33,45].

It should be noted that the compound phase defined above is special in the sense that it contains only A-B bonds. Additional compound phases may also be present at other compositions without changing the bond-counting statistics. The criteria for existence of such compound compositions relates to the existence of a molecular entity from which the network can be generated. The molecular building block can contain both A-B and B-B or A-B and A-A bonds in such a way that the distribution of bond types within and between these units is consistent with the bond-counting statistics.

The concept of local molecular clusters has its origin in some of the early models for the atomic structure of fused silica α -SiO₂ [46,47], having a molecular building block with tetrahedral geometry, SiO_{4/2}: a central Si atom with tetrahedral distribution of four O atoms, each of which is bonded to a Si atom in another tetrahedron, hence the 4/2 notation. The central atom in the molecular cluster is chosen to be the one of higher-coordination and the fractional concentration of the lower-coordination species is then the ratio of the two atomic coordinations and always greater than one. For an alloy of the type A_{1-x}B_x in which the coordination of the A atom is always greater than that of the B atom. The characteristic molecular building block at the special compound composition is then given by AB_{Z_A/Z_B}. Similar procedures have been applied in describing the molecular structure in many other compound chalcogenide glasses [48,49]. In general, the three-dimensional structure of these molecular building blocks reflects the normal covalent

bonding geometry of the central atomic species. $AB_{4/2}$ then has a tetrahedral geometry, whereas the $AB_{3/2}$ unit is a pyramidal structure with a face-apex angle close to 90° . However, the tetrahedral geometry is determined by symmetry with the angles showing an average deviation of about $\pm 10^\circ$. The actual pyramidal apex angle of the $AB_{3/2}$ unit may be estimated by a comparison with crystalline phases in which similar covalent bonding prevails [50] or obtained by an analysis of the X-ray RDFs.

By assuming that the bond-type distribution is determined by chemical driving-forces, the alloy can be divided into two different regimes at the compound composition X_c . In B-rich regime, $1 > x > x_c$, there are A-B and B-B bonds, but not A-A bonds. Each A atom then has only B-type neighbours arranged in a local atomic cluster of the form AB_{Z_A/Z_B} and this is the same cluster that provides the molecular basis for the compound phase at X_c . In the B-rich alloys these molecular clusters are connected through additional B atoms. In chalcogenide alloys $A_{1-x}B_x$ ($B = S, Se, Te$), this type of model for B-rich alloy regime has been designated as a chain-crossing model [32,33,40,43]. Pyramidal ($AB_{3/2}$) or tetrahedral ($AB_{4/2}$) molecular units are interconnected by chain segments of B atoms. Hence the threefold or fourfold coordinated A-type atoms provide points at which chains cross or branch. These have been identified as S_9 ring molecules [51,52] in S-rich As-S [33,45] and Ge-S [32] glasses. In the A-rich alloy regimes, the local molecular order is not simply specified since some of the more highly coordinated A-type atoms must have A-type as well as B-type immediate neighbours. The most general molecular structures can be described in terms of a small set of basic network formers [33]. For the 4:2 alloys, these are tetrahedral units of the form AB_4 , AB_3A , AB_2A_2 , ABA_3 and AA_4 [33,53] and for 3:2 alloys they are the corresponding pyramidal structures AB_3 ,

AB_2A , ABA_2 and AA_3 as pictured in Fig.1.3. For any given alloy composition the fraction of A-type atoms in any one of these local environment is not uniquely defined.

Recently, Phillips proposed a simple dynamical model [54] for network glasses based entirely on topological considerations. This model is treated in detail here since the present thesis explores the applicability of this model to chalcogenide glasses. According to Phillips' theory [54,55,56] of non-equilibrium network glass formation, the glass formation is optimized mechanically when the number of degrees of freedom (N_d) for the atoms in the glassy network equals the number of constraints (N_{con}) in the network at a critical average coordination number m_c . When the average coordination number $m < m_c$, the network is underconstrained and tends to disintegrate into nonpolymerized fragments. For small positive values of $(m_c - m)$ the fragments retain their three dimensional character, but further increase in $(m_c - m)$ produces dimensional contraction, first to quasi planar crossed chains and finally to quasi linear chain bundles. When $m > m_c$, the network is overconstrained. Then the atomic interactions can be separated into intact and broken constraints and the transition from the intact constraints to broken constraints can be explained on the basis of molecular cluster formation [56].

Later Thorpe and co-workers extended this model to predict the elastic behaviour of covalent glasses in terms of the average number of constraints in the system [57-60]. This model treats the network glass as made up of elastically soft or floppy and elastically rigid regions. For low average coordination number m the network is a polymeric glass ($N_d > N_{con}$) in which the rigid regions are isolated. As the mean coordination increases, these rigid regions increase in volume until at $m = m_c$ or $N_d = N_{con}$, the network transforms into a

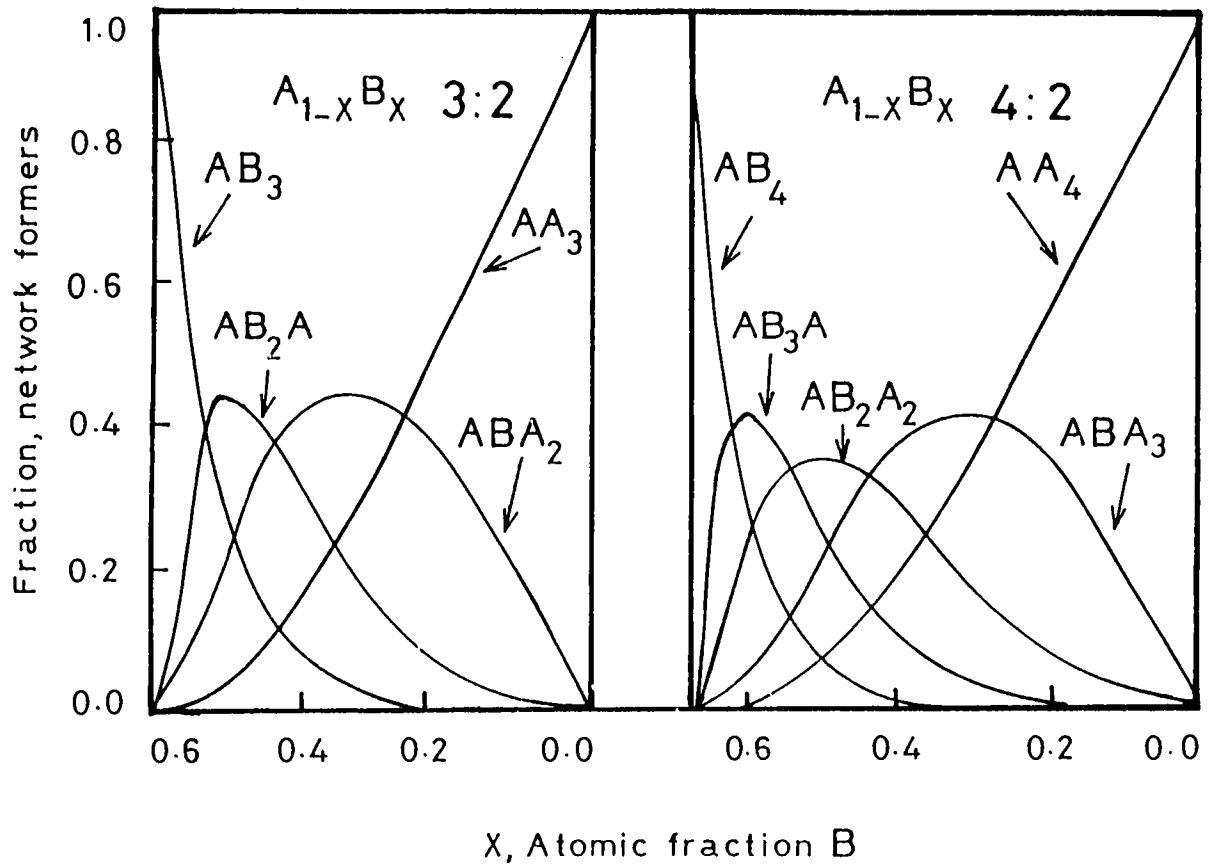


Fig.1.3 Statistically determined local clusters for A-rich alloy regimes in (3:2) and (4:2) networks

completely rigid glassy structure. This transition phenomenon is analogous to the "percolation" phenomenon and the rigidity of the network is said to percolate at $N_d = N_{con}$. This is schematically depicted in Fig.1.4. The soft undercoordinated glasses ($N_d > N_{con}$) can be elastically deformed easily by the application of a shearing force and the system admits the displacement of groups of atoms without the provocation of restoring forces and hence has a number of "floppy" modes.

The fraction of floppy modes in any glassy network is given by

$$f = N_d - N_{con} \quad (1.1)$$

Consider a particular random network with N atoms constructed with n_r atoms having r bonds.

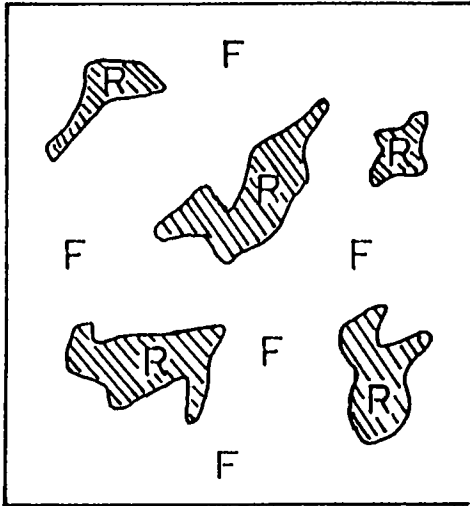
$$\sum_r n_r = N \quad (1.2)$$

This network of well defined bond angles and lengths is relaxed into the local equilibrium for the given topology and small vibrations from an (supposed) equilibrium structure can be described by the potential [60],

$$V = \alpha/2 \sum_{\langle ij \rangle} [(u_i - u_j) \cdot \hat{r}_{ij}]^2 + \beta/2 \sum_{\langle ij \rangle} l_{ij} l_{jk} (\Delta\theta_{ijk})^2 \quad (1.3)$$

This potential is referred to as the covalent potential as it has bond-stretching and bond-bending terms. Here u_i is the displacement of the atom i , and \hat{r}_{ij} is a unit vector connecting nearest-neighbour sites i, j ; l_{ij} is the length of the bond ij and θ_{ijk} is the angle between the bonds ij and jk . The

I Polymeric Glass



II Amorphous Solid

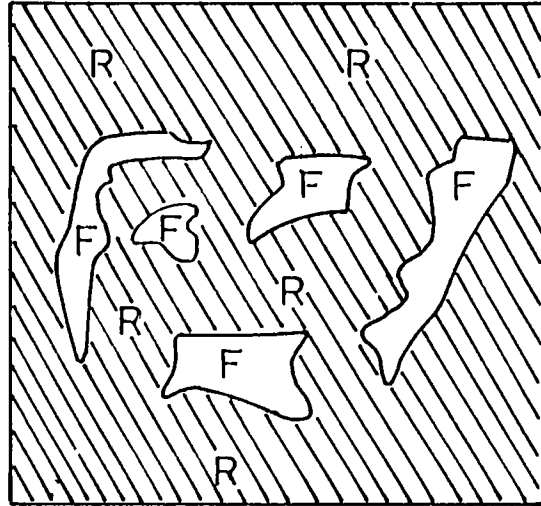


Fig.1.4 Rigid and floppy regions in networks of polymeric glass and amorphous solid

bond-stretching force constant α and the bond-bending force constant β are the largest forces in covalent glasses and other forces are smaller as would be expected from the nature of the covalent bond. When the coordination of the network is low, there are many ways in which the network can be deformed at no cost in energy and the number of these deformations or zero-frequency modes is given by the number of the degrees of freedom ($3N$) minus the number of constraints. There is one constraint associated with each bond and there are $r/2$ constraints associated with each r -coordinated atom. In addition there are constraints associated with the angular forces and for a r -coordinated atom there are a total of $2r-3$ angular constraints [57]. The fraction f of zero-frequency modes is give by

$$f = [3N - \sum_r n_r [r/2 + (2r - 3)]] / 3N \quad (1.4)$$

$$= 2 - 5/6 \langle r \rangle \quad (1.5)$$

where $\langle r \rangle$ is average number of bonds per atom or the "mean coordination number" defined as

$$\langle r \rangle = \sum_r r n_r / \sum_r n_r \quad (1.6)$$

As atoms with higher coordination than two are added to the network, f drops and goes to zero at $\langle r \rangle = 2.4$ and the network becomes rigid. This value of $\langle r \rangle$ at which the transition occurs is termed as the "rigidity percolation threshold" or the "mechanical threshold".

The rigidity percolation threshld predicted by this model depends only on the mean coordination number and is independent of the atomic compostion and therefore the local

structure. The $\langle r \rangle$ value for a ternary network glass of the form $A_x B_y C_{100-x-y}$ is given by

$$\langle r \rangle = \left[xN_A + yN_B + (100-x-y)N_C \right] / 100 \quad (1.7)$$

where N_A , N_B and N_C are the coordination numbers of the elements A, B and C respectively and x and y are the atomic weight percentages of the elements A and B respectively in the network glass.

The model ternary glass Ge-As-Se system which has one of the largest glass-forming regions was naturally the first ternary glassy system studied to verify the threshold behaviour predicted by the percolation model [61]. The ultrasonic pulse-echo overlap technique has been used by these authors to measure the room temperature elastic moduli C_{11} and C_{44} for two sets of Ge-As-Se glasses, one with low-As content and the other with high-As content. Their studies have shown a change of slope at $\langle r \rangle = 2.4$ as predicted by the model. The authors also found that glasses with different compositions but having the same $\langle r \rangle$ value exhibited identical elastic constant values. Further, in the range $2.40 < \langle r \rangle < 2.60$, the authors data could be fitted well with the simulated data [60]. The experimental elastic constant values had non-zero values below $\langle r \rangle = 2.4$ as against the simulated data which could be attributed to the presence of non-central forces which have not been considered in the simulation. Since the structure of a solid significantly affects its physical properties, the signature of any structural changes is bound to show up in properties sensitive to rigidity percolation phenomenon. The experimental reports on a wide variety of physical properties of various binary chalcogenide glasses indicated the threshold behaviour at $\langle r \rangle = 2.40$ [62-74].

Some controversial results have been reported quite recently, indicating a shift in the $\langle r \rangle$ value at which the threshold occurs. There are reports on $\text{Ge}_x\text{Se}_{100-x}$ glasses that a slope change occurs in the elastic constant versus $\langle r \rangle$ plot at 2.60 [75] and at 2.70 [76] against the earlier observations at 2.40 [61]. Also, there have been reports of anomalous behaviour at $\langle r \rangle = 2.4$ and at $\langle r \rangle = 2.67$ in various properties of Ge-Se and Ge-S glasses [77-81,66]. A similar departure in the threshold value in the $\langle r \rangle$ dependence of various physical properties such as photodarkening, molar volume, X-ray diffraction, elastic constants etc. of Ge-As-S glasses have been reported by Tanaka [80-83] and proposed an explanation for the observed shift.

According to Tanaka, the interactions in chalcogenide glasses extend to medium range scale and is not confined to short-range scales as originally proposed by Phillips and Thorpe. It is shown that composition dependence of various properties of chalcogenide alloys exhibit characteristic signatures at the average coordination $\langle r \rangle = 2.67$ and on the basis of topological consideration, the signatures can be connected to the formation of stable layer structures. Considering the planar medium range configurations, the number of angular constraints is reduced to $(r-1)$ instead of $(2r-3)$ as predicted by Thorpe. For an atom in a planar cluster extending in the X-Y plane, the number of constraints reduces to

$$N_{\text{con}} = r/2 + (r-1) \quad (1.8)$$

where the angular term is calculated as excess degrees of r variables in θ over a rotation freedom around the Z axis. If such a cluster is laid in a 3-dimensional space, each atom must have three independent degrees of freedom for stable existence

ie., $N_d = 3$. Therefore the constraint balancing equation $N_d = N_{con}$ becomes

$$3 = r/z + (r-1) \quad (1.9)$$

This expression gives the average coordination number of glasses having stable layer structure as $\langle r \rangle = 2.67$. This means that a two dimensional glass possessing a layered structure appears to be stably fixed in a three-dimensional space, if the coordination number of the glassy network is 2.67.

The controversy of the value at which the mechanical threshold occurs has not been clearly resolved as on date. For many binary V-VI glasses, the 'chemical threshold' coincides with the 'mechanical threshold' and such interferences can be resolved by studies on ternary chalcogenide glasses in which contributions due to each effect can be isolated. New experimental results and old data from literature have been re-analysed by Tanaka [83] in the light of the above arguments. But, unfortunately contributions to structural data from medium-range order cannot be easily distinguished from short-range order. At present no conclusive experimental evidence is available indicating low-dimensional structures in chalcogenide glasses though there exist numerous circumstantial evidences.

Recent report of the studies on IV-V-VI glasses like Ge-As-Te, Ge-Sb-Se and Si-As-Te [84] shows anomalous behaviour in different physical properties near the average coordination value $\langle r \rangle = 2.67$. The studies of the dependence of optical band gap E_g and thermal diffusivity α on average coordination number shows anomaly at $\langle r \rangle = 2.50$ in these systems. The observed shift in the threshold value from $\langle r \rangle = 2.67$ has been attributed to the presence of heavier elements in these glasses.

The photoacoustic studies of optical band gap and thermal diffusivity and the DSC studies on two families of Ge-As-Se systems presented in this thesis shows anomaly around $\langle r \rangle = 2.67$ as predicted by Tanaka. But studies on other systems like As-Sb-Se and As-Te-Se show anomaly at $\langle r \rangle = 2.4$ which suggests more studies are required for a better understanding of the structure of chalcogenide glasses. Any way, the present studies proved that the PA technique is very sensitive to the mechanical threshold in glassy network which undergo topological changes and aims at generalizing a simple theory for a better understanding of the physical properties of ternary chalcogenide glasses.

1.4 Band models

Exciting advances have been made in recent years in understanding the problem of how disorder in amorphous semiconductors influences the band structure and hence the electrical properties. At present, there appears to be widespread agreement that if the short-range order is the same in the amorphous state as in the crystalline one, some basic features of the electronic structure of the crystal are preserved. This can be understood intuitively if one considers that the tight-binding approximation theory uses the atomic wave functions of the individual atoms perturbed only by the presence of the nearest neighbours. In order to account for the translational disorder accompanied by a possible compositional disorder in multicomponent systems, modifications have been proposed for the band structure of the amorphous solid.

Proper interpretation of experimental data of electrical transport properties can only be made if a model for the electronic structure is available. Since the pioneering work

of Bloch it is known that the electronic structure of the crystal shows universal characteristics. For semiconductors, the main features of the energy distribution of the density of electronic states $N(\epsilon)$ of crystalline solids are the sharp structure in the valence and conduction bands, and the abrupt terminations at the valence band maximum and the conduction band minimum. The sharp edges in the density of states produce a well-defined forbidden energy gap and within the band the states are extended, which means that the wave functions occupy the entire volume. The specific features of the band structure are consequences of the perfect short-range and long-range order of the crystal. In an amorphous solid, the long-range order is destroyed, whereas the short-range, i.e., the interatomic distance and the valence angle is only slightly changed. The concept of the density of states is also applicable to noncrystalline solids.

The first effort in generalizing the theory of crystalline semiconductors to amorphous ones was done by Mott [85, 86]. Based on Anderson's theory [7], Mott argued that the spatial fluctuations in the potential caused by the configurational disorder in amorphous materials may lead to the formation of localized states, which do not occupy all the different energies in the band, but form a tail above and below the normal band. Mott postulated furthermore that there should be a sharp boundary between the energy ranges of extended and localized states. The states are localized in the sense that an electron placed in a region will not diffuse at zero temperature to other regions with corresponding potential fluctuations. Mott further suggested that there is a particular density of electronic states above which the states in amorphous solid become extended, leading to the existence of critical energies in each band where there is a sharp jump in mobility, from negligible values to finite ones, takes place. These critical

energies are called the mobility edges and play the same role in amorphous solids that band edges play in crystalline solids. The energy difference between the mobility edges of the valence band and those of the conduction band is called the mobility gap.

The Cohen-Fritzsche-Ovshinsky (CFO) model [87] is an extension of Mott's model. This model assumes the following. (i) The nature of the band tails depends on the extent of the deviations from perfect periodicity (ii) The mobility edges separating the localized and extended states are sharp (iii) the localized band tails overlap in the mobility gap resulting in a finite density of states at the Fermi level (iv) each atom is expected to satisfy the valence requirements locally; thus eliminating any sharp structure in the density of localized states in the gap. The CFO model was specially proposed for multicomponent chalcogenide glasses used in switching devices. This model ensures self compensation and pins the Fermi level close to the middle of the gap. One of the major objections against CFO model has been the high transparency of the amorphous chalcogenides below a well-defined absorption edge and it is now almost certain from different observations that the extent of tailing in chalcogenides is rather limited.

The Davis and Mott model [88] proposes that the tails of localized states should be rather narrow and should extend a few tenths of an eV into the forbidden gap. They proposed furthermore the existence of a band of compensated levels near the middle of the gap, originating from defects in the random network such as dangling bonds, vacancies etc. The energies E_c and E_v separate the ranges where the states are localized and extended. The centre of the band may be split into a donor and an acceptor band, which will also pin the Fermi level. The interval between the energies E_c and E_v act as a pseudogap and is defined as the mobility gap. Cohen [89], proposed a slightly

different picture for the energy dependence of mobility. According to him there should not be an abrupt but a rather continuous drop of the mobility occurring in the extended states just inside the mobility edge. The mean free path of the carriers, in this intermediate range becomes of the order of the interatomic spacing, so that the ordinary transport theory based on the Boltzmann equation cannot be used. Cohen described the transport as a Brownian motion in which the carriers are under the influence of a continuous scattering.

In recent years the experimental evidence, mainly coming from luminescence, photoconductivity and drift mobility measurements, has been found for the existence of various localized gap states, which are split off from the tail states and are located at well defined energies in the gap. These states are associated with defect centres, the nature of which is not always known. Fig.1.5 shows a schematic representation of the electronic structure of amorphous solids based on CFO model, Davis-Mott model and modified Davis-Mott model.

In contrast to the CFO and Davis-Mott ideas, Emin [90] has put forward a different approach to the understanding of the electrical properties of amorphous semiconductors. He suggested that the charge carriers in some amorphous materials might be small polarons. It is generally accepted that the hopping of small polarons is the mechanism responsible for electrical transport in oxide glasses. A disagreement exists, however, in the interpretation of the electrical data obtained on covalent amorphous semiconductors and is not at all clear whether lattice deformation of an extra charge at a given site, is strong enough to cause small-polaron formation.

Kastner has proposed a simple model [91] for the electronic states in chalcogenide glasses based on chemical bonding between atoms. According to this model the electronic

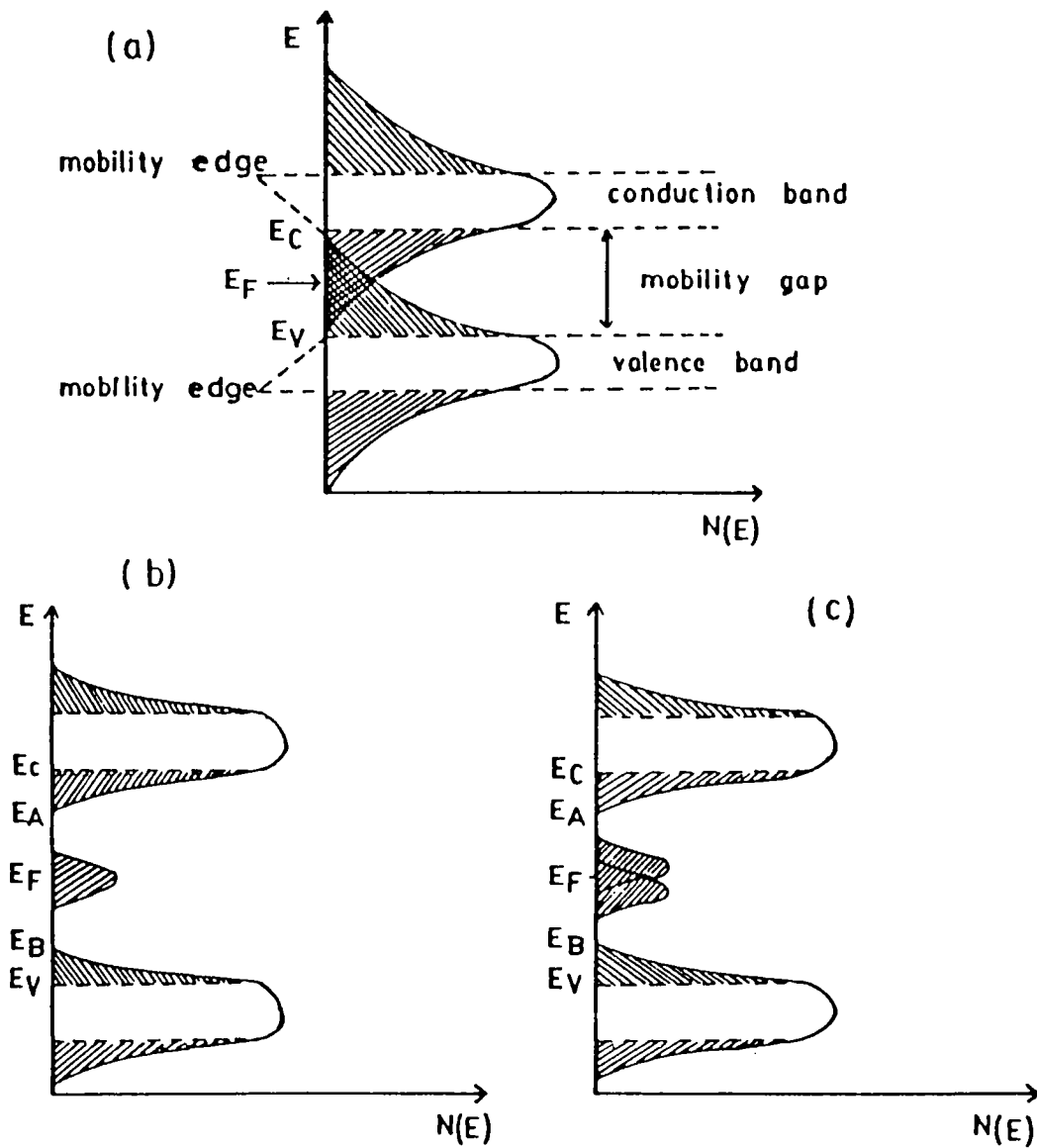


Fig.1.5 Schematic density of states diagrams for amorphous semiconductors (a) the CFO model, (b) the Davis-Mott model, (c) modified Davis-Mott model.

states of a solid may be considered to be a broadened superposition of the molecular orbital states of the constituent bonds. When any two atoms are close enough for their bonding electrons to interact, the energies of their states get shifted by the interaction. Thus group IV elements (Si, Ge) have hybridised sp^3 orbitals which are split into bonding (σ) and antibonding (σ^*) states. In a solid these molecular states are broadened into bands. Thus, in tetrahedral semiconductors the bonding band forms the valence band and the antibonding band forms the conduction band. In group V elements (As, Sb), the presence of three unpaired p electrons does not energetically favour such bonding. In group VI elements (Se, Te), the s states lie well below the p states and need not be considered. Since only two of the three p states can be utilised for bonding, one normally finds chalcogens in two-fold coordination. This leaves one nonbonding electron pair. In a solid these unshared or lone-pair (LP) electrons form a band near the original p-state energy and σ and σ^* bands are split symmetrically with respect to this reference energy. Both the σ and LP bands are occupied. Thus the bonding band is no longer the valence band; this role is played by the LP band. The bonding in Ge and Se are sketched in Fig.1.6. This chemical approach is valid for the chalcogenide glasses in which the chalcogen atom is the major constituent. Kastner also predicted that it is possible to choose a tetrahedral host and a group VI additive so that the LP states fall in the gap. These LP states will be localized at low concentrations. However, when their concentration exceeds a critical value, they become delocalized and an Anderson transition may occur.

1.5 Optical properties of amorphous semiconductors

The sharp structure observed in the fundamental

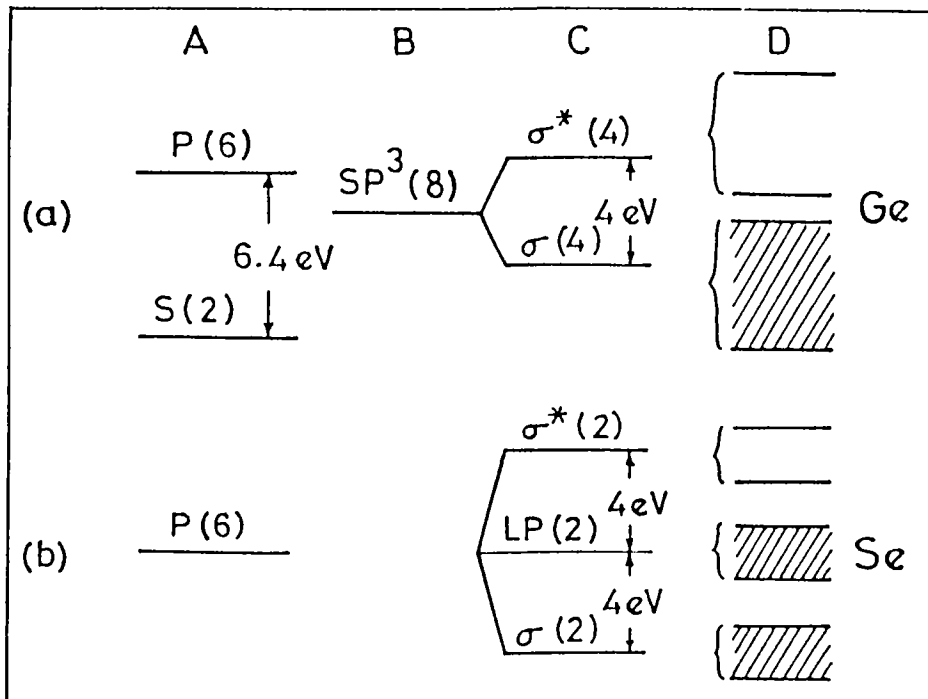


Fig.1.6 Bonding in (a) Ge and (b) Se
 (A) atomic states (B) hybridised states,
 (C) molecular states, (D) States are broad-
 ened into bands in the solid

optical spectra of crystals, both vibrational and electronic, can be classified and interpreted by symmetry arguments based explicitly on the existence of long range order. The sharp structural details which is typical for crystals disappear if the long-range order is destroyed. However, the broad features of the spectra are similar if the short-range order is similar.

The basic nature of a solid depends on the short-range order and more explicitly on the number of first neighbours of the atom i.e., the first coordination number. In order to study the changes in the optical spectra which are caused by the loss of long-range order, one must compare the amorphous materials with the same short-range order; which means that at least the first coordination numbers must be the same. The higher coordination spheres vary differently in different materials, whereas some features of the change caused by the loss of long-range order are similar for all materials, others differ from one class of materials to another. As a general rule, optical transitions between states which may be described by wavefunctions localized over distances of the order of the lattice constant are changed relatively little by disorder. On the other hand, if the valence electron wavefunctions spread over long distances i.e., the bands are very delocalized, the changes are also small.

The structural features of amorphous materials are very much related to the optical properties. In fully coordinated systems, the order within the molecular units is responsible in large part for establishing the electronic bandwidths, which explains the early observation of the similarity of the optical band gaps of many materials in their amorphous and crystalline phases [92]. Conversely, the large differences between the band gaps in which the molecular units are different can also be rationalized. The topological disorder

is responsible for establishing the major features in the density of states [93] though some features are shown to be independent of topology and these are observed in the density of states of crystalline and amorphous phases that are related by their molecular units. Others depend dramatically on ring statistics and these should lead, in principle, to differences in the optical spectra of the two phases. Such changes, however, are heavily masked because in amorphous semiconductors, even at energies well separated from the band edges, the atomic potential is strong enough that even slight distortions of the nearest neighbour bond length and bond angle distributions lead to strong electronic scattering and a short coherence length of the wavefunctions.

In the amorphous state the structure can always adjust itself so that all the valence bands are satisfied and the impurities that may be present are not expected to form distinct absorption centres but would only contribute to the fluctuations of the internal potential. In the optical spectra they would increase the absorption near the absorption edge. However, if the change in potential due to a defect or impurity atom is more profound, exceeding the fluctuations of the internal potential, localized optical transitions can take place. The influence of the fluctuating internal potential in this case is merely a broadening of the lines.

Electronic transitions between the valence and conduction bands in the crystal start at the absorption edge which corresponds to the minimum energy difference E_g between the lowest minimum of the conduction band and the highest maximum of the valence band. If these extrema lie at the same point of the K-space the transitions are called direct. If this is not the case, the transitions are possible only when they are phonon-assisted and are called indirect. The rule governing

these transitions is the conservation of quasimomentum during the transitions, either of the electron alone in direct transitions or the sum of the quasimomenta in indirect transitions. The value of the gap E_g depends in a rather subtle way on the structure and actual values of the pseudo potential in the crystal. It is to be distinguished from the gap E_g , which is the characteristic of the whole absorption band and is connected with the basic chemical properties of the material.

When the semiconductor becomes amorphous, a shift of the absorption edge either towards lower or higher energies may occur. No simple general rule governing these changes has been suggested. In a group of similar materials certain dependencies are observed eg., Rockstand and De Neufville [94] reported a relationship between the optical band gap and the glass transition temperature in chalcogenide glasses. The shape of the absorption curve appears to be similar for many amorphous semiconductors.

The absorption edge in amorphous semiconductors can be generally separated into three regions [95] with absorption coefficients $\beta \geq 10^4 \text{ cm}^{-1}$, $1 \leq \beta \leq 10^{-1} \text{ cm}^{-1}$ and $\beta \leq 1 \text{ cm}^{-1}$ and are referred to as the high absorption region A, the exponential part B which extends over four orders of magnitude of β and the weak absorption tail C as shown in Fig.1.7. The first two regions arise due to transitions within a fully coordinated system perturbed by defects, while the third region arises due to transitions involving defect states directly.

In the high absorption region the absorption coefficient has the following frequency dependence:

$$h\nu \beta(\nu) = B (h\nu - E_o)^r \quad (1.10)$$

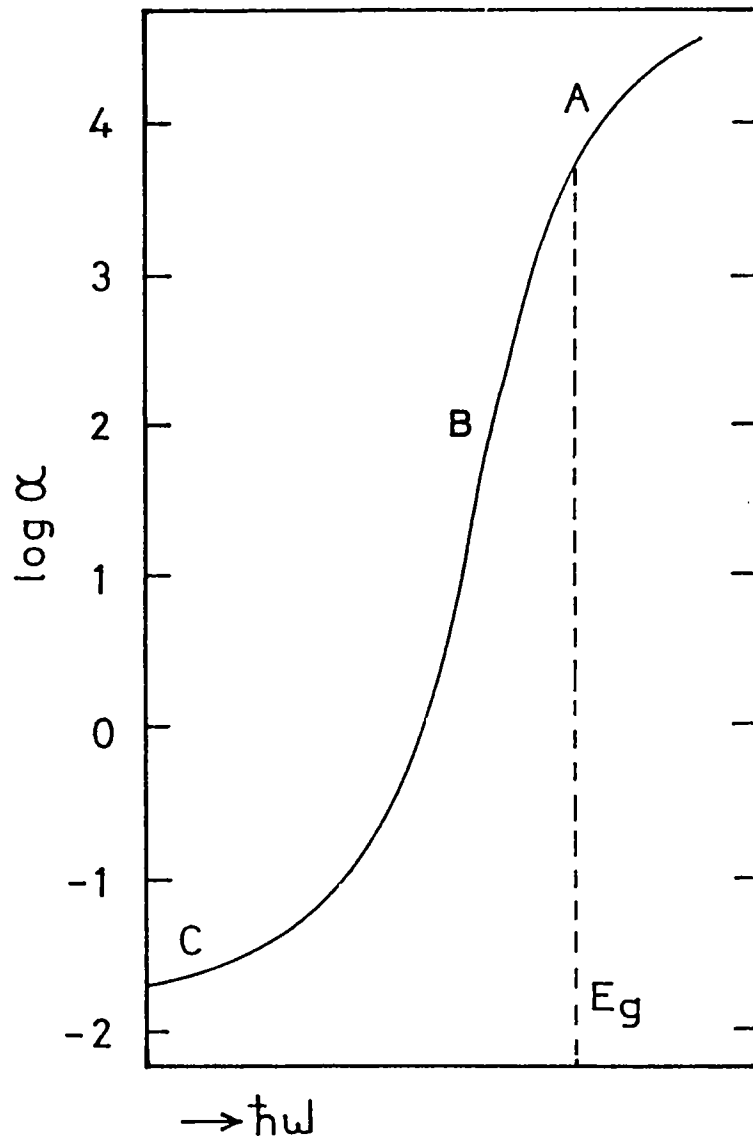


Fig.1.7 Schematic representation of the absorption spectrum of amorphous semiconductors showing three different regions A, B and C.

where ν is the frequency, B is a constant, E_o is the optical band gap and r is a constant. From the above expression an empirical definition for the optical band gap can be made. In amorphous materials, all pairs of extended states with energy differences $h\nu$ can contribute to optical absorption. A plot of $h\nu \beta(\nu)^{1/2}$ vs $h\nu$ yields a straight line. This line when extrapolated to $h\nu$ for which $\beta^{1/2} \rightarrow 0$ gives the optical energy gap E_o .

The exponential region of the absorption edge has the following typical properties :

In the absorption constant range from 1 cm^{-1} (or less) to about 10^4 cm^{-1} , the absorption constant is described by the formula

$$\beta(\nu) = \text{constant} \times \exp (h\nu/E_c) \quad (1.11)$$

where E_c is the energy characterizing the slope. The energy E_c is almost temperature independent at low temperatures and has the value between 0.05 eV and 0.08 eV in many semiconducting glasses. At high enough temperatures the slope decreases with temperature. In many amorphous semiconductors parts A and B move as a whole. The small but non-zero temperature dependence of the slope of the exponential part makes the temperature shift, measured at low absorption levels, somewhat larger than the temperature shift of E_g [96]. The origin of this exponential region is not clear but the suggested possible reasons for the exponential absorption are the disorder induced potential fluctuations [97,98] and strong electron-phonon interaction [99]. In the weak absorption tail region below the exponential part, the strength and shape are found to depend on the preparation, purity and thermal history of the material [100].

A number of areas for concern should have become

apparent in the preceding description of the optical properties of amorphous semiconductors. The theoretical descriptions of optical excitation are semiquantitative at best and qualitative at worst, due to the complexities of calculating the electronic density of states in the absence of long-range order as from the assumptions about the matrix elements for optical transitions between filled and empty states. Moreover, the experimental investigations have been unable in most cases to establish the detailed form of the absorption edge in fully coordinated material. This arises, in some cases, from the difficulty of preparing defect-free material, and in other cases, from an inability to measure precisely the role and magnitude of the electron-phonon interaction. It might be hoped, however, that definite experiments in this area will be performed in the not-too-distant future. Despite these problems, the measurements of the optical properties has played and continues to play a significant role in developing an overall understanding of the structural and electronic properties of amorphous semiconductors.

1.6 Thermal properties of amorphous semiconductors

The phonon mean free path of highly disordered and non-crystalline solids is considerably shorter than that in crystals and correspondingly thermal conductivity is less. The thermal, acoustic and dielectric properties of glasses below 50K show a number of unusual features which have no counterparts in crystals [100]. In low temperature region the thermal conductivity decreases slowly with decreasing temperature. At about 10 K the thermal conductivity is only weakly temperature dependent showing a 'plateau' region and a T^2 dependence at still lower temperatures. Attempts have been made [101] to interpret these variations in thermal conductivity with

temperature using a phonon-fracton anharmonic interaction model. Acoustic and dielectric absorption in amorphous solids is strongly enhanced at low temperatures and in many glasses large absorption peak is found around liquid nitrogen temperature. The linear temperature dependence of the specific heat of amorphous solids at low temperatures is another aspect that has drawn considerable attention in recent years [102,103]. The anomalous features observed in specific heat, thermal conductivity, acoustic and dielectric absorption below 4 K are interpreted using the two-level system (TLS) model [103].

The process of glass transition is another aspect that has been receiving continued attention all the time. The glass transition poses a classification problem: is it a 'new' kind of 'phase transition'? In statistical mechanics, the glass transition may be described in general terms as a transition from ergodic to non-ergodic behaviour [104-106]. Owing to the perpetual atomic motion, of partly vibrational and partly diffusive character, the liquid is driven through its entire 'phase space'. At glass transition the diffusive motion is arrested so that the liquid is locked into a particular cell of phase space which corresponds to the atomic configuration fixed in the glass. A recent theory predicts such a new kind of phase transition: a dynamical transition at which the molecular diffusivity vanishes and the macroscopic viscosity diverges. In view of the experimental data, however, which so far show no evidence of a sharp transition, it seems more natural to ask whether there is a hidden phase transition which might be inferred by extrapolation to longer and longer experimental time scales. One such extrapolation of the excess entropy of the supercooled liquid relative to the same crystalline material leads to a paradoxical situation, named after Kauzmann.

Glass transitions (GT's) are usually characterized by

a phenomenological value T_g of the critical temperature and by a width ΔT_g of the so-called 'glass-transition region' around T_g . In this region the diffusive motion of the melt begins to freeze in, before a glassy structure is achieved with viscosity values typical of solids (10^{14} N s m⁻²). Both T_g and ΔT_g depend smoothly on the cooling rate [107]. It is clear that $\Delta T_g/T_g$ provides a rough estimate of the non-equilibrium effects occurring at the GT, so that $\Delta T_g/T_g \ll 1$ is a necessary condition for any thermodynamical approach. In good glass-forming systems, the above mentioned condition is usually fulfilled at relatively low cooling rates.

Non-isothermal heating studies such as the ones performed in differential scanning calorimetry (DSC) could provide lots of information about the thermal properties of glasses, like the kinetics of crystallization and the thermal stability of the glasses against crystallization apart from being an indispensable characterization tool to investigate glass transition phenomenon. The specific heat at constant pressure (C_p) of a material can be estimated from DSC experiments using the ratio method [108].

PART B: PHOTOACOUSTICS AND PHOTOACOUSTIC SPECTROSCOPY

1.7 Introduction

One of the most effective means employed to study the physical properties of matter is optical spectroscopy, which is based on the interaction of light with matter at the atomic or molecular levels. Almost all the conventional optical spectroscopic methods are either transmission type, which

involves the measurement of the intensity of radiation transmitted through the medium or reflection type which involves the detection and measurement of the intensity of radiation scattered or reflected from the sample material. Optical spectroscopy has been successful in the case of a variety of materials but at the same time there are situations, in which it often fails to give good results, particularly when we try to make measurements on weakly absorbing materials, highly light scattering materials such as powders, amorphous materials etc. and opaque materials. Several techniques like diffuse reflectance [109], attenuated total reflection and internal reflection spectroscopy [110], Raman scattering [111] etc. have been in use in such situations. Even then the application of these techniques are limited to a relatively small category of materials and wavelength ranges and the data obtained are often difficult to interpret.

In recent years the photacoustic technique has become a very powerful method to study those materials that are unsuitable by the conventional transmission or reflection methods [112-115]. This technique, based on the photoacoustic effect originally detected by Alexander Graham Bell in 1880 [116,117], possesses some unique features mainly due to the fact that eventhough the incident energy is in the form of photons, the interaction of these photons with the sample is studied not through subsequent detection and analysis of some of the photons, but through a direct measurement of the energy absorbed by the material as a result of its interactions with the incident photon beam. So this technique can be effectively used with equal success for the study of weakly absorbing samples as well as highly light scattering and optically opaque materials. Also, since the sample itself acts as the radiation detector, no photoelectronic device is necessary and this enables one to carry out studies over a wide range of wavelengths without

changing the detector system.

The photoacoustic effect (PA) is the generation of an acoustic signal when the sample under investigation, placed inside an enclosed volume, is irradiated by an intensity modulated beam of light. The absorption of the incident radiation will excite the internal energy levels of the sample and upon subsequent deexcitation, all or part of the absorbed photon energy is converted into heat through non-radiative deexcitation processes. In the case of gas and liquid samples, which fill the entire volume of the sample chamber, this internal heating causes pressure fluctuations having the same frequency as that of the modulation frequency of the incident radiation and can be detected using an acoustic transducer kept in intimate contact with the sample. In the case of solid samples, which fill only a portion of the sample chamber, the periodic heating of the sample results in a periodic heat flow from the interior of the sample to the surrounding non-absorbing gas medium which in turn produces pressure fluctuations in the gas and detected as an acoustic signal by an electret microphone placed close to the sample.

Photoacoustics is essentially a combination of optical absorption spectroscopy and calorimetry. From the calorimetric view point, the heat input into the sample is supplied indirectly by the incident beam of light and the rise in temperature is detected by another indirect method using an acoustic transducer instead of a thermal detector. For a typical solid sample, using gas-microphone detection system, temperature rise of the order of 10^{-6} °C can be detected. This acoustic detection has several advantages over conventional thermal detection using temperature sensors such as thermistors or thermopiles in terms of sensitivity, detector rise time and the speed at which measurements can be made.

The major advantages of photoacoustics as a spectroscopic tool are evident from the very nature of the technique. Since absorption of optical or electromagnetic radiation is essential for the generation of the PA signal, light that is transmitted or elastically scattered by the sample will not interfere with the inherently absorptive PA measurements. This enables one to work with essentially transparent media or highly light scattering materials such as powders, amorphous solids, gels and colloids. On the other hand, since the technique does not depend upon the detection of photons, it is possible to obtain optical absorption spectra of materials that are completely opaque to transmitted light. The advantages of photoacoustic spectroscopy over other conventional spectroscopic techniques due to the two basic aspects viz., the insensitivity to the non-absorbed light and the non-dependence on the detection of photons, cannot be over-emphasized.

1.8 Theory of photoacoustic effect in solids

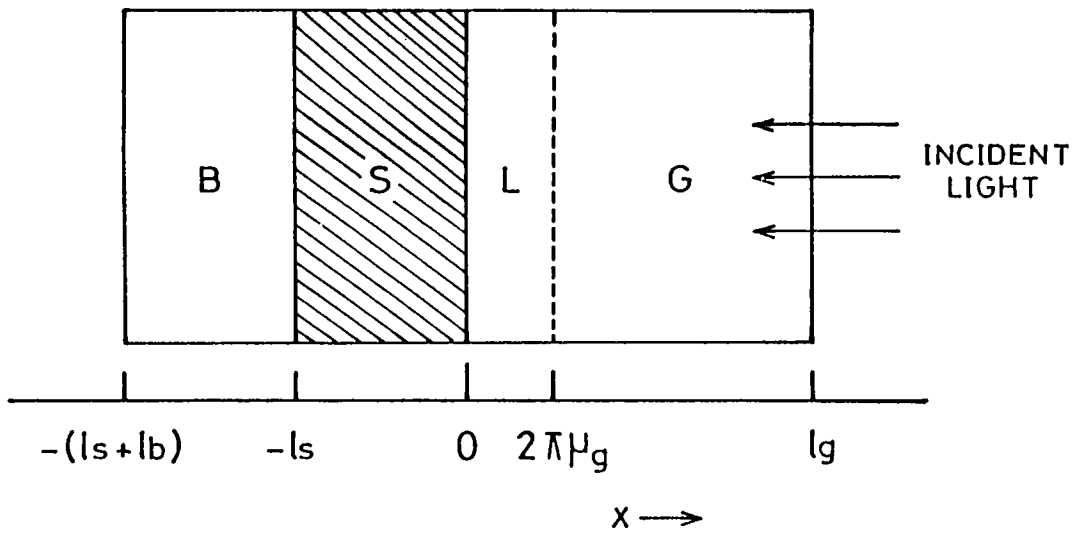
Several theoretical explanations of PA effect have been put forward in the 19th century itself. But the present understanding of the PA effect in solid is based on modern theories developed during the seventies. The first attempt to develop a proper theory of PA effect in solids was carried out by Parker [118] in 1973 in order to give a quantitative explanation for the PA signal emanating from cell windows while performing PA measurements on gases. Later the pioneering works of Rosencwaig and co-workers have resulted in enormous uprise of interest in this field. The general theory of PA effect in solids formulated by Rosencwaig and Gersho [119,120] has been found to be very successful in interpreting most of the experimental observations. The Rosencwaig-Gersho (RG) theory

states that in a gas microphone PA cell, the signal depends both on the generation of an acoustic pressure disturbance at the sample-gas interface and on the transport of this disturbance through the gas to the microphone. The pressure fluctuations at the sample-gas interface are caused by the periodic heat flow from the sample which is governed by thermal diffusion equations. The RG theory gives an exact equation for the magnitude and phase of the PA signal as a function of the optical, thermal and geometrical properties of the sample, the cell and the gas within the cell. Although the thermal part of the theory has been treated exactly, the acoustic part is treated in an approximate heuristic manner which is, however, valid for most experimental conditions. Since RG theory is extensively used in interpreting the results of the present study, the salient features of the theory are briefly discussed below.

The RG Theory is a one-dimensional analysis of the production of the photoacoustic signal in a simple cylindrical cell as shown in Fig.1.8. The cell has a diameter D and length L . It is assumed that the length L is small compared to the wavelength of the generated acoustic signal and the microphone (not shown in the figure) detects the average pressure produced in the cell. The solid sample is considered to be in the form of a disc of diameter D and length l . The sample is mounted in such a way that its back surface is against a poor thermal conductor of thickness l'' . The length of the gas column in the cell is l' . It is also assumed that the gas and the backing material do not absorb light.

The parameters which are important in the theoretical formulation are defined below.

K : the thermal conductivity ($\text{cal cm}^{-1} \text{sec}^{-1} \text{ } ^\circ\text{C}^{-1}$)



B - BACKING MATERIAL
 S - SAMPLE
 L - BOUNDARY LAYER OF GAS
 G - GAS MEDIUM

Fig.1.8 Cross-sectional view of a simple cylindrical photoacoustic cell.

ρ : the density (gm/cm^3)

C : the specific heat ($\text{cal gm}^{-1} \text{ } ^\circ\text{C}^{-1}$)

$\alpha = K/\rho C$: the thermal diffusivity ($\text{cm}^2 \text{ sec}^{-1}$)

$a = (\omega / 2\alpha)^{1/2}$: the thermal diffusion coefficient (cm^{-1})

$\mu = 1/a$: the thermal diffusion length (cm)

ω denotes the modulation frequency of the incident light beam in radians per second. In the following treatment the sample parameters are represented by unprimed symbols and the gas and backing material parameters by singly primed and doubly primed letters respectively.

The intensity I of a sinusoidally modulated monochromatic beam of light with wavelength λ incident on the sample is given by

$$I = 1/2 I_0 (1 + \text{Cos } \omega t) \quad (1.12)$$

where I_0 is the incident monochromatic light flux (W/cm^2). If β denotes the optical absorption coefficient of the solid sample for wavelength λ , the heat density H produced at a point x due to the absorption of light at this point in the solid is given by

$$H = 1/2 \beta I_0 e^{\beta x} (1 + \text{Cos } \omega t) \quad (1.13)$$

where x takes on negative values since the solid extends from $x = 0$ to $x = -l$, with the light incident at $x = 0$. Note also from

fig.1.8 that the gas column extends from $x = 0$ to $x = l'$ and the backing from $x = -l$ to $x = -(l+l'')$.

The thermal diffusion equation in the solid taking into account the distributed heat source can be written as

$$\partial^2 \theta / \partial x^2 = 1/\alpha \partial \theta / \partial t - A e^{\beta x} (1 + e^{i\omega t}) \quad \text{for } -l \leq x \leq 0 \quad (1.14)$$

with

$$A = \beta I_0 \eta / 2K \quad (1.15)$$

where θ is the temperature, η is the efficiency at which the absorbed light at wavelength λ is converted to heat by the non-radiative deexcitation processes. The value of η is taken as unity in the following calculations, a reasonable assumption for most solids at room temperature. The thermal diffusion equations for the backing material and the gas are respectively given by,

$$\partial^2 \theta / \partial x^2 = 1/\alpha'' \partial \theta / \partial t \quad \text{for } -l'' - l \leq x \leq -l \quad (1.16)$$

$$\partial^2 \theta / \partial x^2 = 1/\alpha' \partial \theta / \partial t \quad \text{for } 0 \leq x \leq l' \quad (1.17)$$

The real part of the complex valued solutions $\theta_{\alpha, \omega}$ of equations (1.14) to (1.17) is the solution of physical interest and represents the temperature in the cell relative to ambient temperature as a function of position and time. The actual temperature field in the cell is given by

$$T(x, t) = \text{Re} \theta(x, t) + \phi_0 \quad (1.18)$$

where ϕ_0 is the ambient (room) temperature.

To completely specify the solution $\theta(x, t)$ the

appropriate boundary conditions are obtained from the requirement of temperature and heat flux continuity at the boundaries $x = 0$ and $x = -1$ and from the constraint that the temperature at the cell walls $x = 1'$ and $x = -1-1''$ is at ambient.

The general solutions for $\theta(x,t)$ in the cell neglecting transients can be written as,

$$\theta(x,t) = \begin{cases} 1/1'' (x + 1 + 1'')W_0 + We^{\sigma''(x+1)} e^{i\omega t} , & -1 - 1'' \leq x \leq -1 \\ b_1 + b_2x + b_3e^{\beta x} + (Ue^{\sigma x} + Ve^{-\sigma x} - Ee^{\beta x})e^{i\omega t} , & -1 \leq x \leq 0 \\ (1 - x/1')F + \theta_0 e^{-\sigma'x} e^{i\omega t} , & 0 \leq x \leq 1' \end{cases} \quad (1.19)$$

where W , U , V , E and θ_0 are complex valued constants, b_1 , b_2 , b_3 , W_0 and F are real valued constants, and $\sigma = (1+i)a$. θ_0 and W represent the complex amplitudes of the periodic temperatures at the sample-gas boundary ($x = 0$) and the sample-backing ($x = -1$) respectively. The quantities E and b_3 , determined by the forcing function in (1.14), are given by

$$b_3 = - A/\beta^2 \quad (1.20)$$

$$E = A/(\beta^2 - \sigma^2) = \beta I_0 / 2K(\beta^2 - \sigma^2) \quad (1.21)$$

In the general solution (1.19), the growing exponential components of the solutions to the gas and backing material are omitted because for all frequencies ω of interest,

the thermal diffusion length is small compared to the length of the material and hence the sinusoidal components of these solutions are sufficiently damped so that they are effectively zero at the cell walls. Hence, the growing exponential components of the solutions would have coefficients that are essentially zero in order to satisfy the temperature constraint at the cell walls.

By applying the boundary conditions all the constants of eq. (1.19) and hence the d.c and a.c components of the solution can be obtained. Then the explicit solution for θ_o , the complex amplitude of the periodic temperature at the solid-gas boundary ($x = 0$) is given by,

$$\theta_o = \frac{\beta I_o}{2K(\beta^2 - \sigma^2)} \left[\frac{(r-1)(b+1)e^{\sigma l} - (r+1)(b-1)e^{-\sigma l} + 2(b-r)e^{-\beta l}}{(g+1)(b+1)e^{\sigma l} - (g-1)(b-1)e^{-\sigma l}} \right] \quad (1.22)$$

where

$$b = K''a''/Ka \quad (1.23)$$

$$g = K'a'/Ka \quad (1.24)$$

$$r = (1-i)\beta/2a \quad (1.25)$$

The main source of the acoustic signal is from the periodic heat flow from the solid to the surrounding gas medium. This periodic diffusion process produces a temperature variation in the gas as given by the sinusoidal (a.c) component of the solution (1.19)

$$\theta_{a.c.}(x,t) = \theta_o e^{-a'x} e^{i\omega t} \quad (1.26)$$

The actual physical temperature variation in the gas medium is given by the real part of eq. (1.26) as

$$T_{a.c.}(x,t) = e^{-a'x} \left[\theta_1 \text{Cos} (\omega t - a'x) - \theta_2 \text{Sin} (\omega t - a'x) \right] \quad (1.27)$$

where θ_1 and θ_2 are the real and imaginary parts of θ_o , as given by eq. (1.22). The time dependent component of the temperature in the gas attenuates rapidly to zero with increasing distance from the surface of the solid. The periodic temperature variation in the gas is effectively fully damped out at a distance of $2\pi/a' = 2\pi\mu'$, where μ' is the thermal diffusion length of the gas. It can be assumed to a good approximation that only this boundary layer of gas as shown in fig.1.8 whose thickness is $2\pi\mu'$ is capable of responding thermally to the periodic temperature at the surface of the sample.

The spatially averaged temperature of this boundary layer of gas as a function of time can be determined as,

$$\bar{\theta}(t) = 1/(2\pi\mu') \int_0^{2\pi\mu'} \theta_{ac}(x,t) dx \quad (1.28)$$

Because of the periodic heating of the boundary layer, this layer of gas expands and contracts periodically and thus can be thought of as acting as an acoustic piston on the rest of the gas column, producing an acoustic signal that travels through the entire gas column. The displacement of this gas piston due to the periodic heating can be estimated by the ideal gas law as,

$$\delta x(t) = 2\pi\mu' \bar{\theta}(t)/T_o = (\theta_o\mu'/\sqrt{2} T_o) e^{i(\omega t - \pi/4)} \quad (1.30)$$

Assuming that the rest of the gas responds to this acoustic piston adiabatically, the acoustic pressure in the cell due to the displacement of the piston can be obtained from the adiabatic gas law,

$$PV^\gamma = \text{Constant}$$

where P is the pressure, V is the gas volume in the cell and γ is the ratio of the specific heats of the gas. Then the incremental pressure is given by,

$$\delta P(t) = (\gamma P_o / V_o) \delta V = (\gamma P_o / l') \delta x(t) \quad (1.31)$$

where P_o and V_o are the ambient pressure and volume respectively and $-\delta V$ is the incremental volume.

Then from eq (1.19)

$$\left. \begin{array}{l} \delta P(t) = Q e^{i(\omega t - \pi/4)} \\ Q = \gamma P_o \theta_o / \sqrt{2} l' a' T_o \end{array} \right\} \quad (1.32)$$

Thus the actual physical pressure variation $\Delta P(t)$ is given by the real part of $\delta P(t)$ as

$$\Delta P(t) = Q_1 \text{Cos}(\omega t - \pi/4) - Q_2 \text{Sin}(\omega t - \pi/4) \quad (1.33)$$

or

$$\Delta P(t) = q \text{Cos}(\omega t - \Psi - \pi/4) \quad (1.34)$$

where Q_1 and Q_2 are the real and imaginary parts of Q and q and Ψ are the amplitude and phase of Q , that is,

$$Q = Q_1 + iQ_2 = qe^{i\Psi} \quad (1.35)$$

Thus Q specifies the complex envelope of the sinusoidal pressure variation, and the explicit formula for Q is obtained by combining equations (1.22) and (1.32.)

$$Q = \frac{\beta I_o \gamma P_o}{2\sqrt{2} T_o K l' a' (\beta^2 - \sigma^2)} \left[\frac{(r-1)(b+1)e^{\sigma l} - (r+1)(b-1)e^{-\sigma l} + 2(b-r)e^{-\beta l}}{(g+1)(b+1)e^{\sigma l} - (g-1)(b-1)e^{-\sigma l}} \right] \quad (1.36)$$

Equation (1.36) gives the amplitude and phase of the acoustic wave generated in the cell by photoacoustic effect.

Special cases:

The difficulty in the interpretation of eqn.(1.36) can be reduced by examining the following special cases. The special cases are determined by the relative magnitudes of the optical absorption length $l_\beta = 1/\beta$, the thermal diffusion length μ and thickness l of the sample respectively. Also, it is convenient to define

$$Y = (\gamma P_o I_o) / (2\sqrt{2} T_o l') \quad (1.37)$$

which always appears as a constant factor in the expression for Q .

Case 1 : Optically transparent solids ($l_{\beta} > l$)

In this case light is absorbed throughout the length of the sample and some light is transmitted through the sample.

Case 1(a): Thermally thin solids ($\mu \gg 1; \mu > l_{\beta}$)

Assuming $e^{-\beta l} \approx 1 - \beta l$, $e^{\pm \sigma l} \sim 1$ and $|r| > 1$ in eqn.(1.26), the expression for Q is obtained as,

$$Q = (1-i)\beta l / 2a' (\mu''/K'')Y \quad (1.38)$$

The acoustic signal is thus proportional to βl and since μ''/a'' is proportional to $1/\omega$, the acoustic signal has an ω^{-1} dependence. Also, for this thermally thin case of $\mu \gg 1$, the thermal properties of the backing material come into play in the expression for Q.

Case 1(b): Thermally thin solids ($\mu > 1; \mu < l_{\beta}$)

Setting $e^{-\beta l} \approx 1 - \beta l$, $e^{\pm \sigma l} \approx (1 \pm \sigma l)$ and $|r| < 1$, the expression for Q becomes,

$$Q = (1-i)/2a' (\mu''/K'')Y \quad (1.39)$$

Here again the acoustic signal is proportional to βl and varies as ω^{-1} and depends on the thermal properties of the backing material. Eqn.(1.39) is identical to (1.38).

Case 1(c): Thermally thick solids ($\mu < 1; \mu \ll l_{\beta}$)

Setting $e^{-\beta l} \approx 1 - \beta l$, $e^{-\alpha l} \approx 0$ and $|r| \ll 1$, in eqn.(1.26),

$$Q = -i\beta\mu/2a' (\mu/K)Y \quad (1.40)$$

Here the acoustic signal is proportional $\beta\mu$ instead of βl . This means that only the light absorbed within the first thermal diffusion length contributes to the signal even though absorption takes place throughout the thickness of the solid. Also since $\mu < 1$ the thermal properties of the backing material in eqns. (1.38) and (1.39) are replaced by those of the solid sample. The signal in this case varies as $\omega^{-3/2}$.

Case 2: Optically opaque solids

In this case, most of the light is absorbed within a distance that is small compared to l and essentially no light is transmitted.

Case 2(a): Thermally thin solids ($\mu \gg 1$; $\mu \gg 1/\beta$)

Using the approximations $e^{-\beta l} \approx 0$, $e^{\pm\alpha l} \approx 1$ and $|r| \gg 1$

$$Q \approx (1-i)/2a' (\mu''/K'')Y \quad (1.41)$$

In this case, we have photoacoustic "opaqueness" as well as optical opaqueness, in the sense that our acoustic signal is independent of β . This would be the case for a very black absorber such as carbon black. The signal is quite strong, depends on the thermal properties of the backing material and varies as ω^{-1} .

Case 2(b): Thermally thick solids ($\mu < 1$; $\mu > 1/\beta$)

Setting $e^{-\beta l} \approx 0$, $e^{-\sigma l} \approx 0$ and $|r| > 1$,

$$Q = (1-i)/2a' (\mu/K)Y \quad (1.42)$$

Eqn.(1.42) is similar to (1.41) except that the thermal parameters of the backing material are now replaced by those of the sample. Here also, the acoustic signal is independent of β and varies as ω^{-1} .

Case 2(c): Thermally thick solids ($\mu \ll 1$; $\mu < l_\beta$)

Setting $e^{-\beta l} \approx 0$, $e^{-\sigma l} \approx 0$, $|r| < 1$

$$Q \approx i\beta\mu/2a' (\mu/K)Y \quad (1.43)$$

This is very interesting and important case because eventhough the sample is optically opaque, it is not photoacoustically opaque as long as $\mu < l_\beta$ i.e., the acoustic signal is proportional to β . The signal is also dependent on the thermal properties of the sample and varies as $\omega^{-3/2}$.

The essence of the RG theory as summarized in eqns. (1.38) to (1.43) have successfully been verified by several workers [121-124]. Further theoretical improvements to the theory have been made later by treating the transport of the acoustic signal in the gas more exactly with Navier-Stokes equations [125-128].

Mc Donald and Wetsel [127] extended the theory to include the effect of thermally induced mechanical vibrations of the sample by solving coupled equation for thermal and acoustic

waves in both the sample and gas. Although these refinements did not change the basic results of the RG theory for most experimental conditions, they were able to account for the observed deviations from the RG theory at very low modulations frequencies.

1.9 Applications of the photoacoustic effect

Since the PA technique basically incorporates spectroscopic as well as calorimetric aspects, applications of the PA effect can be correspondingly divided into two classes. The first one is basically the study of the interaction of photons with matter and the second one is the study of thermal and acoustic properties of materials. The applications of the PA techniques in various branches of science and technology have been enormous during the past few years. The following paragraphs briefly outline some of the principal applications of the PA effect.

The most basic and earliest applications of the PA effect is spectroscopy. One of the principal advantages of PA spectroscopy is that it enables one to obtain spectra similar to the optical absorption spectra of any type of solid or semisolid material, whether it be crystalline, powder, amorphous, smear or gel. Also, it has been found experimentally that good optical absorption data can be obtained using PA technique on materials that are completely opaque [113,129] or essentially transparent [130] to incident light. The PA spectroscopy has already found important applications in research and analysis of inorganic, organic and biological specimens [112,129-131].

With the advent of laser PA systems, PA technique has been used in overtone spectroscopy, trace analysis and pollution monitoring [132-136]. The PA technique can be used to study

insulators, semiconductors and even metallic systems that cannot be readily studied by conventional absorption techniques. In the case of insulators, PA spectra could provide information about the optical absorption bands in the material [112] and in semiconductors both direct and indirect transitions can be detected [113,129].

The spectroscopic application of PA technique also include the study of deexcitation processes in materials. The selective sensitivity of the PA technique to non-radiative deexcitation channel can be used to study fluorescence and photosensitivity of materials. The PA effect has been effectively utilized for deexcitation studies in rare earth oxides and doped crystals [132,133]. A combination of conventional fluorescence spectroscopy and PA spectroscopy can provide information about the relative strength of the radiative and non-radiative deexcitation processes in solids.

Another useful application of PA technique is in the study of photovoltaic deexcitation processes in semiconductors. In such processes part of the incident radiation is converted into electrical energy resulting in a corresponding reduction in the thermal energy produced and hence the PA signal depends upon the energy conversion efficiency of the process. Cahen has reported [132] the measurement of photoelectrical generation efficiency of silicon solar cells using PA technique. There are reports on the use of PA method to determine photoconductive quantum efficiency of a thin organic dye film [133], and photocarrier generation quantum efficiency of a Schottky diode [134].

One of the unique applications of PA technique is that by changing the chopping frequency, it is possible to obtain a depth profile analysis of the optical and thermal properties of

a material. At high chopping frequencies information about the sample near the surface is obtained, while at low frequencies data comes from deeper regions within the sample. Such applications are very useful in thin films, layered and optically opaque samples etc. Depth profiling is also important in the study of doped semiconducting materials, laser windows whose surfaces have absorption properties different from that of bulk and biological tissues.

Recently attention has turned to the possibility of using PA technique for imaging applications [135-139]. By scanning the amplitude modulated focused light beam across the surface of the sample and recording the amplitude and phase of the PA response, it is possible to construct an image that is characteristic of the optical and thermal properties within a part of the sample. By varying the chopping frequency, one can obtain PA images at various depths of the sample material. The PA image is due to the spatial variation in the optical and thermal properties of the material. The imaging application of PA technique can also be applied for subsurface imaging and detecting flaws in samples like semiconductor chips. The techniques of photoacoustic microscopy makes use of the imaging applications of PA effect.

The potential application of PA technique has also been extended for the investigation of thermal properties of materials. The thermal and acoustic waves generated by optical irradiation can be used to investigate different properties such as thermal diffusivity, sound velocity, flow velocity, thickness of thin films, subsurface defects and so on. Adams and Kirkbright [140] were the first to make use PA technique to obtain thermal diffusivity values of copper and glass by using rear surface illumination. Later several workers [141-146] investigated the use of PA technique for the measurement of

thermal parameters in detail and various methods have developed in this area.

Apart from the above described applications of PA effect, it has gained wide interest as a powerful tool for the study of phase transitions in solids recently. In phase transition studies, photoacoustics constitutes a complementary technique to the conventional calorimetric methodology. Several reports have been appeared on the use of photoacoustic technique for the investigation of phase transitions in solids including high T_c superconductors [141-146].

1.10 Work presented in the thesis

The composition dependence of various properties of chalcogenide glasses is expected to show up two features mainly - the chemical and the mechanical thresholds. In this work a detailed investigation of the composition dependence of three ternary chalcogenide systems, As-Sb-Se, As-Te-Se and Ge-As-Se, has been performed using photoacoustic and calorimetric techniques. Ternary glasses have been chosen because the effect of the addition of another element of the mechanical and chemical thresholds can be separated out in these glassy systems. It is also expected that different physical phenomena may have varying sensitivities to rigidity percolation and chemical ordering in glassy networks. Also, the presented work demonstrates the potential use of PA technique as a calorimetric tool for the investigation of glass transition temperature in glassy systems. The details of the various experiments performed on these systems and the results obtained are presented in the following chapters.

REFERENCES

1. B. T. Kolomiets, Proc. Int. Cof. on Semiconductor Physics, Prague 1960 (Czechoslovak Academy of Sciences, 1961) p.884; Phys. Stat. Solidi, 7, 359, 713 (1964)
2. W. E Spear, Proc. Phys. Soc. (London), 870, 1139 (1957); 76, 826 (1960)
3. J. Tauc, R. Grigorovici and A. Vanacu, Phys. Stat. Solidi, 15, 267 (1966)
4. S. R. Ovshinsky, Phys. Rev. Lett., 21, 1450 (1968)
5. F. Bloch, Z. Physik., 52, 555 (1928)
6. A. H. Wilson, Theory of Metals (Cambridge University Press, New York, 1936)
7. P. W. Anderson, Phys. Rev. 109, 1492 (1958)
8. K. Ishii, Suppl. Prog. Theor. Phys., 53, 77 (1973)
9. D. T. Thouless, J. Phys C 3, 1559 (1970)
10. D. C. Licciardello and E. N. Economou, Phys. Rev. B 11, 3697 (1975)
11. D. C. Licciardello and D. J. Thouless, J. Phys. C, 8, 4157 (1975); J. Phys. C, 11, 935 (1977)
12. D. Weaire and V. Srivastava, Solid State Commun., 23, 863 (1977)

13. K. Tsujino, A. Tokunaga, M. Yamamoto and F. Yonezawa, *Solid State Commun.*, **30**, 531 (1979)
14. E. N. Economou and P. D. Antoniou, *Solid State Commun.*, **21**, 28 (1977)
15. A. Abrahams, P. W. Anderson, D. C. Licciardello and T. V. Ramakrishnan, *Phys. Rev. Lett.*, **42**, 673 (1979)
16. P. A. Lee and T. V. Ramakrishnan, *Rev. Mod. Phys.*, **57**, 287 (1985).
17. D. J. Thouless, in *Ill Condensed Matter*, ed: L. R. Balian, R. Maynard and G. Toulouse (North-Holland, Amsterdam, 1978) p.5
18. N. F. Mott and E. A. Davis, *Electronic Processes in Non-Crystalline Materials* (Clarendon Press, 1971)
19. R. Zallen, *The Physics of Amorphous Solids* (John Wiley, 1983)
20. S. R. Elliot, *Physics of Amorphous Materials*, 2nd Edn. (Longman, London, 1990)
21. W. H. Zachariasen, *J. Am. Chem. Soc.*, **54**, 3841 (1932)
22. D. E. Polk, *J. Non-Cryst. Solids*, **5**, 365 (1971)
23. N. J. Shevchik, W. Paul, *J. Non-Cryst. Solids*, **8-10**, 381 (1972)
24. D. Henderson, F. Herman, *J. Non-Cryst. Solids*, **8-10**, 359 (1972)

25. D. E. Polk, D. S. Boudreaux, Phys. Rev. Lett., 31 , 92 (1973)
26. G. N. Greaves, E. A. Davis, Phil. Mag., 29, 1201 (1974)
27. M. Long, P. Galison, R. Alben, G A N Connell, Phys. Rev. B13, 1821 (1976)
28. G. Lucovsky, A. Mooradian, W. Taylor, G. B. Wright, R. C. Keezer, Solid state commun., 5 , 113 (1967)
29. A. Mooradian, G. B. Wright : In Physics of Selenium and Tellurium, ed: by W. C. Cooper (Pergamon Press, Oxford 1967) p.269
30. M. Gorman, S. A. Solin, Solid State Commun., 18, 1401 (1976)
31. R. J. Nemanich, G. Lucovsky, W. Pollard, J. D. Joannopoulos, Solid State commun., 26, 137, (1978)
32. G. Lucovsky, F. L. Galeener, R. C. Keezer, R. H. Geils, H. A. Six, Phys. Rev. B10, 5134 (1974)
33. G. Lucovsky, F. L. Galeener, R. H. Geils, R. C. Keezer, In The Structure of Non-Crystalline Materials, ed: by P. H. Gaskell (Taylor and Francis, London 1977) p.127.
34. R. J. Bell, P. Dean, Discuss. Faraday Soc., 50, 55 (1970)
35. G. Locovsky, R. J. Nemanich, F. L. Galeener, In Amorphous and Liquid Semiconductors, ed: by W. E. Spear (G. G. Stevenson, Dundee 1977) p.130
36. N. F. Mott, E. A. Davis, R. A. Street, Phil. Mag. 32, 961 (1975)

- R. A. Street, N. F. Mott; Phys. Rev. Lett., **35**, 1293 (1975)
37. M. Kastner, D. Adler, H. Fritzsche, Phys. Rev. Lett., **37**, 1504 (1976)
38. S. G. Bishop, U. Storm, P. C. Taylor, Phys. Rev. Lett., **34**, 1346 (1975); Phys. Rev. Lett., **36**, 543 (1976)
39. S. G. Bishop, U. Storm; in Optical Properties of Highly Transparent Solids, ed: by S. S. Mitra, B. Bendow (Plenum, New York 1975) p.317.
40. F. Betts, A. Bienenstock, S. R. Ovshinsky, J. Non-Cryst. Solids, **4**, 554 (1970)
41. S. C. Rowland, S. C. Narasimhan, A. Bienenstock, J. Appl. Phys., **43**, 2741 (1972)
42. L. Cervinka, A. Haruby; In Amorphous and Liquid Semiconductors, ed: by J. Stuko, W. Brening (Taylor and Francis, London, 1974) p 431.
43. R. W. Fawcett, C. N. J. Wagner, C. S. Cargill III, J. Non-Cryst. Solids, **8-10**, 369 (1972)
44. G. Yu. Poltavtsev, V. M. Pozdnyadova, Ukr. Fiz. Zh., **18**, 679 (1973)
45. P. S. E. Even, M. Sik, A. E. Owen, In The structure of Non-Crystalline Materials, ed: by P. Gaskell (Taylor and Francis, London 1977) p. 231
46. F. Ordway, Science **143**, 800 (1964)
47. D. L. Evans, S. R. King, Nature (London), **212**, 1353 (1966)

48. G. Lucovsky, J. P. de Neufville, F. L. Galeener, Phys. Rev. B8, 5947 (1973)
49. G. Lucovsky, R. M. Martin, J. Non-Cryst. Solids, 8-10, 185 (1972)
50. G. Lucovsky, R. M. White, Phys. Rev. B8, 660 (1973)
51. A. T. Ward, J. Phys. Chem., 72, 744, 4133 (1968).
52. D. W. Scott, J. P. Mc Cullough, F. H. Kruse, J. Mol. Spect., 13, 313 (1964)
53. H. R. Philipp, J. Non-Cryst. Solids, 8-10, 627 (1972)
54. J. C. Phillips , J. Non-Cryst. solids, 34 , 153 (1979)
55. J. C. Phillips , J. Non-Cryst. solids, 43, 37 (1981)
56. J. C. Phillips , Phys. Stat. Solidi (b) 101, 473 (1980)
57. M. F. Thorpe, J. Non-Cryst. Solids, 57, 355 (1983)
58. J. C. Phillips and M. F. Thorpe, Solid State commun., 53, 699 (1985)
59. S. Feng, M. F. Thorpe and E. Garboczi, Phys., Rev. B31, 276 (1985)
60. H. He and M. F. Thorpe, Phys. Rev. Lett., 54, 2107 (1985)
61. B. L. Halfpap and S. M. Lindsay, Phys. Rev. Lett., 57, 847 (1986)
62. R. Ota, T. Yamate, N. Soga and M. Kunugi, J. Non-Cryst.

- Solids, 29, 67 (1978)
63. K. Murase, K. Yakushiji and T. Fukunaga, J. Non-Cryst. Solids, 59-60, 855 (1983)
 64. M. Bensoussan, Rev. Phys. Appl., 12, 753 (1977)
 65. K. S. Gilroy and W. A. Phillips, Phil. Mag., B47, 655, (1983)
 66. K.N. Madhusoodanan and J.Philip, Phys. Stat. Solidi (a), 108, 775 (1988)
 67. A. Deneuville, J. P. Keradec, P. Gerrad and A. Mini, Solid State Commun., 14, 341 (1974)
 68. K. N. Madhusoodanan, J. Philip, G. Parthasarathy, S. Asokan and E. S. R. Gopal, Phil. Mag., B58, 123 (1988)
 69. K.E. Peterson, U. Birkholz and D. Adler, Phys. Rev. B8, 1453 (1973)
 70. S. Asokan, G. Parthasarathy and E. S. R. Gopal, Phys. Rev. B35, 8269 (1987)
 71. K. N. Madhusoodanan, J. Philip, S. Asokan, G. Parthasarathy and E. S. R. Gopal, J. Non-Cryst. Solids, 109, 255 (1989)
 72. K. N. Madhusoodanan, K. Nandakumar, J. Philip, S. S. K. Titus, S. Asokan and E. S. R. Gopal, Phys. Stat. Solidi (a), 114, 525 (1989)
 73. R. Ota, N. Soga and M. Kunugi, Yogyokyokai-Shi, 81, 131 (1973)

74. K. N. Madhusoodanan and J. Philip, *Pramana- J. Phys*, **33**, 705 (1989)
75. S. S. Yun, H. Li, R. L. Cappeletti, R. N. Enzweiler and P. Boolchand, *Phys. Rev.* **B39**, 8702 (1989)
76. J. Y. Duquesne and G. Bellessa, *Europhys. Lett.*, **9**, 453 (1989)
77. A. Feltz, H. Aust and A. Blayer, *J. Non-Cryst. Solids*, **55**, 179 (1983)
78. S. Asokan, M. V. N. Prasad, G. Parathasarathy and E. S. R. Gopal, *Phys. Rev. Lett.*, **62**, 808 (1989)
79. R. A. Street, R. J. Nemanich and G. A. N. Connell, *Phys. Rev.* **B18**, 6915 (1978)
80. K. Tanaka, T. Nakagawa and A. Odajima, *Phil. Mag.*, **B54**, L3 (1986)
81. K. Tanaka, Y. Kasanuki and A. Odajima, *Thin Solid Films*, **117**, 251 (1984)
82. K. Tanaka, *Solid State Commun.*, **60**, 295 (1986)
83. K. Tanaka, *Phys. Rev.* **B39**, 1270 (1989)
84. A. Sreenivasan, Ph.D thesis, Indian Institute of Science, Bangalore, India (1991)
85. N. F. Mott, *Phil. Mag.*, **22**, 7 (1990)
86. N. F. Mott and E. A. Davis, *Electronic Processes in Non-Crystalline Materials* (Clarendon Press, 1971)

87. M. H. Cohen , H. Fritzsche and S. R. Ovshinsky, Phys. Rev. Lett., **22**, 1065 (1969)
88. E. A. Davis and N. F. Mott, Phil. Mag. **22**, 903 (1970)
89. M. H. Cohen, J. Non-Cryst. Solids, **4**, 391 (1970)
90. D. Emin, in Electronic and Structural Properties of Amorphous Semiconductors, ed: by P. G. Le Comber and J. Mort (Academic Press, London, NewYork 1973) p.261
91. M. Kastner, Phys. Rev. Lett., **28**, 355 (1972)
92. A. F . Ioffe, A. R. Regel, Prog. Semicond., **4**, 237 (1960)
93. D. Weaire , M. F. Thorpe, Phys. Rev. **B4**, 2508, 3518 (1971)
94. H. K. Rockstand and J. P De Neufville, Proc 5th Int. Conf. on Amorphous and Liquid Semiconductors in Garnisch-Partenkirchen (Taylor and Fracis ,London 1973)
95. J. Tauc , in Amorphous and Liquid Semiconductors, ed: J. Tauc, (Plenum Press 1974)
96. F. Kosek and J. Tauc , Czech. J. Phys., **B20**, 94 (1970)
97. J. Tauc , Mat. Res. Bull., **5**, 721 (1970)
98. J. D. Dow and D.Redfield, Phys. Rev. **B5**, 594 (1972)
99. R. A. Street, Solid State Commun., **24**, 363 (1977)
100. R. C. Zeller and R.O Pohl, Phys. Rev. **B4**, 2029 (1971)

101. S. Alexander, O.E. Wohlman and R. Orbach, Phys. Rev. B34, 2726 (1986)
102. W. A. Phillips (ed) Amorphous Solids: Low Temperature Properties (Springer 1981)
103. P. W. Anderson, B. I. Halperin and C. M. Varma, Phil. Mag. 25, 1 (1971)
104. S. F. Edwards, Polymer, 17, 933 (1976)
105. J. Jackle, Phil. Mag., B44, 533 (1981)
Physica B, 127, 79 (1984)
Rep. Prog. Phys., 49, 171 (1986)
106. R. G. Palmer, Adv. Phys., 31, 669 (1982)
107. N. H. Ritland, J. Am. Ceram. Soc., 37, 370 (1954)
108. M. J. O'Neill, Anal. Chem., 38, 1331 (1966)
109. W. W. Wendlandt and H. G. Hecht, Reflection Spectroscopy (Wiley, New York 1966)
110. P. A. Walks Jr. and T. Hirschfeld, Appl. Spectrosc. Rev. 1, 99 (1968)
111. G. B. Wright (ed.), Light Scattering in Solids (Springer-Verlag, Berlin, 1969)
112. A. Rosencwaig, Opt. Commun., 7, 305 (1973)
113. A. Rosencwaig, Anal. Chem., 47, 592A (1975)

114. A. Rosencwaig, *Advances in Electronic and Electron Physics*, Vol. 46, ed. L. Morton (Academic Press, New York 1978) p.207
115. A. Rosencwaig, *Photoacoustics and Photoacoustic Spectroscopy* (Wiley, New York 1980)
116. A. G. Bell, *Amer. J. Sci.*, 20, 305 (1880)
117. A. G. Bell, *Phil. Mag.*, 11, 510 (1881)
118. J. G. Parker, *Appl. Opt.*, 12, 2974 (1973)
119. A. Rosencwaig and A. Gersho, *J. Appl. Phys.*, 47, 64 (1976)
120. A. Rosencwaig and A. Gersho, *Science*, 190, 556 (1975)
121. M. J. Adams, G. F. Kirkbright and K. R. Menon, *Anal. Chem.*, 51, 508 (1979)
122. J. F. McClelland and R. N. Kniseley, *Appl. Phys. Lett.*, 28, 467 (1976)
123. G. C. Wetsel Jr. and F. A. McDonald, *Appl. Phys. Lett.*, 30, 252 (1977)
124. E. M. Monahan Jr. and A. W. Nolle, *J. Appl. Phys.*, 48, 3519 (1977)
125. H. S. Bennett and R. A. Forman, *Appl. Opt.*, 15, 2405 (1976)
126. L. C. Aamodt, J. C. Murphy and J. G. Parker, *J. Appl. Phys.*, 48, 927 (1977)

127. F. A. McDonald and Wetsel Jr., J. Appl. Phys., 49, 2313 (1978)
128. F. A. McDonald, Appl. Opt., 18, 1363 (1979)
129. A. Rosencwaig, Phys. Today, 28, 23 (1975)
130. A. Rosencwaig, Science, 181, 657 (1973)
131. A. Rosencwaig and S. S. Hall, Anal. Chem., 47, 548 (1978)
132. D. Cahen, Appl. Phys. Lett., 33, 810 (1978)
133. A. C. Tam, Appl. Phys. Lett., 37, 978 (1980)
134. W. Thielemann and H. Neumann, Phys. Stat. Solidi (a) 61, K123 (1980)
135. G. F. Kirkbright and R. M. Miller, Analyst, 107, 798 (1982)
136. A. Rosencwaig and G. Busse, Appl. Phys. Lett., 36, 725 (1980)
137. Y. H. Wong, R. L. Thomas and G. F. Hawkins, Appl. Phys. Lett., 32, 538 (1978)
138. H. K. Wickramasighe, R. L. Brag, V. Jipson, C. F. Quate and J. R. Saleeda, Appl. Phys. Lett., 33, 923 (1978)
139. K. N. Madhusoodanan, K. Nandakumar and J. Philip, J. Acoust. Soc. Ind., Vol XVIII (3&4), 28, (1990)
140. M. J. Adams and G. F. Kirkbright, Analyst, 102, 281 (1977)

141. M. A. A. Siqueira, C. C. Ghizoni, J. I. Vargas, E. A. Menezes, H. Vargas and L. C. M. Miranda, J. Appl. Phys. **51**, 1403 (1980)
142. P. Korpiun and R. Tilgner, J. Appl. Phys., **51**, 6115 (1980)
143. T. Somasundaram, P. Ganguly and C. N. R. Rao, J. Phys. C, **19**, 2137 (1986)
144. Yang Sup Song, Ho Keun Lee and Nak Sam Chung, J. Appl. Phys., **65**, 2568 (1989)
145. Yang Sup Song and Nak Sam Chung, J. Appl. Phys., **67**, 935 (1990)
146. Jorney Isaac, Jacob Philip and B. K. Chaudhury, Pramana-J. Phys., **32**, L167 (1989)

CHAPTER II

EXPERIMENTAL TECHNIQUES USED IN THE PRESENT INVESTIGATIONS

In this chapter, the details of the various experimental techniques used for the investigations of various physical properties of the chalcogenide glass samples are briefly described. The photoacoustic spectrometer, the differential scanning calorimeter and the UV-Vis-NIR spectrophotometer are the experimental tools employed for the present investigations of optical and thermal properties of the samples. The results given in the following chapters III, IV, V, VI, and VII, are based on the experimental techniques outlined in this chapter.

2.1 General considerations of a photoacoustic spectrometer

The essential parts of a PA spectrometer are (i) a radiation source of sufficient intensity in the spectral range of interest (ii) means for intensity or frequency modulation of light (iii) PA cell in which the sample is situated, which also incorporates the acoustic transducer and (iv) signal processing unit. The block diagram of a basic PA spectrometer is shown in Fig. 2.1.

2.1.1 Radiation source

Incandescent or arc lamps and lasers are two popular types of light sources currently in use for PA experiments. The lamp-monochromator combination can provide continuous tunability over a wide wavelength range from the infrared to the

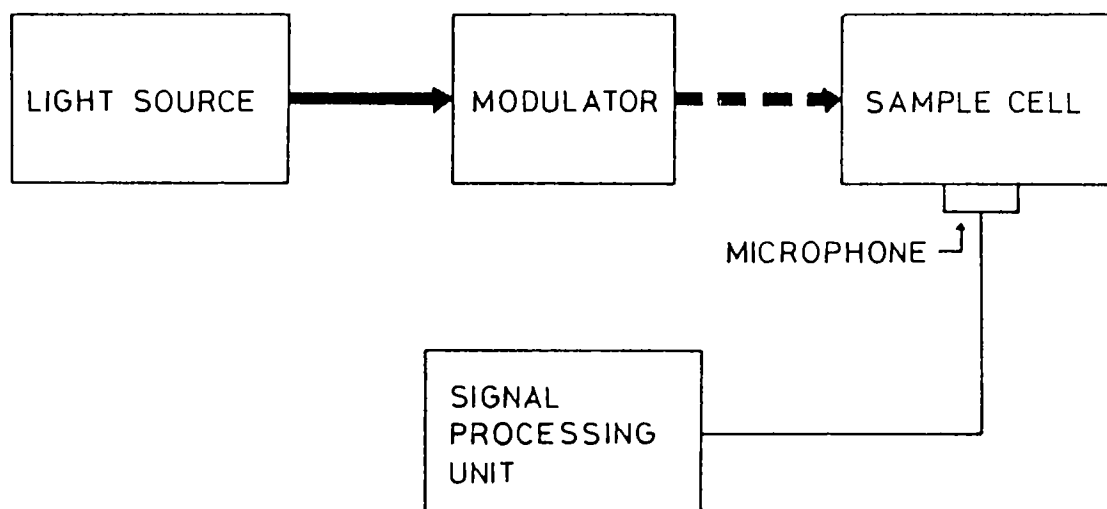


Fig.2.1 The basic experimental setup for a gas-microphone PA spectrometer.

vacuum ultraviolet. High pressure Xe arc lamps, high pressure Hg lamps, tungsten lamps, Nerst glowers etc. are the commonly used incandescent sources. A major drawback of these sources is the relatively low bandwidth-throughput product. A monochromator output power of 0.1 mW is typical for 1 nm resolution using a high pressure Xe arc lamp. Consequently, the lamp-monochromator combination is used with strongly absorbing samples or where low resolution suffices. Lasers are widely accepted light sources in PA experiments, especially for measuring weak absorption. This is mainly because of their high spectral radiance resulting from the extremely narrow line widths and high collimation. Because of spectral purity, lasers can be effectively used for high resolution PA spectroscopy experiments. One main drawback of lasers is their limited tunability.

2.1.2 Modulation

Modulation of the incident light beam is essential for the generation of PA signals. Either the amplitude or frequency of the incident beam can be modulated, amplitude modulation being the more commonly used method. Amplitude modulation can be achieved by one of the several methods such as mechanical, electrical, electro-optic etc. One of the inexpensive, efficient and common method to accomplish amplitude modulation is to use a mechanical chopper. The depth of modulation in this case is $\approx 100\%$. Care should be taken, while using mechanical chopper, to minimize the vibration noise as this may interfere with the PA signal and cannot be filtered off even by lock-in detection. In the case of electrical CW lasers, modulation can be achieved by varying the discharge tube current. Electro-optic modulation involves changing the plane of an incoming polarized light beam in a nonlinear crystal (such as KDP or ADP) by the application of a modulated electric field across the crystal. Frequency

modulation can be employed to eliminate the PA signals generated due to wavelength independent absorption at the cell windows. In dye lasers, rapid frequency change can be obtained by using an electro-optic tuner in place of a birefringent filter. Frequency modulation is well suited for narrow line width absorbers such as atomic and diatomic species.

2.1.3. The photoacoustic cell

The heart of a PA spectrometer is the PA cell in which the sample is placed and the signal is generated. Proper design of the cell is very important for the generation of PA signal of detectable amplitude. Some of the important criteria governing the design of a PA cell are outlined below.

(i) There should be good acoustic isolation of the cell from the ambient. The cell should be designed with good acoustic seals and with walls of sufficient thickness to form good acoustic barriers. Precautions to isolate the whole PA cell from building vibrations should also be taken.

(ii) In order to minimize the PA signal arising due to the absorption in cell windows and walls, windows should be as transparent as possible for the wavelength region of interest, and the interior of the cell highly reflecting. Although the cell walls will absorb some of the incident and scattered light, the resulting PA signal will be quite weak as long as the thermal mass of the walls is quite large. The cell geometry should be such that the amount of scattered light reaching the microphone diaphragm is as minimum as possible. Moreover, the interior surfaces of the cell should be free from any contamination.

(iii) Since the PA signal varies inversely with the volume of the gas inside the cell [1], the cell dimensions should be so chosen that the volume of the cell is minimum. However, care

must be taken to avoid the dissipation of acoustic signal produced appreciably, to the cell windows and walls before reaching the microphone. Also for all chopping frequencies of interest the length of the gas column l_g in the cell should be greater than the thermal diffusion length μ_g , since it is this boundary layer of gas that acts as an acoustic piston generating the signal inside the cell. Tam [2] has suggested the optimum gas column length to be $l_g \approx 1.8 \mu_g$. Another important parameter that should be considered in the design of a PA cell is the thermoviscous damping. This could be a source of signal dissipation at the cell boundaries. Thermoviscous damping coefficient varies as $\omega^{1/2}$ and becomes important at high frequencies whereas thermal diffusion length which varies as $\omega^{-1/2}$ is predominant at low frequencies. Taking into account all these effects the distance between the sample and window can be chosen to be 1-3 mm [3].

Various cell designs have appeared in literature [4,5], depending upon the nature of the investigations to be carried out. The most common cell design adopts cylindrical geometry in which the light beam is centered along the axis. Such cells can be operated either in the resonant mode or in the non-resonant mode. The pressure variations produced due to PA effect propagates radially outwards, perpendicular to the exciting beam. The hydro-dynamic equation describing the time variation of pressure at a given point in the cell have been solved for cylindrical [3,6-8] and other [9] cell geometries. The pressure distribution P within a cylinder of length L and radius R is given by [3],

$$P(r, \phi, z, t) = \text{Cos}(m\phi) \text{Cos}(k\pi z/L) J_m(\alpha_{m,n} \pi r/R) \exp(-i\omega t) \quad (2.1)$$

where J_m is the Bessel function of the first kind of order m and the eigenvalues k, m and n relate to longitudinal ($k = 1, m = n = 0$), azimuthal ($m = 1, k = n = 0$) and radial ($n = 1, k = m = 0$) acoustic modes respectively. It is found that the cell exhibits a number of acoustic resonances. The resonance frequencies are given by [3],

$$f_{res} = C_o/2 \left[(k/L)^2 + (\alpha_{m,n}/R)^2 \right]^{1/2} \quad (2.2)$$

where C_o is the sound velocity in the gas and $\alpha_{m,n}$ is the n^{th} root of the equation $dJ_m/dr|_{r=R} = 0$. Numerical values for the lowest order roots are $\alpha_{0,0} = 0$, $\alpha_{0,1} = 1.226$ and $\alpha_{1,0} = 0.589$. Cell resonances amplify the acoustic power at the resonance frequency. Geometries other than cylindrical have also been employed in PA cell design. Ioli et.al [10] directed the laser radiation transverse to a cylindrical sample cell and this configuration allows the excitation of a lower frequency longitudinal resonance, with simultaneous placement of the microphone along the axis of the PA cell for more efficient coupling of the acoustic energy onto a small diaphragm microphone.

Another geometry for PA cell makes use of the Helmholtz resonator type configuration [11-13]. In this configuration, the sample and microphone compartments having volumes V_1 and V_2 are connected by a narrow tube of length L and cross-sectional area A , and the resonance frequency is given by [3],

$$2\pi f_{res} = C_o \left[A/L V_r \right]^{1/2} \quad (2.3)$$

where

$$V_r = V_1 V_2 / (V_1 + V_2) \quad (2.4)$$

With this configuration, light scattering from the sample, sample holder and window onto the microphone, causing spurious acoustic signals due to absorption at microphone surface, may be reduced. Also by using a sufficiently long connecting tube, the sample chamber can be kept at a very high or very low temperature to perform temperature dependent PA studies, with the microphone being kept at room temperature [14,15].

The PA cell also incorporates an acoustic transducer, usually a microphone, to detect the acoustic signals generated. Both conventional condenser microphones with external biasing and electret microphones with internal self-biasing provided by a charged electret foil, are widely used to detect photoacoustic signal.

2.1.4 Signal processing

Since the PA signal is very weak, often several orders of magnitudes lower than the ambient noise, care must be taken in processing the microphone output signal. In order to maximize the signal to noise ratio, the signal from the microphone preamplifier should be processed by an amplifier tuned to the chopping frequency. The phase as well as the amplitude of the signal can be measured using a phase sensitive lock-in amplifier [16]. A lock-in amplifier is used also to eliminate noise from other sources. Using a dual phase lock-in amplifier the measurements can be made more easily particularly when both amplitude and phase vary simultaneously. When a pulsed laser is used as the excitation source a boxcar averager is used instead

of a lock in amplifier.

In spectroscopic applications one should normalize the PA spectrum with the power spectrum of the radiation source, since the PA signal is proportional to the intensity of the incident beam. The power spectrum of the source can be obtained either by using a conventional power meter or another reference PA cell with a saturable absorber like carbon black as the sample. While using a reference PA cell, part of the incident modulated beam is allowed to fall on to the reference cell using a beam splitter and the signal from the sample cell is divided by that of the reference cell using a ratiometer and the spectrum is directly recorded.

2.2 The present experimental setup

A single beam PA spectrometer has been assembled for the investigations described in this thesis, block diagram of which is shown in Fig. 2.2. The essential parts of the spectrometer are (1) a 1 KW Xe arc lamp (2) a grating monochromator (3) an electromechanical chopper (4) PA cell and (5) a lock in amplifier.

A 1KW high pressure Xenon arc lamp (M/s Spectroscopy instruments, Model SVX 1000) has been used as the light source. It has got a continuous emission from 280 nm to 2500 nm with high intensity in the visible region and some intense lines between 800 nm and 1000 nm. The power of the lamp can be varied between 600 and 1000 W. The intensity of the lamp is found to be highly stable.

To select the wavelength of the incident radiation a source monochromator (Oriel Model 7240) has been used. This monochromator can be used over a wide range of wavelengths from

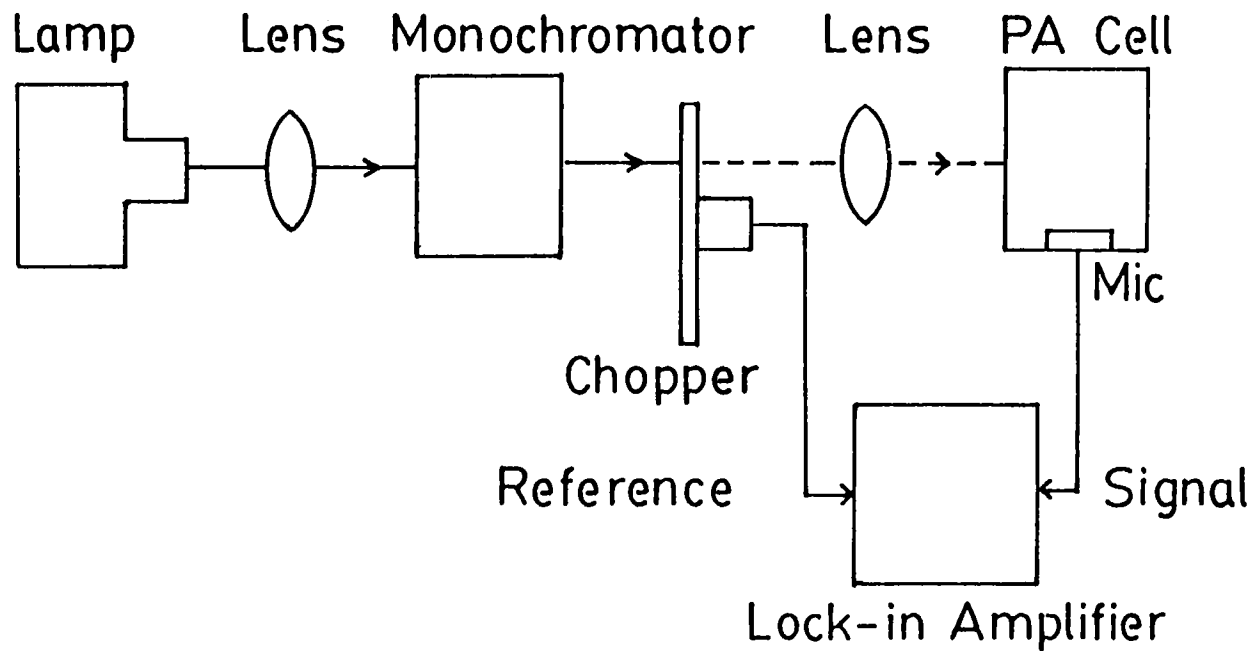


Fig.2.2 Schematic representation of the PA spectrometer.

190 nm to 240 μm with appropriate gratings. A variable slit having adjustable width from 0 to 3.2 mm is used. This allows band widths of 0.8 to 20 nm in the visible region. The wavelength can be read in nm on a three digit mechanical counter. In order to scan the wavelength automatically over the selected range a monochromator drive controller, (Oriel Model 78200) which is a bidirectional wavelength drive using a stepper motor, is used. The scan speed is adjustable and a six digit LED display shows wavelength in nm directly.

For intensity modulation of the incident light beam, a mechanical chopper (Photon Technology International, Model OC 4000) is used. With the two discs provided the chopping frequency can be continuously varied from 4 to 4000 Hz. The chopper also provides the reference signal for the lock-in amplifier.

The PA signal detected by the microphone is processed using a single-phase lock-in amplifier (Stanford Research Systems, Model SR 510). The lock-in amplifier has a full scale sensitivity of 10 nV to 500 mV and an operating frequency range 0.5 Hz to 100 KHz. Phase can be adjusted in large steps of 90° and fine steps of 0.025° . Phase shift as well as the frequency can be read on a four digit LC display. The signal amplitude can be read either on the analogue meter or on the autoranging digital display.

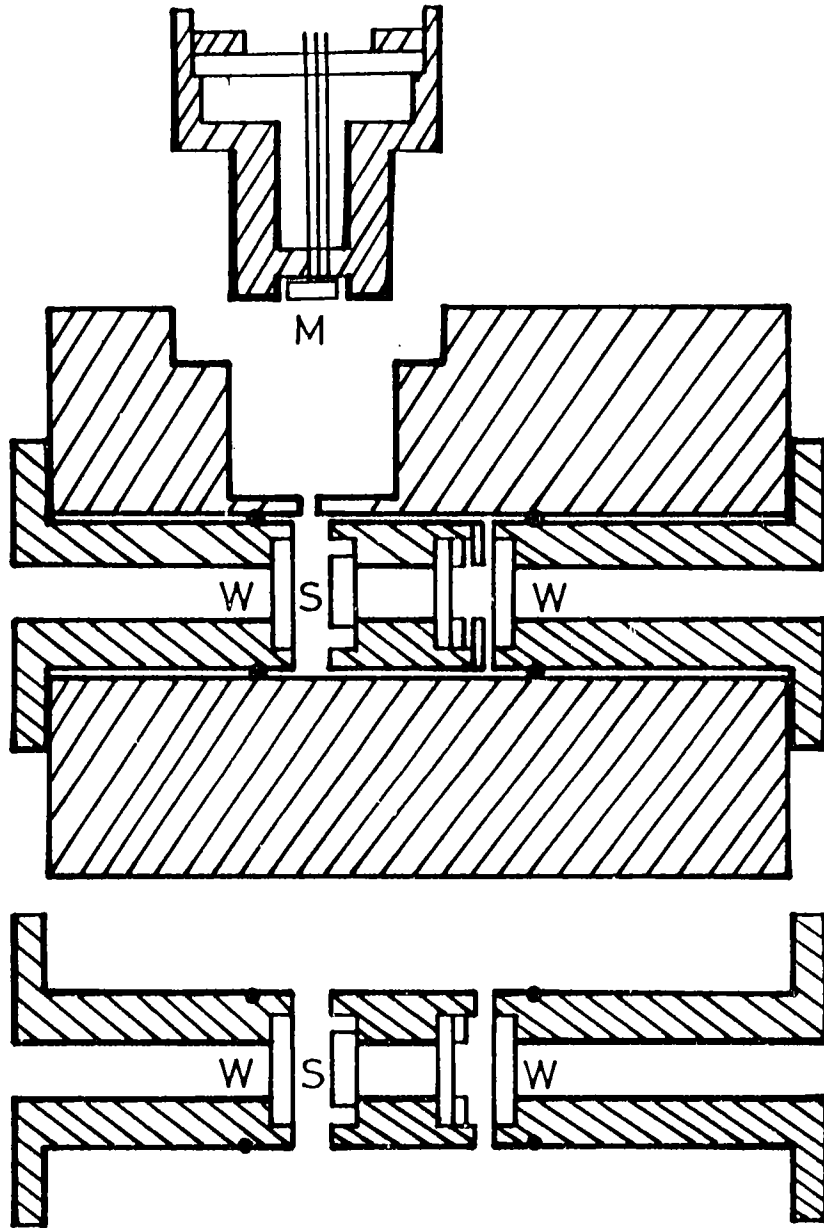
2.2.1 Description of the PA cells

The PA cell is the most important part of any PA spectrometer. Two types of PA cells, one for room temperature measurements and another for high temperature measurements have been used for the present investigations. The detailed

description of these two PA cells are given below.

The small volume non-resonant cell for room temperature measurements is made out of aluminium. The Fig. 2.3 depicts the cell with its various parts. An axial bore of diameter 2.2 cm is made in a solid aluminium rod of diameter 10 cm and length 12 cm which constitutes the cell body. The sample holder which is also made of aluminium can be just fitted into this bore. The design of the sample holder is such that different backing materials can be used for the sample. Two windows are provided, which enable to use both front and rear surface illumination of the sample. The acoustical isolation of the cell volume from outside is achieved by using 'O' rings on the window holders. The provisions provided to change the backing material and to use the rear and front surface illuminations are necessary for the investigation of thermal properties [17] of solid samples.

The PA signal is detected using a microphone kept very close to the sample compartment in a separate port. A small size, high sensitive electret microphone (Knowles, Model BT 1759) having a built-in FET preamplifier has been used for the detection of the acoustic signal. It has got a flat frequency response in the frequency range 10 to 5000 Hz. The microphone output is fed to the lock-in amplifier through a BNC connector attached to the microphone port. The minimum distance between the sample and window is 2mm. This is very much greater than the thermal diffusion length of air which is 0.06 mm at a chopping frequency of 10 Hz. The minimum volume of the sample chamber is ≈ 1 cc. The distance between the window and sample can be varied by moving the window holder. The resonance frequencies of the cell (longitudinal, radial and azimuthal) are very much above the operating frequency range of interest.



W - WINDOW

S - SAMPLE

M - MICROPHONE

Fig.2.3 Cross-sectional view of the room temperature PA cell.

The calibration of the PA cell has been carried out using carbon black as the reference sample. Modulated light beam is focused on the carbon black sample and by varying chopping frequency, the PA signal amplitude as well as the phase have been measured. The log-log plot of the PA signal amplitude versus chopping frequency for the carbon black sample is shown in Fig. 2.4. This plot clearly shows the ω^{-1} dependence of the PA signal as predicted by the RG theory [1] for optically opaque materials. The corresponding variation in phase is shown in Fig. 2.5. For a saturated PA signal the RG theory predicts the phase shift at the sample surface to be a constant, viz., $-\pi/2$ with respect to the modulated light beam. However variations from this can be attributed to the system electronics and the frequency dependence of signal propagation in the gas medium.

The high temperature PA cell employs Helmholtz resonator type configuration with which measurement can be made upto 300°C . The cross sectional view of the high temperature PA cell is shown in Fig. 2.6. It has a sample compartment and a separate microphone compartment, both connected by a stainless steel tube of inner diameter 1.6 mm and length 7 cm. The sample compartment is made of a brass rod of diameter 2cm and length 6 cm. Heating wires are wound on this rod to keep the sample at the desired temperature. One end of the rod is drilled to form a sample compartment of depth 1 cm and diameter 1 cm. A glass window is provided at the top of this compartment and this volume is sealed with a silicone 'O' ring. The volume of the sample chamber can be slightly adjusted by placing metal discs of appropriate thickness in the chamber. Also different backing materials can be used for the sample. The sample compartment is kept inside a metallic chamber of inner diameter 15 cm and wall thickness 6mm. The microphone compartment is attached to this outer chamber and acoustic sealing is achieved using an 'O'

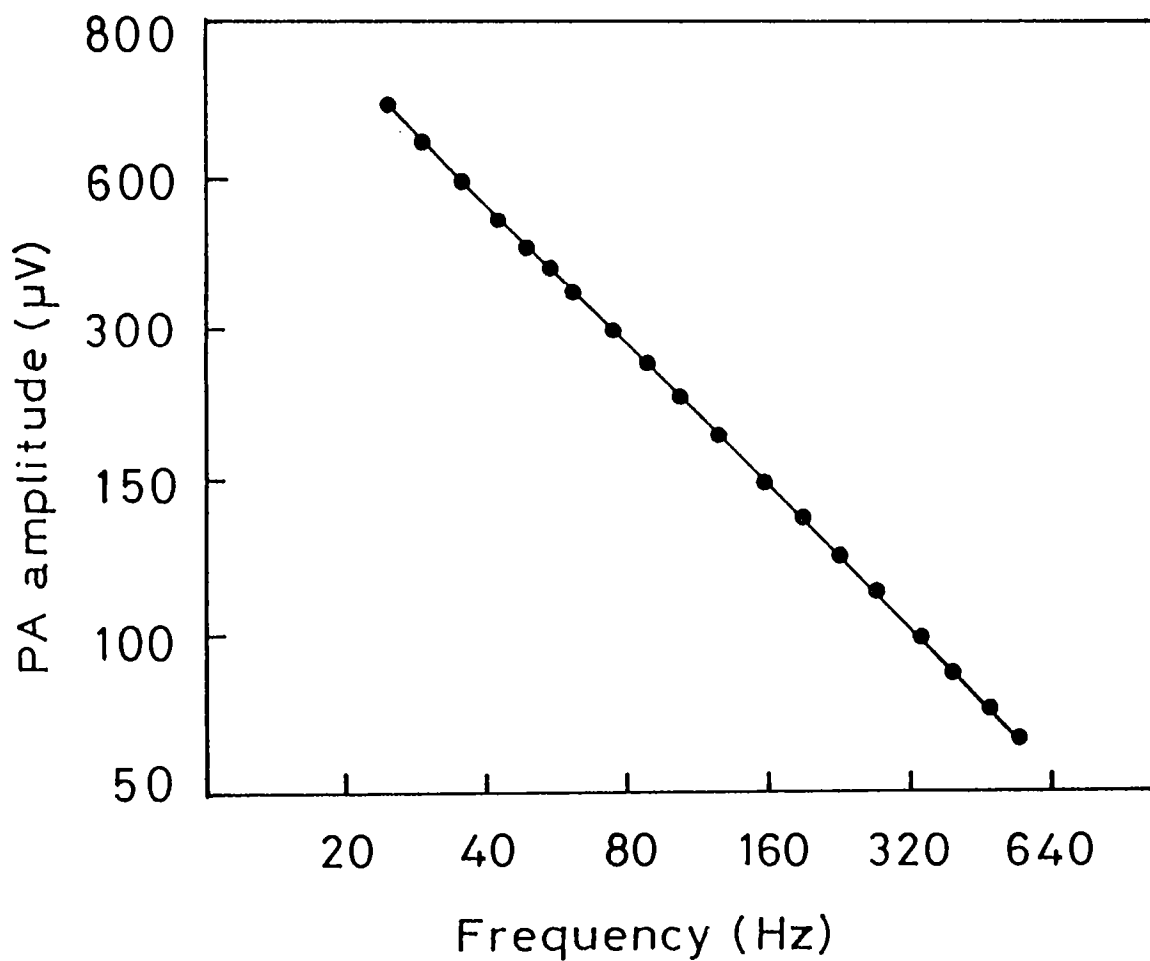


Fig.2.4 Log-log plot of the PA signal amplitude versus chopping frequency for carbon black sample.

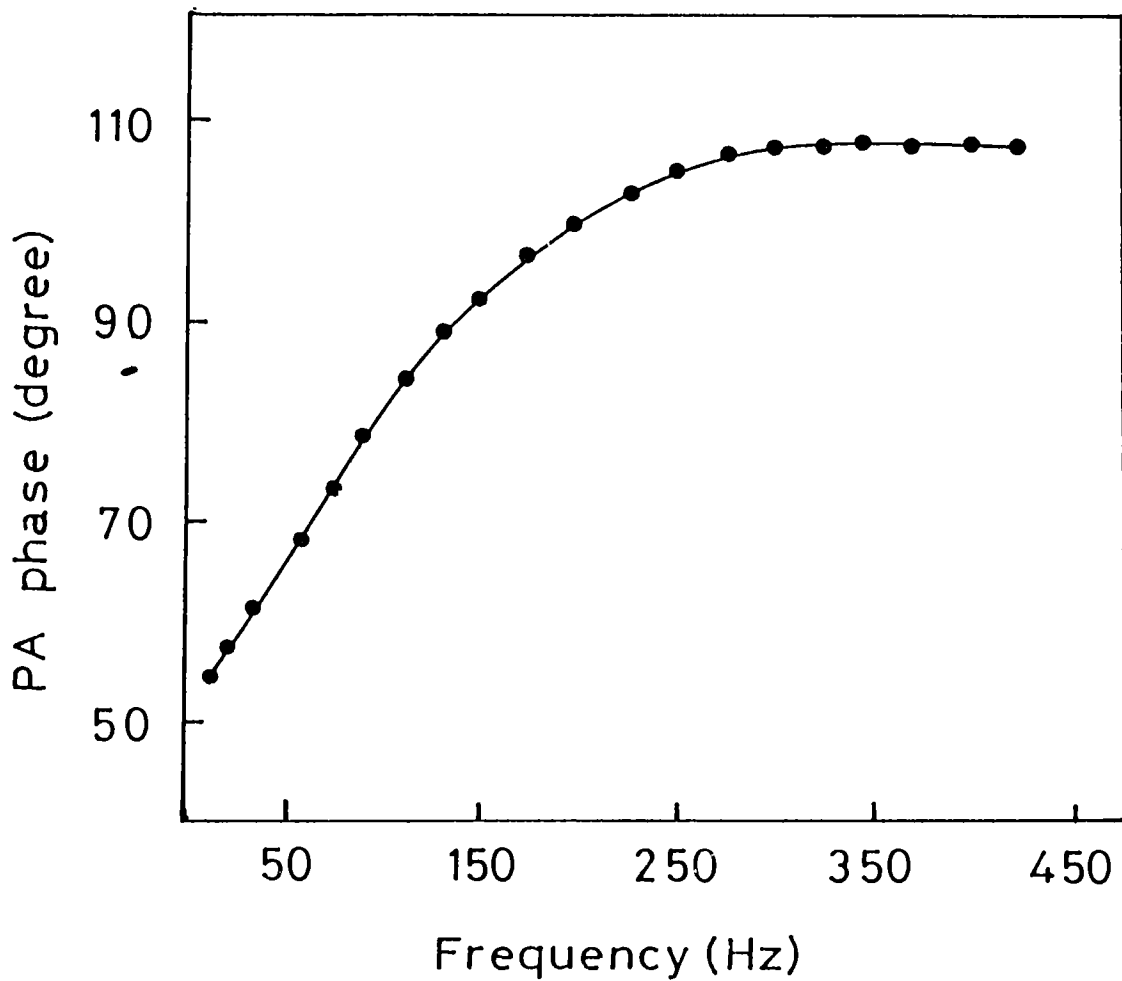
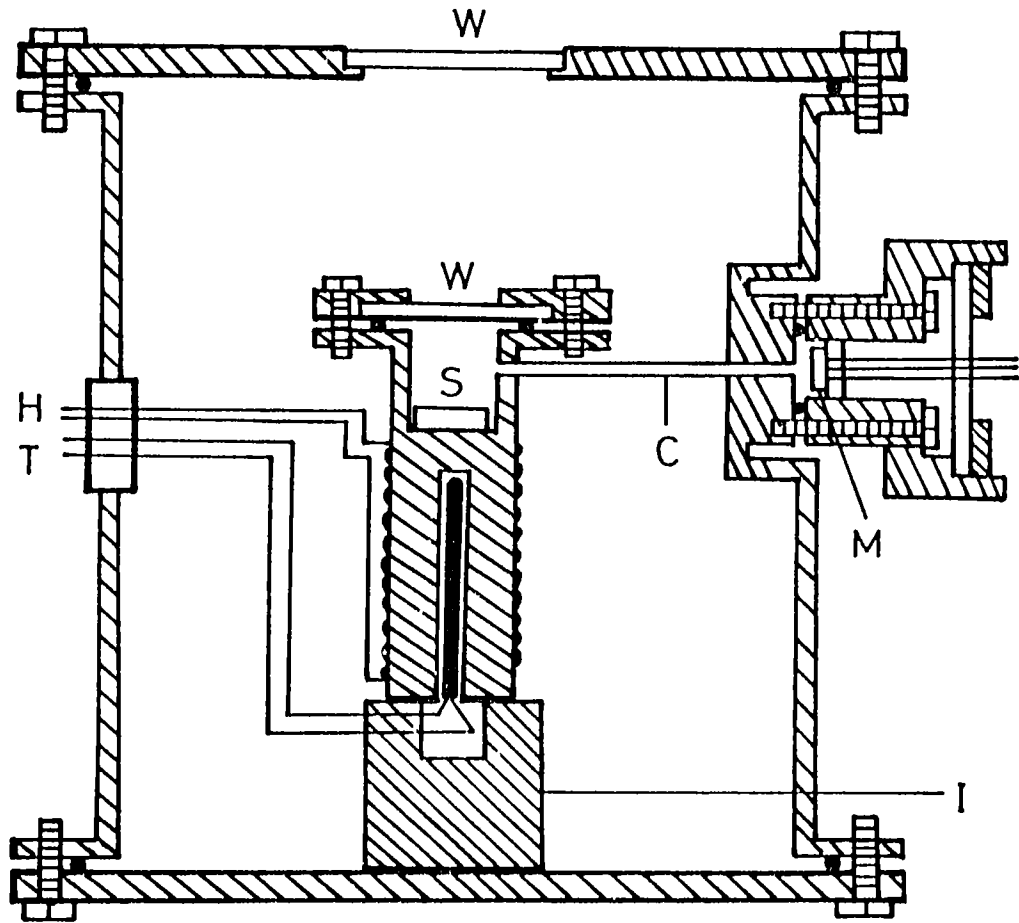


Fig.2.5 Variation of PA phase with chopping frequency for carbon black sample.



- W - WINDOW
- M - MICROPHONE
- S - SAMPLE
- I - INSULATING MATERIAL
- C - CONNECTING STEEL TUBE
- T - TEMPERATURE SENSOR
- H - HEATER

Fig.2.6 Cross-sectional view of high temperature PA cell.

ring. The acoustic signal generated in the sample compartment reaches the microphone compartment through a stainless steel connecting tube and the microphone can always be kept at room temperature. The outer chamber is suitably insulated from the sample compartment. The sample temperature is measured using a platinum resistor placed very close to the sample. The electrical connections are taken through the walls of the outer chamber with proper insulation. The temperature sensor and the heating element can be connected to a temperature controller.

The calibration of this cell has also been done using carbon black sample. Fig. 2.7 shows the variation of the PA signal amplitude with chopping frequency for carbon black sample at two different temperatures. The corresponding variation in phase is shown by Fig. 2.8. The temperature dependent variations of the PA signal amplitude and phase for two different frequencies are shown in Fig. 2.9 and Fig. 2.10 respectively. As the temperature is increased the PA signal amplitude decreases and the phase shift increases. This is mainly due to the temperature dependence of the sample parameters and sound attenuation in the transmitting gas column.

The PA spectrometer, consisting of the modules described above, has been set up on a sturdy table which helps to isolate building vibrations to a large extent. The performance of the PA spectrometer is found to be very good.

2.3 Differential scanning calorimetry

Differential Scanning calorimetry (DSC) is a dynamic thermal analysis technique, with which the thermal behaviour of any sample can be studied over a wide temperature range, under nonisothermal conditions. Whenever a material undergoes a change

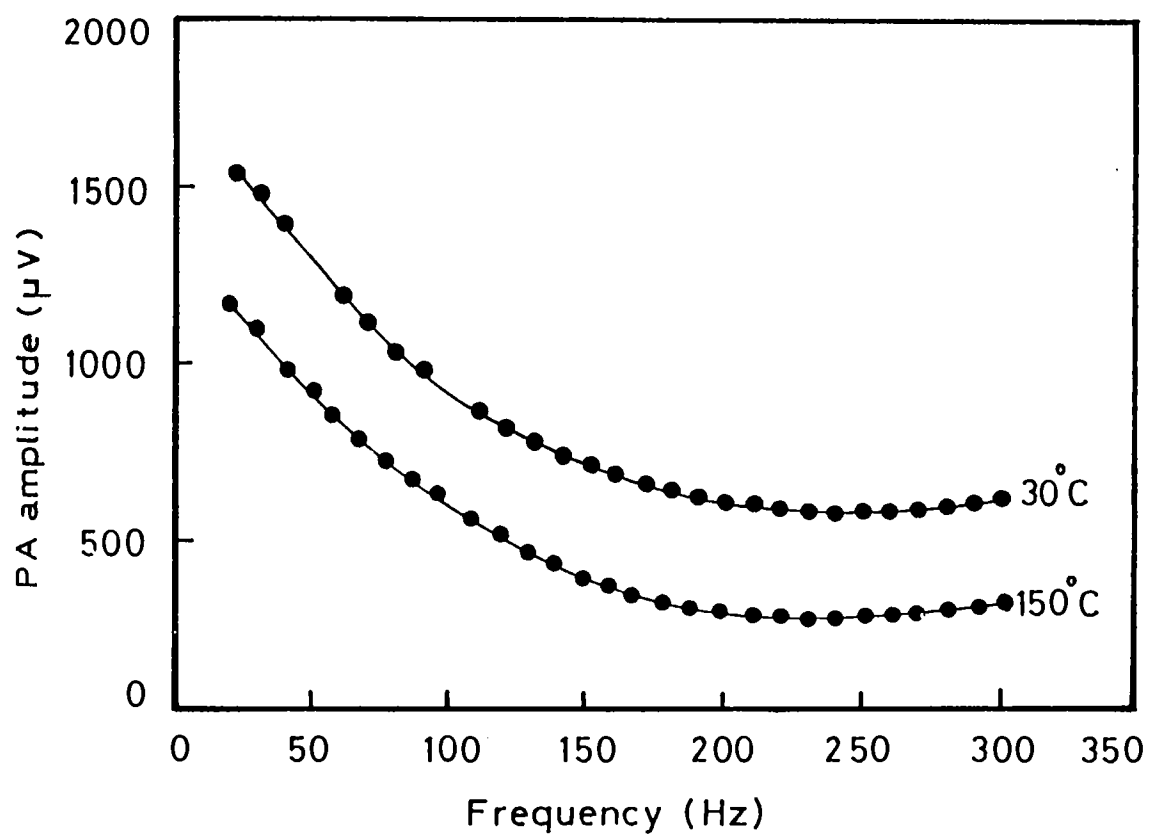


Fig.2.7 Variation of PA signal amplitude with chopping frequency for carbon black sample measured using high temperature PA cell.

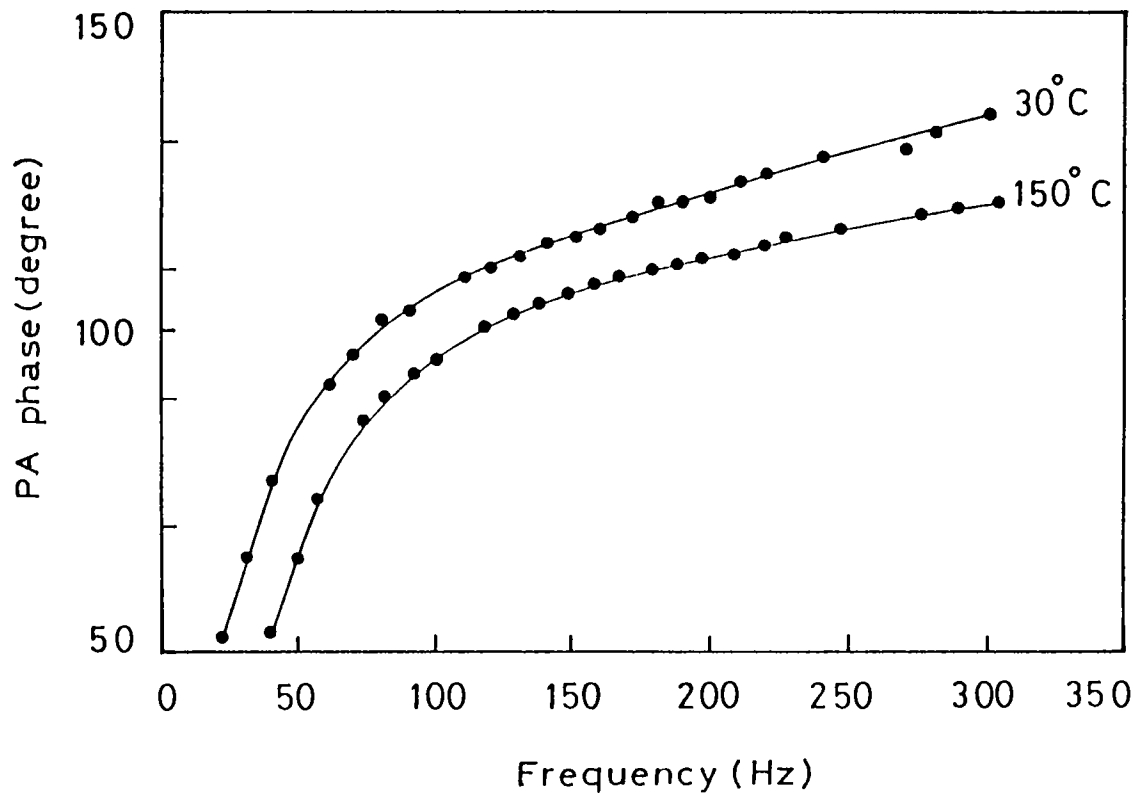


Fig.2.8 Variation of PA phase with chopping frequency for carbon black sample measured using high temperature PA cell.

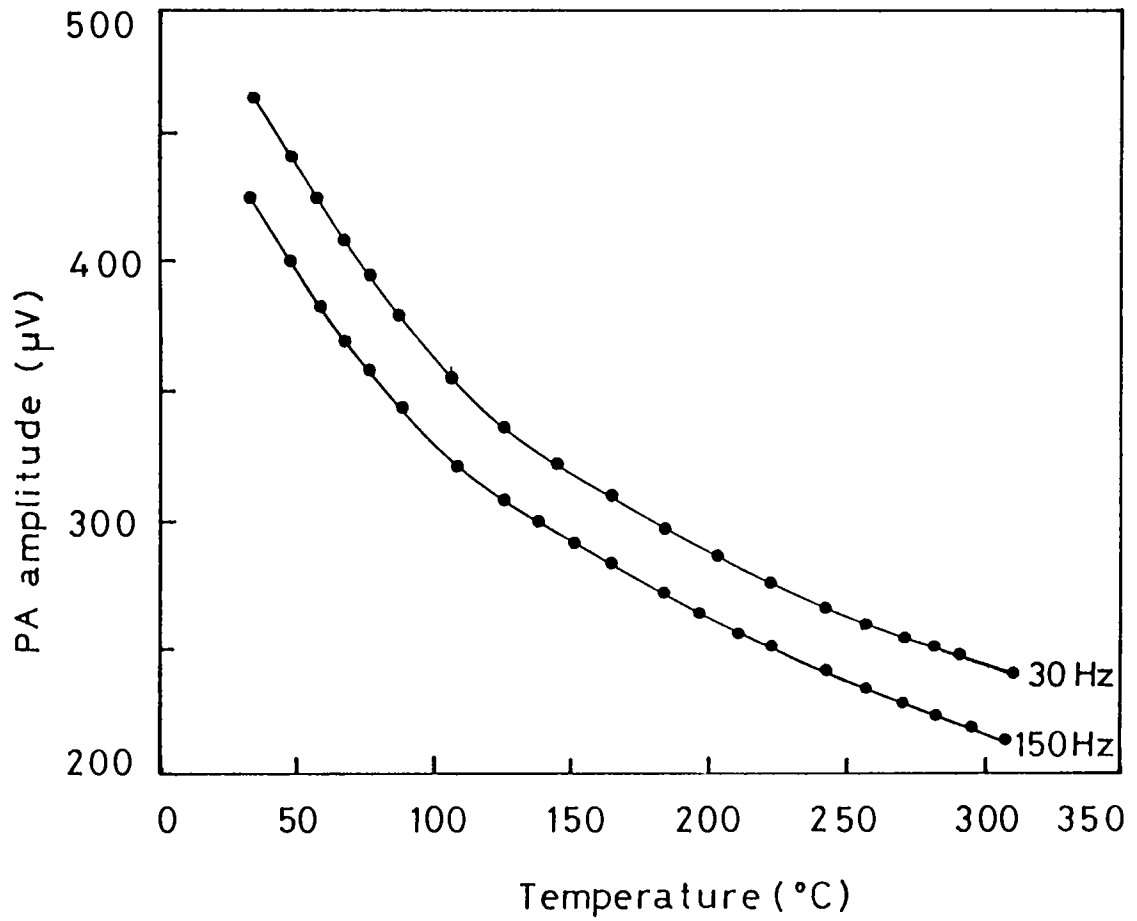


Fig.2.9 Variation of PA signal amplitude with temperature for carbon black sample.

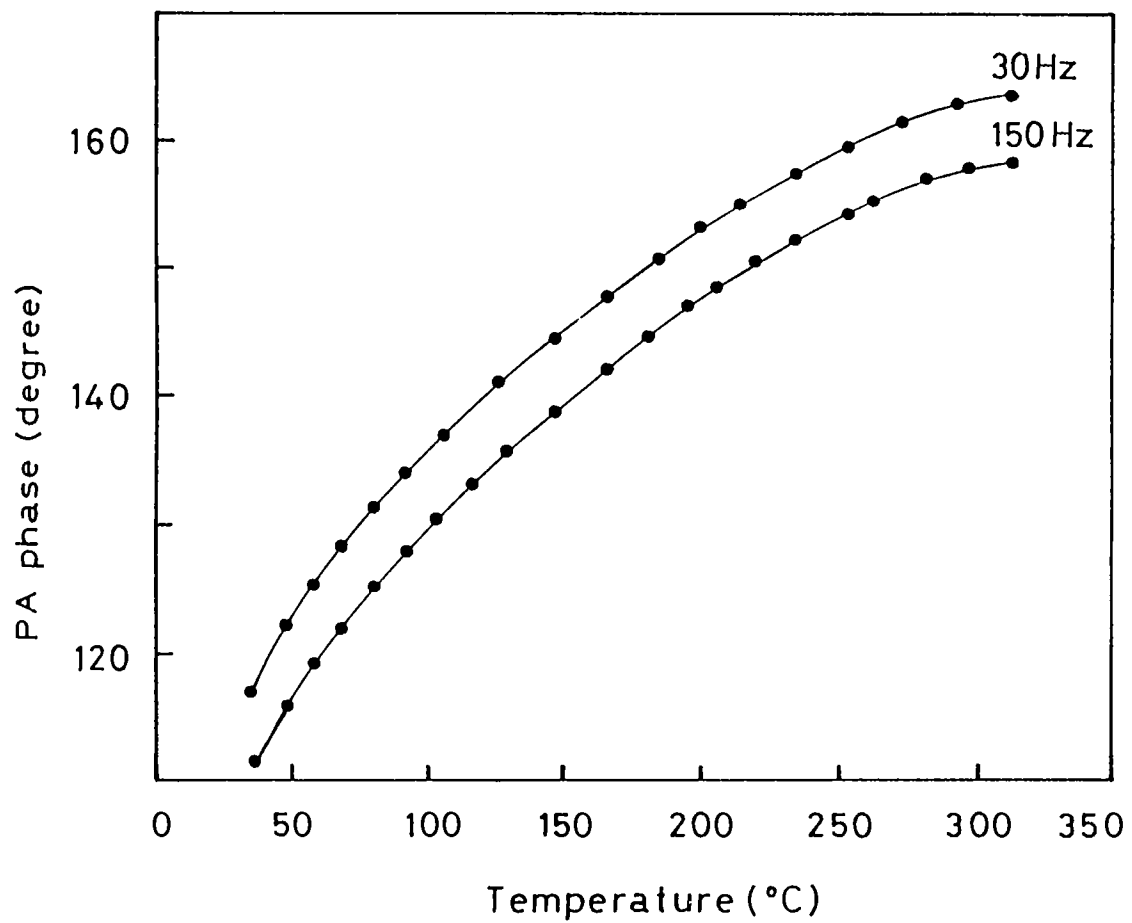


Fig.2.10 Variation of PA phase with temperature for carbon black sample.

in its physical state such as melting or transition from one crystalline form to another or whenever it reacts chemically, heat is either absorbed or liberated. Many such processes can be initiated simply by raising the temperature of the material. In DSC, the enthalpies of these processes are determined by measuring the differential heat flow required to maintain a sample material and an inert reference at the same temperature. This temperature is usually programmed to scan a temperature range by increasing linearly at a predetermined rate. Thermal changes in a sample are due to exothermic or endothermic enthalpic transitions or reactions. Such enthalpic changes can be caused by phase changes, fusion, crystalline inversions, boiling, sublimation, vapourisation, oxidation, reduction or other chemical reactions. Generally, phase transitions, dehydration, reduction and some decomposition reactions are endothermic in nature, whereas crystallisation, oxidation and some decomposition reactions are exothermic. The phenomenon of glass transition exhibits itself in a DSC curve as an endothermic baseline shift. Although DSC yields data which are inherently more qualitative and more amenable to theoretical interpretation than the differential thermal analysis (DTA) data, it does not seem to have been used as widely as the latter. The DSC technique has been applied, however, to diverse types of compounds and reviews on the application of DSC to petroleum products, plastics, biological systems and metal complexes etc. have appeared [18-21] in literature. Barrall and Johnson [22] have reviewed the subject in some detail, particularly on aspects relevant to polymer materials. Wendlandt [23] has surveyed the commercially available instruments for both DSC and DTA, and also reviewed thermal methods of analysis from an analytical view point [24]. Some of the trends in the general field of thermal analysis has been analyzed by Redfern [25].

The relative advantages of the DSC over conventional calorimetric technique are [26] (i) rapidity in the determination of thermal properties over a wide temperature range (ii) small amounts of sample required for measurements (iii) easy data analysis procedure and (iv) ability to study many different types of reactions. The main disadvantages of this technique are (i) relatively low accuracy and precision (5-10% accuracy), (ii) inability to conveniently determine the ΔH of overlapping reactions and (iii) inaccuracy in the determination of peak areas due to baseline changes during the transition or reaction.

We have used the DSC-7 Differential scanning calorimeter (Perkin-Elmer) to study the glass transition temperature and specific heat of the samples. With the 3700 Data Station, the modular DSC-7 permits direct calorimetric measurement, characterization, and analysis of thermal properties of materials. Under the control of the computer, the DSC-7 is programmed from an initial to a final temperature through transitions in the sample material (such as glass transition, melting, crystallization). Usually, the DSC-7 is programmed to scan a temperature range by changing at a linear rate over a temperature ramp for the study of the endothermic and exothermic reactions. With the liquid nitrogen attachment the temperature can be varied from ≈ 77 K to 1000 K. Before any quantitative measurements are made the calorimeter must be calibrated to obtain a calibration constant in units of $\text{mcal}(\text{unit area})^{-1}$ and fix the temperature scale accurately. Correct sampling techniques must also be used. High purity metals with accurately known enthalpies of fusion are generally used as calibration standards. The most commonly used calibrants are Indium and Zinc, which can be used to calibrate the instrument over a wide temperature range.

A typical DSC curve of a glassy sample is shown in Fig. 2.11. The characteristic feature of the glass, viz., the glass transition temperature shows up as an endothermic baseline shift designated as T_g in the DSC curve. An unstable glass generally shows one or more exothermic crystallisation (T_c) peak(s) and the melting T_m as an endothermic peak. This is the general behaviour expected from a glass and ofcourse there are exceptions to this. Certain glasses are thermally very stable and may not show any sharp crystalline exotherms. In such glasses, the amorphous structure may be so complex that easy segregation of crystalline phases may not be possible. On the other hand, certain glasses that are very unstable and may show multiple crystallisation. The T_g values reported in this thesis correspond to the on set of the glass transition. This value is estimated as the temperature corresponding to the intercept of the tangent drawn to the baseline and the endothermic baseline shift as shown in Fig. 2.11.

Differential scanning calorimetry can also be used to measure the specific heat C_p of materials. When a sample material is subjected to a linear temperature increase, the rate of heat flow into the sample is proportional to the instantaneous specific heat. By measuring this rate of heat flow as a function of temperature and comparing it with a standard material under the same conditions, one can obtain the specific heat C_p as a function of temperature [27,28].

The procedure is briefly described as follows. Empty aluminium pans are placed in the sample and reference holders. An isothermal base line is recorded at the lower temperature and the temperature is then programmed to increase over a range. An isothermal baseline is then recorded at the higher temperature as indicated in the lower part of Fig. 2.12. The two isothermal

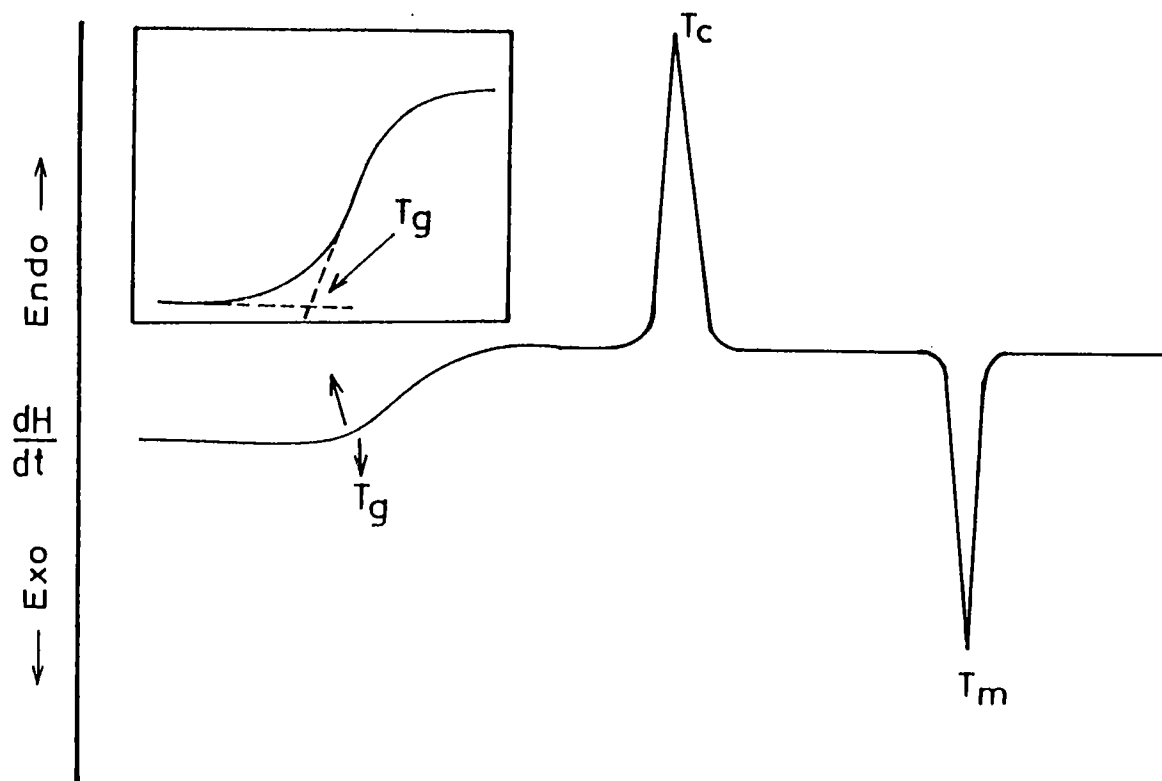


Fig.2.11 Typical DSC curve of a glassy sample showing the procedure by which the various reaction temperatures are measured.

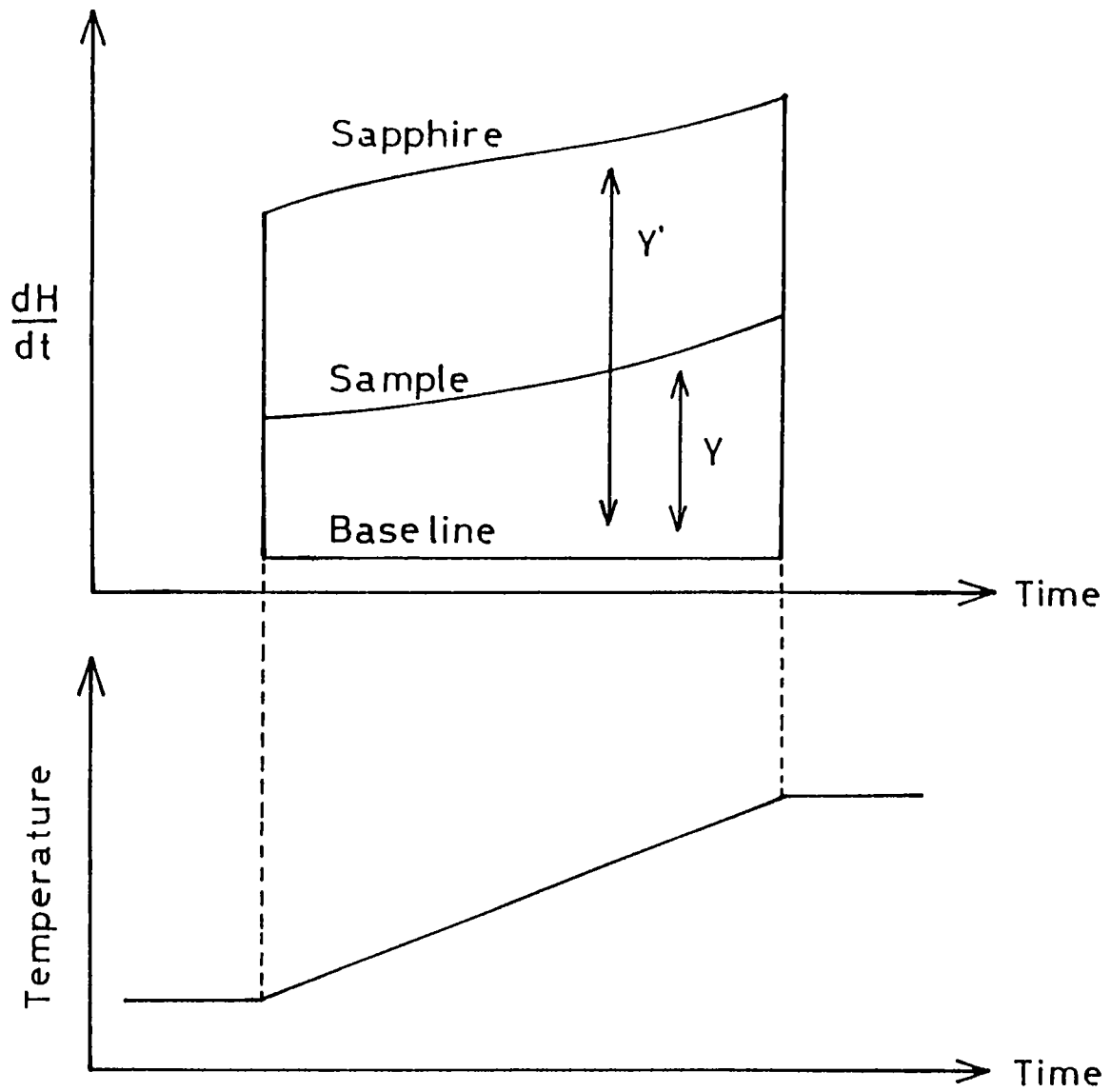


Fig.2.12 Specific heat determination by ratio method.

baselines are used to interpolate a baseline over the scanning section as shown in the upper part of Fig. 2.12. The procedure is repeated with known mass of sample in the sample pan and a trace of dH/dt against time is recorded. There is a pen displacement due to the absorption of heat by the sample, then

$$dH/dt = m C_p dT_p/dt \quad (2.5)$$

where m is the mass of the sample in grams, C_p is the specific heat in $\text{cal g}^{-1} \text{K}^{-1}$ and dT_p/dt is the programmed rate of temperature increase.

This equation could be used to obtain values of C_p directly, but any errors in ordinate read-out dH/dt , and in programming rate dT_p/dt , would reduce the accuracy. To minimize these errors the procedure is repeated with a known mass of sapphire, the specific heat of which is well established [29] and a new trace is recorded. Thus at any temperature T ,

$$K y = m C_p dT/dt \quad (2.6)$$

$$K y' = m' C_p' dT/dt \quad (2.7)$$

where y and y' are the ordinate deflections due to the sample and the standard respectively, m' and C_p' are the mass and specific heat of the standard, and K is the calibration factor in $\text{cal cm}^{-1} \text{sec}^{-1}$.

Dividing equation (2.6) by equation (2.7) and rearranging terms

$$C_p/C_p' = m' y / m y' \quad (2.8)$$

Thus the calculation requires only the comparison of two ordinate deflections at the same temperature.

2.4 UV-Vis-NIR Spectrophotometer

Apart from photoacoustic (PA) spectroscopy, UV-Vis-NIR Spectrophotometry has also been employed to measure the optical band gap E_g of the samples for comparison. Hitachi Model U-3410 Recording spectrophotometer has been employed for this purpose. The model U-3410 comprises a monochromator section (including control section), display section, floppy disk section, graphics plotter and operating section. The system is equipped with various functions which can be used in combination with the variety of optional accessories in all types of analytical fields and is especially suited for material characterization. This unit has a wavelength range 187 to 2600 nm with 0.07 nm resolution. The wavelength accuracy is 0.2 nm in the UV-Vis range and +/-1nm in the NIR range. The monochromator adopts the model 340 prism/ grating double monochromatic system. The lenses used in the conventional monochromator have all been replaced with mirrors to eliminate image deviation due to chromatic aberration. The PbS detector converges the light beam with a toroidal mirror located below the photomultiplier. This permits placing the PbS symmetrically against the sample and reference beams whereby the two beams are completely balanced. A mechanical chopper is placed before the first monochromator to chop the light beam, which minimizes deviation in zero signal. The long life, easily replaceable iodine free tungsten lamp is used as the visible wavelength light source. The photometric output from the detector is fed through the preamplifier to an A/D convertor and input into the computer where it is discriminated into reference signal, sample signal and zero

signal for storage by gate signals obtained in synchronization with rotation of the sector mirror for splitting the light beam. The reference signal is compared with a predetermined standard value and used for controlling the voltage applied to the dynode of the photomultiplier.

REFERENCES

1. A. Rosencwaig and A. Gersho, J Appl. Phys, **47**, 64 (1976)
2. A. C. Tam, in Ultrasensitive Laser Spectroscopy, ed: Klinger (Academic Press, New York, 1983) p.1
3. A. Rosencwaig, Photoacoustics and Photoacoustic spectroscopy (Wiley, New York, 1980)
4. L. G. Rosengren, Appl. Opt., **14**, 1960 (1975)
5. C. F. Dewey, in Optoacoustic Spectroscopy and Detection, ed: Y. H. Pao (Academic Press, New York, 1977) p.47
6. P. M. Morse, Vibration and Sound (McGraw-Hill, New York, 1948)
7. L. A. Farrow and R. E. Richton, J. Appl. Phys., **48**, 4962 (1977)
8. C. F. Dewey Jr., R. D. Kamm and C. E. Hackett, Appl. Phys, Lett., **23**, 633 (1973)
9. E. Kritchman, S. S. Shtrikman and M. Statkine, J. Opt. Soc. Amer., **68**, 1257 (1978)
10. N. Ioli, P. Violino and M. Meucci, J Phys. E, **12**, 168 (1979)
11. N. C. Fernelius and T. W. Hass, Appl Opt., **17**, 3348 (1978)
12. N. C. Fernelius, Appl. Opt., **18**, 1784 (1979)

13. R. S. Quimby, P. M. Selzer and W. M. Yen, *Appl. Opt.*, **16**, 2630 (1977)
14. J. C. Murphy and L. C. Aamodt, *J. Appl. Phys.*, **48**, 3502 (1977)
15. P. A. Bechthold, M. Campagna and J. Chatzipetros, *Opt. Commun.*, **36**, 369 (1981)
16. M. L. Meade, *Lock-in Amplifier: Principles and Applications* (Peter Peregrinus Ltd., London, 1983)
17. K. N. Madhusoodanan, M. R. Thomas and J. Philip, *J. Appl. Phys.*, **62**, 1162 (1987)
18. F. Pochetti, *Riv. Combust.*, **25**, 461 (1971)
19. V. Era and A. Savolainen, *Suom. Kemi.*, A **44**, 50 (1971)
20. J. M. Steim, *Instrument News*, Vol 19, 12 (Norwalk, Conn: Perkin-Elmer Corporation, 1968)
21. C. T. Mortimer, *Calorimetry in Chemical and Biological Systems*, **9** (London: LKB Producer AB, 1969)
22. Barrall EM II and J. F. Johnson, *Tech. Methods. Polymer Eval.*, **2**, 1 (1970)
23. W. W. Wendlandt, *J. Chem. Educ.*, **49**, A671, A674, A676 (1972)
24. W. W. Wendlandt, *MTP International Review of Science, Physical Chemistry series I*, **13**, 177, ed: T. S. West (London: Butterworths, 1973)

25. J. P. Redfern, *Pure Appl. Chem.*, **25**, 849 (1971)
26. W. M. Wendlandt, *Thermal Analysis* (John Wiley & Sons, 1964)
27. M. J. O'Neill, *Anal. Chem.*, **38**, 1331 (1966)
28. *Thermal Analysis Newsletter*, No.3 (Norwalk, Conn: Perkin-Elmer Corporation)
29. D. C. Ginnings and G. T. Furukawa, *J Amer. Chem Soc.*, **75**, 522 (1953).

CHAPTER III

ENERGY GAP STUDIES ON As-Sb-Se GLASSES

537, 229.2: 539.213: 537-321

3.1 Introduction

NAY



Since the announcement of the discovery of reversible switching phenomena in certain types of chalcogenide glasses [1], much effort has been devoted towards characterization, improvement, and understanding of the properties of these materials [2]. This interest has been stimulated both by the basic scientific questions that remain to be answered in order to understand the structures and properties of these alloys and by their obvious potential use as reversible threshold and memory switching elements in a wide variety of electronic devices [2,3]. One advantage of these materials is that they can be prepared over a very wide composition range. Since the physical properties do change with composition, it enables composition dependent tunability of various physical properties. So an understanding of the composition dependence of their physical properties is necessary to select the proper composition for the desired technological applications.

A good understanding of the gap states in disordered systems is of particular interest because they govern the electron transport in these materials. Glassy chalcogenide semiconductors have great varieties of band gaps. Several correlations of glass transition temperature and band gaps have been proposed [4,5]. Although they are not very successful when extended beyond a single narrow family of materials, they do provide an idea how to produce materials with the desired band gap.

Among the glass forming alloys of the group

$A_x^V B_{100-x}^{VI}$, where A is a group V element such as As, Sb, Bi etc. and B is a group VI element such as S, Se and Te etc., the $As_x Se_{100-x}$ family is probably the most studied one [6-9]. But there are not many investigations on the effect of replacing As in the As-Se system by other elements. Addition of Sb to certain extent to the As-Se system could form good ternary glasses. The glass forming region in the ternary As-Sb-Se system is illustrated in Fig. 3.1, in accordance with the data obtained for alloys quenched in air. Results of the measurement of electrical conductivity, density, elastic constant, thermal expansion coefficient and calorimetric studies of several glasses of the As-Sb-Se system have been reported earlier [11-14].

We have carried out a systematic investigation of the composition dependence of the optical band gap E_g in bulk As-Sb-Se glasses using PA technique. As already discussed in chapter I, the PA technique has proved to be a very effective method for the study of both crystalline and amorphous semiconductors [15-19]. The advantage of PA technique over conventional spectroscopic technique makes it convenient for the study of glassy semiconductors. The energy gap measurements carried out at room temperature on As-Sb-Se glasses are described in this chapter. Such investigations will greatly help in selecting materials of the desired energy gap and optical absorption properties for special technological applications.

3.2 Experimental details

Materials on which measurements have been made can generally be represented as $As_x Sb_y Se_{100-x-y}$ and classified into four groups depending on the Sb content as $As_x Sb_5 Se_{95-x}$ ($x = 25, 30, 35, 40$ and 45), $As_x Sb_{10} Se_{90-x}$ ($x = 20, 25, 30, 35$ and 40), $As_x Sb_{15} Se_{85-x}$ ($x = 15, 20, 25, 30$ and 35) and $As_x Sb_{20} Se_{80-x}$ (x

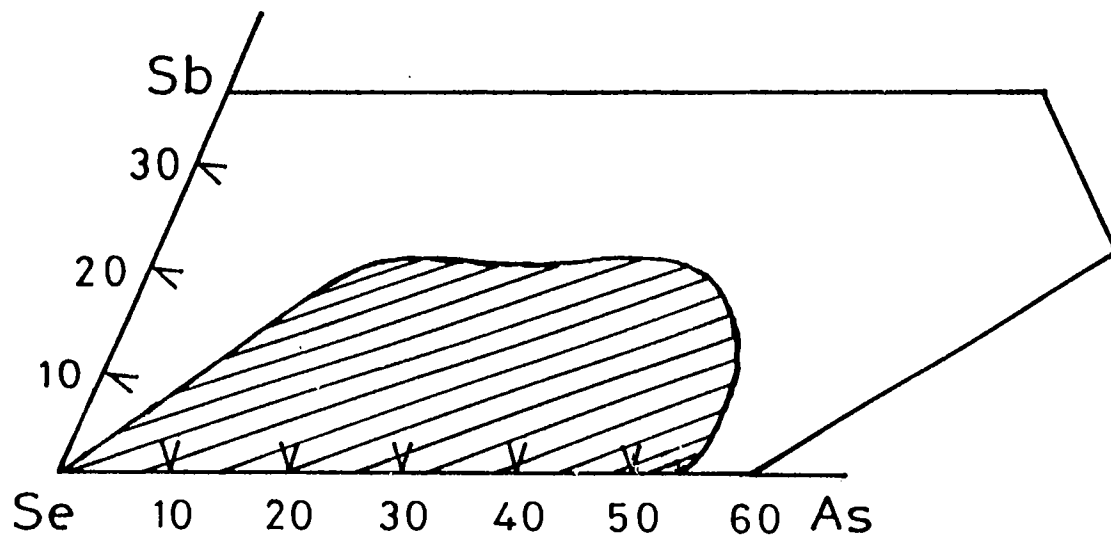


Fig.3.1 Glass forming regions of As-Sb-Se system.

= 10, 15, 20, 25 and 30). In each group, the compositions $(\text{As,Sb})_{40}\text{Se}_{60}$ fall along the pseudobinary section $\text{As}_2\text{Se}_9\text{-Sb}_2\text{Se}_9$ and represent the so-called 'stoichiometric' compositions of the As-Sb-Se system. With this stoichiometric compositions as the reference sample, glasses with more than 60 at. % of Se are referred to as Se-rich glasses, while those with less than 60 at. % of Se are referred to as the As-rich glasses.

3.2.1 Sample preparation

Bulk glasses of the compositions mentioned above have been prepared by the conventional melt-quenching technique. Appropriate proportions of spectroscopically pure (99.999%) constituent elements are taken in previously evacuated quartz ampoules and sealed. Each ampoule is then kept in a rotary furnace at about 850°C for 24 hours. For homogeneous mixing of the melt, the ampoule is rotated periodically and quenched in ice water to obtain the glass samples. The quenching rate is about 200°C s^{-1} . The amorphous nature of the samples has been checked by X-ray diffractometry. Powdered samples have been used for recording the PA spectra to measure the optical band gap.

3.2.2 Photoacoustic measurements

The PA spectrometer already described in chapter II has been used for the present investigations. For recording the PA spectrum of each sample, the PA signal amplitude as a function of the wavelength of the exciting radiation is measured at a fixed chopping frequency using the room temperature PA cell. The chopping frequency used is 22 Hz. The power spectrum of the light source has initially been recorded as the variation of the PA signal amplitude for a carbon black sample as a function of wavelength at the same chopping frequency. The

normalized PA signal is then obtained by dividing the PA signal amplitude of the sample by that of the carbon black sample, which is the reference, at corresponding wavelengths. The PA spectrum of the sample is then obtained by plotting the normalized PA signal Vs wavelength of the incident radiation.

3.3 Photoacoustic spectra of As-Sb-Se glasses

The normalized PA spectra recorded for the four groups of samples of the As-Sb-Se family are shown in Fig. 3.2 to 3.5. Since the PA signal amplitude is directly proportional to the optical absorption coefficient [20], these spectra provide information about the features of optical absorption in the samples. The normalized PA signal increases as the photon energy is increased and reaches a saturation level for photon energy $h\nu > E_o$, where E_o is the optical energy gap. A slight decrease in the normalized PA signal in the saturated region could be attributed to the increased reflection of the incident beam from the sample surface [21]. As described by Tauc [22], for an amorphous semiconductor there are three different regions in the optical absorption curve corresponding to three different ranges of the optical absorption coefficient β . The saturated region of the normalized PA signal is characterized by a very high value for the absorption coefficient ($\beta \geq 10^4 \text{ cm}^{-1}$). R-G theory [23] predicts this type of behaviour for highly absorbing samples with $l_\beta < l_s$ and $\mu_s > l_\beta$. In this region the absorption coefficient β has an energy dependence given by

$$h\nu\beta(h\nu) = B (h\nu - E_o)^2 \quad (3.1)$$

where B is a constant [23].

The absorption edge in amorphous semiconductors has an

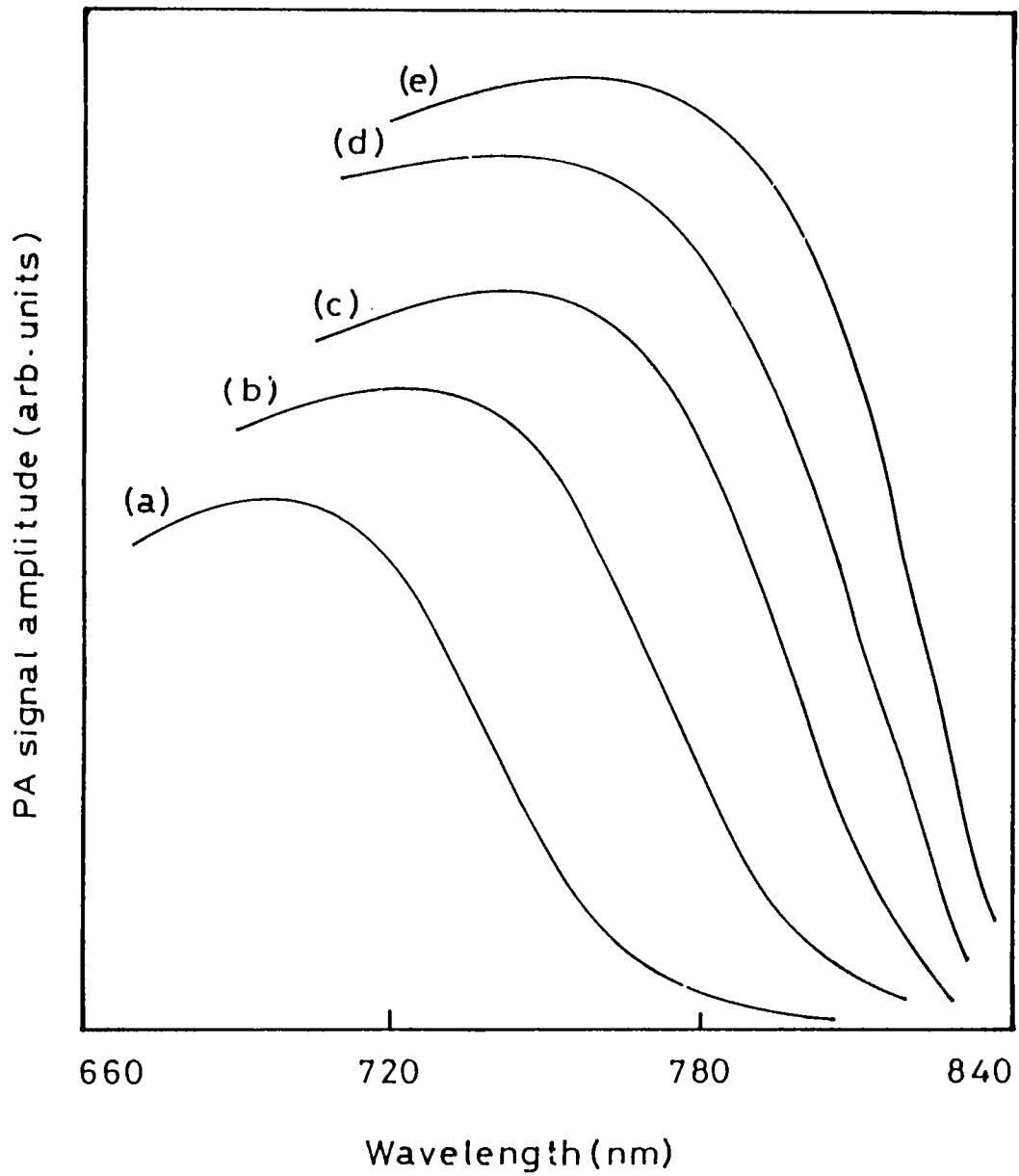


Fig.3.2 PA spectra of $As_xSb_5Se_{90-x}$ glasses.
 (a) $As_{25}Sb_5Se_{70}$, (b) $As_{30}Sb_5Se_{65}$,
 (c) $As_{35}Sb_5Se_{60}$, (d) $As_{40}Sb_5Se_{55}$ and
 (e) $As_{45}Sb_5Se_{50}$

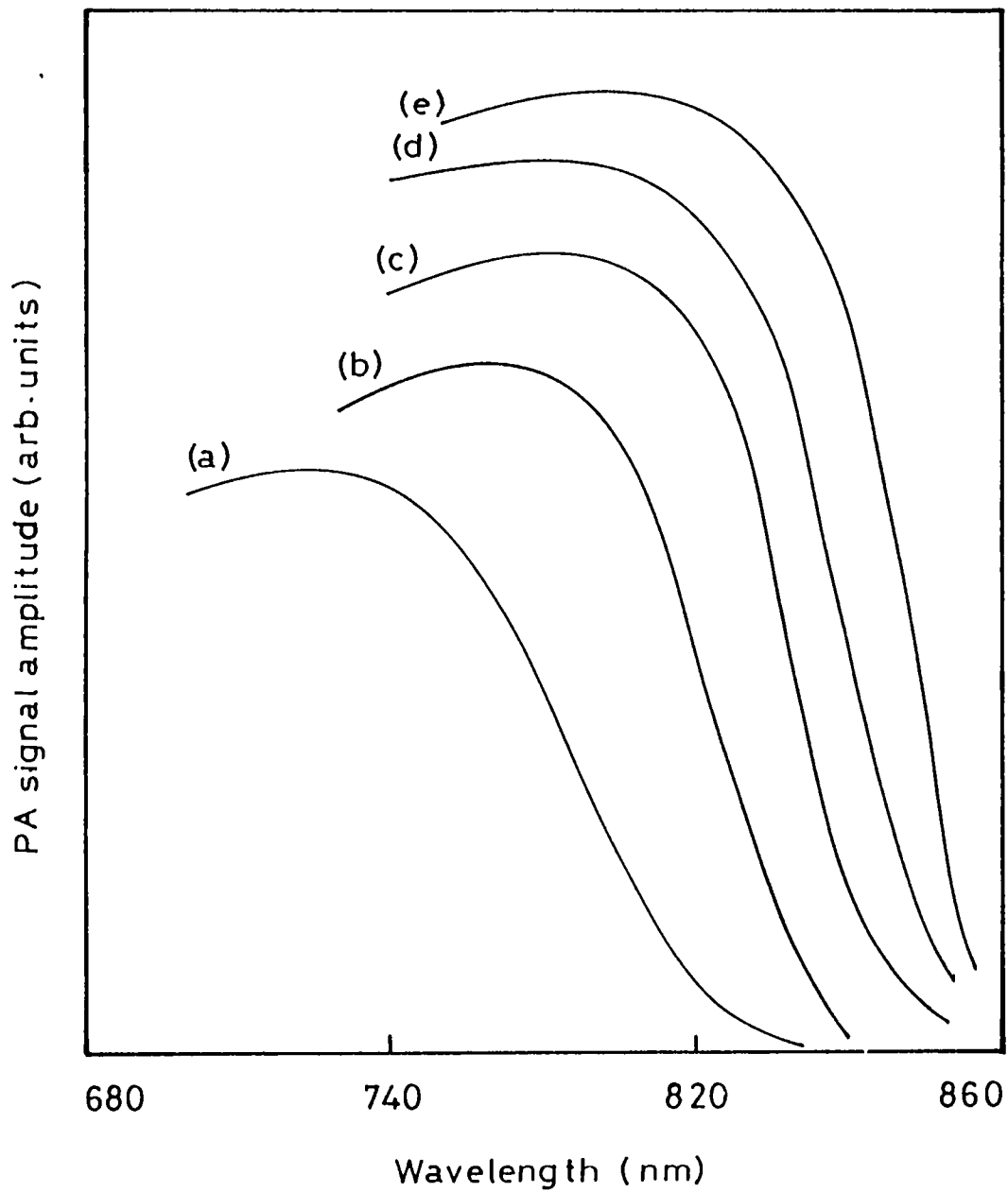


Fig.3.3 PA spectra of $\text{As}_x\text{Sb}_{10}\text{Se}_{90-x}$ glasses.
 (a) $\text{As}_{20}\text{Sb}_{10}\text{Se}_{70}$, (b) $\text{As}_{25}\text{Sb}_{10}\text{Se}_{65}$,
 (b) $\text{As}_{30}\text{Sb}_{10}\text{Se}_{60}$, (d) $\text{As}_{35}\text{Sb}_{10}\text{Se}_{55}$ and
 (e) $\text{As}_{40}\text{Sb}_{10}\text{Se}_{50}$

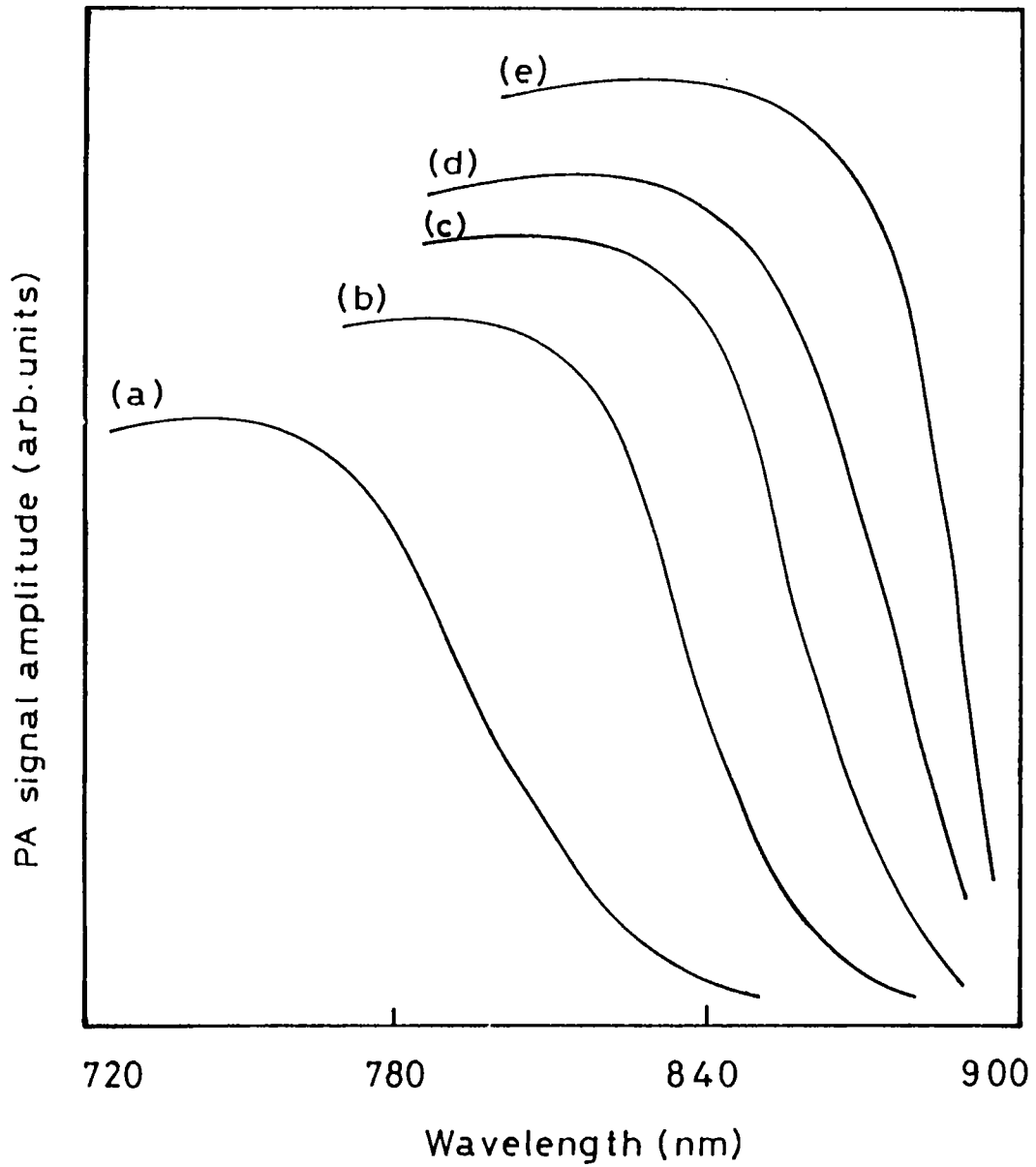


Fig.3.4 PA spectra of $\text{As}_x\text{Sb}_{15}\text{Se}_{85-x}$ glasses.
 (a) $\text{As}_{15}\text{Sb}_{15}\text{Se}_{70}$, (b) $\text{As}_{20}\text{Sb}_{15}\text{Se}_{65}$,
 (c) $\text{As}_{25}\text{Sb}_{15}\text{Se}_{60}$, (d) $\text{As}_{30}\text{Sb}_{15}\text{Se}_{55}$ and
 (e) $\text{As}_{35}\text{Sb}_{15}\text{Se}_{50}$

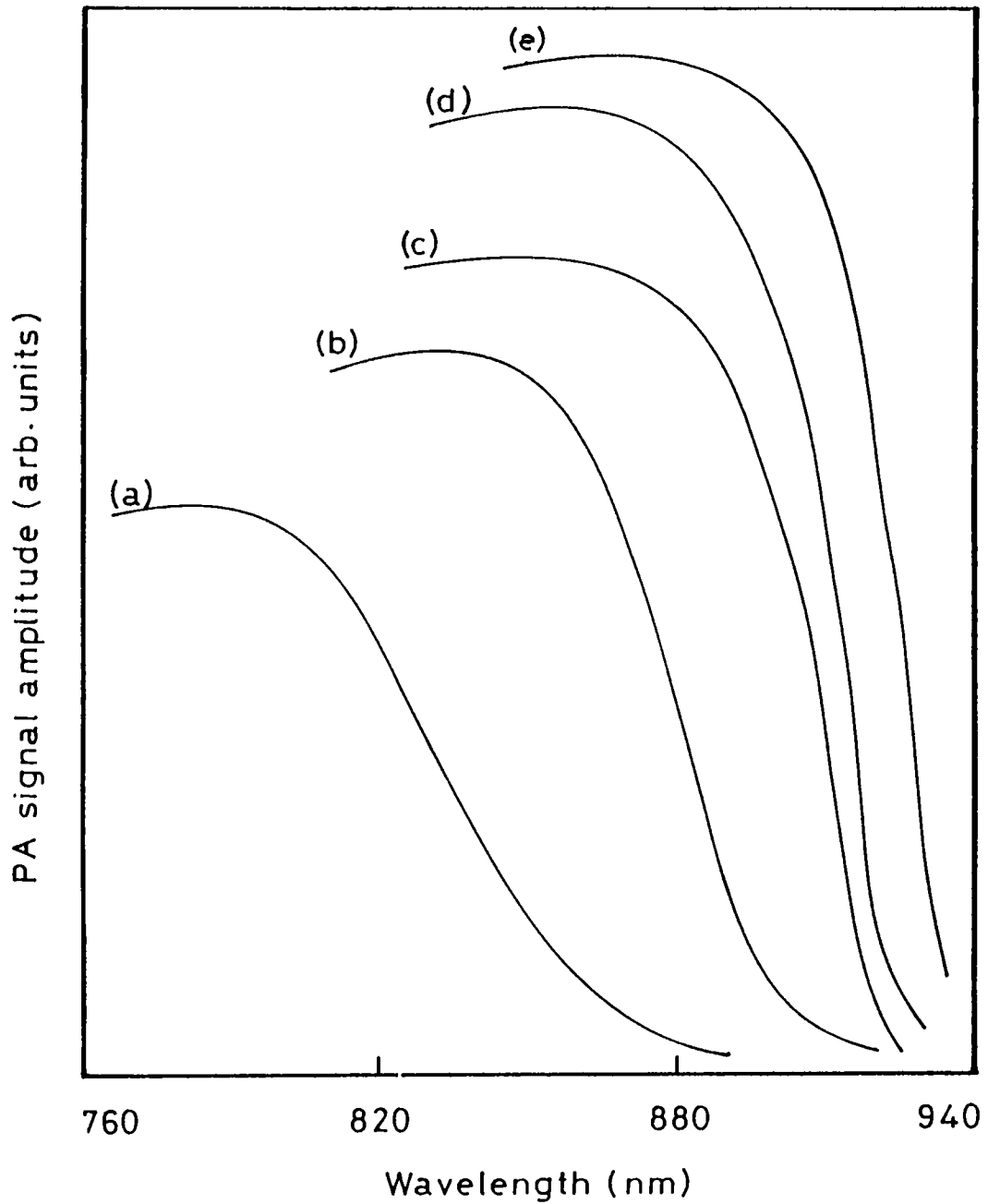


Fig.3.5 PA spectra of $\text{As}_x\text{Sb}_{20}\text{Se}_{80-x}$ glasses.
 (a) $\text{As}_{10}\text{Sb}_{20}\text{Se}_{70}$, (b) $\text{As}_{15}\text{Sb}_{20}\text{Se}_{65}$,
 (c) $\text{As}_{20}\text{Sb}_{20}\text{Se}_{60}$, (d) $\text{As}_{25}\text{Sb}_{20}\text{Se}_{55}$ and
 (e) $\text{As}_{30}\text{Sb}_{20}\text{Se}_{50}$

exponential part associated with disorder induced potential fluctuations which extends in the absorption coefficient range $1\text{cm}^{-1} \leq \beta \leq 10^4 \text{ cm}^{-1}$. The absorption in this region depends on the photon energy according to the relation

$$\beta (h\nu) = \beta_0 \exp (h\nu/E) \quad (3.2)$$

where E characterizes the slope of the exponential absorption region. In the PA spectra this corresponds to the region where the normalized PA signal increases with photon energy. In this region the normalized PA signal is proportional to the absorption coefficient as predicted by R-G theory for optically transparent solids [23].

In the weak absorption tail region with $\beta < 1 \text{ cm}^{-1}$, where the absorption depends upon the preparation, purity and thermal history of the material is not of much interest in the present studies and so is not discussed any further.

The optical energy gap E_0 of all the samples has been determined from the PA spectra. This has been done graphically by drawing tangents at the PA saturation region and the region where the absorption increases exponentially with photon energy in the PA spectra of each sample. The point where the two tangents meet corresponds to E_0 . The optical energy gap has also been determined using UV-Vis-NIR spectrophotometer. The values of E_0 determined using PA technique as well as UV-Vis-NIR spectrophotometry are tabulated in Table.3.1

3.4 Composition dependence of optical band gap

The variation of optical band gap E_0 with As concentration for the four groups of glasses viz., $\text{As}_x\text{Sb}_5\text{Se}_{95-x}$,

Table 3.1 The optical band gap of As-Sb-Se glasses using PA technique and UV-Vis-NIR spectrophotometry.

No.	Composition As:Sb:Se	E_o (eV) (PA technique)	E_o (eV) (UV-Vis-NIR)
1.	25:5:70	1.76	1.74
2.	30:5:65	1.69	1.68
3.	35:5:60	1.64	1.64
4.	40:5:55	1.63	1.62
5.	45:5:50	1.61	1.61
6.	20:10:70	1.68	1.65
7.	25:10:65	1.61	1.60
8.	30:10:60	1.58	1.56
9.	35:10:55	1.57	1.57
10.	40:10:50	1.56	1.55
11.	15:15:70	1.64	1.54
12.	20:15:65	1.54	1.55
13.	25:15:60	1.50	1.48
14.	30:15:55	1.48	1.46
15.	35:15:50	1.45	1.45
16.	10:20:70	1.56	1.55
17.	15:20:65	1.46	1.46
18.	20:20:60	1.42	1.41
19.	25:20:55	1.41	1.40
20.	30:20:50	1.39	1.38

$As_xSb_{10}Se_{90-x}$, $As_xSb_{15}Se_{85-x}$ and $As_xSb_{20}Se_{80-x}$ are shown in Fig.3.6. It is clear that for a particular Sb concentration, E_o decreases gradually as the As concentration increases and shows a marked change in its rate of decrease at a particular concentration at which the As content and Sb content together is 40 atomic percent. this is the stoichiometric composition of the As-Sb-Se system of glasses. The rate of decrease of E_o is higher for compositions with $(x+y) < 40$ than for those with $(x+y) > 40$.

Fig.3.7 shows the variation of optical band gap E_o with Sb concentration for the stoichiometric compositions of the As-Sb-Se system. as the Sb concentration is increased from 0 to 20 at. %, the optical band gap decreases linearly.

The observed behaviour of the As-Sb-Se family of glasses can be explained on the basis of chemical bonding between atoms and the changes in the short-range order that occurs in the glass network. Based on the chemically ordered network (CON) model [6], the As-Sb-Se glasses can be thought of as made up of completely cross-linked three-dimensional structural units of $As_2Se_3-Sb_2Se_3$ with either As or Se in excess. In the Se-rich glasses some of the original As_2Se_3 structural units are replaced by Se and the two coordinated Se atoms form $(Se)_n$ chains or $(Se)_8$ rings. In the As-rich glasses, three coordinated As atoms break these $(Se)_8$ rings or $(Se)_n$ chains to satisfy its coordination number and form very complex network structure. The chemical order is maintained for As atoms as As_2Se_3 structural units. With the introduction of Sb atoms, the Se atom chains get interconnected with both As and Sb atoms and the composition dependence is brought about by the occupation of Se atoms in favourable positions in the network.

Apart from As-Se, Sb-Se and Se-Se bonds, As-As and Sb-Sb bonds will also be involved in the formation of the network. The bond energies of As-Se, Sb-Se, Se-Se, As-As and

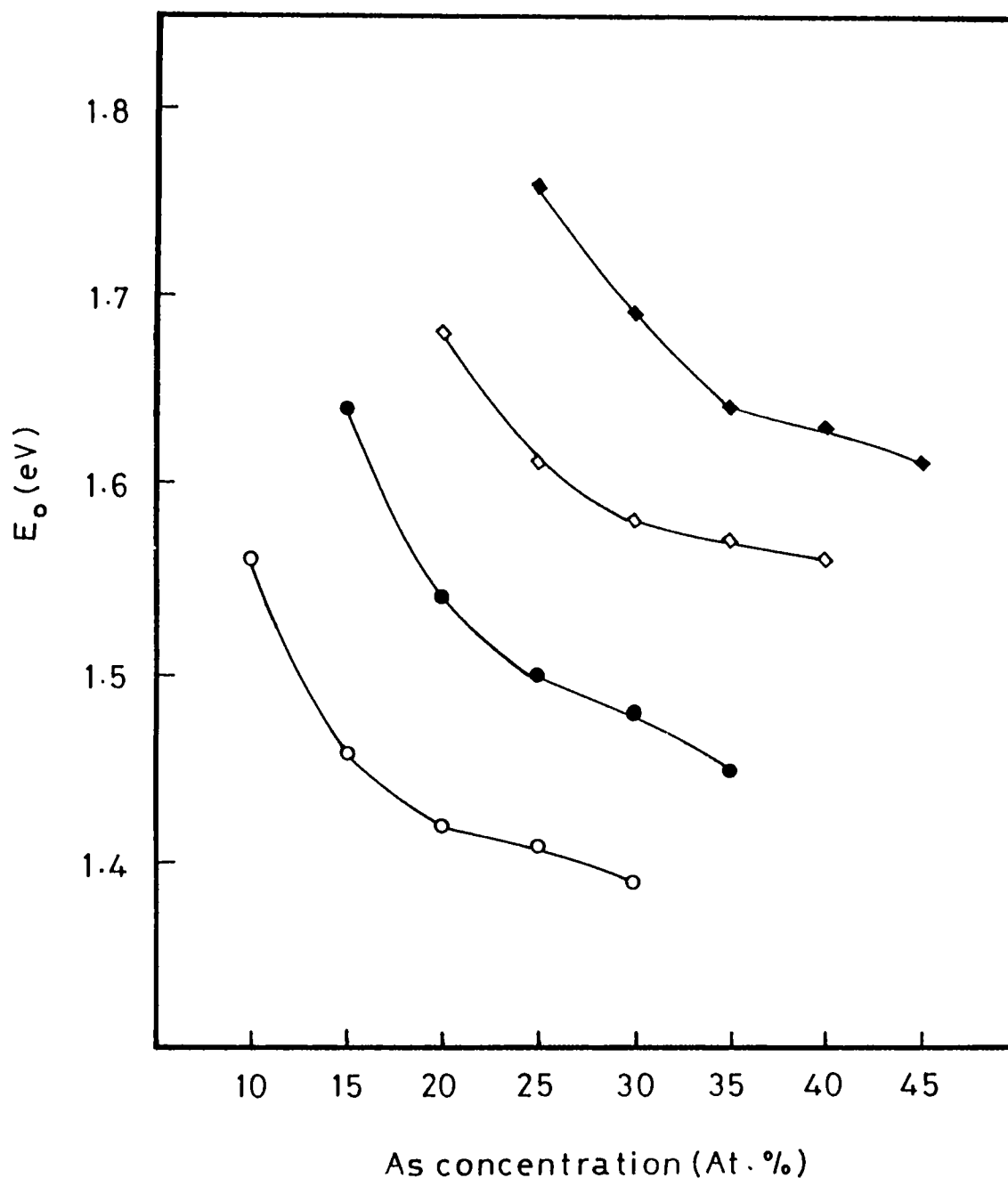


Fig.3.6 The variation of optical band gap E_o with As concentration for As-Sb-Se glasses.

(■) $As_xSb_5Se_{95-x}$, (◻) $As_xSb_{10}Se_{90-x}$,
 (●) $As_xSb_{15}Se_{85-x}$ and (○) $As_xSb_{20}Se_{80-x}$

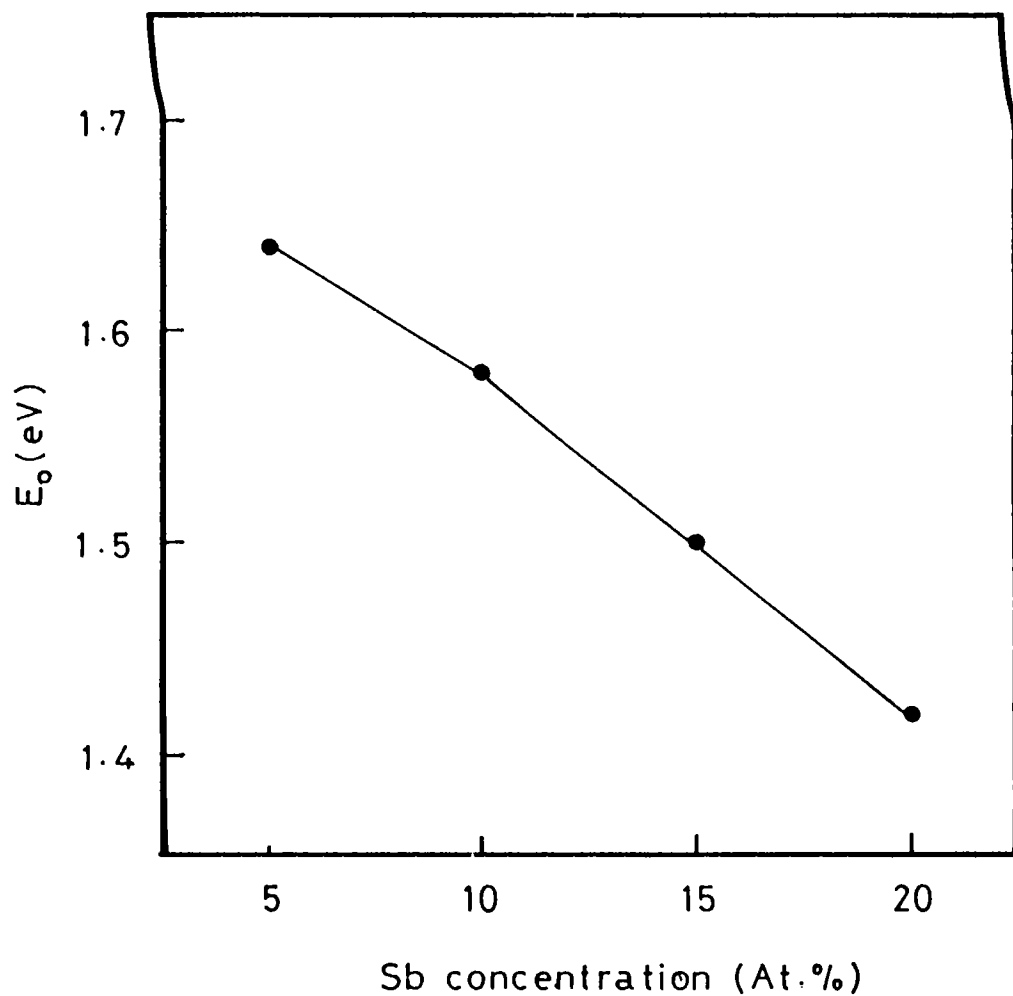


Fig.3.7 Variation of optical band gap E_o with Sb concentrations for the stoichiometric compositions of the As-Sb-Se glasses.

Sb-Sb bonds are 52, 51, 49, 46 and 42 Kcal/mol respectively [24]. With decrease in Se content in As-rich glasses the $\text{Sb}_2\text{Se}_3/\text{As}_2\text{Se}_3$ ratio progressively increases resulting in a decrease in average bond energy of the system. Using Kastner's model [25] for the band structure of chalcogenide glasses, the decrease in average bond energy of the system tends to decrease the energy of the conduction band edge. This effectively decreases the optical band gap E_o . For the Se-rich glasses more As_2Se_3 structural units are present in the network than the Sb_2Se_3 structural units and results in an increase of average bond energy which in turn increases the optical band gap. However, the marked variation at the stoichiometric compositions, which corresponds to an average coordination number $\langle r \rangle = 2.4$, could be attributed to the interactions between the lone pair p electrons which broadens the lone pair band resulting in a decrease in E_o .

For the stoichiometric compositions, one can not expect any drastic change in the basic structure of the glass network by replacing As by Sb since As and Sb are isovalent. However, as Sb concentration increases the probability for the formation of Sb-Sb and Sb-Se bonds increases. Hence the average bond energy of the system is reduced which effectively reduces E_o .

REFERENCES

1. S. R. Ovshinsky, Phys. Rev. Lett., 21, 1450 (1968)
2. S. R. Ovshinsky, in : Physical Properties of Amorphous Materials, eds., D. Adler, B. B. Schwartz and M. C. Steele, Institute for Amorphous Studies Series, Vol.1, Ch.2 ,(Plenum, New York 1985)
3. S. R. Ovshinsky, J. de Phys., C4, Suppl.10, 42, C4-1095 (1981)
4. M. Nunoshita et. al., Solid State Commun., 11, 213 (1972)
5. A. Feltz et.al., J. Non-Cryst. Solids, 8-10, 64 (1972)
6. G. Lucovsky and T. M. Hayes; in Amorphous Semiconductors ed., M. H. Brodsky (Springer-Verlag, Berlin 1979)
7. R. J. Nemanich, G. A. N. Connell, T. M. Hayes and R. A. Street, Phys. Rev. B18, 6900 (1978)
8. R. A. Street, R. J. Nemanich and G. A. N. Connell, Phys. Rev. B18, 6915 (1978)
9. K. N. Madhusoodanan and J. Philip, Phys. Rev. B39, 7922 (1989)
10. G. M. Orlova, O. Z. Rasina and N. P. Krivenkova, Zl. Prikl. Khim. 47, 510 (1974)
11. A. Giridhar and Sudha Mahadevan, J. Non-Cryst. Solids, 51, 305 (1982)
12. A. Giridhar, Sudha Mahadevan and A. K. Singh, Bull. Mater. Sci., 6, 1001 (1984)

13. A. Giridhar, Sudha Mahadevan and A. K. Singh, Bull. Mater. Sci., **8**, 53 (1986)
14. Sudha Mahadevan, A. Giridhar and A. K. Singh, J. Non-Cryst. Solids, **88**, 11 (1986)
15. A. Mandelis and E. K. M. Siu, Phys. Rev. **B34**, 7209; 7222 (1986)
16. A. K. Bhatnagar and S. V. Subramanyam, Solid State Commun., **42**, 81 (1982)
17. Y. Yamasaki, Phil. Mag. **B56**, 79 (1987)
18. K. Nagata, Y. Miyamoto, H. Nishimura, H. Suzuki and S. Yamasaki, Jpn. J. Appl. Phys., **24**, L8 58 (1985)
19. M. Kitamura, T. Ogawa and t. Arai, J. Non-Cryst. Solids, Pt. 2, **59-60**, 917 (1983)
20. A. Rosencwaig, Photoacoustics and Photoacoustic Spectroscopy (New York - Wiley, 1980)
21. K. N. Madhusoodanan, Ph.D. thesis, Cochin University of Science & Technology, Cochin, India (1988)
22. J. Tauc, in Amorphous and Liquid Semiconductors ed: J. Tauc (Plenum Press, New York 1974) p. 159
23. A. Rosencwaig and A. Gersho, J. Appl. Phys., **47**, 64 (1976)
24. G. C. Das, N. S. Platakis and M. B. Bever, J. Non-Cryst. Solids, **15**, 30 (1974)
25. M. Kastner, Phys. Rev. Lett., **28**, 355 (1972)

CHAPTER IV

THERMAL DIFFUSIVITY MEASUREMENTS ON As-Sb-Se GLASSES

4.1 Introduction

Thermal diffusivity α is of direct importance in thermal transport properties as it determines the rate of periodic or transient heat propagation through a medium. Since thermal diffusivity is the ratio of thermal conductivity to the specific heat and density of the material, a knowledge of thermal diffusivity can be used to calculate the thermal conductivity, provided the other two parameters of the material are known. Although thermal conductivity and thermal diffusivity are directly related, measurement of these two parameters are made by completely different experimental procedures. Thermal conductivity, when measured directly by a steady state method, requires the measurement of the thermal flux and temperature gradient. Thermal diffusivity requires the measurement of the time for a thermal disturbance to propagate to a known distance in the medium. This points out the importance of thermal diffusivity measurements because lengths and time intervals can be measured more easily and accurately than heat fluxes and temperature gradients.

Two kinds of techniques have been commonly used to determine thermal diffusivities: transient heat-flow methods [1] and periodic heat-flow methods [2]. In the transient heat-flow method, an addition or removal of thermal energy from the sample induces a transitory temperature change and α is determined from a measurement of the temperature as a function of time at one or more points along the sample. In periodic heat-flow methods the thermal energy supplied to the sample is modulated at a fixed period. Consequently the temperatures at all points in the sample vary with the same period and α is then determined from

the measurement of the amplitude and phase of thermal wave in the sample.

The PA technique [3], which belongs to the periodic heat flow method, is an effective method for determining thermal parameters of various materials when the PA signal is measured as a function of chopping frequency for thermally thin samples. The method enables one to measure indirectly and with high sensitivity the surface temperatures of the sample by noncontact means. Ever since Rosencwaig and Gersho formulated their theory of PA effect based on thermal diffusion characteristics [4], this technique has been utilized for measuring the thermal diffusivity of a wide variety of samples [5-11]. Charpentier et.al [12] have studied the theoretical and experimental problems which are encountered when PA technique is used. They presented a frequency analysis of the PA signal for the determination of thermal diffusivity by extending the RG theory. An account of the mechanical vibrations of the sample due to its periodic dilation, known as drum effect, has also been discussed by them. An extensive study of the variation of PA signal phase with different sample thicknesses have been made by Lachaine [13] and could obtain the thermal parameters of lead samples.

In this chapter the necessary theory behind thermal diffusivity measurements using PA technique and the results of such measurements done on As-Sb-Se glasses are described in detail.

4.2 RG theory of thermal diffusivity measurement

The theory of Rosencwaig and Gersho shows that the complex expression for the pressure variations Q inside a photo-acoustic cell can be written as

$$Q = q e^{-i\psi} \quad (4.1)$$

where q is the amplitude of the PA signal and ψ is the phase shift between Q and the excitation. The above equation can be rewritten as the product of two terms A and B such that A depends on the modulation frequency f , and B is independent of f as given by,

$$B = \frac{P_0 \gamma^2 W_{\alpha} l}{2 l' T_0 K} \frac{\sqrt{\alpha'}}{\sqrt{\alpha}} \quad (4.2)$$

$$\text{and } A = \left[1 + g \frac{d^+ + d^-}{d^+ - d^-} \right] \left[\frac{d^+ + d^-}{d^+ - d^-} + g \right] \frac{1}{(\sigma l)^2} \quad (4.3)$$

$$\begin{aligned} \text{where } d^+ &= \exp(\sigma l) \\ d^- &= \exp(-\sigma l) \\ \sigma &= (1 + i) (\pi f / \alpha)^{1/2} \end{aligned} \quad (4.4)$$

and g , the ratio between the effusivities of the backing material (e'') and the sample (e), is given by

$$g = e''/e = (K''/K) (\alpha/\alpha'')^{1/2} \quad (4.5)$$

In the above expressions l , K and α are the thickness, thermal conductivity and thermal diffusivity respectively. Unprimed quantities refer to sample parameters, singly primed quantities refer to gas parameters and doubly primed ones to the backing material. T_0 and P_0 are respectively the static temperature and pressure of the gas, γ is the ratio of specific heats of the gas and W_{α} is the amount of absorbed light. It is assumed that the effusivity of the gas in the cell is negligible compared to the effusivity of the sample. The term A depends on the modulation frequency through the product σl which can be

written as,

$$\sigma l = (1+i) (\pi f / f_c)^{1/2} \quad (4.6)$$

where the characteristic frequency f_c is defined by,

$$f_c = \alpha / l^2 \quad (4.7)$$

The thermal diffusivity α can be determined by measuring the amplitude of the PA signal as a function of chopping frequency. One of the parameters which determines the amplitude of the PA signal is the thermal diffusion length (μ) given by

$$\mu = [\alpha / \pi f]^{1/2} \quad (4.8)$$

where α is the thermal diffusivity of the sample and f is the chopping frequency. In the thermally thick regime ($\mu < l$, where l is the sample thickness) the PA signal is independent of the thermal properties of the backing material on which the sample is mounted, whereas in the thermally thin regime ($\mu > l$) the PA signal gets modified by the thermal properties of the backing material as well. For an appropriate sample thickness, one can obtain a crossover from thermally thin regime to thermally thick regime by increasing the chopping frequency. Hence the amplitude versus chopping frequency plot shows a change in slope at the characteristic frequency f_c at which the crossover takes place.

Charentier *et al* [12] have demonstrated the dependence of A on the modulation frequency for different values of g . when $f > f_c$, the variation of A is independent of α and decreases as f^{-1} . When $f < f_c$ the variation of A depends both on α and the ratio of effusivities, g . Thus it is possible to determine f_c by measuring the amplitude of the PA signal as a function of chopping frequency, f . However if $g = 1$, (same

effusivity for sample and backing) the variation of the amplitude is the same for all frequencies and the determination of f_c becomes impossible. Once f_c is determined, thermal diffusivity can be determined from eq.(4.7) as

$$\alpha = f_c l^2 \quad (4.9)$$

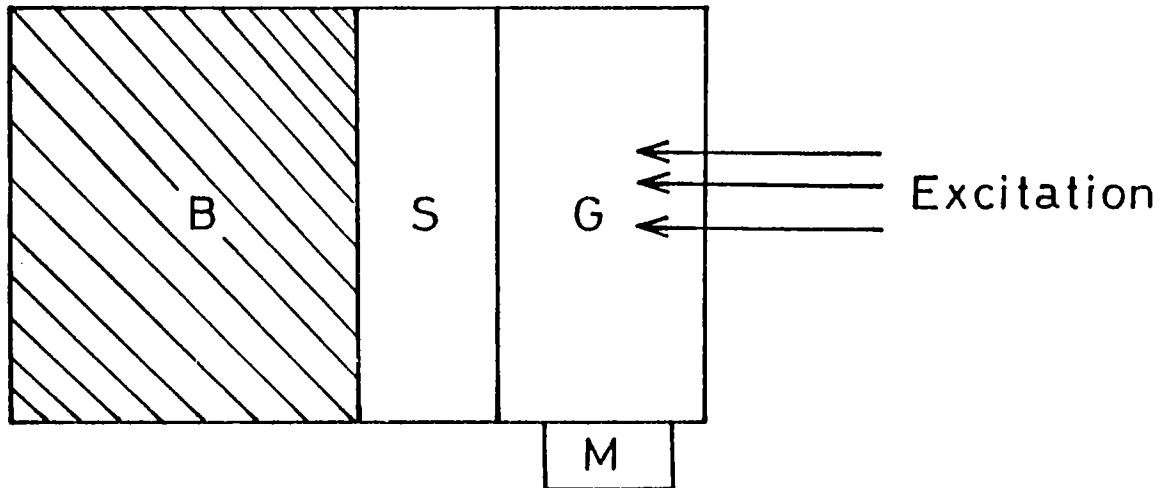
The thermal diffusivity α can also be determined by measuring the variation of PA phase as a function of chopping frequency. For determining the characteristic frequency f_c above which the PA signal is independent of the effect of the backing material, the PA phase of a thermally thick reference sample and that of the experimental sample are measured as a function of the chopping frequency. Then f_c is determined as the frequency at which the difference between these two phases, $\Delta\phi$, tends to zero. Knowing f_c , thermal diffusivity α is determined using eq. (4.9).

4.3 Thermal diffusivity measurements on As-Sb-Se glasses

The theoretical formulations presented above account for the frequency dependence and the effect of backing material on the PA signal phase and amplitude. The thermal diffusion length is confined within the sample for thermally thick sample in the entire chopping frequency range and consequently the thermal reflection coefficient will be zero. When the sample is thermally thin, the heat generated within the sample propagates into the backing material which is thermally thick. Since the thermal diffusion length decreases as the chopping frequency increases, by properly choosing the sample thickness, it is possible to find out the characteristic frequency f_c , above which the PA signal is independent of the effect of the backing material.

The thermal diffusivity α of several glasses belonging to the As-Sb-Se system have been measured using the PA technique. The compositions studied are $\text{As}_x\text{Sb}_5\text{Se}_{95-x}$ (with $x = 25, 30, 35, 40$ and 45), $\text{As}_x\text{Sb}_{10}\text{Se}_{90-x}$ (with $x = 20, 25, 30, 35$ and 40), $\text{As}_x\text{Sb}_{15}\text{Se}_{85-x}$ (with $x = 15, 20, 25, 30$ and 35) and $\text{As}_x\text{Sb}_{20}\text{Se}_{80-x}$ (with $x = 10, 15, 20, 25$ and 30). In each group the glasses $(\text{As,Sb})_{40}\text{Se}_{60}$ fall along the pseudobinary section representing the stoichiometric compositions of the As-Sb-Se system. The samples are prepared by the melt-quenching technique as described in chapter III. For the thermal diffusivity measurements disc type samples of appropriate thickness are prepared by hand lapping and polishing such that the characteristic frequency, at which a crossover from thermally thin to thermally thick regime takes place as the chopping frequency is varied, lies well within the operating range of our spectrometer. Typical sample thickness is in the range 100-130 μm . The sample of appropriate thickness is fixed on to a thermally thick backing material which has been a copper or aluminium disc in our experiments. Proper thermal contact between the sample and the backing material is ensured during each measurement. The sample is properly placed in the room temperature PA cell and the measurements have been carried out using front surface illumination. The front surface illumination geometry used in the experiments is shown schematically in Fig. 4.1.

The characteristic frequency f_c of each sample is determined by measuring the variation of PA signal phase as a function of chopping frequency. For this, first of all the variation of the phase of the PA signal for a thermally thick sample (thickness $\approx 1\text{mm}$) as a function of chopping frequency is measured. Then the experiment is repeated with the experimental samples of appropriate thickness. Then the difference in phase between the reference sample and the experimental sample, $\Delta\phi$, is plotted as a function of chopping frequency. The difference in



B – Backing material

S Sample

G Gas medium

M Microphone

Fig.4.1 The front surface illumination geometry used in the experiment.

phase $\Delta\phi$ tends to zero for $f > f_c$. Figs 4.2 to 4.5 shows the variation of $\Delta\phi$ with chopping frequency for the four groups of As-Sb-Se glasses. The characteristic frequency f_c of each sample is determined from these plots. Once f_c is determined, α is calculated using eqn.(4.9) for each sample. Table 4.1 shows the average coordination number, sample thickness, characteristic frequency and thermal diffusivity of the samples investigated.

4.4 Composition dependence of thermal diffusivity in As-Sb-Se glasses

The variation of thermal diffusivity α with As concentration for the four groups of glasses belonging to the As-Sb-Se system is shown in Fig.4.6. For each group the thermal diffusivity increases with increase in As concentration and shows a change in its rate of increase at the stoichiometric composition where $(x+y) = 40$. This composition corresponds to an average coordination number $\langle r \rangle = 2.4$.

The average coordination number $\langle r \rangle$ is an important parameter in determining the composition dependence of various physical properties of chalcogenide glasses. If N_{As} , N_{Sb} , N_{Se} are the coordination numbers of As, Sb and Se atoms respectively, then the average coordination number of $As_xSb_ySe_{100-x-y}$ system can be written as

$$\langle r \rangle = \left[xN_{As} + yN_{Sb} + (100-x-y)N_{Se} \right] / 100 \quad (4.10)$$

Taking $N_{As} = 3$, $N_{Sb} = 3$ and $N_{Se} = 2$, $\langle r \rangle$ lies in the range $2.3 \leq \langle r \rangle \leq 2.5$ for the four groups of compositions we have studied. According to Phillips' constraint theory [14] and percolation model [15,16], corresponding to the average coordination number $\langle r \rangle = 2.4$, the number of valence force field constraints are equal to the number of atomic degrees of freedom if

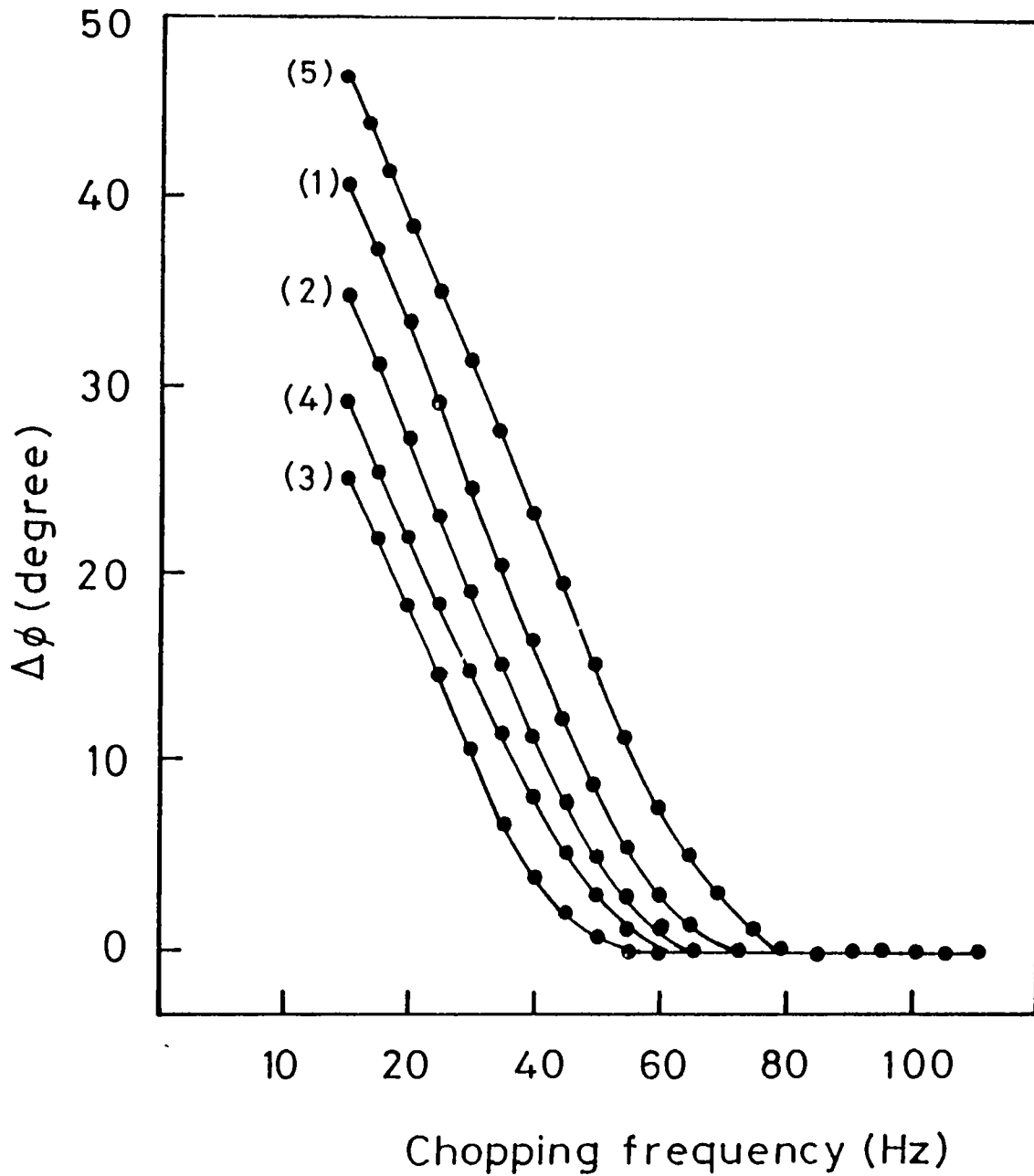


Fig.4.2 Variation of $\Delta\phi$ with chopping frequency for (1) $\text{As}_{25}\text{Sb}_5\text{Se}_{70}$, (2) $\text{As}_{30}\text{Sb}_5\text{Se}_{65}$, (3) $\text{As}_{35}\text{Sb}_5\text{Se}_{60}$ (4) $\text{As}_{40}\text{Sb}_5\text{Se}_{55}$ and (5) $\text{As}_{45}\text{Sb}_5\text{Se}_{50}$ glasses.

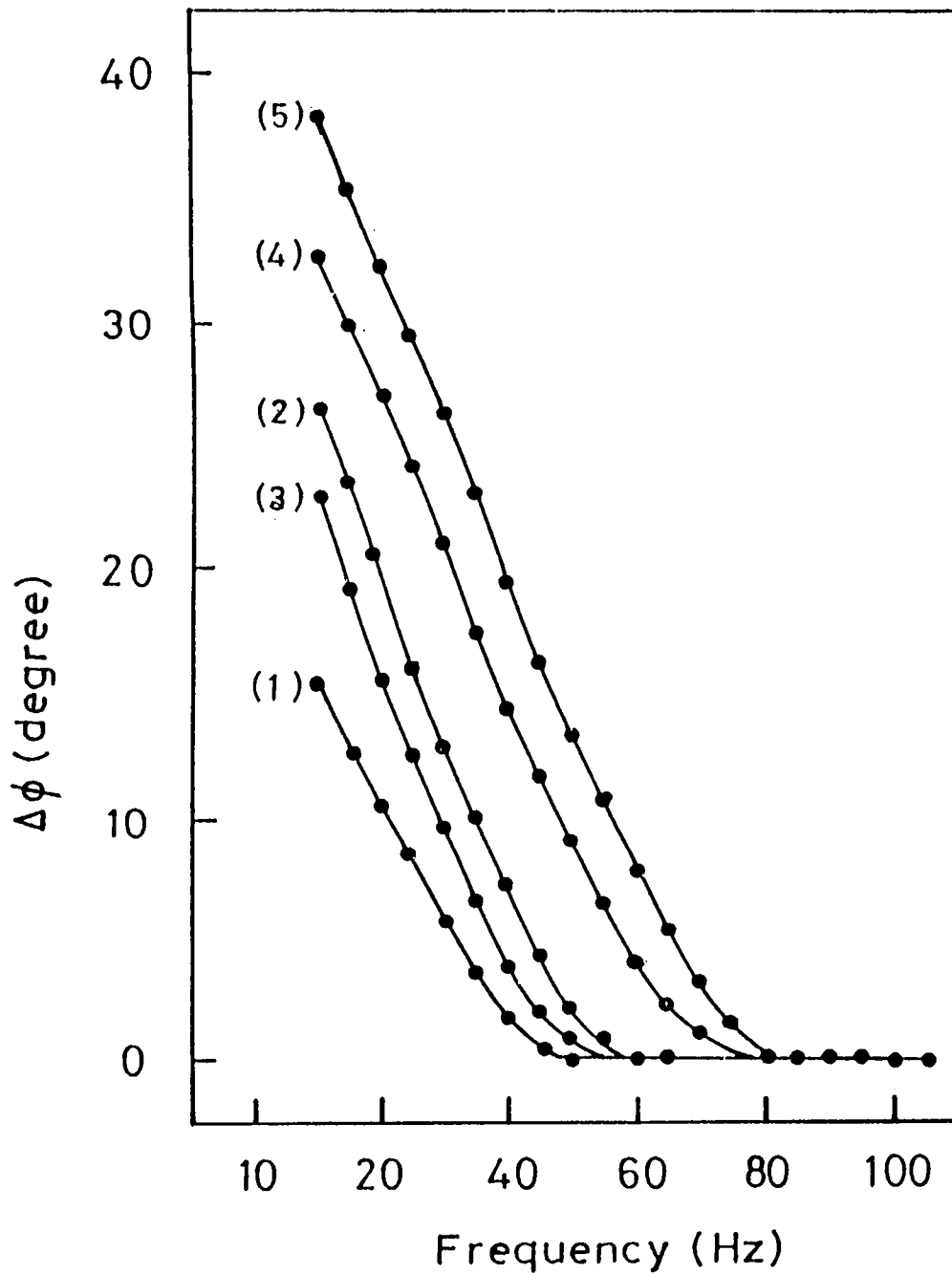


Fig.4.3 Variation of $\Delta\phi$ with chopping frequency for (1) $\text{As}_{20}\text{Sb}_{10}\text{Se}_{70}$, (2) $\text{As}_{25}\text{Sb}_{10}\text{Se}_{65}$, (3) $\text{As}_{30}\text{Sb}_{10}\text{Se}_{60}$, (4) $\text{As}_{35}\text{Sb}_{10}\text{Se}_{55}$ and (5) $\text{As}_{40}\text{Sb}_{10}\text{Se}_{50}$ glasses.

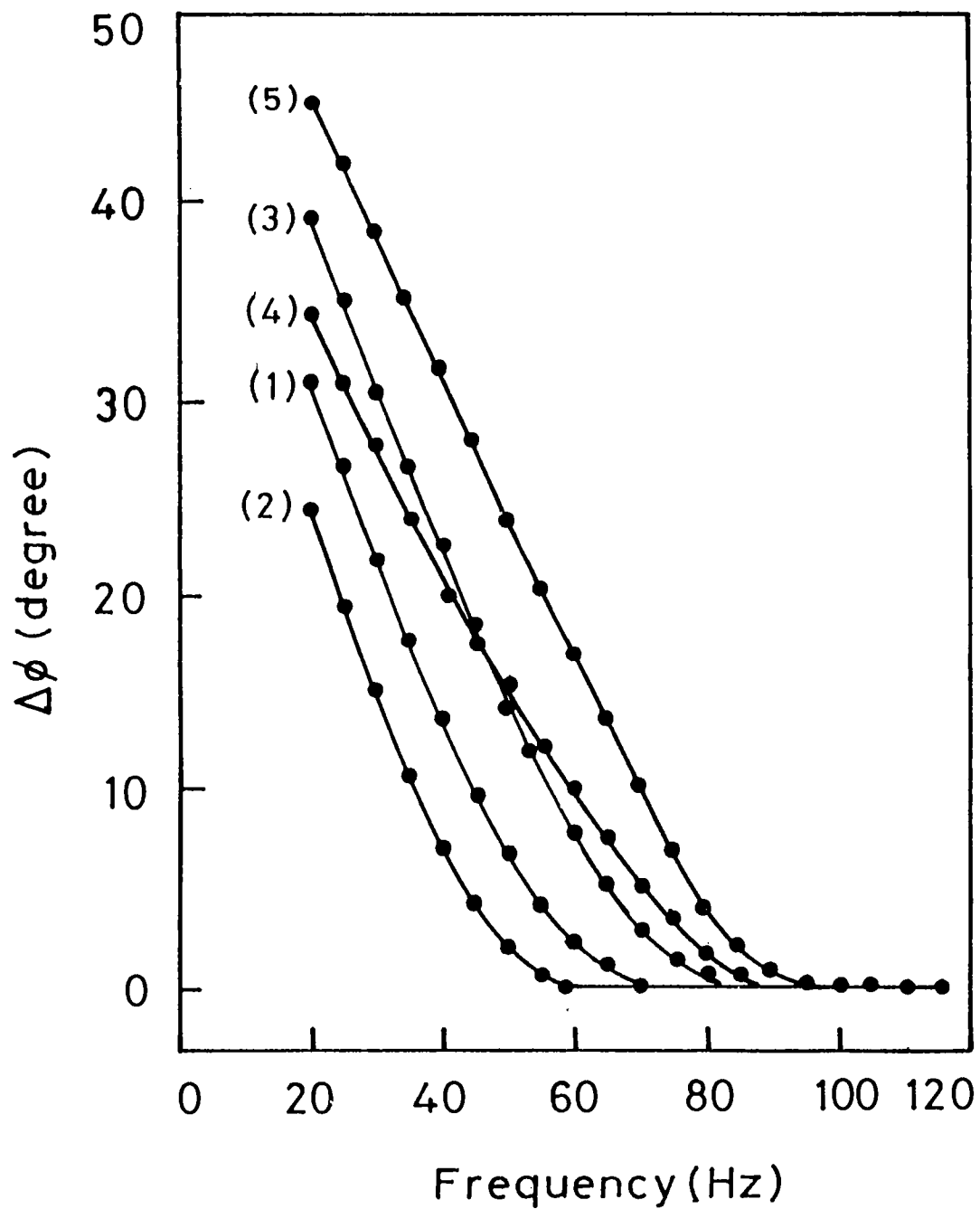


Fig.4.4 Variation $\Delta\phi$ with chopping frequency for
 (1) $\text{As}_{15}\text{Sb}_{15}\text{Se}_{70}$, (2) $\text{As}_{20}\text{Sb}_{15}\text{Se}_{65}$,
 (3) $\text{As}_{25}\text{Sb}_{15}\text{Se}_{60}$, (4) $\text{As}_{30}\text{Sb}_{15}\text{Se}_{55}$ and
 (5) $\text{As}_{35}\text{Sb}_{15}\text{Se}_{50}$ glasses.

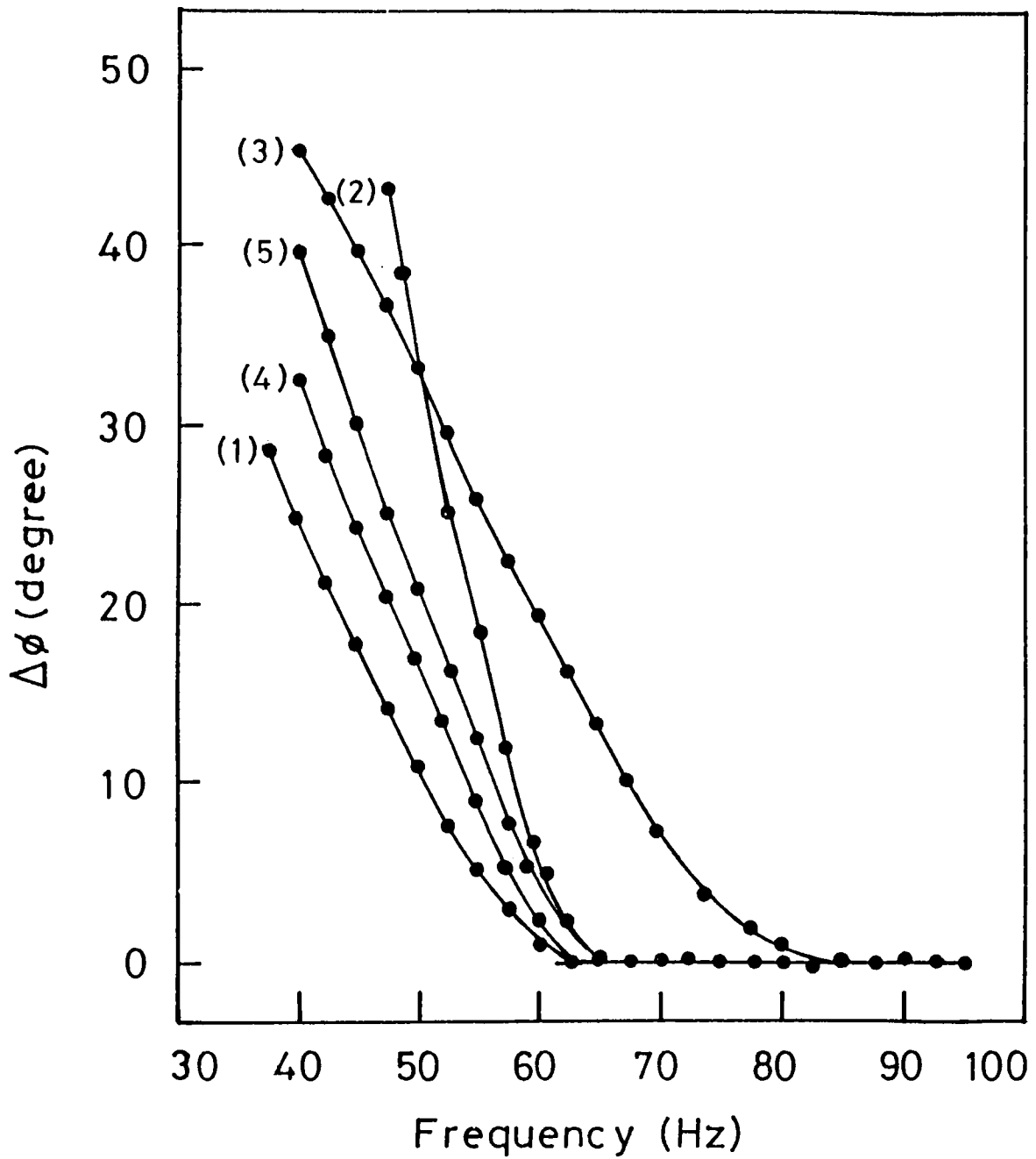


Fig.4.5 Variation of $\Delta\phi$ with chopping frequency for
 (1) $\text{As}_{10}\text{Sb}_{20}\text{Se}_{70}$, (2) $\text{As}_{15}\text{Sb}_{20}\text{Se}_{65}$,
 (3) $\text{As}_{20}\text{Sb}_{20}\text{Se}_{60}$, (4) $\text{As}_{25}\text{Sb}_{20}\text{Se}_{55}$ and
 (5) $\text{As}_{30}\text{Sb}_{20}\text{Se}_{50}$ glasses.

Table 4.1 Composition, average coordination number $\langle r \rangle$, characteristic frequency f_c , thickness l and thermal diffusivity α of As-Sb-Se glasses.

No.	Composition As:Sb:Se	$\langle r \rangle$	f_c (Hz)	l (μm)	α ($\times 10^{-2} \text{ cm}^2/\text{s}$)
1.	25:5:70	2.30	68	100	0.68
2.	30:5:65	2.35	65	110	0.79
3.	35:5:60	2.40	53	130	0.89
4.	40:5:55	2.45	64	120	0.92
5.	45:5:50	2.50	79	110	0.95
6.	20:10:70	2.30	49	120	0.70
7.	25:10:65	2.35	58	120	0.83
8.	30:10:60	2.40	56	130	0.94
9.	35:10:55	2.45	79	110	0.96
10.	40:10:50	2.50	81	110	0.98
11.	15:15:70	2.30	72	100	0.72
12.	20:15:65	2.35	58	120	0.84
13.	25:15:60	2.40	81	110	0.99
14.	30:15:55	2.45	86	110	1.05
15.	35:15:50	2.50	91	110	1.10
16.	10:20:70	2.30	63	110	0.76
17.	15:20:65	2.35	65	120	0.93
18.	20:20:60	2.40	85	110	1.03
19.	25:20:60	2.45	63	130	1.06
20.	30:20:50	2.50	65	130	1.10

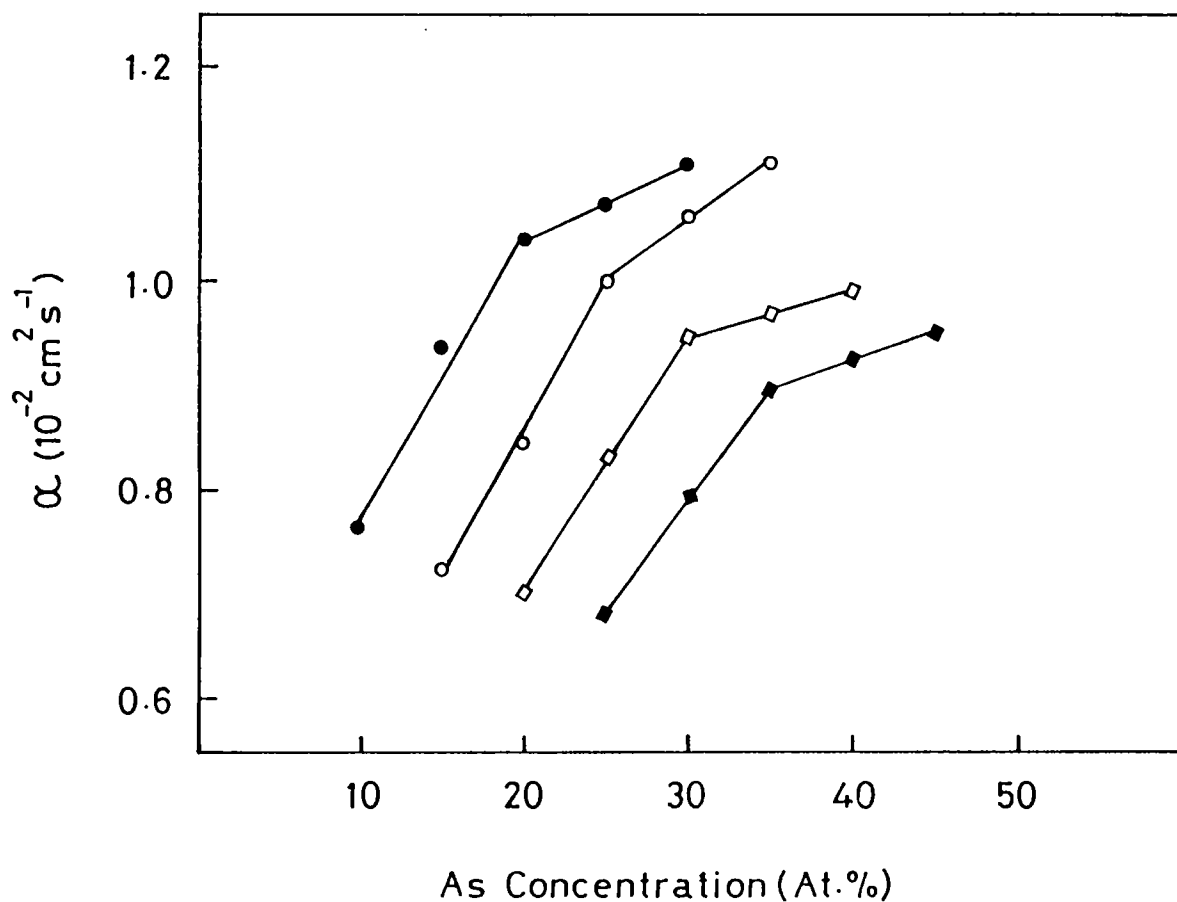


Fig.4.6 Variation of thermal diffusivity with As concentration for As-Sb-Se glasses.

(■) $\text{As}_x \text{Sb}_5 \text{Se}_{95-x}$, (□) $\text{As}_x \text{Sb}_{10} \text{Se}_{90-x}$,
 (○) $\text{As}_x \text{Sb}_{15} \text{Se}_{85-x}$ and (●) $\text{As}_x \text{Sb}_{20} \text{Se}_{80-x}$

bond-stretching and bond-bending constraints are taken into account. For a three-dimensional network, the average covalent coordination number is $\langle r \rangle = 2.4$ and corresponds to a mechanical threshold at which a transition from a floppy polymeric glass to a rigid amorphous solid takes place. The system forms an ideal glass at this composition and the number of zero frequency modes would be minimum at this composition. Beyond this composition, corresponding to the percolation threshold for rigidity, the variation of α with As concentration is small. This can be attributed to the gradual increase in resistance to the propagating thermal waves offered by the glass network beyond this critical composition.

The variation of thermal diffusivity α with Sb concentration for the stoichiometric compositions is shown in Fig.4.7. The thermal diffusivity increases gradually as the Sb concentration is varied from 5 to 20 atomic percent. Even though the system forms an ideal glass at the stoichiometric compositions, the ratio Sb_2Se_3/As_2Se_3 increases as the Sb content increases and this gives rise to a gradual increase of thermal diffusivity.

4.5 Composition dependence of glass transition temperature using PA technique

Glass transition and the observed relaxational behaviour is an old problem but a first principle, microscopic model of glass transition has developed only a few years ago by Götze and coworkers [17-20]. According to this the freezing-in of the liquid amorphous structure is a dynamic transition which can be idealized as the extreme case of atomic motion that the self-diffusion coefficient becomes zero and therefore the viscosity goes to infinity. Characteristics of glass transition are its nonequilibrium nature and the associated jump in

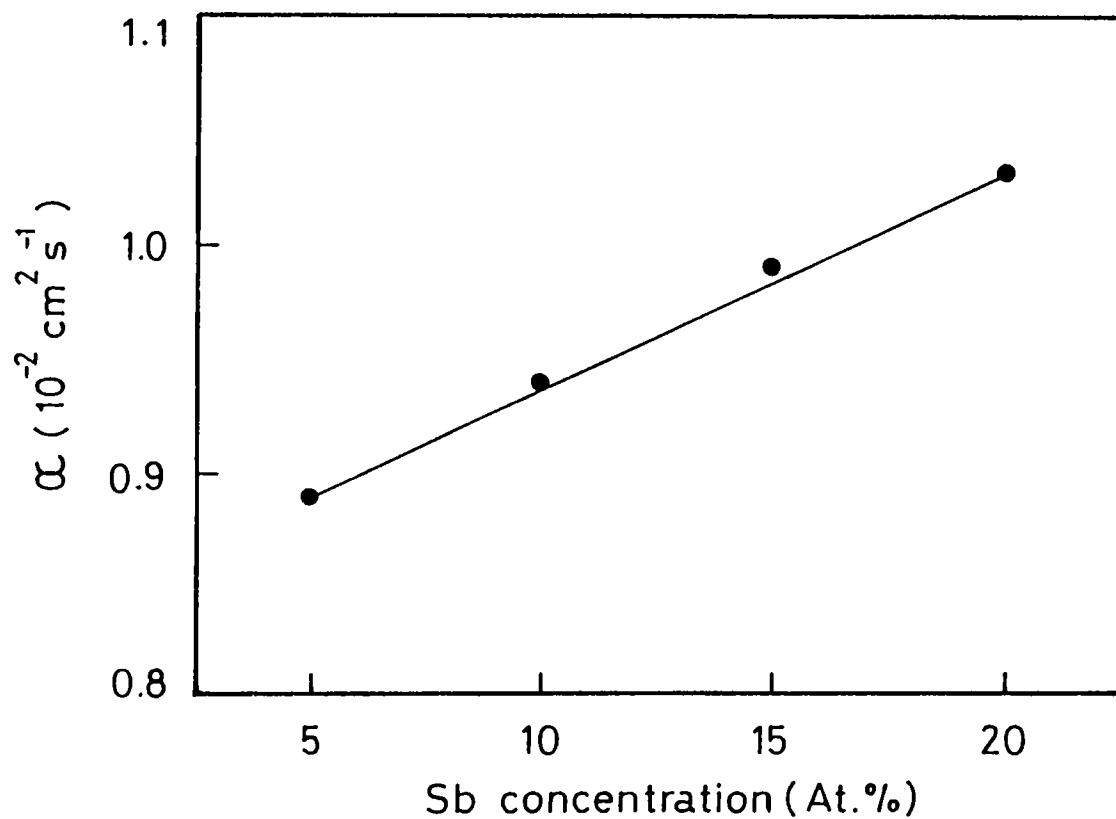


Fig.4.7 Variation of thermal diffusivity with Sb concentration for the stoichiometric compositions of the As-Sb-Se glasses.

compressibility, thermal expansion coefficient and specific heat.

Certain liquids transform continuously into a mechanically solid material (glass) upon cooling. The temperature at which the transformation occurs is called the glass transition temperature and the properties of the resulting glass depend to some degree on the rate of cooling. Some liquids form glasses only if cooled at very high cooling rates. Glasses made from good glass-formers possess a high degree of mechanical and chemical stability and stability against crystallization (or devitrification).

The process of glass transformation and the phenomenon of glass transition can be readily understood from the volume versus temperature behaviour shown in Fig.4.8. When a liquid is cooled from beyond its melting point T_m , two events may occur. Ordinary liquids having low viscosity at their melting point undergo a sudden change in volume and solidify into an ordered crystalline phase. A glass-forming liquid on the other hand, could be supercooled below T_m without crystallising. The $V(T) - T$ plot for a supercooled liquid (Fig.4.8) gently changes slope after T_m indicating that the glass formation process is thermodynamically different from crystallisation process. The liquid-glass transition occurs in a narrow temperature interval near T_g , the glass transition temperature. There is no volume discontinuity, instead $V(T)$ bends over to acquire the small slope characteristic of the low thermal expansion of a solid.

At the glass transition, the first derivative of the free energy such as volume, entropy and enthalpy show a continuous change. The specific heat at constant pressure and thermal expansivity on the other hand, show an abrupt change at T_g . Since C_p is the second derivative of the free energy, the glass transition is considered to be a "second-order" phase

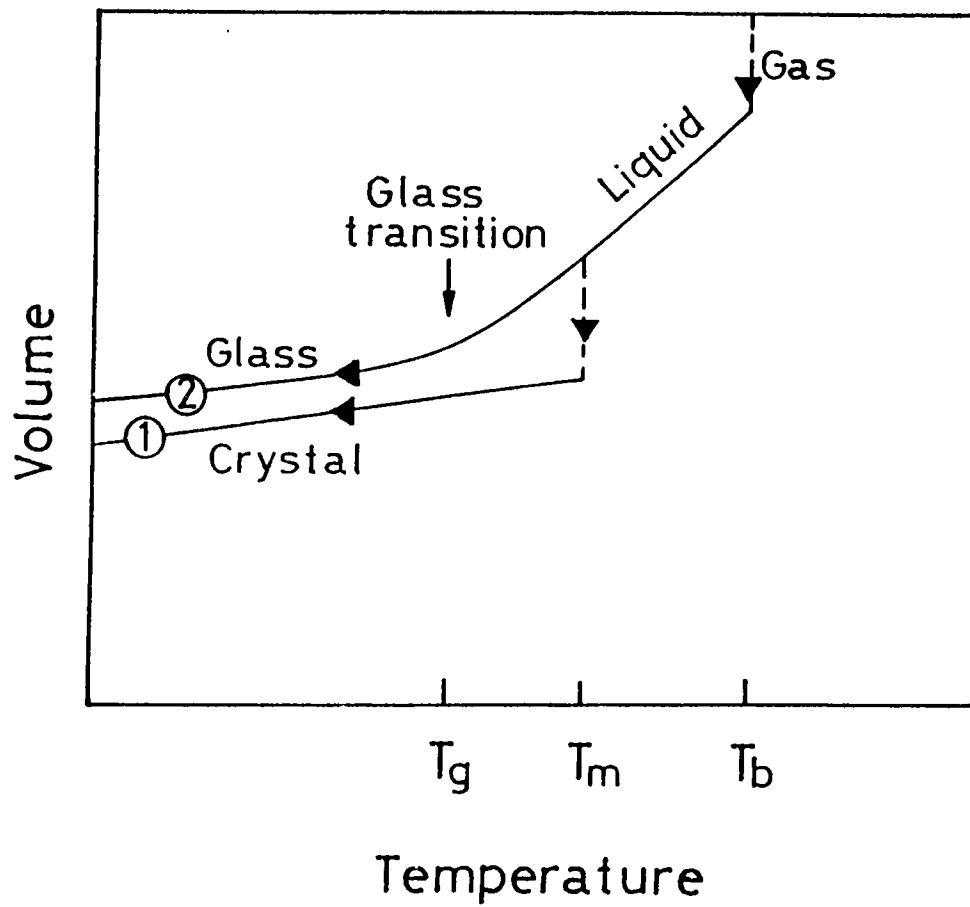


Fig.4.8 The two general routes by which an assembly of atoms can condense into the solid state. Route (1) is the path into crystalline state; route (2) is the rapid-quench path to the amorphous solid state.

transition.

Eventhough the use of the PA effect for studying first and second order phase transitions have been demonstrated by several workers before [21-26], not much work has been done on probing the features of glass transition using this technique. Since the PA signal depends on the thermal properties such as specific heat, thermal expansion and thermal conductivity of the sample, on going through a phase transition, the PA response essentially reflects the thermodynamic changes that are taking place in the sample. Hence the PA studies will provide information about the thermal properties of samples at glass transition temperature, which in turn can provide valuable information about the mechanism of this transition.

The variation of PA signal amplitude and phase have been measured as a function of temperature using white light from the Xe lamp chopped at a frequency of 31Hz. The high temperature PA cell has been used for the measurements. The samples used for these measurements are thermally thick at this chopping frequency so that the thermal properties of the backing material do not affect the PA signal. The variation of PA signal amplitude with temperature of the glasses $As_xSb_5Se_{95-x}$ with $25 \leq x \leq 45$, $As_xSb_{10}Se_{90-x}$ with $20 \leq x \leq 40$, $As_xSb_{15}Se_{85-x}$ with $15 \leq x \leq 35$, and $As_xSb_{20}Se_{80-x}$ with $10 \leq x \leq 30$ are shown in Figs.4.9 to 4.12 respectively. The corresponding variations in PA phase with temperature are shown in Figs.4.13 to 4.16.

For each sample the PA amplitude decreases as the temperature is increased and this decrease becomes faster as glass transition is approached and shows a minimum at T_g . The minimum value for the PA amplitude at T_g indicates that the sample has minimum thermal diffusivity or maximum thermal resistance at T_g . Consequently it takes longer time for the generated thermal waves to travel through the sample and to get

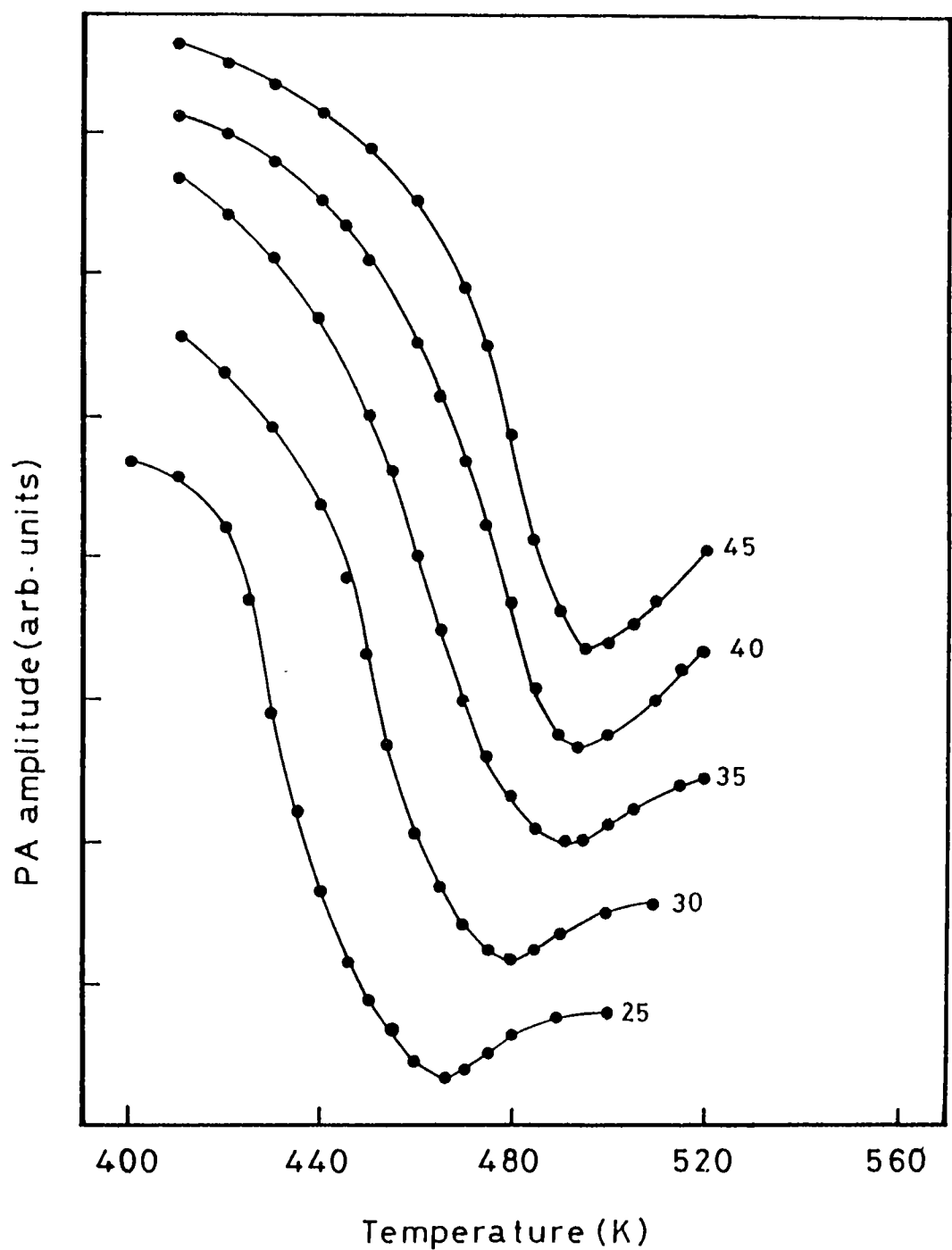


Fig.4.9 Variation of PA amplitude with temperature for $As_xSb_5Se_{95-x}$ glasses. The x values are noted on the curves.

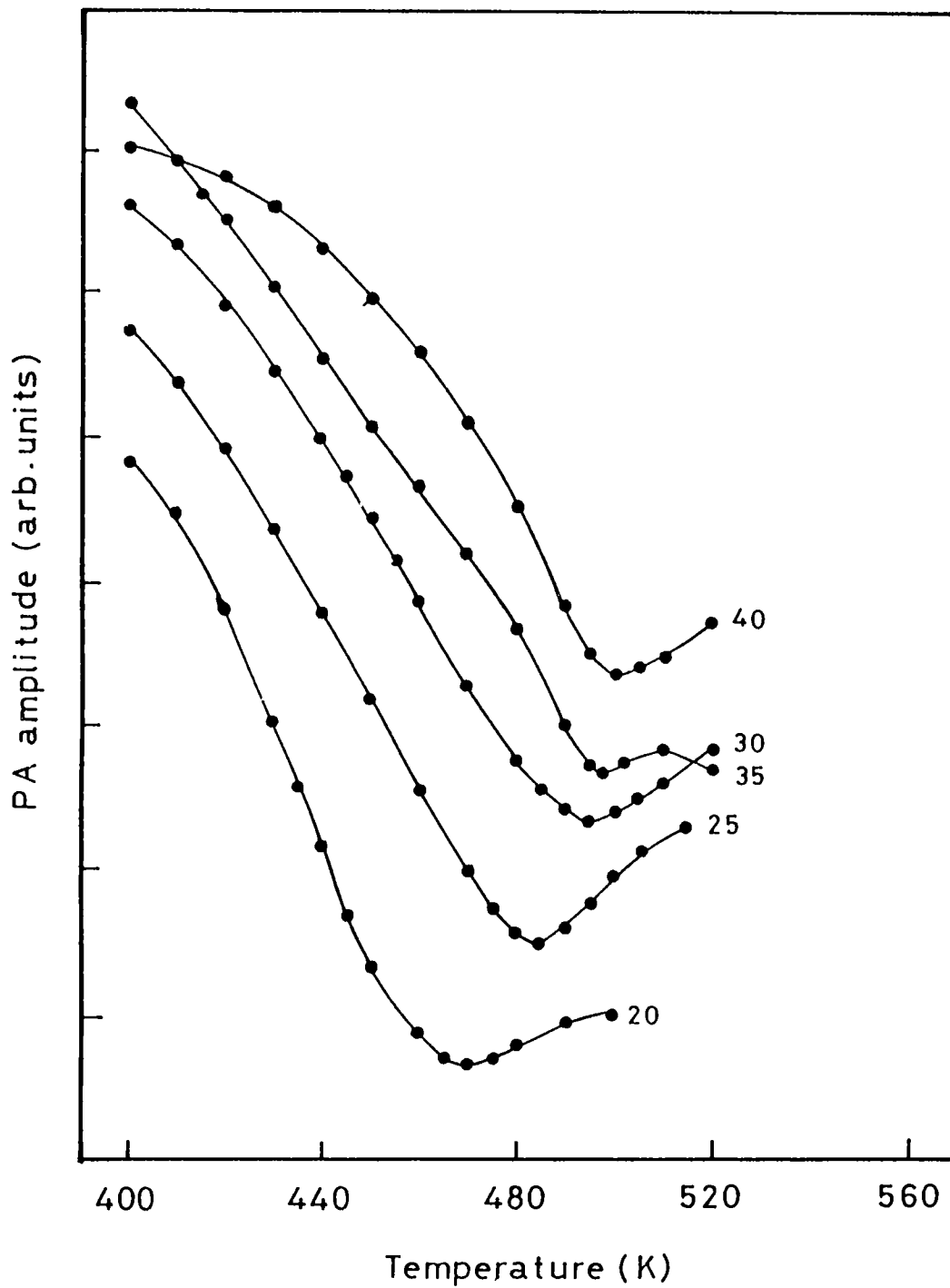


Fig.4.10 Variation of PA amplitude with temperature for $As_xSb_{10}Se_{90-x}$ glasses. The x values are noted on the curves.

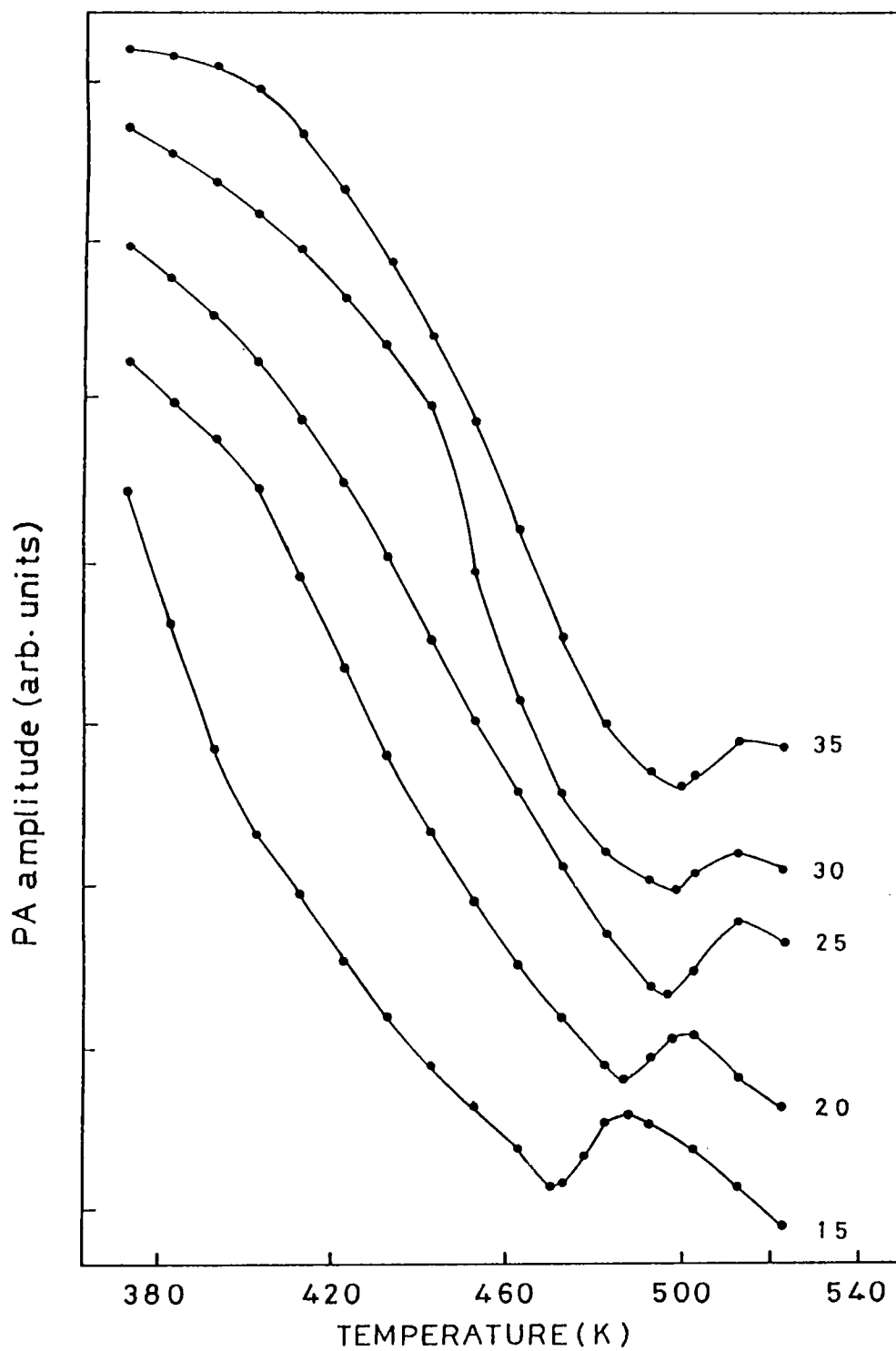


Fig.4.11 Variation of PA amplitude with temperature for $\text{As}_x\text{Sb}_{15}\text{Se}_{85-x}$ glasses. The x values are noted on the curves.

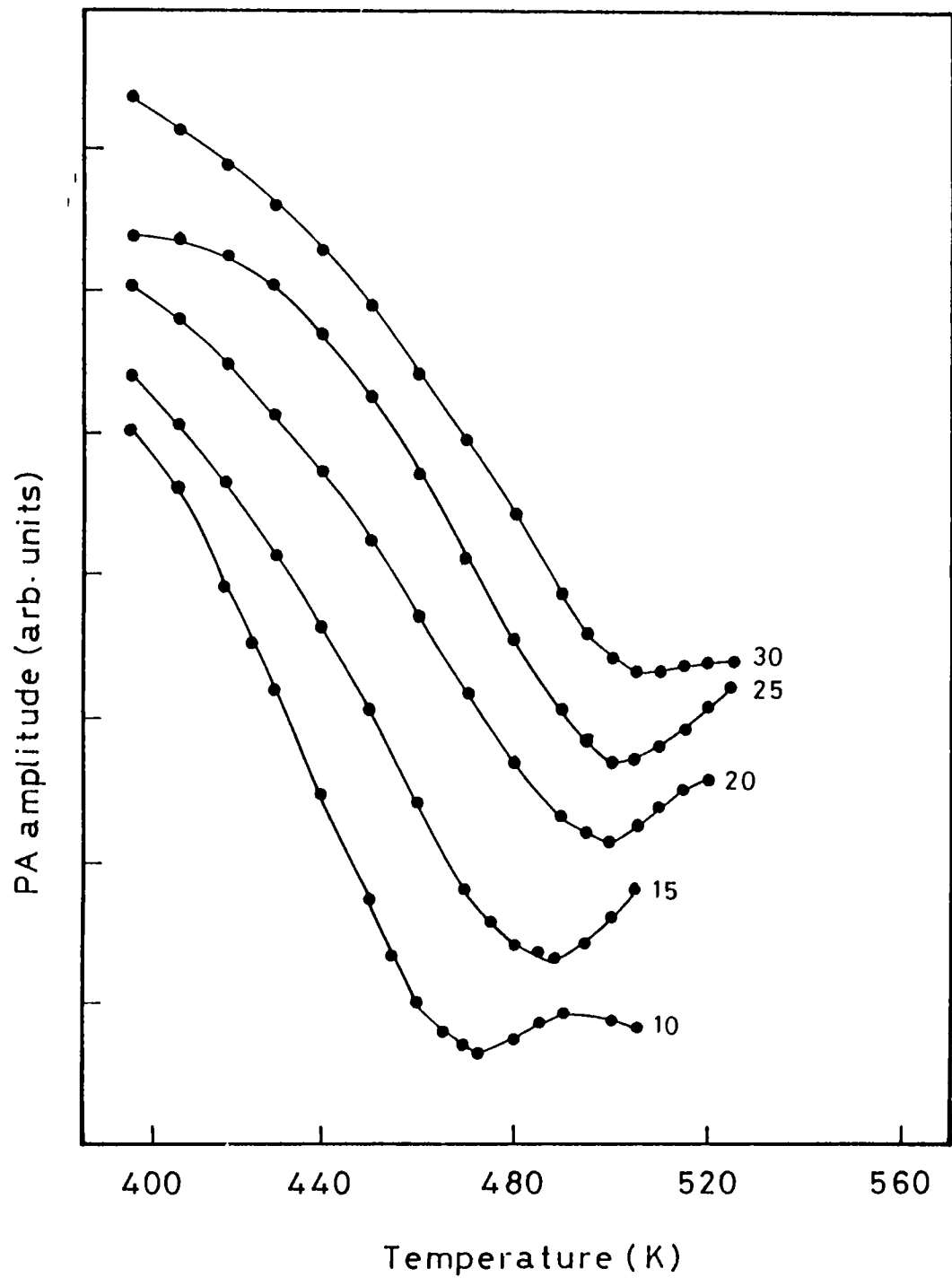


Fig.4.12 Variation of PA amplitude with temperature for $As_xSb_{20}Se_{80-x}$ glasses. The x values are noted on the curves.

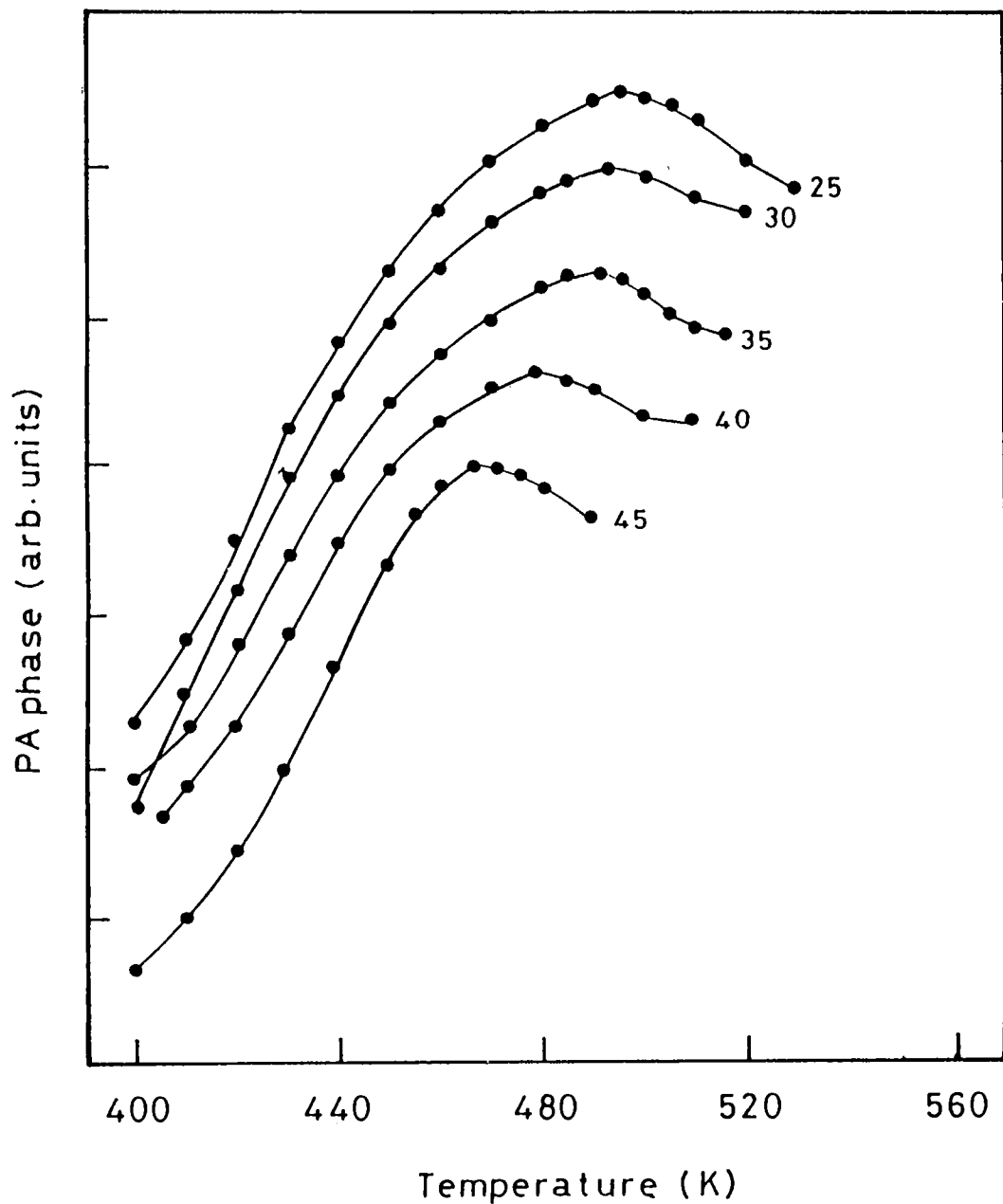


Fig.4.13 Variation of PA phase with temperature for $As_xSb_5Se_{95-x}$ glasses. The x values are noted on the curves.

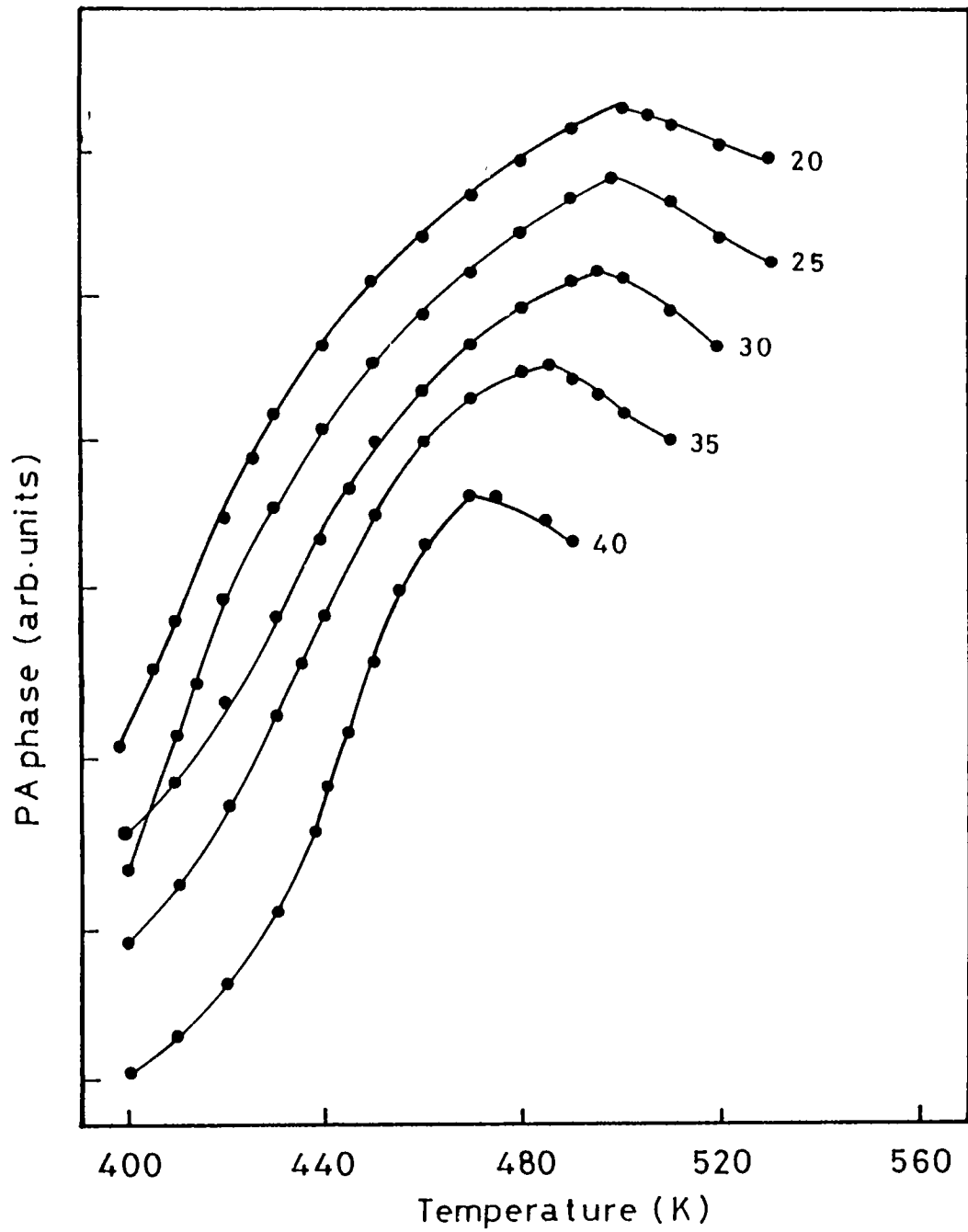


Fig.4.14 Variation of PA phase with temperature for $\text{As}_x\text{Sb}_{10}\text{Se}_{90-x}$ glasses. The x values are noted on the curves.

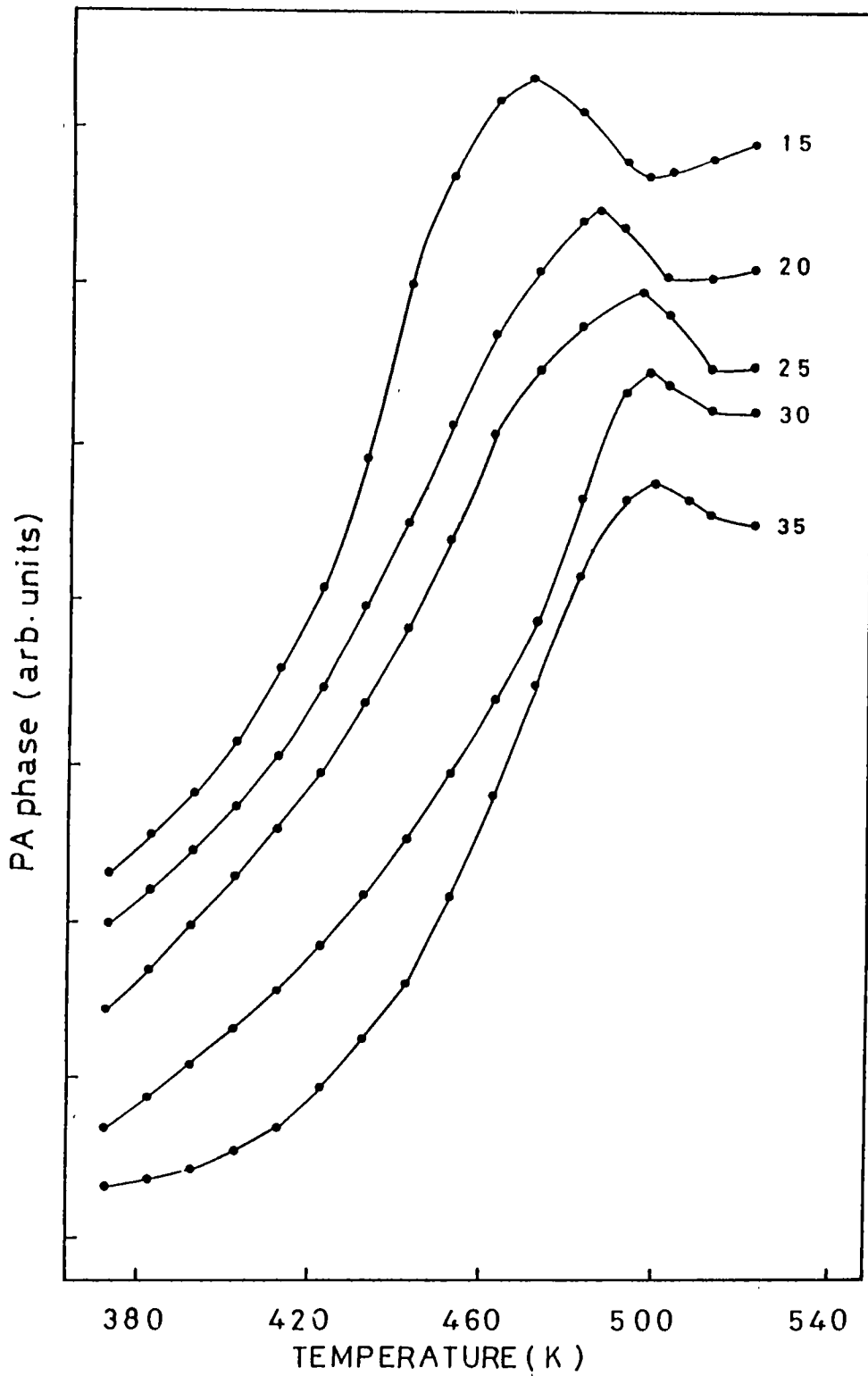


Fig.4.15 Variation of PA phase with temperature for $As_xSb_{15}Se_{85-x}$ glasses. The x values are noted on the curves.

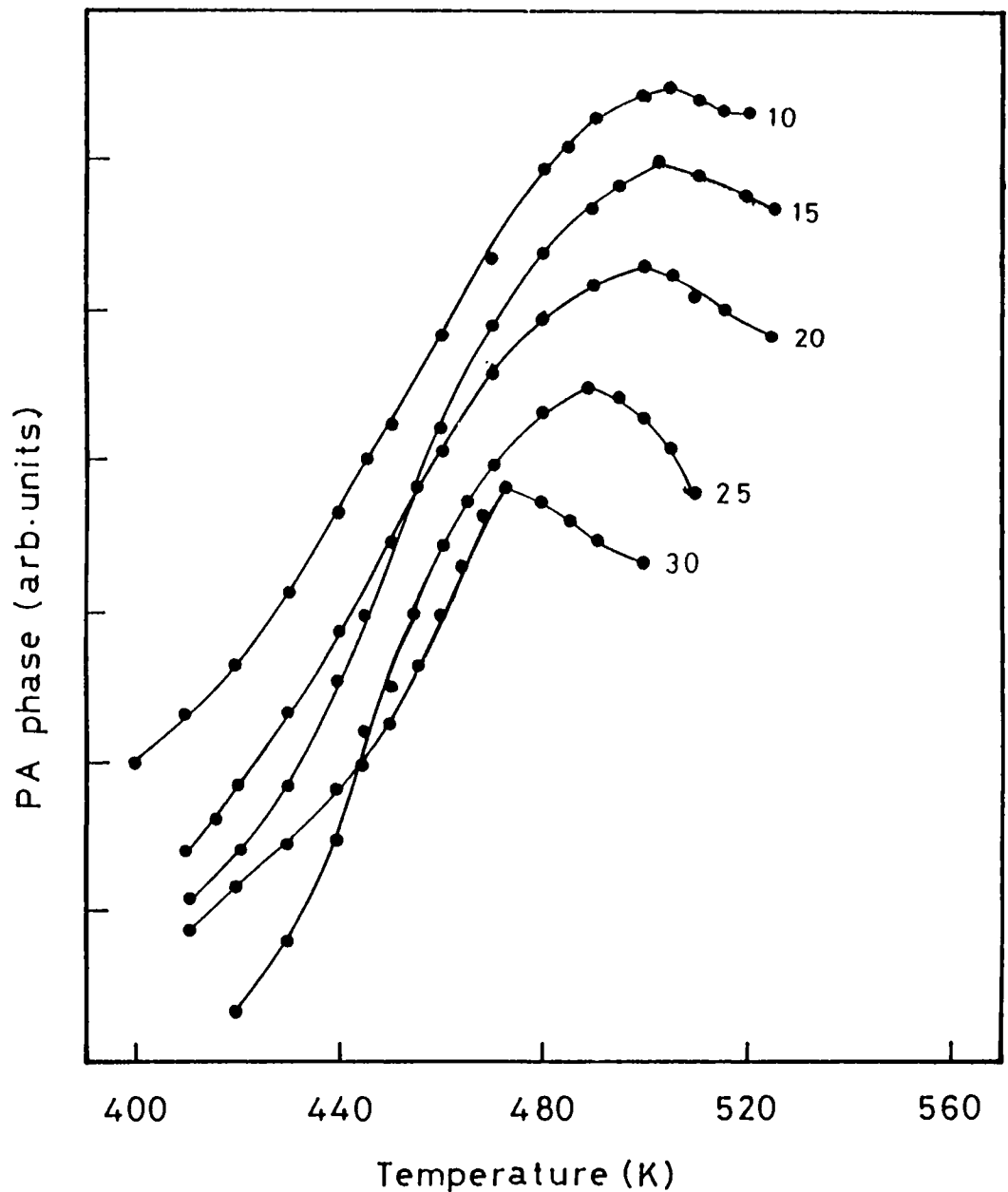


Fig.4.16 Variation PA phase with temperature for $As_xSb_{20}Se_{80-x}$ glasses. The x values are noted on the curves.

converted into pressure waves. Hence the PA phase delay is maximum at T_g . The T_g values obtained by the amplitude and phase measurements are exactly the same. The T_g values of $As_xSb_{15}Se_{85-x}$ with $15 \leq x \leq 35$ and some of the $(As,Sb)_{40}Se_{60}$ compositions have been reported earlier [25] using differential scanning calorimetry (DSC). The T_g values obtained using PA technique are slightly higher than these reported values using DSC. This could be attributed to the difference in the preparative conditions and heating rates used for the investigations. The present investigations prove the use of PA technique as a calorimetric tool to investigate the glass transition temperature of semiconducting glasses.

The variation of glass transition temperature with composition parameter x for the four groups of As-Sb-Se glasses is shown in Fig.4.17. It is observed that for a particular Sb concentration, as the As concentration increases (ie., Se concentration decreases) T_g increases gradually and shows a marked change in its rate of increase at the stoichiometric composition at which the As content and Sb content together is 40 atomic percent. The rate of increase is higher for compositions with $(x+y) < 40$ than for those with $(x+y) > 40$. With the stoichiometric composition as the reference, glasses with more than 60 at. % of Se are referred to as Se-rich glasses and those with 40 at. % of As are referred to as As-rich glasses. It is clear from Fig.4.17 that T_g decreases rapidly for the Se-rich glasses and increases slightly for the As-rich glasses. According to CON model, at the stoichiometric composition the formation of heteropolar bonds are favoured over the formation of homopolar bonds. Based on the same model the Stoichiometric compositions of the As-Sb-Se system can be pictured to be made up of cross linked three-dimensional structural units of As_2Se_3 and Sb_2Se_3 . As the As content in the glass is increased from 60 at. %, some of the original As_2Se_3 structural units are replaced by Se atoms. Se is generally found

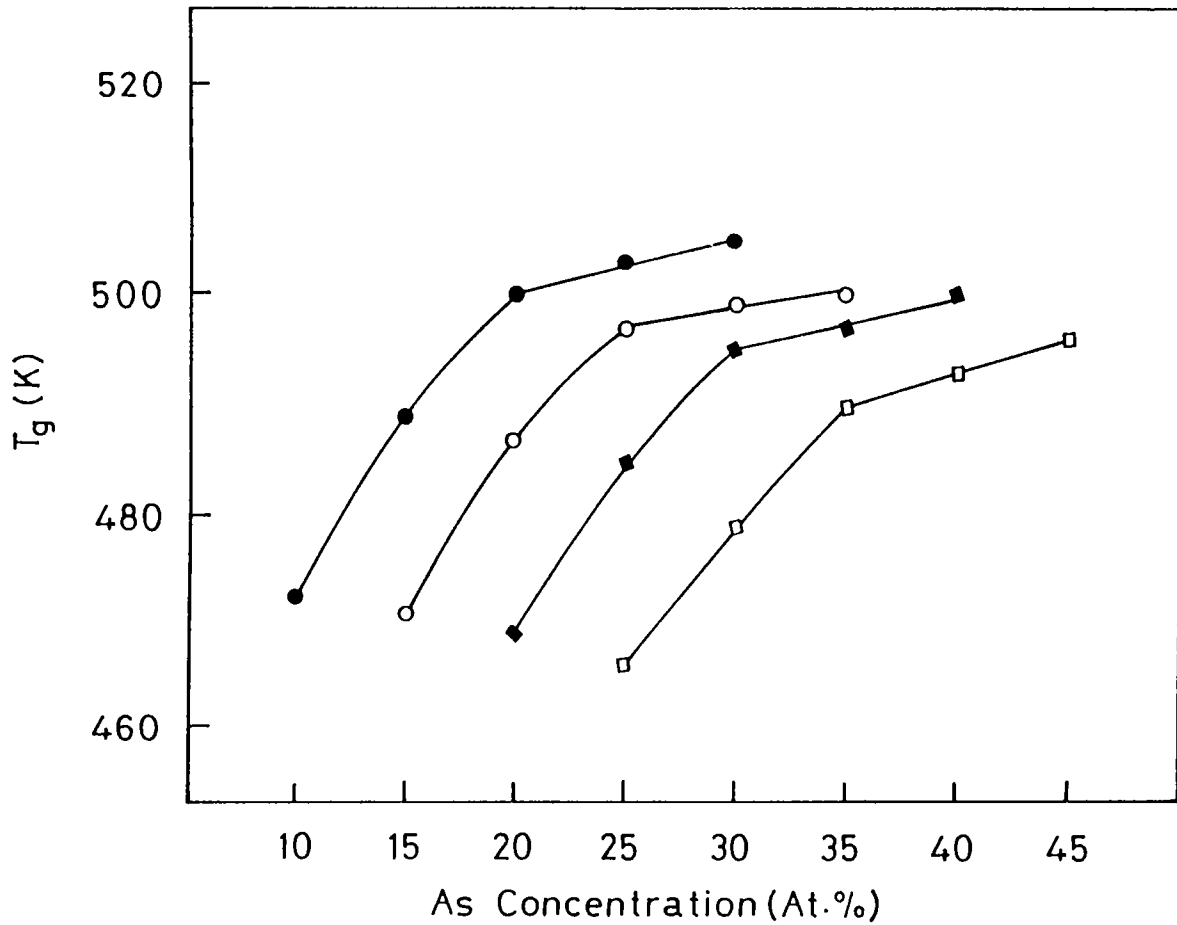


Fig.4.17 Variation of glass transition temperature with As concentration for As-Sb-Se glasses.

(□) $As_xSb_5Se_{95-x}$, (■) $As_xSb_{10}Se_{90-x}$,
 (○) $As_xSb_{15}Se_{85-x}$ and (●) $As_xSb_{20}Se_{80-x}$

in two-fold coordination. Thus, based on the lower coordination number and lower bond energy, the steep decrease of T_g of Se-rich glasses can be understood. For As-rich glasses, some of the As_2Se_3 structural units are replaced by As which is generally found in three-fold coordination, which registers a slight increase of T_g with increasing As content.

The variation of T_g with Sb concentration for the stoichiometric compositions is shown in Fig.4.18. A slight increase in T_g as the Sb concentration is varied from 5 to 20 at. % has been observed. With increase in Sb content for the stoichiometric glasses, some of the original As_2Se_3 structural units are replaced by Sb_2Se_3 units. Since As and Sb are isovalent, a drastic change in T_g is not expected with increase of Sb content. The observed increase in T_g is probably due to the increase in the effective molecular weight with increase in Sb concentration and more ionic character of Sb-Se bonds compared to As-Se bonds.

4.6 Temperature dependence of thermal diffusivity of $As_xSb_{15}Se_{85-x}$ glasses

Measurements of the temperature dependence of thermal diffusivity α of $As_xSb_{15}Se_{85-x}$ glasses with $15 \leq x \leq 35$ have been carried out using PA technique. The measurements have been done upto the glass transition temperature determined using PA technique. The high temperature PA cell has been used for these measurements, the details of which are given in chapter II. The thermal diffusivity α is determined by measuring the variation of PA signal phase of a thick reference sample and that of the experimental samples as described earlier. The experiment is repeated at fixed temperatures at regular temperature intervals and in each case α is calculated by the same procedure.

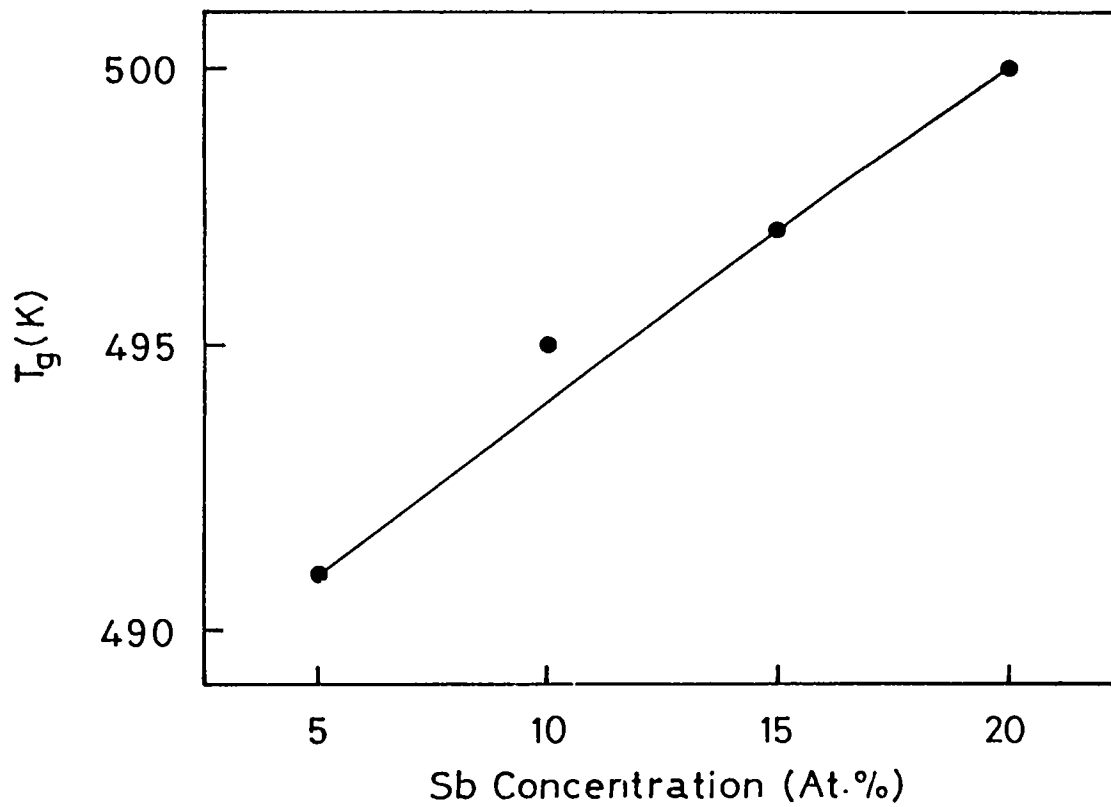


Fig.4.18 Variation of glass transition temperature with Sb concentration for the stoichiometric compositions of the As-Sb-Se glasses.

The variation of thermal diffusivity as a function of temperature for $\text{As}_x\text{Sb}_{15}\text{Se}_{85-x}$ glasses with $15 \leq x \leq 35$ are shown in Fig.4.19. The thermal diffusivity decreases as the temperature is increased and shows a sharp decrease at T_g in all cases. As the temperature increases there will be a decrease in the phonon mean free path due to an increase in collision rates leading to a decrease in thermal conductivity. As T_g is approached the mean free path has decreased substantially which in turn retards the thermal transport to the maximum extent. At T_g the anomalous increase taking place in the specific heat will also be reflected in thermal diffusivity. Both these effects work in the same direction which results in the observed decrease in α at T_g .

Fig.4.20 shows the variation of thermal diffusivity α of $\text{As}_x\text{Sb}_{15}\text{Se}_{85-x}$ glasses with composition parameter x at room temperature and at T_g . The variation in thermal diffusivity shows a marked change at the stoichiometric composition where the average coordination number $\langle r \rangle = 2.4$ both at room temperature and at T_g . This observation can be attributed to the mechanical stiffening of the network at the critical composition corresponding to an average coordination number $\langle r \rangle = 2.4$ due to threshold percolation of rigidity and a corresponding threshold in the internal stress [14,15,16]. The present result indicate that the critical coordination is fixed as the glass is formed at T_g and the network rigidity is kept intact at all temperatures below the glass transition temperature.

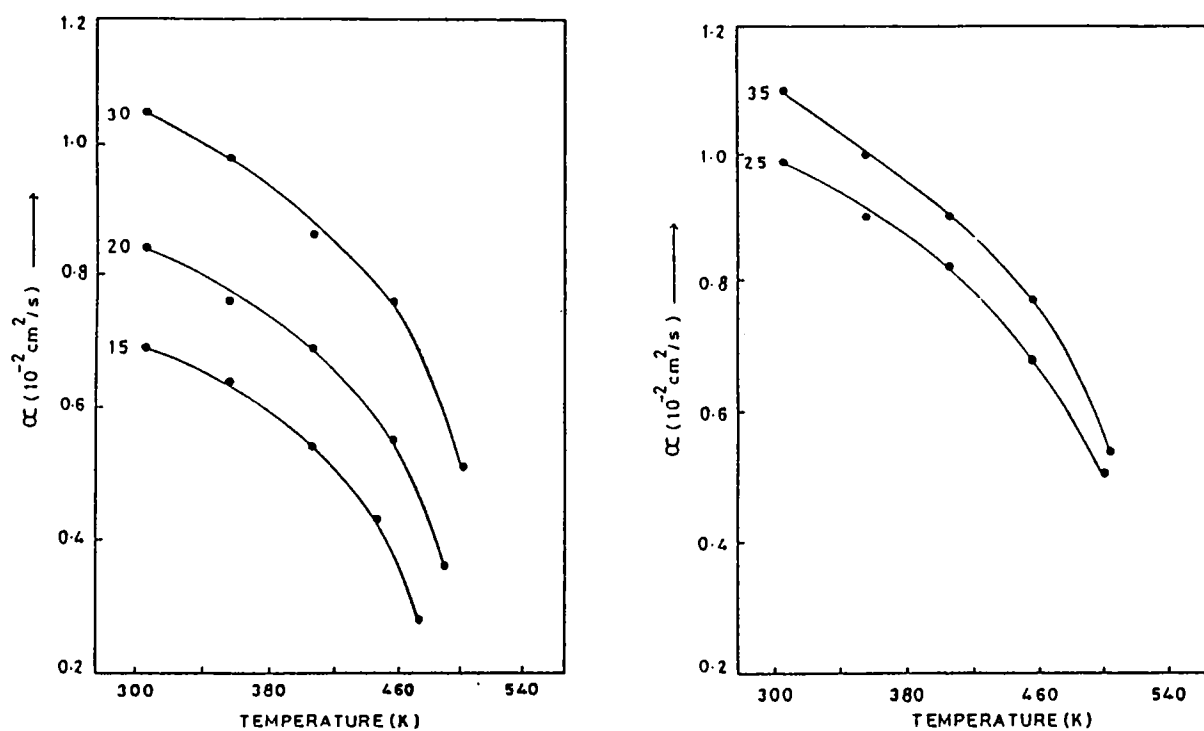


Fig.4.19 Variation of thermal diffusivity with temperature for $\text{As}_x\text{Sb}_{15}\text{Se}_{85-x}$ glasses. The x values are noted on the curves.

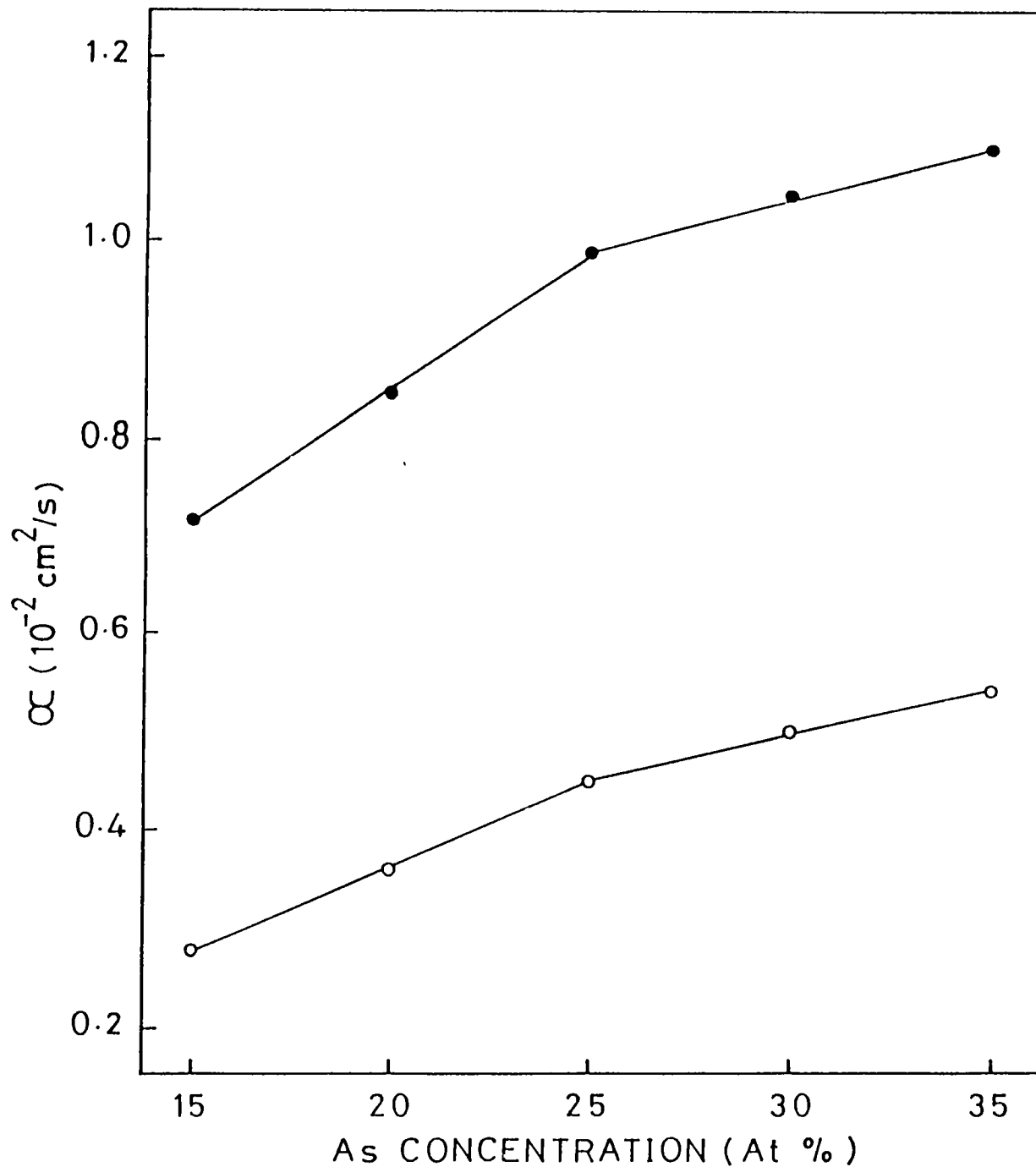


Fig.4.20 Variation of thermal diffusivity with As concentration for $\text{As}_x\text{Sb}_{15}\text{Se}_{85-x}$ glasses; (●) at room temperature and (○) at glass transition temperature.

REFERENCES

1. W. J. Parker, R. J. Jenkins, C. P. Butler, G. L. Abdot, J. Appl. Phys., **32**, 1679 (1961)
2. B. Abeles, G. D. Cody, D. S. Beers, J. Appl. Phys., **31**, 1585 (1960)
3. A. Rosencwaig, Photoacoustics and Photoacoustic Spectroscopy (Wiley-New York 1980)
4. A. Rosencwaig and A. Gersho, J. Appl. Phys., **47**, 64 (1976)
5. M. J. Adams and G. F. Kirkbright, Analyst, **102**, 678 (1977)
6. M. J. Adams and G. F. Kirkbright, Analyst, **102**, 281 (1977)
7. K. Yamashita, H. Kasahara, K. Yamamoto and K. Abe, Jpn. J. Appl. Phys., **21**, Suppl. 21-23, 107 (1982)
8. U. Zammit, M. Marinelli, F. Scudieri and S. Martellucci, High Temp-High Pressures, **18**, 551 (1986)
9. R. T. Swimm, Appl. Phys. Lett., **42**, 955 (1983)
10. A. Lachaine and P. Poulet, Appl. Phys. Lett., **45**, 953 (1984)
11. K. N. Madhusoodanan, Mini. R. Thomas and J. Philip, J. Appl. Phys., **62**(4), 1162 (1987)
12. P. Charpentier, F. Lepoutre and L. Bertrand, J. Appl. Phys., **53**, 608 (1982)
13. A. Lachaine, J. Appl. Phys., **57**, 5075 (1985)

14. J. C. Phillips, *J. Non-Cryst. Solids*, **34**, 153 (1979)
15. M. F. Thorpe, *J. Non-Cryst. Solids*, **57**, 355 (1983)
16. J. C. Phillips and M. F. Thorpe, *Solid State Commun.*, **53**, 699 (1985)
17. U. Bengtzelius, W. Götze and A. Sjolander, *J. Phys. C*, **17**, 5815 (1984)
18. H. De Raedt and W. Götze, *J. Phys. C*, **19**, 2607 (1986)
19. W. Götze, in *Amorphous and Liquid Materials*, ed: by E. Luscher, G. Fritsch, G. Jacucci (M. Nijhoff Publishers, Dodrecht 1987) p.34
20. E. Leutheusser, *Phys. Rev.A***29**, 2965 (1984)
21. T. Somasundaram, P. Ganguly and C. N. R. Rao, *J. Phys. C*, **19**, 2137 (1986)
22. P. S. Bechthold, M. Campagna and T. Schober, *Solid State Commun.*, **36**, 225 (1980)
23. J. Etxebarria, S. Uriate, J. Fernandez, M. J. Tello and A. J. Cuevas, *J. Phys. C*, **17**, 6601 (1984)
24. P. Korpiun and R. Tilgner, *J. Appl. Phys.*, **51**, 6115 (1980)
25. Sudha Mahadevan, A. Giridhar and A. K. Singh, *J. Non-Cryst. Solids*, **88**, 11 (1986)
26. J. Isaac and J. Philip, *J. Appl. Phys.*, **69**, 7765 (1991)

CHAPTER V

OPTICAL ENERGY GAP AND THERMAL DIFFUSIVITY IN As-Te-Se GLASSES

5.1 Introduction

The freedom associated with lifting the restrictions of crystalline symmetry allows large deviations from stoichiometric compositions in non-crystalline semiconductors and many new structural configurations. This freedom is often the origin of unique properties that open new possibilities for applications. The chalcogenide glasses form one group of the range of amorphous semiconductors and are distinguished from other groups in that they are solid, as opposed to liquid and do not contain oxygen. They are easily produced in bulk from melt and do not require the more rapid quenching processes entailed in thin film production.

Studies on semiconducting chalcogenide glasses based on As and Se have received considerable attention because of their photoconducting and switching properties. Though there are reports on the effect of addition of Cu, Ag, Sn, Bi, Mg, Ga etc. on the electrical properties of As_2Se_3 [1-4], there are not many reports on the effect of the replacement of Se by other elements on various physical properties. The interaction of the components of the As-Se-Te system has been investigated mainly along the As_2Se_3 - As_2Te_3 tie line. Fig.5.1 shows the glass formation region for As-Se-Te compositions obtained by quenching melts in air [5]. A high crystallization ability is possessed by glasses whose compositions lie on the As_2Se_3 - As_2Te_3 tie line and also glasses considerably richer in tellurium. Results of measurements of the effects of As and Te on the crystallization and optical band gap of selenium [6], the dielectric and photoelectric properties of glasses of the As_2Se_3 - As_2Te_3 system

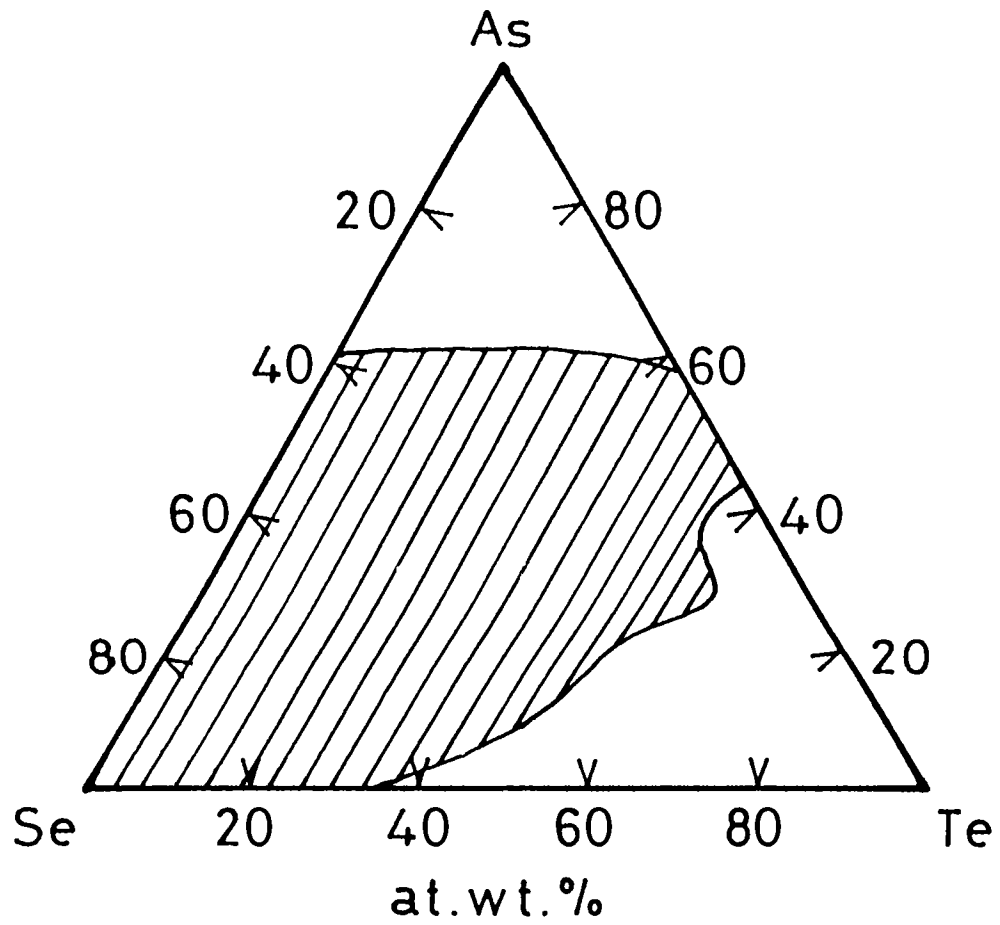


Fig.5.1 Glass forming region of As-Te-Se system.

[7], the electrical conductivity, thermoelectric power and the optical absorption of selected glasses and melts in $As_2Se_9-As_2Te_9$ system have been reported earlier [8]. But none of these reports are based on a systematic investigation of the effect of replacement of the basic constituent atoms by others. The results of our work on the composition dependence of optical band gap E_0 and thermal diffusivity α of As-Te-Se glasses are described in this chapter.

5.2 Experimental details

The compositions under study in this work can be categorized into three groups depending on the Te content as $As_xTe_5Se_{95-x}$, $As_xTe_{10}Se_{90-x}$ (with $x = 30, 35, 40, 45$ and 50) and $As_{40}(Te,Se)_{60}$ with Te content varying from 0 to 20 at.%, which are the stoichiometric compositions of the As-Te-Se system. Bulk glasses of these compositions have been prepared by the well established melt-quenching technique as described earlier in chapter III. The amorphous nature of the samples has been checked by X-ray diffractometry.

The single beam PA spectrometer used for the present investigations is already described in chapter II. The optical band gap E_0 is determined by measuring the variation of the normalized PA signal amplitude with incident wavelength. The chopping frequency used is 22 Hz for absorption measurements. Powdered samples have been used for recording the PA absorption spectra. The PA spectrum obtained for a highly absorbing carbon black sample is used to normalize the PA spectrum obtained for each sample.

The normalized PA spectra of $As_xTe_5Se_{95-x}$, $As_xTe_{10}Se_{90-x}$ (with $x = 30, 35, 40, 45$ and 50) and

$\text{As}_{40}(\text{Te},\text{Se})_{60}$ glasses are shown in Figs. 5.2 to 5.4. The optical band gap E_0 is determined from these spectra as described in chapter III. The optical band gap has also been determined using UV-Vis-NIR spectrophotometer. The E_0 values determined for each sample using PA technique as well as UV-Vis-NIR spectrophotometry are tabulated in Table 5.1.

The variation of the PA signal amplitude with chopping frequency is measured to determine the thermal diffusivity α of each sample. Samples of appropriate thickness have been prepared in the form of thin discs from single pieces for these measurements. Each sample is mounted on a thermally thick backing material during measurements. The light beam used for these measurements need not be monochromatic. At first, the variation of the PA signal amplitude with chopping frequency is obtained for a thick sample (thickness ≈ 1 mm) which is taken as the reference sample. This reference sample is thermally thick in the entire chopping frequency range used in these measurements. Then the measurement is repeated with the experimental samples of appropriate thickness such that the sample is thermally thin for $f < f_c$ and thermally thick for $f > f_c$, where f_c is the characteristic frequency. At $f = f_c$, the sample goes from a thermally thin regime to a thermally thick regime. For $f > f_c$, the PA signal is independent of the thermal properties of the backing medium.

The log-log plots of the PA signal amplitude versus chopping frequency for the three groups of samples are shown in Figs. 5.5 to 5.7, along with that of the reference sample. The slope of the curve changes at the characteristic frequency f_c for the experimental samples because in the thermally thin region the heat generated at the the surface of the sample is propagated into the backing medium for $f < f_c$. For $f > f_c$ the slope of the curve is the same as that of the reference sample.

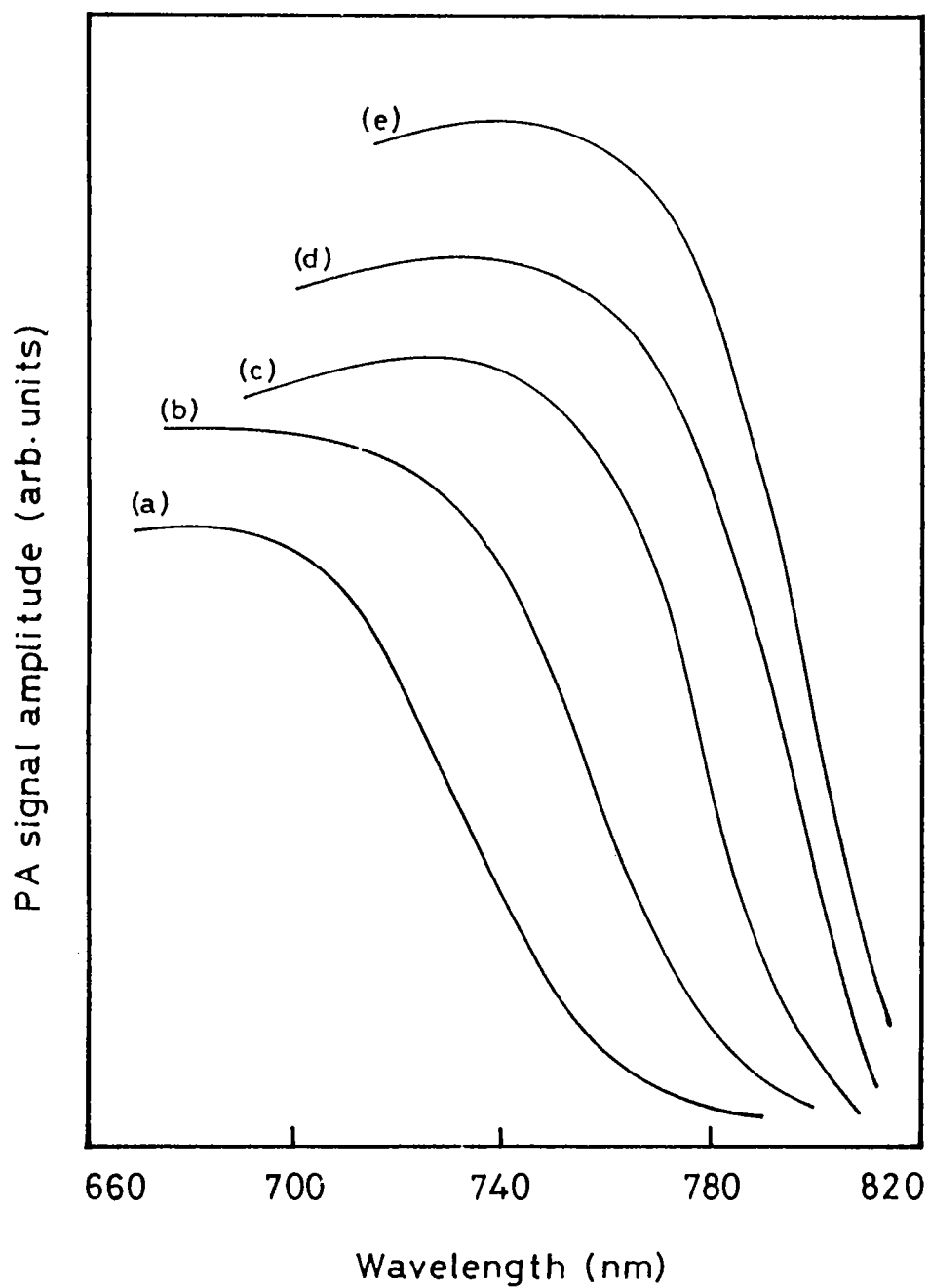


Fig.5.2 PA spectra of $\text{As}_x\text{Te}_5\text{Se}_{95-x}$ glasses.
 (a) $\text{As}_{30}\text{Te}_5\text{Se}_{65}$, (b) $\text{As}_{35}\text{Te}_5\text{Se}_{60}$,
 (c) $\text{As}_{40}\text{Te}_5\text{Se}_{55}$, (d) $\text{As}_{45}\text{Te}_5\text{Se}_{50}$,
 (e) $\text{As}_{50}\text{Te}_5\text{Se}_{45}$

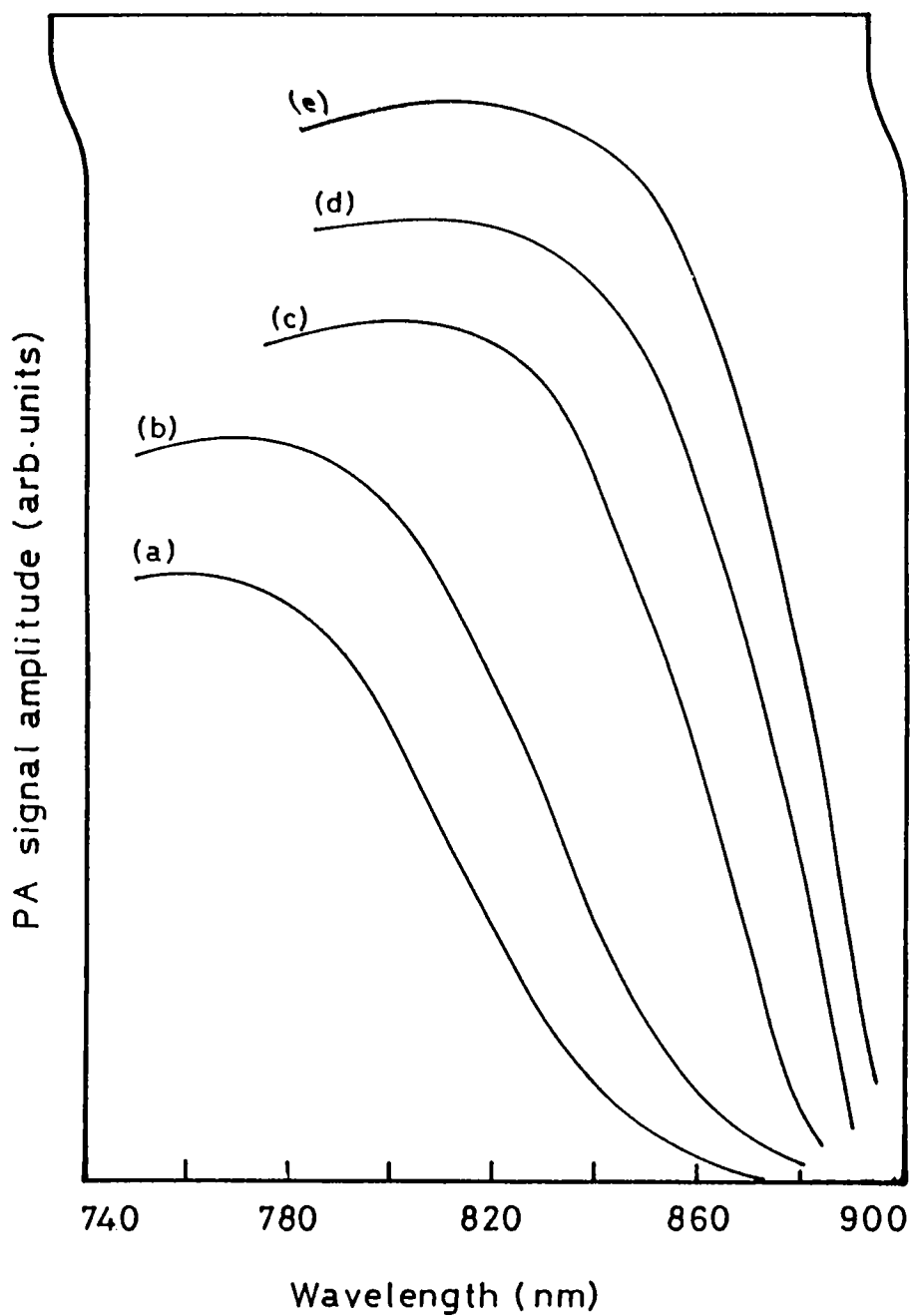


Fig.5.3 PA spectra of $\text{As}_x\text{Te}_{10}\text{Se}_{90-x}$ glasses.
 (a) $\text{As}_{30}\text{Te}_{10}\text{Se}_{60}$, (b) $\text{As}_{35}\text{Te}_{10}\text{Se}_{55}$,
 (c) $\text{As}_{40}\text{Te}_{10}\text{Se}_{50}$, (d) $\text{As}_{45}\text{Te}_{10}\text{Se}_{45}$,
 (e) $\text{As}_{50}\text{Te}_{10}\text{Se}_{40}$

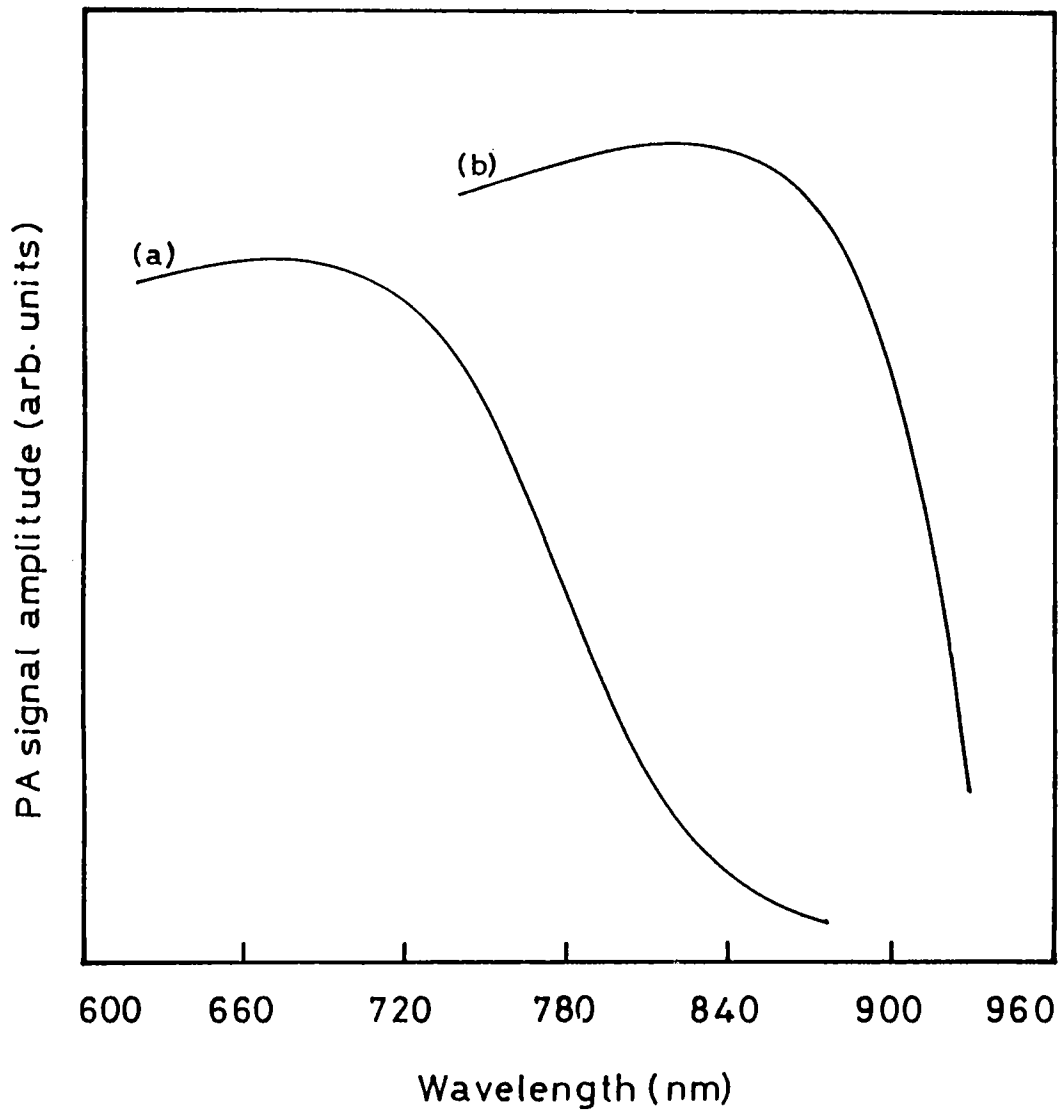


Fig.5.4 PA spectra of As(Te,Se) glasses.
 (a) $As_{40}Se_{60}$, (b) $As_{40}Te_{15}Se_{45}$

Table 5.1 The glass composition, optical band gap E_o measured using PA technique and UV-Vis-NIR spectrophotometry.

No.	Composition As:Te:Se	E_o (eV) PA technique	E_o (eV) UV-Vis-NIR
1.	30:5:65	1.78	1.77
2.	35:5:60	1.72	1.71
3.	40:5:55	1.66	1.65
4.	45:5:50	1.65	1.64
5.	50:5:45	1.63	1.60
6.	30:10:60	1.62	1.62
7.	35:10:55	1.56	1.56
8.	40:10:50	1.50	1.50
9.	45:10:45	1.49	1.48
10.	50:10:40	1.48	1.47
11.	40:00:60	1.78	1.76
12.	40:15:45	1.46	1.44

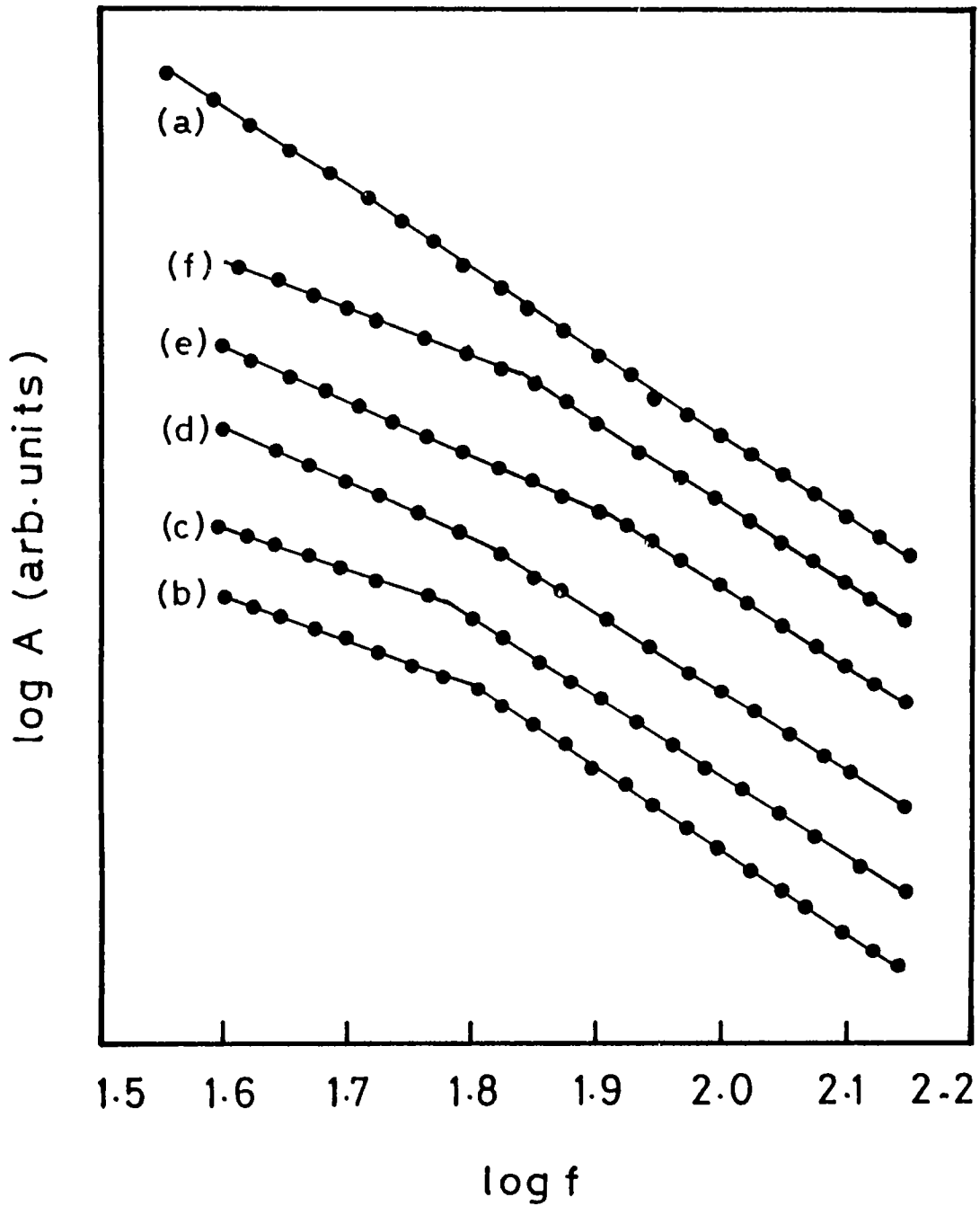


Fig.5.5 Log-log plots of variation of PA signal amplitude with chopping frequency for $\text{As}_x\text{Te}_5\text{Se}_{95-x}$ glasses.
 (a) Reference sample, (b) $\text{As}_{30}\text{Te}_5\text{Se}_{65}$,
 (c) $\text{As}_{35}\text{Te}_5\text{Se}_{60}$, (d) $\text{As}_{40}\text{Te}_5\text{Se}_{55}$,
 (e) $\text{As}_{45}\text{Te}_5\text{Se}_{50}$, (f) $\text{As}_{50}\text{Te}_5\text{Se}_{45}$

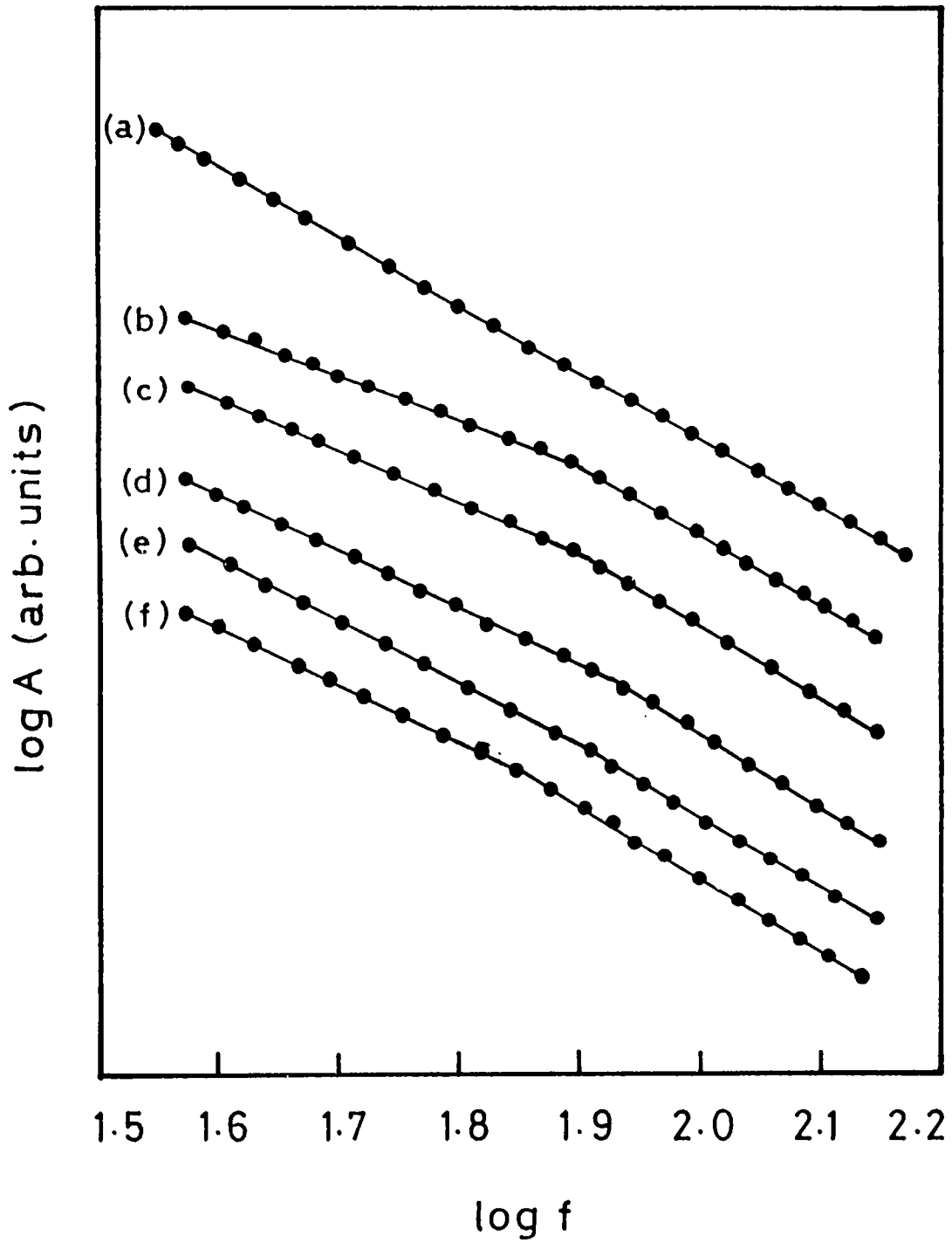


Fig.5.6 Log-log plots of variation of PA signal amplitude with chopping frequency for $\text{As}_x\text{Te}_{10}\text{Se}_{90-x}$ glasses.
 (a) Reference sample, (b) $\text{As}_{30}\text{Te}_{10}\text{Se}_{60}$,
 (c) $\text{As}_{35}\text{Te}_{10}\text{Se}_{55}$, (d) $\text{As}_{40}\text{Te}_{10}\text{Se}_{50}$,
 (e) $\text{As}_{45}\text{Te}_{10}\text{Se}_{45}$, (f) $\text{As}_{50}\text{Te}_{10}\text{Se}_{40}$

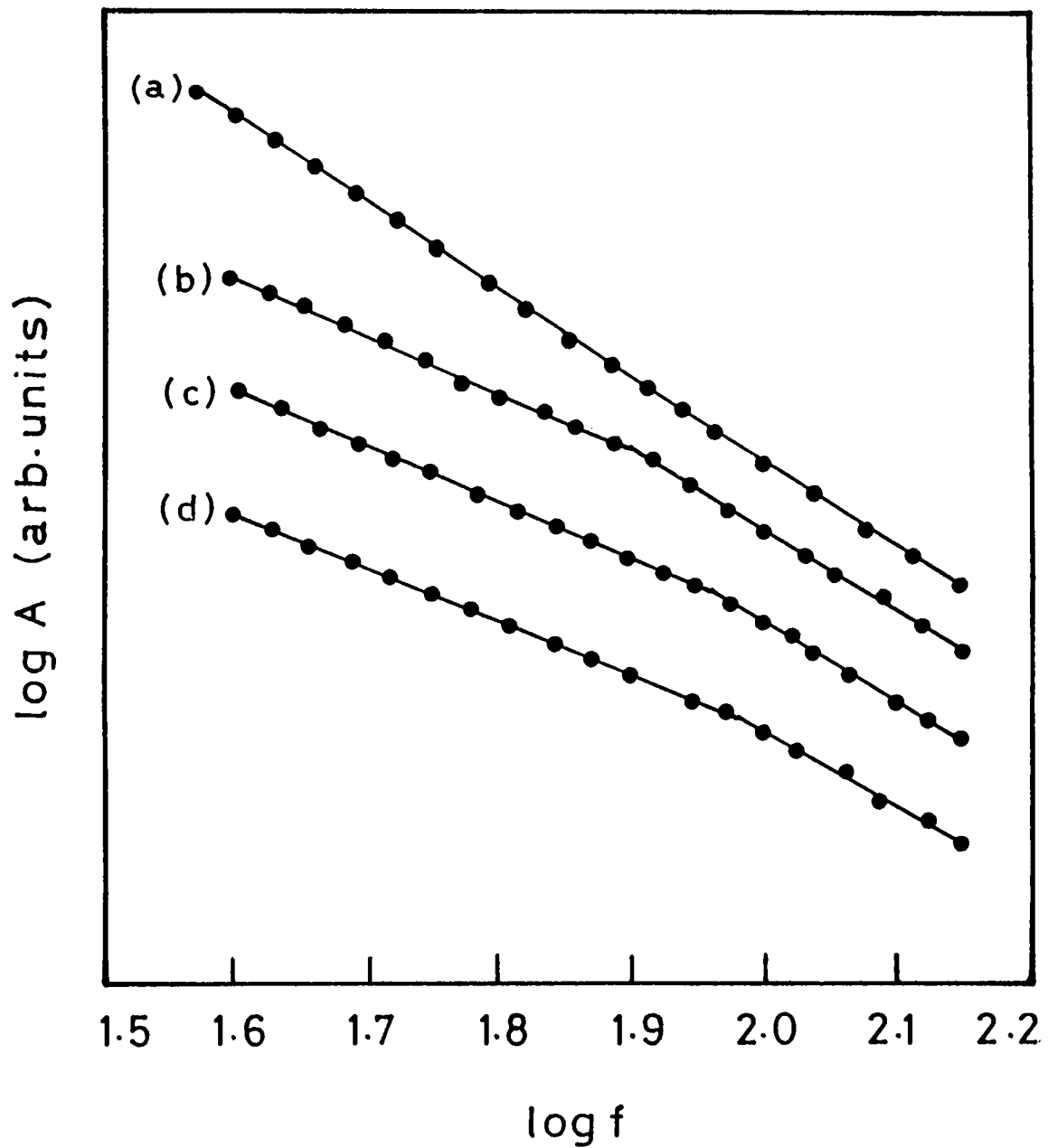


Fig.5.7 Log-log plots of variation of PA signal amplitude with chopping frequency for $\text{As}_{40}(\text{Te},\text{Se})_{60}$ glasses.
 (a) Reference sample, (b) $\text{As}_{40}\text{Se}_{60}$,
 (c) $\text{As}_{40}\text{Te}_{15}\text{Se}_{45}$, (d) $\text{As}_{40}\text{Te}_{20}\text{Se}_{40}$

The values of f_c determined from these plots are used to calculate the thermal diffusivity of the samples given by $\alpha = f_c l^2$, where l is the sample thickness [9]. Table 5.2 shows the sample, average coordination number, characteristic frequency sample thickness l and thermal diffusivity of the samples investigated.

5.3 Composition dependence of optical band gap in As-Te-Se system

Fig.5.8 shows the variation of optical band gap with composition parameter x for $As_xTe_5Se_{95-x}$ and $As_xTe_{10}Se_{90-x}$ (with $x = 30, 35, 40, 45$ and 50) systems. As can be seen from the figure, the optical band gap decreases with increase in As content. For a particular Te concentration, with increase in As content the optical band gap decreases gradually and shows a marked change in its rate of decrease at the stoichiometric composition at which the As content is 40 at. %. The rate of decrease is higher for compositions with $x < 40$ than for those with $x > 40$. Fig.5.9 shows the variation of the optical band gap with Te concentration for the stoichiometric compositions. The optical band gap decreases gradually as the Te concentration is varied from 0 to 15 at. %.

Based on the chemically ordered network model [10], the As-Te-Se system can be described as a completely cross-linked three-dimensional structural units of As_2Se_9 and As_2Te_9 with either As or Se in excess. In Se rich glasses, the network is dominated by Se atom chains and addition of As atoms leads to the formation of branching chains on three-fold coordination of As atoms into the basic Se structural units. The two-coordinated Se atoms form $(Se)_n$ chains or $(Se)_6$ rings, and the addition of three-coordinated As atoms will break these chains or rings to satisfy its coordination number and form a

Table 5.2 The glass composition, average coordination number $\langle r \rangle$, characteristic frequency f_c , thickness l and thermal diffusivity α of As-Te-Se glasses.

No.	Composition As:Te:Se	$\langle r \rangle$	f_c (Hz)	l (μm)	α ($\times 10^{-2} \text{ cm}^2/\text{s}$)
1.	30:5:65	2.30	62.81	160	1.61
2.	35:5:60	2.35	76.74	150	1.73
3.	40:5:55	2.40	84.72	150	1.91
4.	45:5:50	2.45	81.28	150	1.83
5.	50:5:45	2.50	69.18	160	1.77
6.	30:10:60	2.30	79.07	150	1.78
7.	35:10:55	2.35	76.03	160	1.95
8.	40:10:50	2.40	85.11	160	2.18
9.	45:10:45	2.45	122.2	130	2.07
10.	50:10:40	2.45	90.99	150	2.05
11.	40:00:60	2.40	79.07	150	1.78
12.	40:15:45	2.40	118.9	140	2.33
13.	40:20:40	2.40	95.94	160	2.46

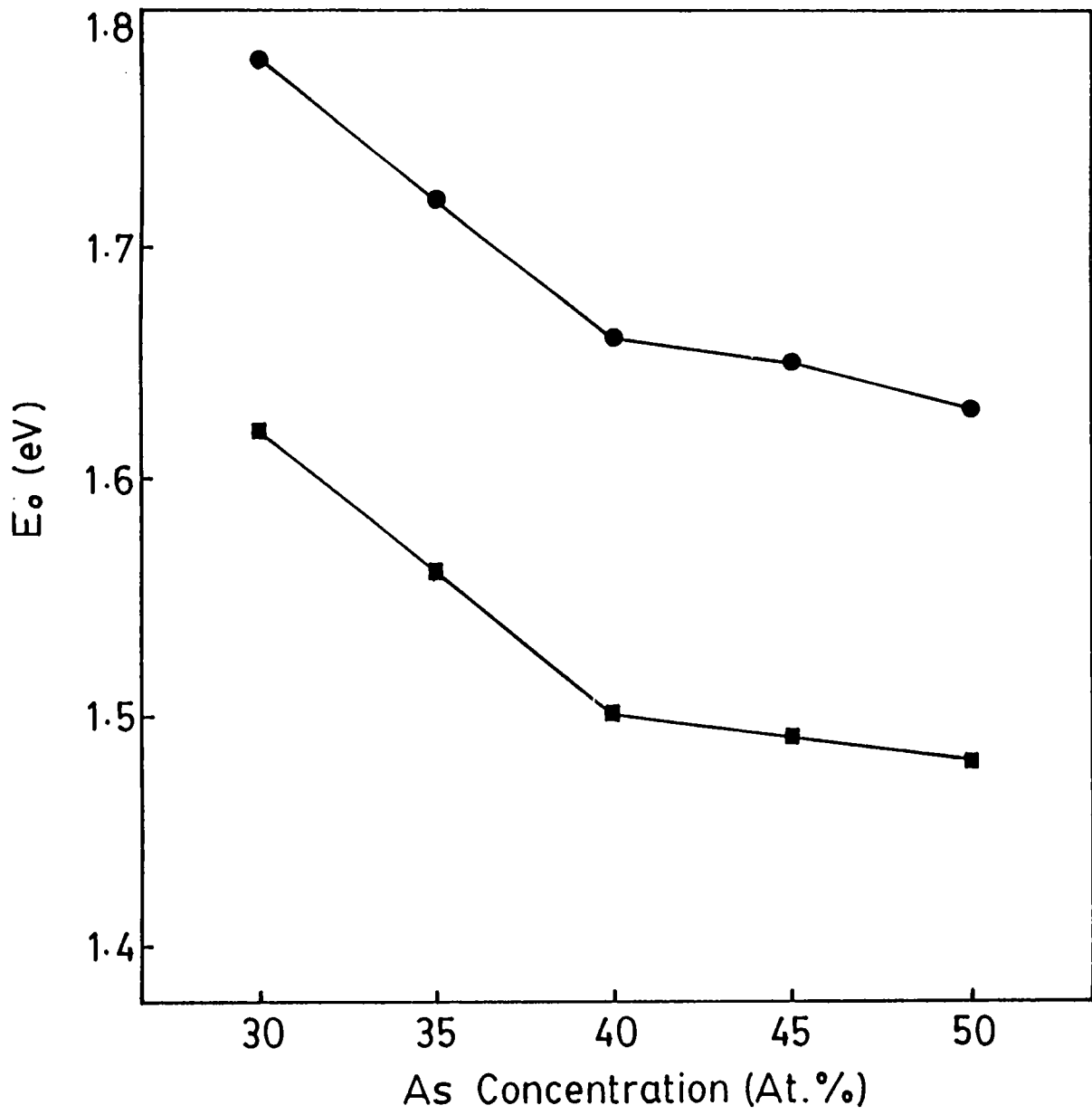


Fig.5.8 Variation of optical band gap (E_o) with As concentration of As-Te-Se glasses.
 (●) $As_xTe_5Se_{95-x}$, (■) $As_xTe_{10}Se_{90-x}$

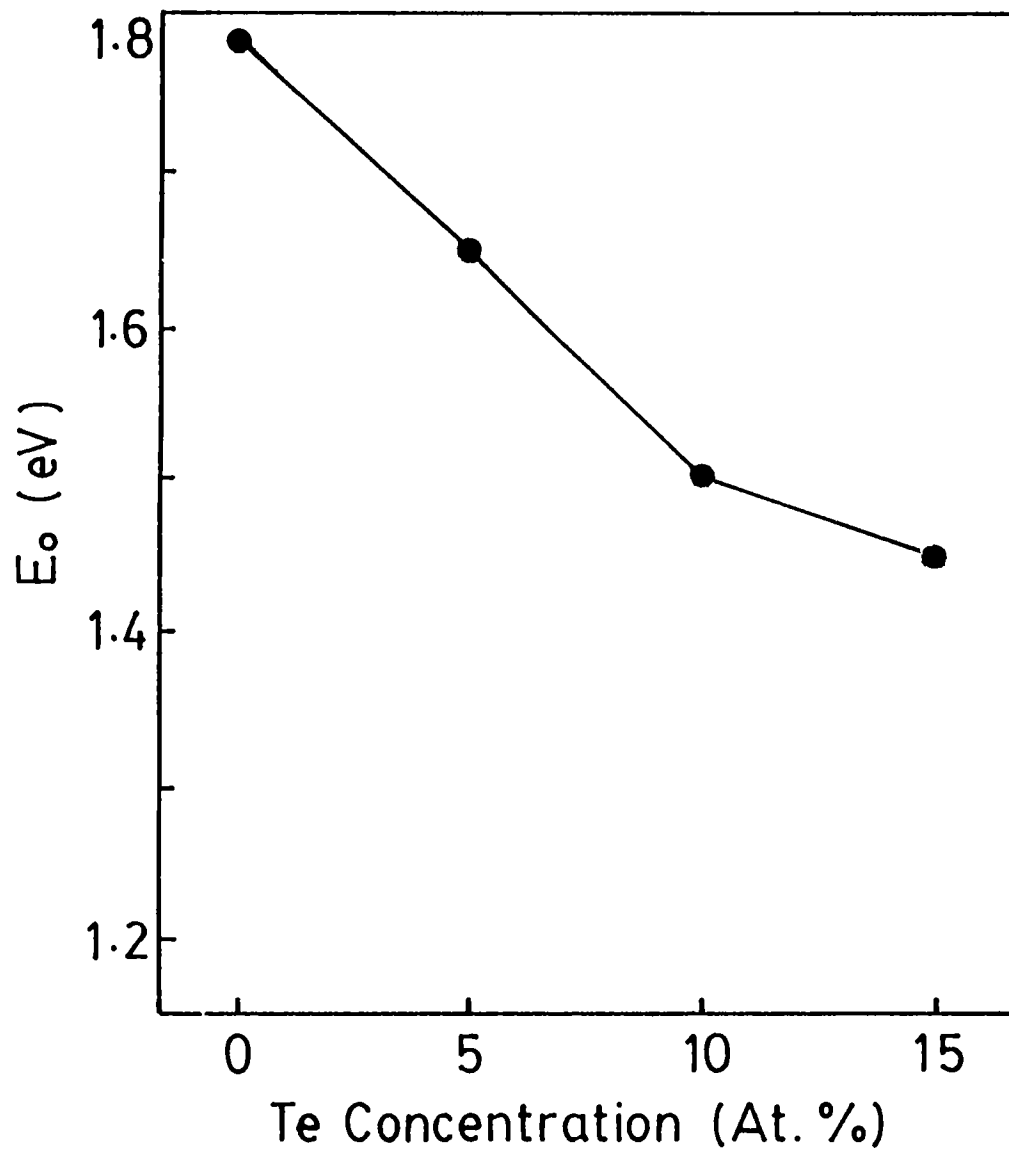


Fig.5.9 Variation of optical band gap (E_o) with Te concentration for the stoichiometric compositions of the As-Te-Se glasses.

large complex atomic group structure in the glass. The introduction of Te into the system leads to the formation of copolymer chains replacing Se chains. Apart from As-As, As-Se and Se-Se bonds in the network, As-Te, Te-Te and Se-Te bonds will also be involved in the formation of the network. The bond energies of As-As, As-Se, As-Te, Se-Te, Se-Se and Te-Te bonds are 46.0, 52.0, 45.4, 54.8, 49.0 and 38.0 kCal/mol, respectively. When As concentration increases, more and more As-Te bonds will be formed in addition to Te-Se and Te-Te bonds. Since the energies of the bonds involving Te on an average less than the bonds involving As and Se alone, this difference will lead to a reduction of the energy of the conduction band edge resulting in a decrease in E_o with increase in As content. Eventhough the system forms an ideal glass at the stoichiometric compositions, with increase in Te concentration the probability for the formation of As-Te bonds increases. Hence the bond energy of the system on an average is reduced which effectively reduces E_o .

5.4 Composition dependence of thermal diffusivity in As-Te-Se system

The variation of thermal diffusivity α with the composition parameter x for $As_xTe_5Se_{95-x}$ and $As_xTe_{10}Se_{90-x}$ (with $x = 30, 35, 40, 45$ and 50) glasses is shown in Fig.5.10. For both sets of glasses the thermal diffusivity shows a threshold maximum at the composition $x = 40$ which corresponds to an average coordination number $\langle r \rangle = 2.4$. Fig.5.11 shows the variation of thermal diffusivity α with Te concentration for the stoichiometric compositions. The thermal diffusivity increases gradually as the Te concentration is increased from 0 to 20 at. %.

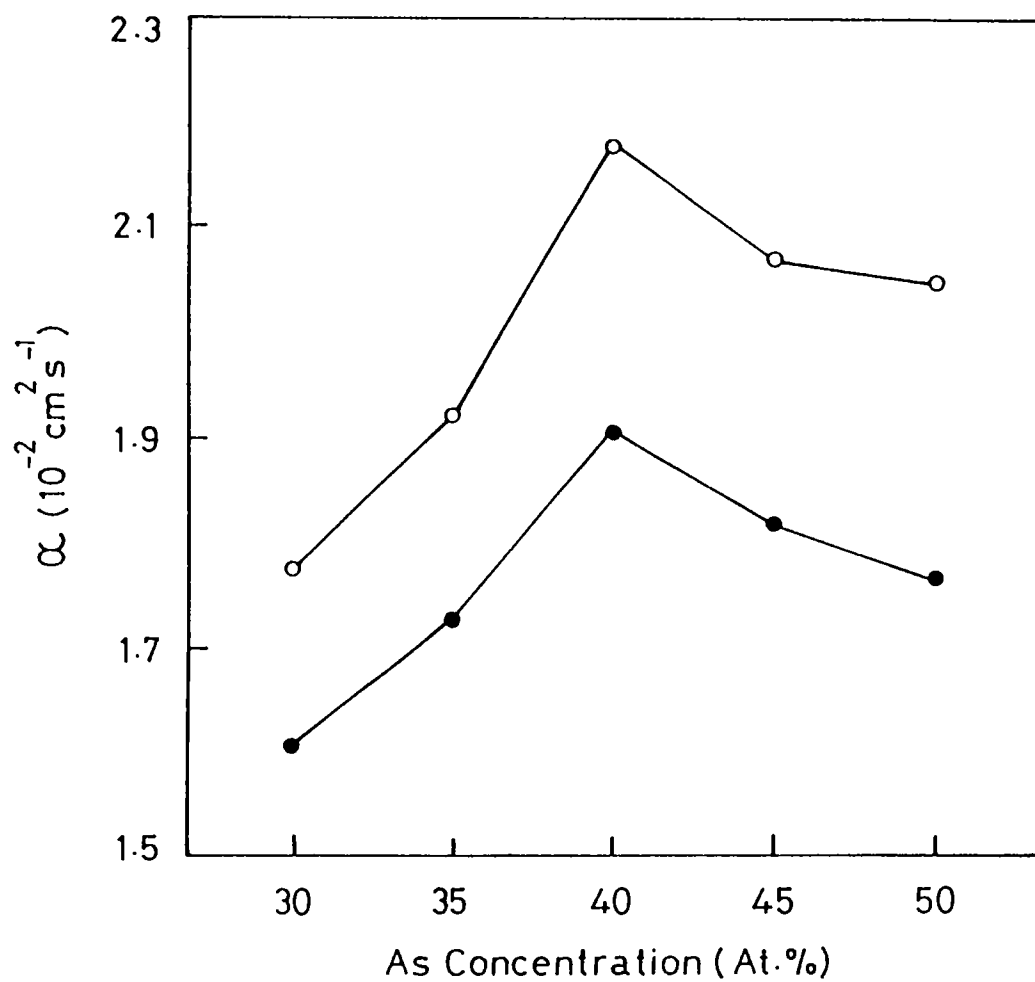


Fig.5.10 Variation of thermal diffusivity (α) with As concentration of As-Te-Se glasses.

(●) $\text{As}_x \text{Te}_5 \text{Se}_{95-x}$, (O) $\text{As}_x \text{Te}_{10} \text{Se}_{90-x}$

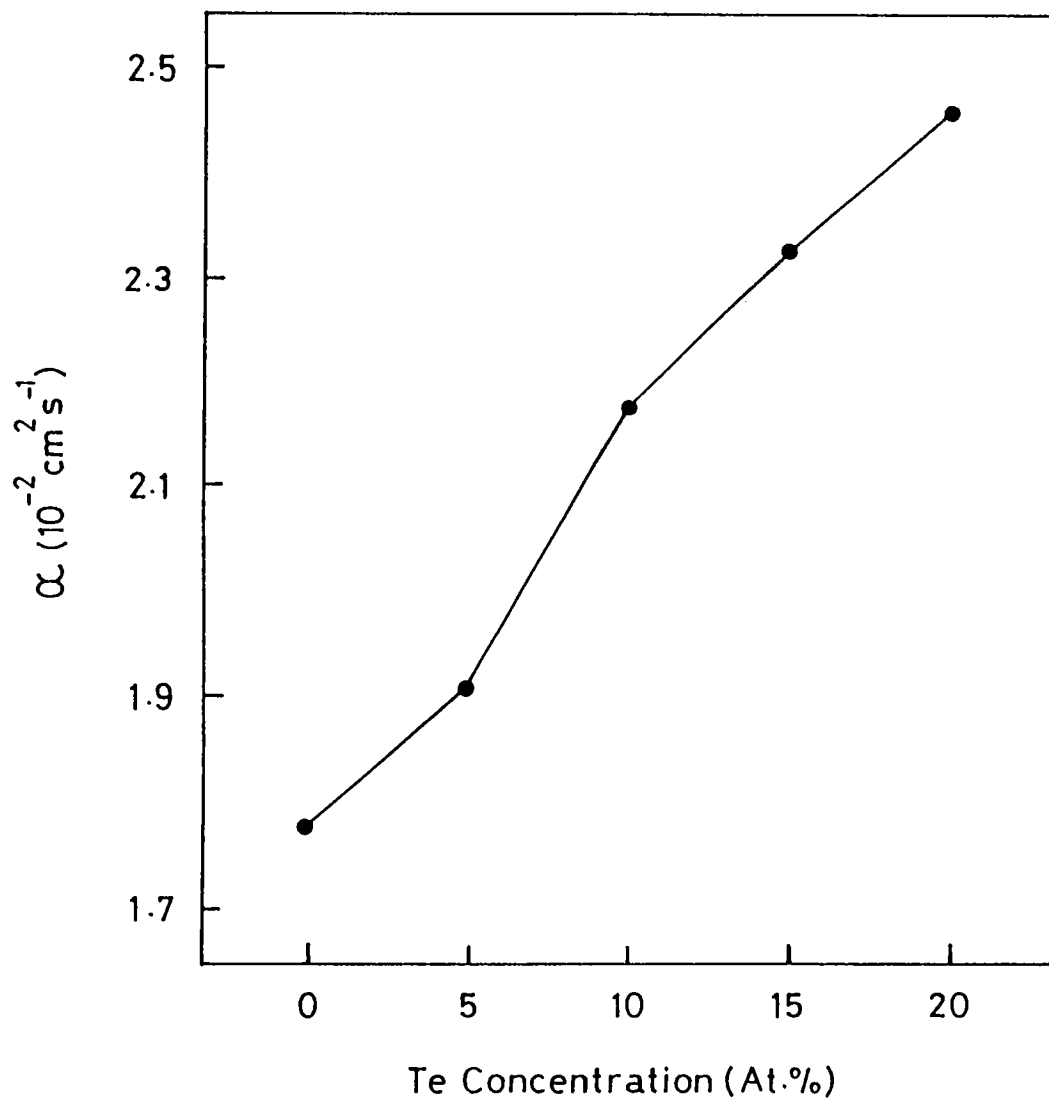


Fig.5.11 Variation of thermal diffusivity α with Te concentration for the stoichiometric compositions of the As-Te-Se glasses.

The observed variation of thermal diffusivity α with composition can be explained in terms of average coordination number $\langle r \rangle$ which is an important parameter in determining the composition dependence of various physical properties of chalcogenide glasses. If N_{As} , N_{Se} and N_{Te} are the coordination numbers of As, Se and Te atoms respectively, then the average coordination number of $As_xTe_ySe_{100-x-y}$ system can be written as

$$\langle r \rangle = \left[x N_{As} + y N_{Te} + (100-x-y)N_{Se} \right] / 100 \quad (5.1)$$

Taking $N_{As} = 3$, $N_{Se} = 2$ and $N_{Te} = 2$, $\langle r \rangle$ lies in the range $2.3 \leq \langle r \rangle \leq 2.5$ for the compositions we have investigated. $\langle r \rangle = 2.4$ corresponds to the stoichiometric compositions of the As-Te-Se system with As concentration equals 40 at. %. According to Phillips' constraint theory [11] and percolation model [12], corresponding to the average coordination number $\langle r \rangle = 2.4$, the number of valence force field constraints are equal to the number of atomic degrees of freedom if bond-stretching and bond-bending constraints are taken into account. The composition corresponding to $\langle r \rangle = 2.4$ is a composition for this system at which a percolation transition takes place from a polymeric glass to a rigid network or amorphous solid. The threshold behaviour in thermal diffusivity exhibited by the As-Te-Se system can be attributed to the mechanical stiffening of the glass network at the critical composition $x = 40$ due to the threshold percolation of rigidity and the corresponding threshold in the internal stress. The system forms an ideal glass at $x = 40$ and the number of zero frequency modes would be minimum at this composition [12]. At this composition the network offers minimum resistance to propagating thermal waves and consequently thermal diffusivity has a maximum value. The observed increase in thermal diffusivity for the stoichiometric compositions is attributed to the increase in the effective

molecular weight with increase in Te content which results in the formation of isostructural units. The thermal conductivity and specific heat of the system change in such a way that the thermal diffusivity is increased with increase in Te content.

REFERENCES

1. R. L. Myuller, in: Solid State Chemistry, Ed., Z. U. Borisova (Consultants Bureau, New York, 1966)
2. Y. Sawan, F. G. Wakim, M. El. Gabaly and M. El. Rayees, J. Non-Cryst. Solids, **41**, 319 (1980)
3. Y. Sawan, F. G. Wakim, M. El. Gabaly and R. Prasad, J. Non-Cryst. Solids, **30**, 293 (1979)
4. B. T. Kolomiets, Yu. V. Rukhlyadev and V. P. Shilo, J. Non-Cryst. Solids, **5**, 389 (1971)
5. Z. U. Borisova, in: Glassy Semiconductors (Plenum Press, New York, 1981)
6. Yang Hanmei, Wang Weizhong and Min Szukwei, J. Non-Cryst. Solids, **80**, 503 (1986)
7. O. I. Andreievskii and G. F. Kashirin, Vestn. L'vovsk. Politekh. Inst. No. **48**, 3-9 (1970)
8. J. T. Edmond, Br. J. Appl. Physics, **17**, No.8, 979 (1966)
9. A. Lachaine and P. Poulet, Appl. Phys. Lett., **45**, 953 (1984)
10. G. Lucovsky and T. M. Hayes, in: Amorphous Semiconductors, ed., M. H. Brodsky (Springer-Verlag, Berlin 1979)
11. J. C. Phillips, J. Non-Cryst. Solids, **34**, 153 (1979)
12. M. F. Thorpe, J. Non-Cryst. Solids, **57**, 355 (1983)
13. J. C. Phillips and M. F. Thorpe, Solid State Commun., **53**, 699 (1985)

CHAPTER VI

OPTICAL BAND GAP AND THERMAL DIFFUSIVITY IN Ge-As-Se GLASSES

6.1 Introduction

The role of microscopic topology in determining the properties of glass-forming compounds has been explored theoretically for several years. The concept of an average atomic coordination number is used by Phillips [1] in constraint counting arguments explaining the strong glass-forming tendency of certain alloy compositions. These ideas have been later refined by Thorpe and coworkers [2-4], who, by evaluating the number of zero-frequency "floppy" modes as a function of the coordination number predicted that a rigidity percolation transition from a soft to a rigid structure should occur at an average coordination number of $\langle r \rangle = 2.4$. According to this, stable glasses satisfy the relation $N_{co}(r) = 3$, where $N_{co}(r)$ is the number of constraints per atom given as

$$N_{co}(r) = r/2 + (2r-3), \quad (6.1)$$

for covalent glasses. In this equation, the first term on the right-hand side represents the bond-stretching constraint and the second term denotes the number of angular (bond-bending) constraints.

Later Tanaka has extended Phillips' ideas to two-dimensional glassy structures [5,6]. Assuming a hypothetical material having a plane lattice laid in three-dimensional space, the constraint balancing equation for the layer material gets modified as

$$3 = r/2 + (r-1) \quad (6.2)$$

The expression gives $r = 2.67$, ie. the coordination number of glasses having stable layer structure is 2.67.

The ternary system Ge-As-Se is particularly well suited to testing the validity of these topological concepts because the large glass-forming region makes it possible for a given value of the average coordination number $\langle r \rangle$ (given in this case by $\langle r \rangle = 4X_{Ge} + 3X_{As} + 2X_{Se}$, where X is the mole fraction) to be realized with a continuous range of chemical compositions, allowing purely topological effects to be distinguished from chemical effects. The fact that germanium, arsenic and selenium are elements in groups IV, V and VI respectively of the same period brings about the covalent character of the interaction between their atoms. The result is a broad glass formation region in the Ge-As-Se system as shown in Fig 6.1. It is possible to introduce into the glassy alloys upto 70 at.% of arsenic and upto 50 at.% of germanium. In the three component Ge-As-Se system, selenium will react primarily with germanium and produce structural units of $GeSe_{4/2}$. When germanium is introduced into arsenic selenides, gradual composition changes take place in the system forming $GeSe_{4/2}$ and $AsSe_{3/2}$ structural units. Introduction of germanium into the glassy arsenic selenide can be accompanied also by formation of the complex structural units $As_2Ge_{4/2}Se_{4/2}$ of the glass forming Ge-As-Se system. Approximate thermochemical calculations indicate that in the three component Ge-As-Se system, there can be several sections with different contents of structural units, and consequently with different physical and chemical properties. There can be sections in which the structure is determined mainly by bonds of the selenium type [7].

Recently, experimental reports correlating the elastic constants of Ge-As-Se glasses with $\langle r \rangle$ suggest the occurrence of a threshold at $\langle r \rangle = 2.4$ [8]. But this data do not match with

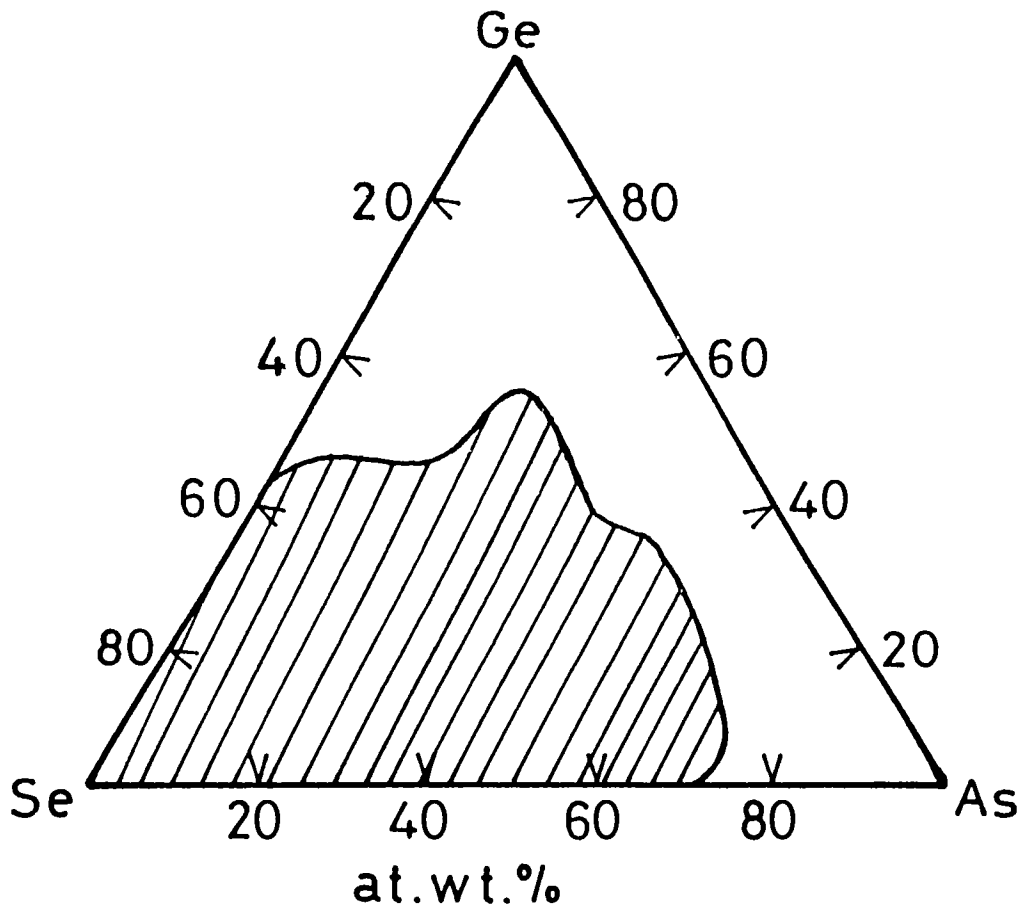


Fig.6.1 Glass forming region of Ge-As-Se system.

the previous report by Tillie and coworkers [9] and their samples contained oxygen inclusions. Hence, their report could not be taken as conclusive evidence for the observation of the threshold at $\langle r \rangle = 2.4$. The persistent infrared spectral hole burning studies of the effects of network topology on low-temperature relaxation in Ge-As-Se glasses show no indication of a rigidity transition or any other unusual features at $\langle r \rangle = 2.4$ [10]. Another study of the $\langle r \rangle$ dependence on excess heat capacity ΔC_p measured at T_g shows minimum at $\langle r \rangle = 2.4$ whereas excess expansion coefficient $\Delta \alpha$ shows absence of any anomaly at $\langle r \rangle = 2.4$ in selected Ge-As-Se glasses [11]. Their studies on the $\langle r \rangle$ dependence of glass transition temperature T_g shows no significant variation at $\langle r \rangle = 2.4$. Moreover, studies on other ternary systems, for example, $\langle r \rangle$ dependence of the optical band gap E_o and thermal diffusivity α of bulk Ge-As-Te glasses show subtle features at $\langle r \rangle = 2.6$ indicating the occurrence of a threshold at this value of $\langle r \rangle$ [12]. Studies of photodarkening and elastic constants of Ge-As-S glasses show the occurrence of a threshold in the vicinity of $\langle r \rangle = 2.67$ with no significant change at $\langle r \rangle = 2.4$ [13,14].

In order to clarify the disparity in the value of the threshold in Ge-As-Se systems, experimental techniques which are sensitive to probe the composition dependence should be used. Unlike binary systems, ternary systems can be prepared over a wide composition range and are good candidates for this type of studies. Also, in ternary systems, chemical threshold effects occurring at stoichiometric compositions can be distinguished from the mechanical threshold. This is possible because the stoichiometric compositions depend upon the percentage of individual elements present in the glass whereas the mechanical threshold depends only on $\langle r \rangle$.

The composition dependence of the optical band gap E_o and thermal diffusivity α of two sets of glasses belonging to

the Ge-As-Se system investigated using photoacoustic (PA) technique are described in this chapter. The compositions studied can be represented as $\text{Ge}_x\text{As}_{10}\text{Se}_{90-x}$ (with $x = 5, 10, 15, 20, 25, 28.5, 30, 35$ and 40) and $(\text{Ge}_{0.5}\text{As}_{0.5})_x\text{Se}_{100-x}$ (with $x = 10, 20, 28.7, 30, 40, 44, 50$ and 60). The compositions have been chosen to produce an average atomic coordination $\langle r \rangle$ ranging from 2.15 to 2.9. The samples are prepared by the well established melt-quenching technique described earlier. Identical preparation conditions have been followed while preparing all the samples. This is necessary because any change in the preparative conditions may affect the properties of glasses. The amorphous nature of the samples have been checked by X-ray diffractometry.

6.2 Composition dependence of optical band gap in Ge-As-Se glasses

The variation of the normalized PA signal amplitude with wavelength of the incident radiation is measured to determine the optical band gap E_o of each sample. The room temperature PA cell has been used for this purpose. The chopping frequency used is 22 Hz. For recording the absorption spectra, powdered samples have been used. The PA spectrum obtained for a highly absorbing carbon black sample is used to normalize the PA spectrum obtained for each sample.

The normalized PA spectra of the compositions mentioned above are shown in Figs. 6.2 - 6.5. The optical band gap E_o is determined by the tangent drawing procedure as described in chapter-III. The optical band gap has also been determined using the UV-Vis-NIR spectrophotometer. The E_o values determined for each sample using the PA technique as well as UV-Vis-NIR spectrophotometry along with their $\langle r \rangle$ values are tabulated in Table 6.1.

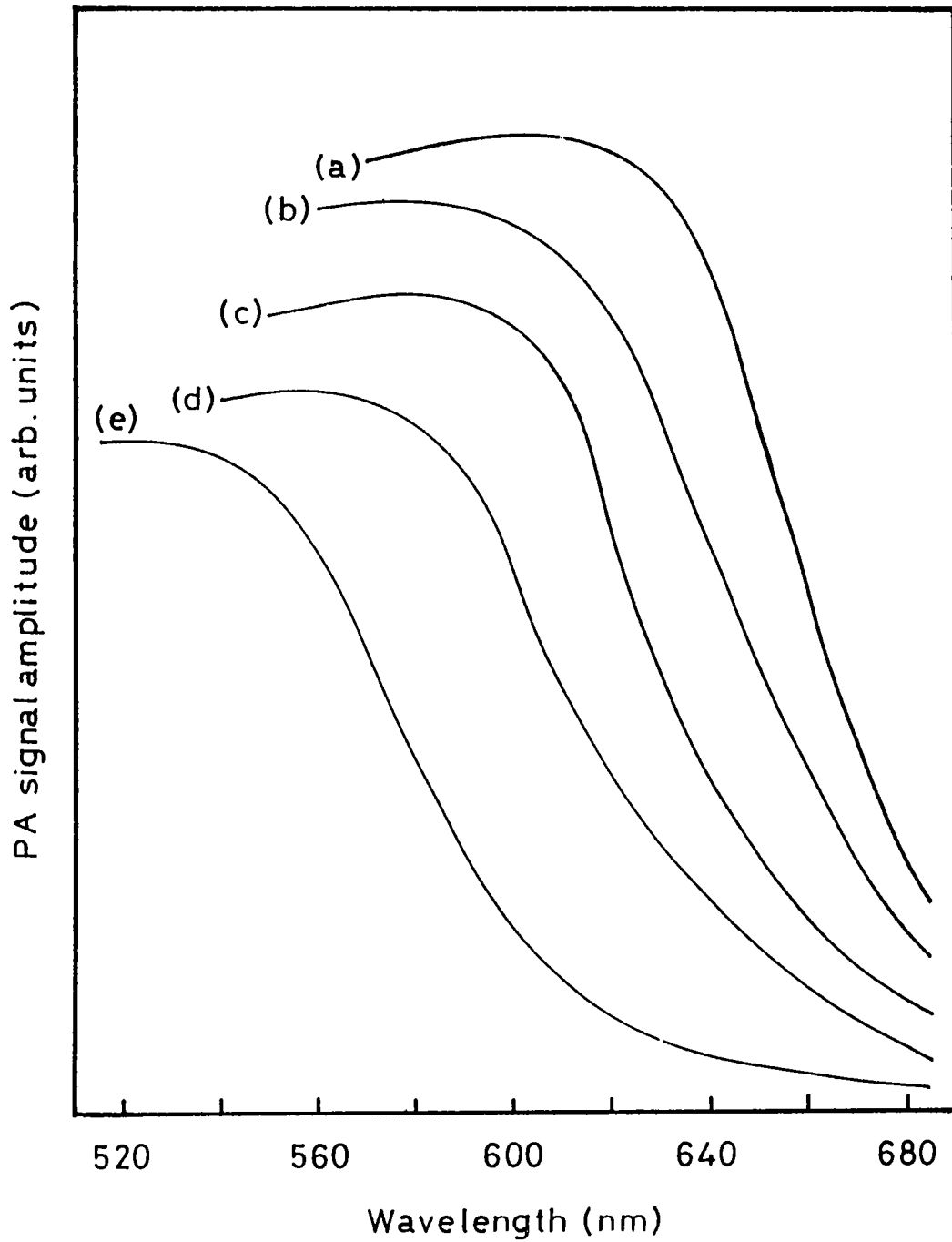


Fig.6.2 Normalized PA spectra of $\text{Ge}_x\text{As}_{10}\text{Se}_{90-x}$ glasses.
 (a) $\text{Ge}_5\text{As}_{10}\text{Se}_{85}$, (b) $\text{Ge}_{10}\text{As}_{10}\text{Se}_{80}$
 (c) $\text{Ge}_{15}\text{As}_{10}\text{Se}_{75}$, (d) $\text{Ge}_{20}\text{As}_{10}\text{Se}_{70}$
 (e) $\text{Ge}_{25}\text{As}_{10}\text{Se}_{65}$

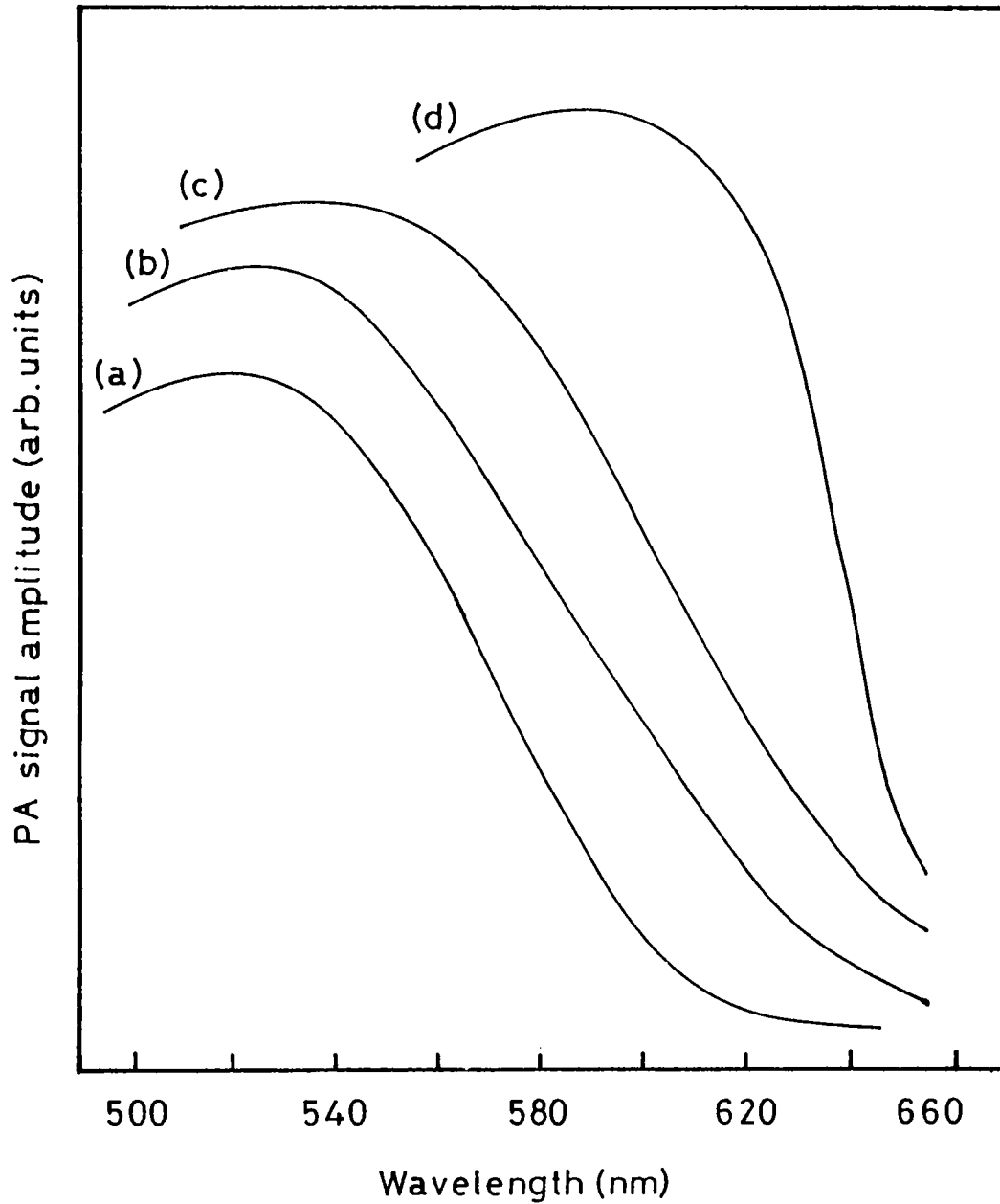


Fig.6.3 Normalized PA spectra of $\text{Ge}_x\text{As}_{10}\text{Se}_{90-x}$ glasses.
 (a) $\text{Ge}_{28.5}\text{As}_{10}\text{Se}_{61.5}$, (b) $\text{Ge}_{30}\text{As}_{10}\text{Se}_{60}$
 (c) $\text{Ge}_{35}\text{As}_{10}\text{Se}_{55}$, (d) $\text{Ge}_{40}\text{As}_{10}\text{Se}_{50}$

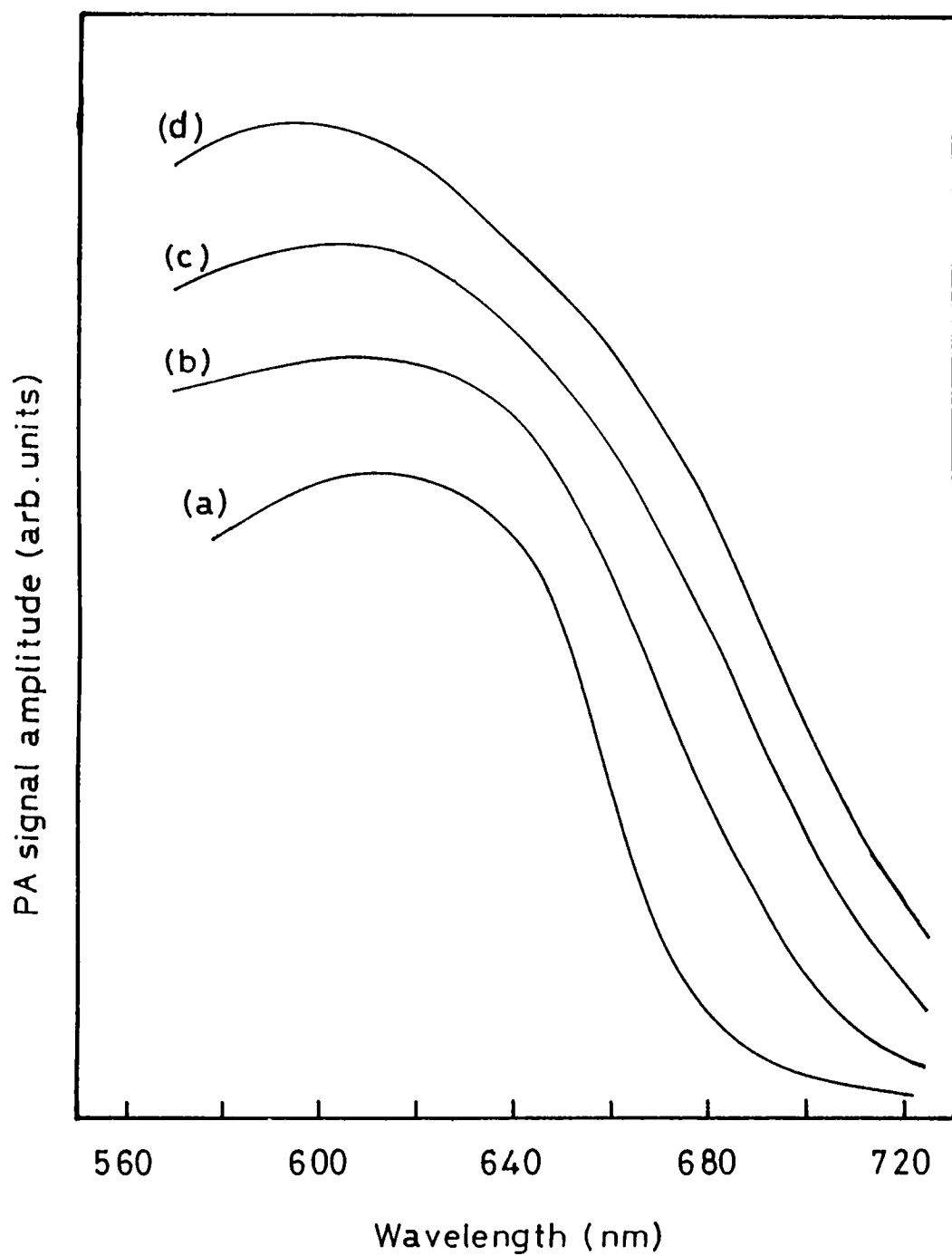


Fig.6.4 Normalized PA spectra of $(\text{Ge}_{0.5}\text{As}_{0.5})_x\text{Se}_{100-x}$ glasses.

(a) $\text{Ge}_5\text{As}_5\text{Se}_{90}$, (b) $\text{Ge}_{10}\text{As}_{10}\text{Se}_{80}$

(c) $\text{Ge}_{13.95}\text{As}_{13.95}\text{Se}_{73.3}$, (d) $\text{Ge}_{15}\text{As}_{15}\text{Se}_{70}$

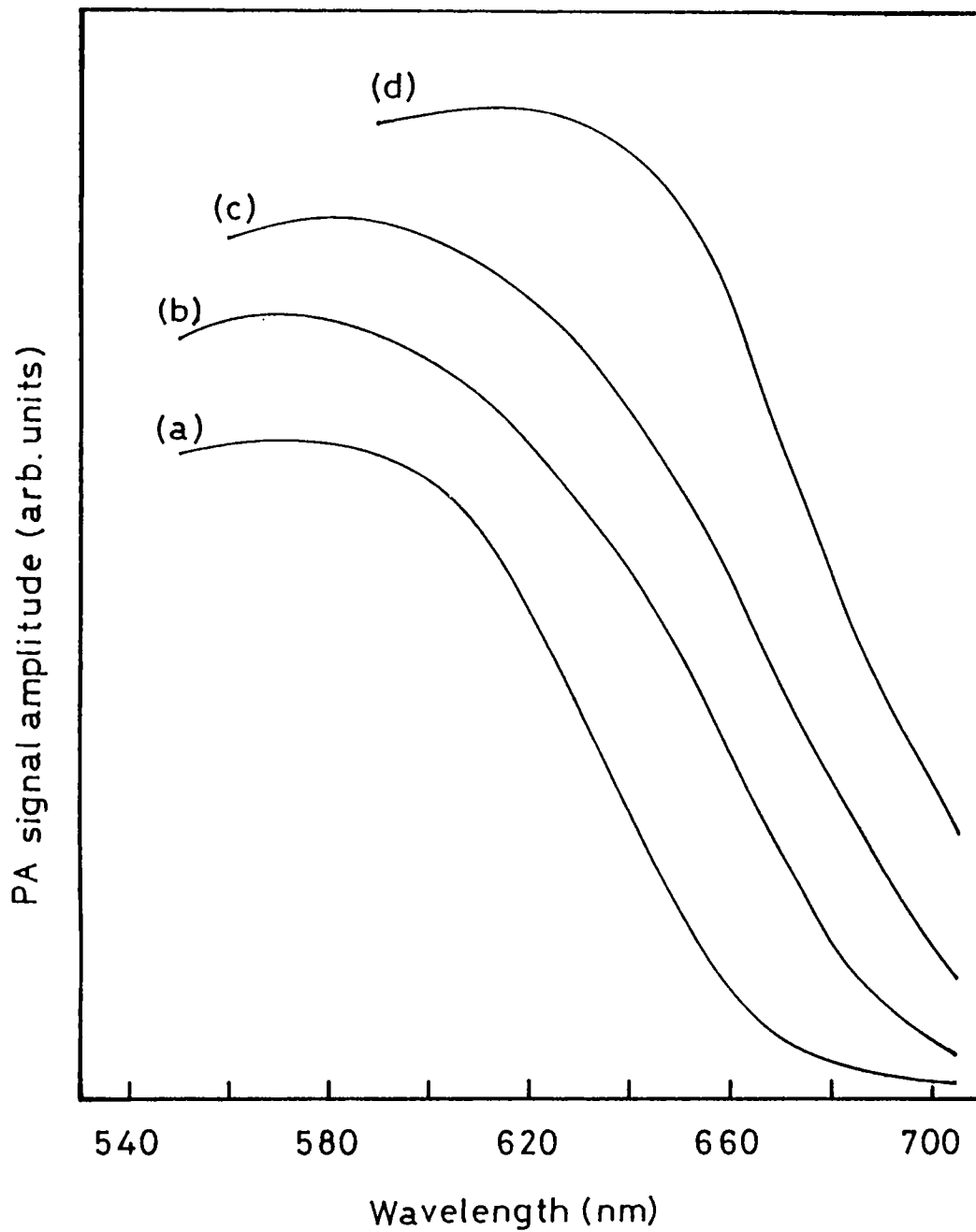


Fig.6.5 Normalized PA spectra of $(\text{Ge}_{0.5}\text{As}_{0.5})_x\text{Se}_{100-x}$ glasses.

- (a) $\text{Ge}_{20}\text{As}_{20}\text{Se}_{60}$, (b) $\text{Ge}_{22}\text{As}_{22}\text{Se}_{56}$
(c) $\text{Ge}_{25}\text{As}_{25}\text{Se}_{50}$, (d) $\text{Ge}_{30}\text{As}_{30}\text{Se}_{40}$

Table 6.1 The glass composition, average coordination number, optical band gap of the two families of Ge-As-Se glasses.

No.	Composition Ge:As:Se	$\langle r \rangle$	E_g (eV) PA technique	E_g (eV) UV-Vis-NIR
1.	5:10:85	2.20	1.98	1.96
2.	10:10:80	2.30	2.01	2.00
3.	15:10:75	2.40	2.07	2.10
4.	20:10:70	2.50	2.14	2.12
5.	25:10:65	2.60	2.27	2.24
6.	28.5:10:61.5	2.67	2.33	2.32
7.	30:10:60	2.70	2.32	2.32
8.	35:10:55	2.80	2.25	2.26
9.	40:10:50	2.90	2.04	2.20
10.	5:5:90	2.15	1.98	1.98
11.	10:10:80	2.30	2.00	1.98
12.	13.35:13.35:73.3	2.40	2.02	2.00
13.	15:15:70	2.45	2.05	2.04
14.	20:20:60	2.60	2.12	2.10
15.	22:22:56	2.67	2.14	2.14
16.	25:25:50	2.75	2.06	2.04
17.	30:30:40	2.90	1.97	1.94

The variation of the optical band gap of these glasses with $\langle r \rangle$ is shown in Fig.6.6. It can be seen that the optical band gap increases gradually as $\langle r \rangle$ is increased and shows maxima around $\langle r \rangle = 2.67$ for both $\text{Ge}_x\text{As}_{10}\text{Se}_{90-x}$ and $(\text{Ge}_{0.5}\text{As}_{0.5})_x\text{Se}_{100-x}$ glasses. Beyond the value of $\langle r \rangle = 2.67$, the optical band gap decreases gradually.

In order to understand the variation of E_o with $\langle r \rangle$ in Ge-As-Se glasses, it is necessary to have an idea of the single covalent bond energy of the various bonds present in the network. The single bond energies of the various bonds in the Ge-As-Se glasses, namely, Ge-Ge, As-As, Se-Se, Ge-As, Ge-Se and As-Se are 49.1, 47.7, 44.0, 46.6, 55.2 and 51.3 respectively.

The variation of optical band gap with average coordination number can be interpreted as follows. In Se-rich glasses of the Ge-As-Se system, the two-fold coordinated Se will form flexible chains of Se in the glass network. The addition of the three-fold coordinated element As and the four-fold coordinated Ge results in branching and cross-linking of these chains. These configurational changes result in the formation of a two-dimensional structure which is stabilized by the medium-range intermolecular interactions. In both $\text{Ge}_x\text{As}_{10}\text{Se}_{90-x}$ and $(\text{Ge}_{0.5}\text{As}_{0.5})_x\text{Se}_{100-x}$ glasses, an increase in Ge concentrations (which corresponds to an increase in $\langle r \rangle$) increases the possibility for the formation of more Ge-Se bonds. Since the bond energy of Ge-Se bond is higher than all the other possible bonds in the system, the average bond energy of the system increases. According to Kastner's model [15] for band structure of chalcogenide glasses, an increase in the average bond energy of the system tends to increase the energy of the conduction band edge. This effectively increases the optical band gap E_o of the system.

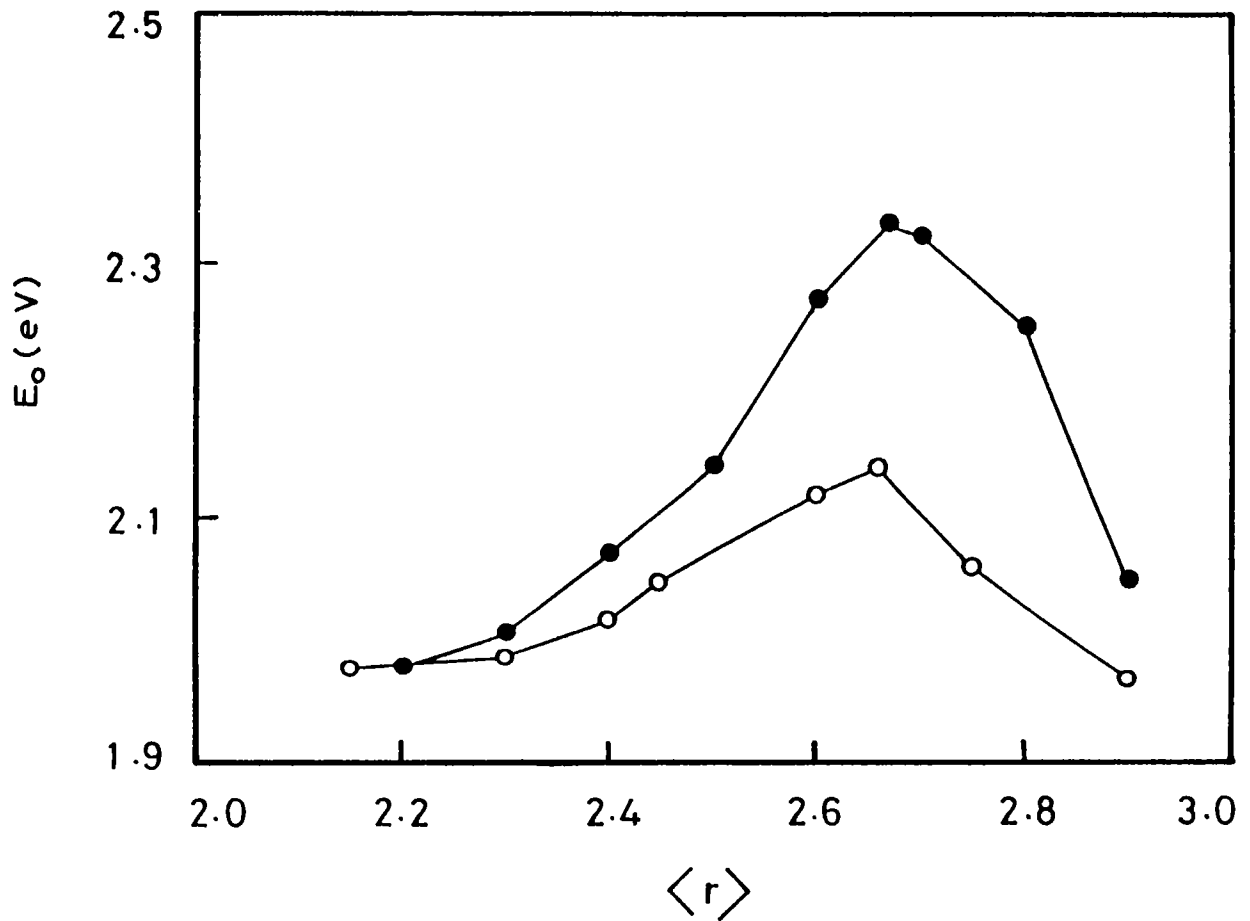


Fig.6.6 Variation of optical band gap with average coordination number for Ge-As-Se glasses.

(●) $\text{Ge}_x\text{As}_{10}\text{Se}_{90-x}$, (○) $(\text{Ge}_{0.5}\text{As}_{0.5})_x\text{Se}_{100-x}$

The optical band gap E_o attains a maximum value around $\langle r \rangle = 2.67$ for both $Ge_xAs_{10}Se_{90-x}$ and $(Ge_{0.5}As_{0.5})_xSe_{100-x}$ glasses. The 2-d layered structure is fully developed at this composition and the system goes over to a rigid 3-d structure and the system will be rigid beyond this composition. The cross-linking of the layered structure and the formation of rigid 3-d structure beyond this composition changes the interaction between lone pair p electrons which can broaden the lone pair band resulting in a gradual decrease of optical band gap. This could be the reason for the small decrease in E_o beyond the compositions corresponding to $\langle r \rangle = 2.67$ for the two sets of glasses of the Ge-As-Se system. The occurrence of a maximum around $\langle r \rangle = 2.67$ in these glasses supports the idea of a structural phase transition at $\langle r \rangle = 2.67$ as suggested by Tanaka [5].

6.3 Composition dependence of thermal diffusivity in Ge-As-Se glasses

The thermal diffusivity measurements on $Ge_xAs_{10}Se_{90-x}$ and $(Ge_{0.5}As_{0.5})_xSe_{100-x}$ glasses have been performed by the procedure already outlined in previous chapters. The log-log plots of the PA signal amplitude versus chopping frequency of the samples investigated are shown in Figs. 6.7 and 6.8. The slope of the curve changes at the characteristic frequency f_c because for $f < f_c$ the heat generated at the surface of the sample is propagated into the backing medium. Once f_c is determined, the thermal diffusivity is calculated using the relation $\alpha = f_c l^2$, where l is the sample thickness. Table 6.2 shows the average coordination number, characteristic frequency, sample thickness and thermal diffusivity of each sample investigated.

The variation of thermal diffusivity α with average

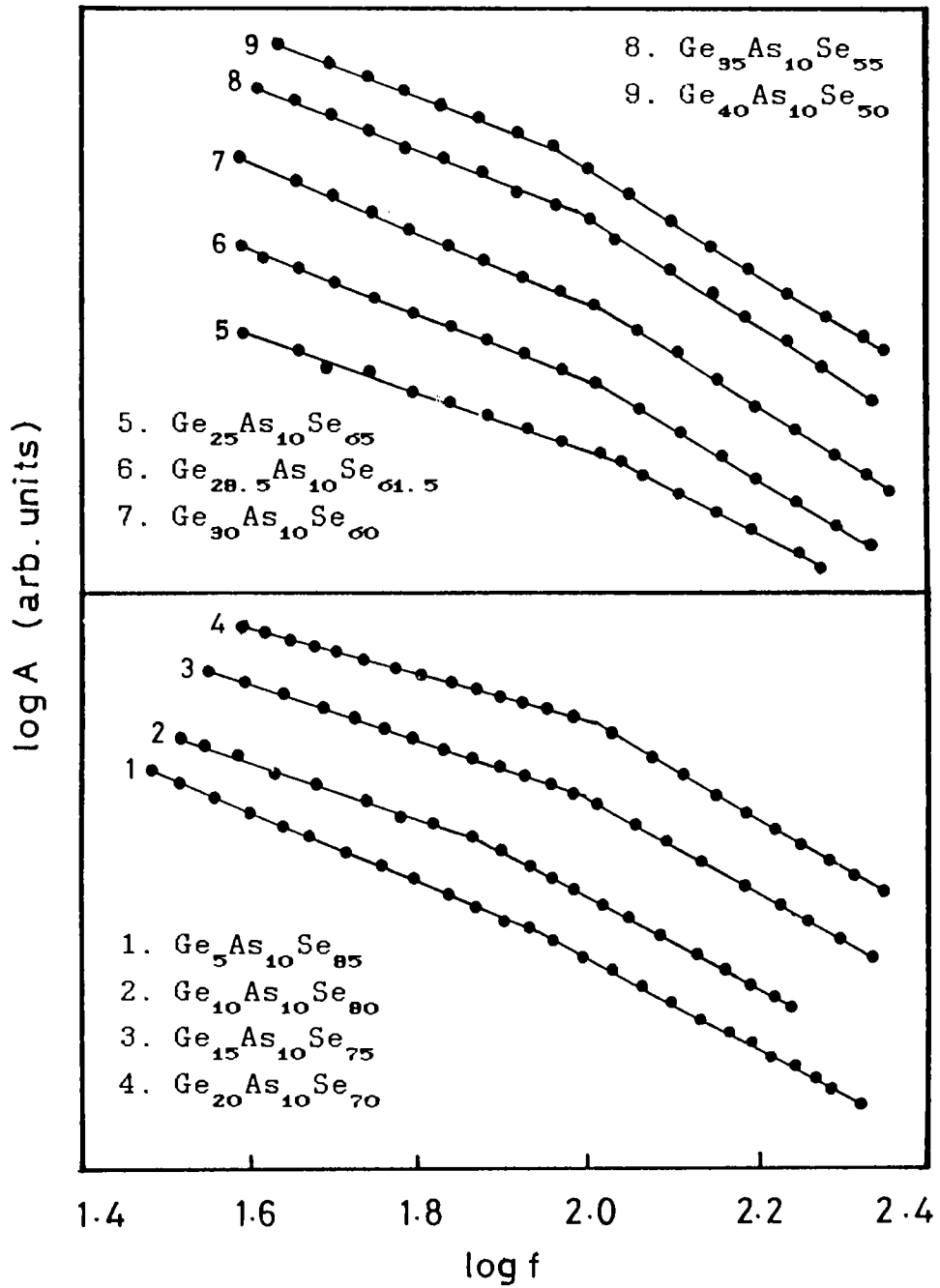


Fig.6.7 Log-log plots of PA amplitude with chopping frequency of $\text{Ge}_x\text{As}_{10}\text{Se}_{90-x}$ glasses.

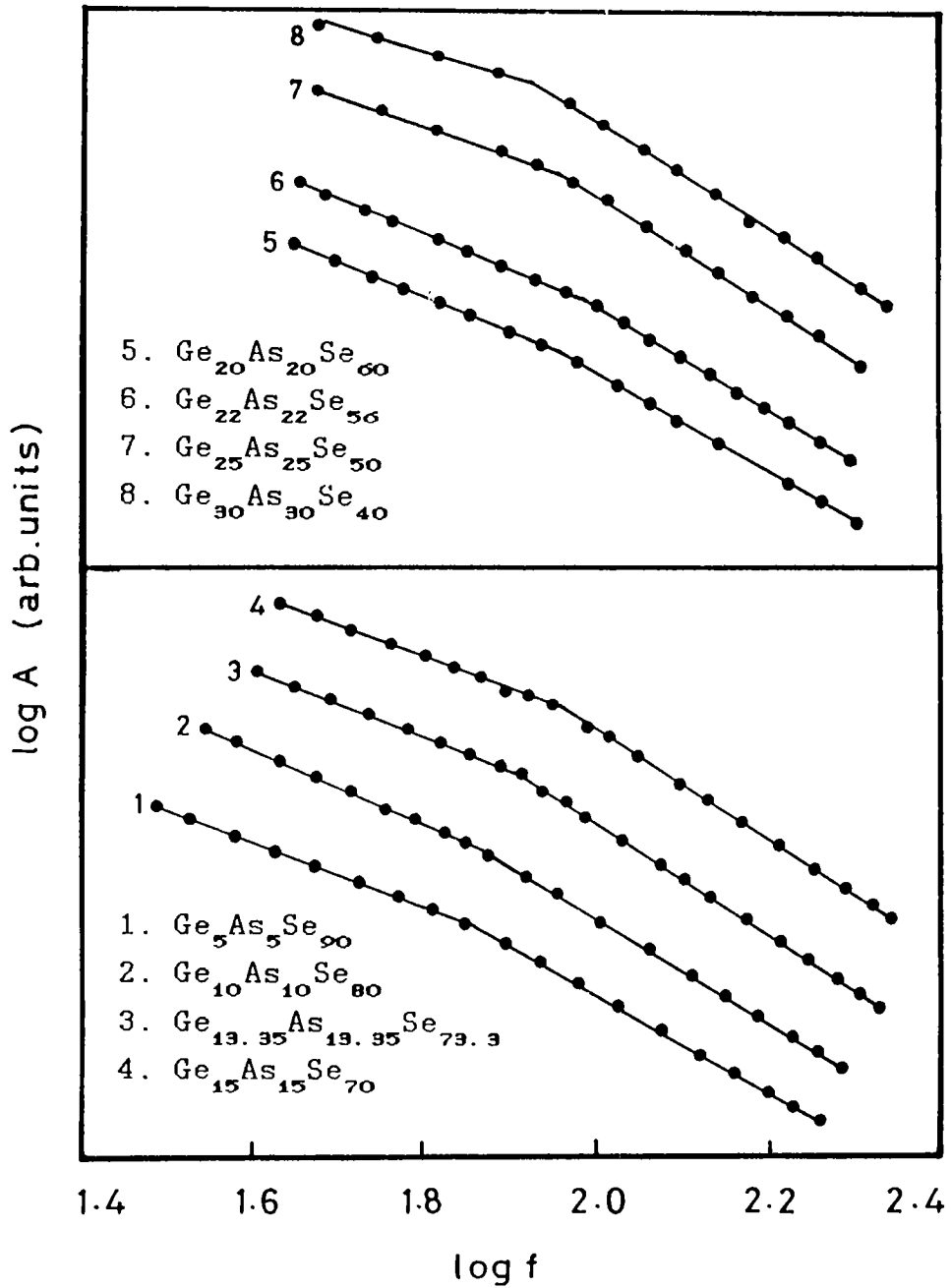


Fig.6.8 Log-log plots of PA amplitude with chopping frequency of $(\text{Ge}_{0.5}\text{As}_{0.5})_x\text{Se}_{100-x}$ glasses.

Table 6.2 Composition, average coordination number, characteristic frequency, thickness and thermal diffusivity of Ge-As-Se glasses.

No.	Composition Ge:As:Se	$\langle r \rangle$	f_c (Hz)	l (μm)	α ($10^{-2} \text{ cm}^2/\text{s}$)
1.	5:10:85	2.20	87.86	90	0.712
2.	10:10:80	2.30	73.23	100	0.732
3.	15:10:75	2.40	95.79	100	0.958
4.	20:10:70	2.50	104.4	100	1.044
5.	25:10:65	2.60	110.6	100	1.106
6.	28.5:10:61.5	2.67	113.8	100	1.138
7.	30:10:60	2.70	105.3	100	1.053
8.	35:10:55	2.80	97.16	100	0.972
9.	40:10:50	2.90	90.40	100	0.904
10.	5:5:90	2.15	72.24	100	0.722
11.	10:10:80	2.30	73.23	100	0.732
12.	13.35:13.35:73.3	2.40	80.52	100	0.805
13.	15:15:70	2.45	90.42	100	0.904
14.	20:20:60	2.60	90.42	110	1.094
15.	22:22:56	2.66	95.76	110	1.159
16.	25:25:50	2.75	90.42	110	1.094
17.	30:30:45	2.90	86.6	110	1.048

coordination number $\langle r \rangle$ is plotted in Fig.6.9. As $\langle r \rangle$ is increased α increases gradually and shows a threshold maximum around $\langle r \rangle = 2.67$ for both $\text{Ge}_x\text{As}_{10}\text{Se}_{90-x}$ and $(\text{Ge}_{0.5}\text{As}_{0.5})_x\text{Se}_{100-x}$ glasses. The variation of α with $\langle r \rangle$ can be interpreted in terms of the change in network topology and dimensionality. It can be inferred that α increases as the two-dimensional layered structure develops through cross-linking of Se atom chains. This change in dimensionality as $\langle r \rangle$ is increased reduces the flexibility of the network as it goes over to a three-dimensional rigid structure. The maximum value of α around $\langle r \rangle = 2.67$ could be attributed to the formation of layered structure and a medium range order fully getting developed through intermolecular interactions and the system tending to form a three-dimensional structure. The slight decrease in α beyond $\langle r \rangle = 2.67$ may be due to the large number of bonding defects present in the three-dimensional structure. It is well known that the thermal conductivity depends crucially on the phonon mean free path in the system. Since α is directly related to the thermal conductivity, the threshold maximum in α occurring around $\langle r \rangle = 2.67$ may be a signature of the development of a more ordered and rigid structure at this composition.

The observed behaviour of Ge-As-Se glasses shows that the average coordination number $\langle r \rangle$ is an important parameter for understanding the properties of network glasses and is valid even for complicated glasses like Ge-As-Se. The absence of any observable change in both the optical band gap and thermal diffusivity in these systems at $\langle r \rangle = 2.4$ rules out the validity of Phillips' and Thorpes's prediction of the mechanical threshold at $\langle r \rangle = 2.4$ in these systems. The observed maxima around $\langle r \rangle = 2.67$ indicates that medium-range interactions have an important role in determining the network topology in these glasses as suggested by Tanaka. The present studies establish the sensitivity of thermal diffusivity to rigidity percolation in covalent network glasses.

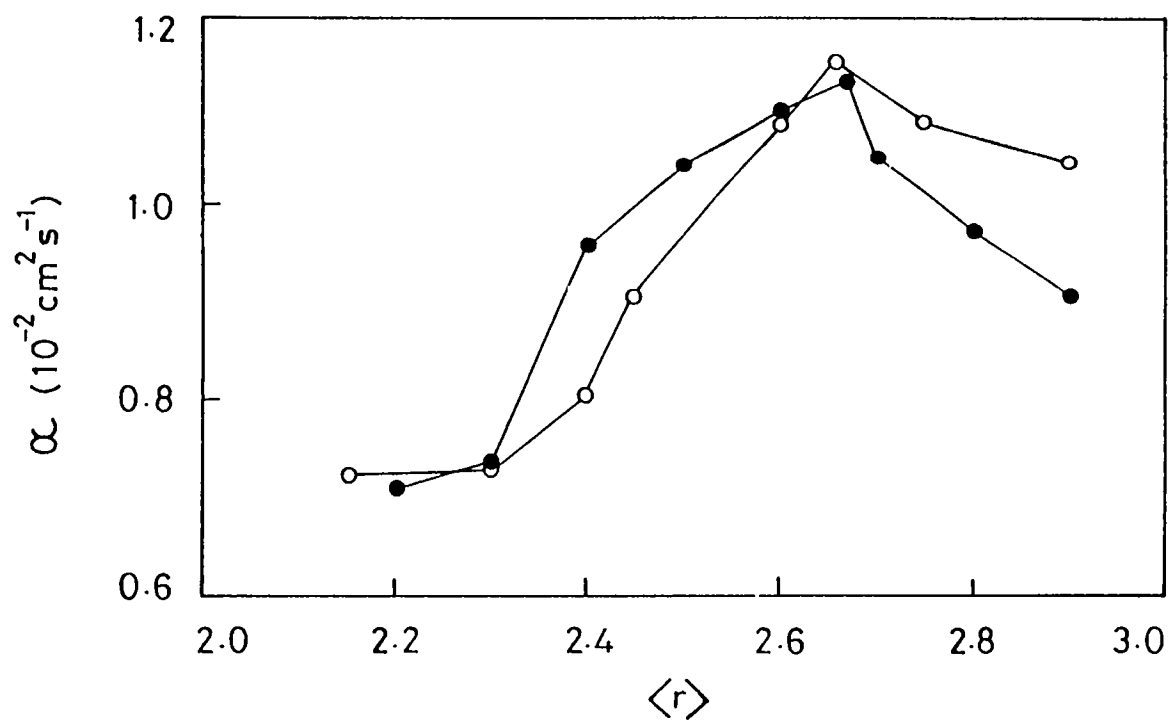


Fig.6.9 Variation of thermal diffusivity with average coordination number for Ge-As-Se glasses.
 (●) $\text{Ge}_x \text{As}_{10} \text{Se}_{90-x}$, (○) $(\text{Ge}_{0.5} \text{As}_{0.5})_x \text{Se}_{100-x}$

REFERENCES

1. J. C. Phillips, *J. Non-Cryst. Solids*, **34**, 153 (1979)
2. M. F. Thorpe, *J. Non-Cryst. Solids*, **57**, 355 (1983)
3. H. He and M. F. Thorpe, *Phys. Rev. Lett.*, **54**, 2107 (1985)
4. S. Feng and M. F. Thorpe, *Phys. Rev B***31**, 276 (1985)
5. K. Tanaka, *J. Non-Cryst. Solids*, **103**, 149 (1988)
6. K. Tanaka, *Phys. Rev B***39**, 1270 (1989)
7. Z. U. Borizova, in: *Glassy Semiconductors* (Plenum Press, New York, 1981)
8. B. L. Halfpap and S. M. Lindsay, *Phys. Rev. Lett.*, **57**, 847 (1986)
9. U. Tillie, G. H. Frishat, K. J. Leers, *Fourth International Conference on Physics of Non-Crystalline Solids*, Clausthal, Germany (Aedermansdorf, Switzerland and *Trans. Tech. S. A.* 1977) p. 631
10. S. P. Love, A. J. Sievers, B. L. Halfpap and S. M. Lindsay, *Phys. Rev. Lett.*, **65**, 1792 (1990)
11. M. Tatsumisago, B. L. Halfpap, J. L. Green, S. M. Lindsay and C. A. Angell, *Phys. Rev. Lett.*, **64**, 1549 (1990)
12. A. Srinivasan, K. N. Madhusoodanan, E. S. R. Gopal and J. Philip, *Phil. Mag B***65**, 99 (1992)

13. K. Tanaka, Solid State Commun., 60, 295 (1986)
14. K. Tanaka, T. Nakagawa and A. Odajima, Phil. Mag B54, L3 (1986)
15. M. Kastner, Phys. Rev. Lett., 28, 355 (1972)

CHAPTER VII

CALORIMETRIC MEASUREMENTS ON As-Te-Se AND Ge-As-Se GLASSES

7.1 Introduction

Due to their interesting electronic and opto-electronic properties, glassy chalcogenide semiconductors have been studied extensively [1]. Since in these applications the materials are activated by light or an electrical signal, primarily their optical and electrical properties have been investigated. On the other hand, little effort has been devoted to the determination of the thermodynamic properties of these materials. All known amorphous solids are less stable than their crystalline counterparts, which may be homogeneous or phase separated. Thus for an amorphous solid to form and persist, a thermodynamically preferred crystallization process must be bypassed and then suppressed [2]. Glass formation in melt quenching is possible only when the resistance to homogeneous crystal nucleation remains high as the melt is deeply undercooled through its liable regime to the glass transition temperature, which implies that the crystallization process in glass forming materials must be one in which the short range order is reconstructed.

The glass transition phenomenon and the process of glass formation can be understood from the volume-temperature behaviour already described in chapter-IV. The glass transition temperature T_g is not a well defined temperature and if the melt is cooled more slowly, it can be supercooled to lower temperatures and subsequently T_g gets lowered. T_g can take up

any value within a range depending upon the thermal history of the material and can vary from 10% to 20% depending upon the cooling rate. Using free-volume theory an expression relating T_g and cooling rate R can be derived [3] as,

$$R = R_o \exp \left[-1/C (1/T_g - 1/T_m) \right] \quad (7.1)$$

where C and R_o are constants and T_m denotes the melting point.

Historically the metastability of glasses has been discussed from many different view points (the early history is reviewed in Ref.(4)). In the early 1930s Simons introduced a kinetic approach and he distinguished between the measured glass transition temperature T_g , at which the supercooled liquid freezes with rapid drops in specific heat, thermal expansion, compressibility, etc., and the ideal glass transition temperature T_o obtained from the viscosity η which is fitted very well by the relation $\ln \eta = A/(T-T_o)$. In 1948 Kauzmann [5] pointed out that thermodynamically certain glass transition temperatures T_x could be defined by linear extrapolation of the "configurational" quantities $\Delta x = x(\text{liquid}) - x(\text{crystal})$ to zero, where for x one can choose entropy, enthalpy or volume. On the basis of the fragmentary data available at that time Kauzmann guessed that $T_o = T_s$. The conjecture was based on a hypothetical configurational third law of thermodynamically metastable systems.

The chemical systematics of glass formation also suggests that $T_o = T_s$. If we define the quality of a glass in terms of the inverse of its minimal quenching rate which can be employed without crystallization of the supercooled liquid, then the best inorganic glasses are formed from materials with network (covalently bonded) structures. Such structures have low

coordination numbers and lower densities than non-covalently bonded systems. However, since glassy materials are not in equilibrium, their properties strongly depend on the thermal history of the samples. In the glass transition region, the properties are dependent on time because, in this region, the experimental time scale becomes comparable to the time scale for structural rearrangements; the material will relax towards equilibrium and so many physical properties will exhibit anomalous changes near glass transition temperature.

In this chapter, the calorimetric investigations performed on two groups of glasses viz., As-Te-Se and Ge-As-Se are described in detail. The glass transition temperature T_g and specific heat at constant pressure C_p of these two families of glasses have been determined using a differential scanning calorimeter (Perkin-Elmer DSC-7). The variation in glass transition temperature T_g and heat capacity ΔC_p with composition during glass transition are discussed in detail.

7.2 Experimental details

The samples belonging to the As-Te-Se and Ge-As-Se systems have been prepared by the conventional melt quenching technique. In the As-Te-Se system, the compositions investigated are $As_xTe_5Se_{95-x}$, $As_xTe_{10}Se_{90-x}$ (with $x = 30, 35, 40, 45$ and 50) covering an average coordination number $\langle r \rangle$ in the range 2.3 to 2.5 and $As_{40}(Te,Se)_{60}$ with Te concentration varying from 0 to 20 at.% which are the stoichiometric compositions of the As-Te-Se system. In the Ge-As-Se system, the compositions studied can be categorized into two sets as $Ge_xAs_{10}Se_{90-x}$ (with $x = 5, 10, 15, 20, 25, 28.5, 30, 35$ and 40) and $(Ge_{0.5}As_{0.5})_xSe_{100-x}$ (with $x = 10, 20, 26.7, 30, 40, 44, 50$ and 60) covering an average

coordination number $\langle r \rangle$ ranging from 2.15 to 2.9.

Differential scanning calorimetry (DSC) is a widely used thermal analysis technique which provides a great deal of information about the thermal behaviour of any sample over a wide temperature range. In this technique the sample and the reference material, which is thermally inert, are maintained at the same temperature by proper application of electrical energy as they are heated or cooled at a predetermined linear rate. The heat flow, dH/dt (in mcal/sec or mW) is recorded as a function of temperature. Any thermal changes that take place inside the sample will be reflected on a DSC curve which is a plot of the heat flow into (or out of) the sample against temperature.

The initial calibration of the instrument has been carried out using standard calibrants such as Indium and Zinc, over a temperature range of 50°C to 450°C. Samples in the form of powder are sealed in aluminium pans and scanned through their T_g . The heating rate used for all the samples is 20°C/min. The DSC curves of selected samples belonging to the As-Te-Se and Ge-As-Se systems are shown in Fig.7.1 and Fig.7.2 respectively. The glass transition temperature T_g is determined as the temperature corresponding to the onset of glass transition which appears as an endothermic baseline shift of the DSC curve as described already in chapter II of this thesis. Moreover, the DSC curves do not show any trace of crystallization in any of the samples investigated suggesting that these glasses are highly glass forming over a wide composition range.

The DSC technique has also been used to estimate the specific heat at constant pressure C_p of each sample of the As-Te-Se and Ge-As-Se systems using the ratio method [6]. In this method, the baseline corresponding to the temperature range

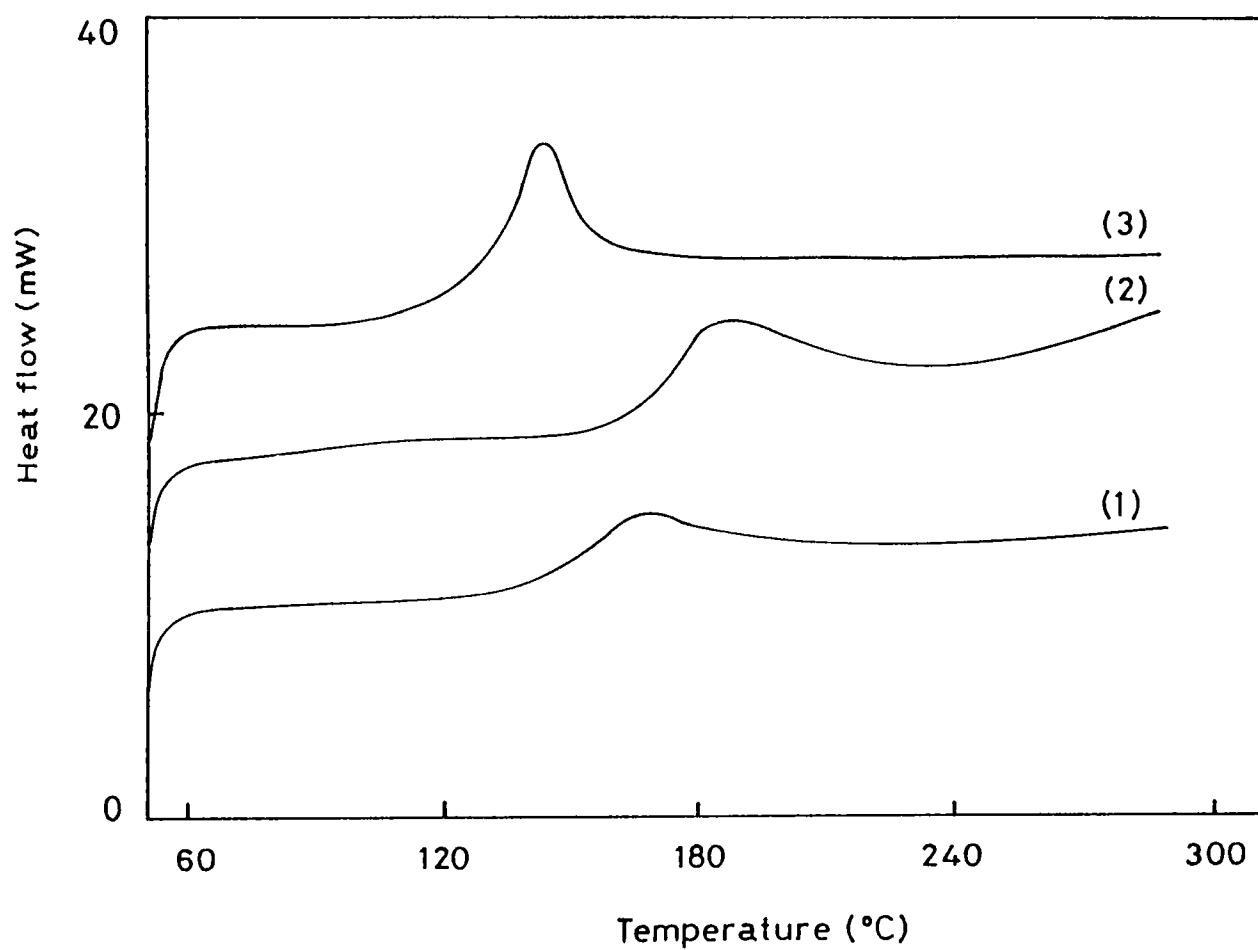


Fig.7.1 DSC curves of selected As-Te-Se glasses.
 (1) $As_{30}Te_{20}Se_{40}$, (2) $As_{45}Te_{10}Se$,
 (3) $As_{30}Te_5Se_{65}$

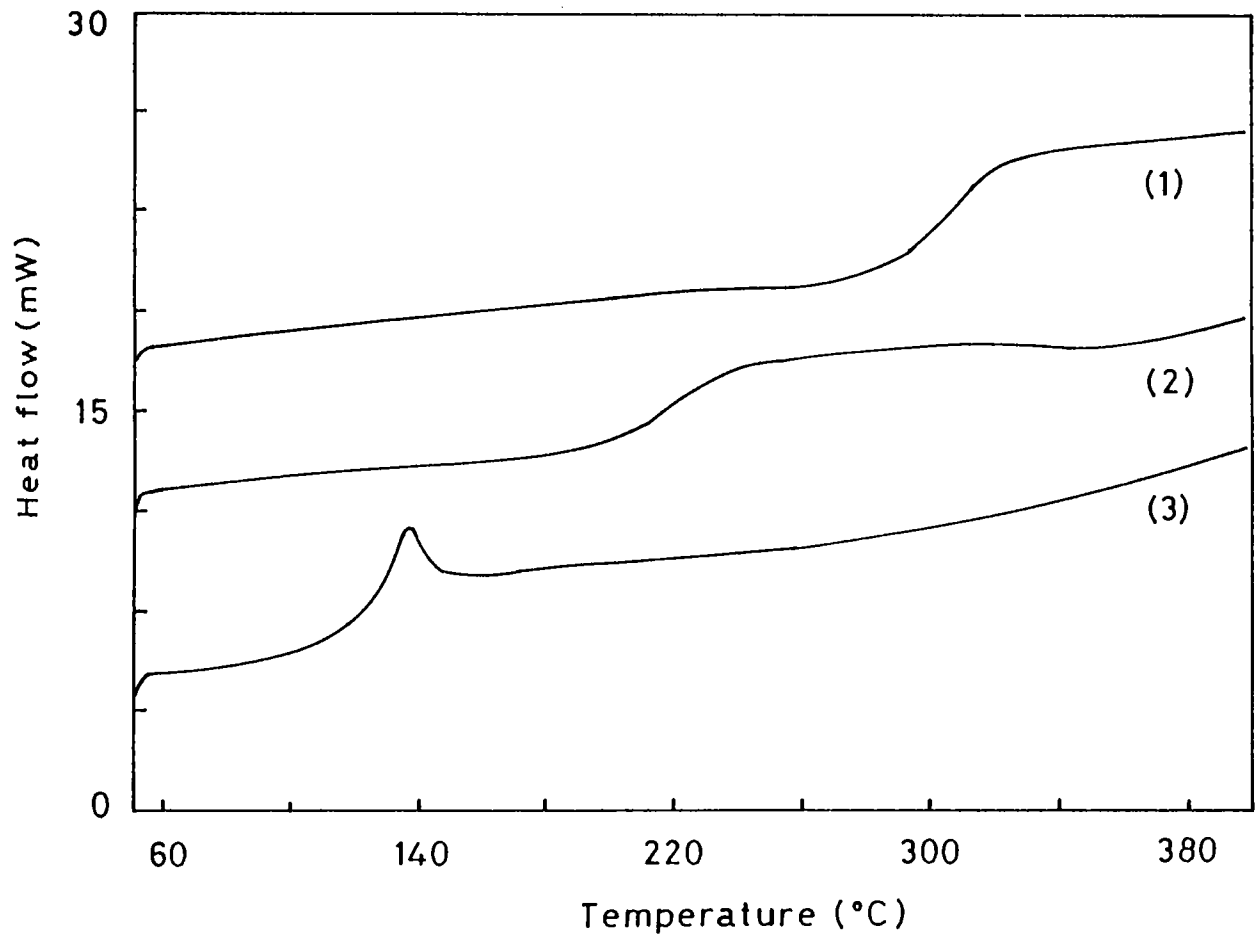


Fig.7.2 DSC curves of selected Ge-As-Se glasses.
 (1) $\text{Ge}_{25}\text{As}_{10}\text{Se}_{65}$, (2) $\text{Ge}_{20}\text{As}_{10}\text{Se}_{70}$
 (3) $\text{Ge}_{10}\text{As}_{10}\text{Se}_{80}$

of interest is first obtained. After this, two independent DSC runs are performed under identical conditions; one with a weighed quantity of the standard reference sample ($\alpha\text{-Al}_2\text{O}_3$ or sapphire) and the other with a weighed quantity of the experimental sample. All runs are performed at a constant heating rate of $20^\circ\text{C}/\text{min}$. Then, the specific heat C_p of the sample can be calculated using the relation

$$C_p/C_p' = m'y/my' \quad (7.2)$$

where, C_p' , m' and y' are the specific heat at constant pressure, mass and ordinate deflection of the reference standard. y and m are the ordinate deflection and mass of the experimental sample. The procedure has already been discussed in chapter II. All parameters given in equation (7.2) correspond to the same temperature. Since specific heat of $\alpha\text{-Al}_2\text{O}_3$ is available from literature [7], the C_p of the sample can be calculated using equation (7.2). This technique claims an accuracy of 5-10%.

7.3 Composition dependence of glass transition temperature in As-Te-Se and Ge-As-Se glasses

The glass transition temperature T_g of all samples belonging to the As-Te-Se and Ge-As-Se systems have been determined and are tabulated in Table 7.1 and Table 7.2 respectively. The average coordination numbers of the samples are also given in these tables. The variation of T_g with average coordination number $\langle r \rangle$ (with increase in As concentration) for $\text{As}_x\text{Te}_5\text{Se}_{95-x}$ and $\text{As}_x\text{Te}_{10}\text{Se}_{90-x}$ glasses are shown in Fig. 7.3. The glass transition temperature T_g gradually increases as the As concentration increases from 30 to 50 at.%. The rate of

Table 7.1 The composition, average coordination number $\langle r \rangle$ and glass transition temperature T_g of As-Te-Se glasses.

No	Composition As:Te:Se	$\langle r \rangle$	$T_g(K)$
1.	30:5:65	2.30	398
2.	35:5:60	2.35	431
3.	40:5:55	2.40	444
4.	45:5:50	2.45	447
5.	50:5:45	2.50	449
6.	30:10:60	2.30	390
7.	35:10:55	2.35	428
8.	40:10:50	2.40	439
9.	45:10:45	2.45	442
10.	50:10:40	2.50	446
11.	40:00:60	2.40	453
12.	40:15:45	2.40	431
13.	40:20:40	2.40	420

Table 7.2 The composition, average coordination number $\langle r \rangle$ and glass transition temperature T_g of Ge-As-Se glasses.

No.	Composition Ge:As:Se	$\langle r \rangle$	$T_g(K)$
1.	5:10:85	2.20	382
2.	10:10:80	2.30	391
3.	15:10:75	2.40	433
4.	20:10:70	2.50	470
5.	25:10:65	2.60	556
6.	28.5:10:61.5	2.67	576
7.	30:10:60	2.70	618
8.	35:10:55	2.80	645
9.	40:10:50	2.90	646
10.	5:5:90	2.15	378
11.	10:10:80	2.30	391
12.	13.35:13.35:73.3	2.40	448
13.	15:15:70	2.45	438
14.	20:20:60	2.60	545
15.	22:22:56	2.66	570
16.	25:25:50	2.75	603
17.	30:30:40	2.90	605

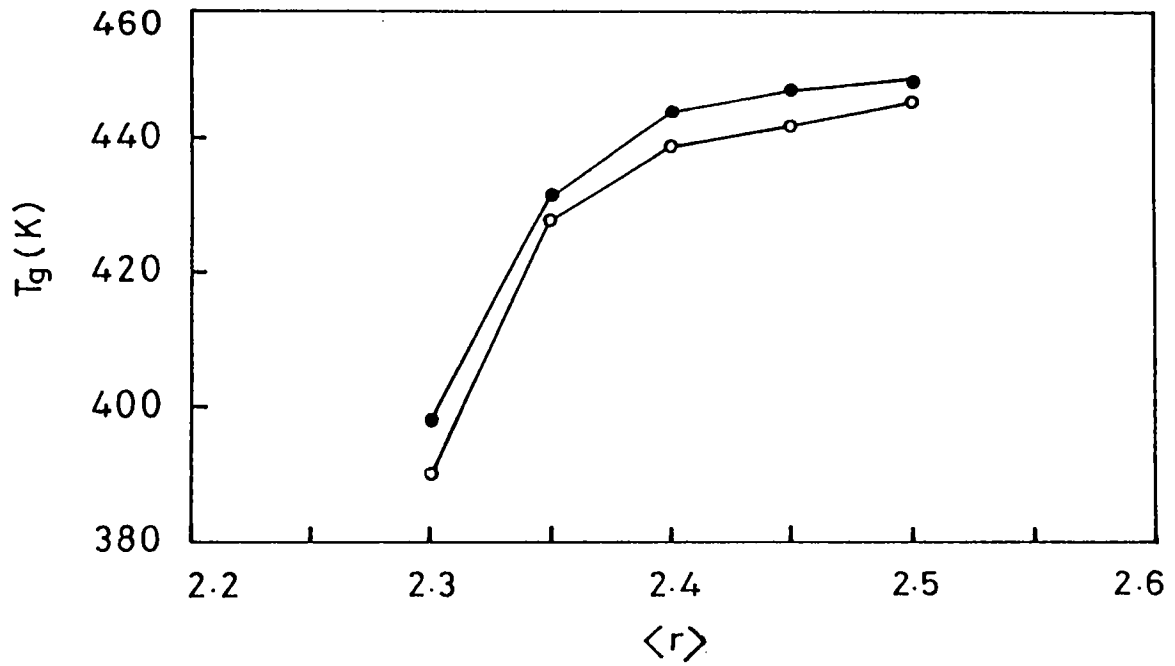


Fig.7.3 Variation of glass transition temperature (T_g) with average coordination number $\langle r \rangle$ of (●) $\text{As}_x\text{Te}_5\text{Se}_{95-x}$, (○) $\text{As}_x\text{Te}_{10}\text{Se}_{90-x}$ glasses.

increase is higher for compositions with $x < 40$ than for those with $x > 40$, in both cases. The variation of glass transition temperature with Te concentration for the stoichiometric compositions is shown in Fig. 7.4. The glass transition temperature gradually decreases as the Te concentration increases from 0 to 20 at.%.

The As-Te-Se system basically behaves similar to a binary-like system with As_2Se_3 and As_2Te_3 structural units. With the stoichiometric composition as reference ($x = 40$), which corresponds to an average coordination number $\langle r \rangle = 2.4$, the T_g values increases more rapidly for the Se-rich glasses than for As-rich glasses. This suggests that the variation of different physical properties do depend on the average coordination number as predicted by the rigidity percolation model. There is, however, no sudden upturn in the $\langle r \rangle$ dependence of T_g to signal any threshold crossing. T_g generally represents the "strength" or "rigidity" of the glass structure. As the average coordination number is increased the system gradually undergoes a percolation transition from a polymeric glass state to a rigid network structure registering a gradual increase in T_g for both $As_xTe_5Se_{95-x}$ and $As_xTe_{10}Se_{90-x}$ glasses. Moreover, for binary-like ternary systems it is reported that the mechanical and chemical thresholds coincide at $\langle r \rangle = 2.4$ [8]. For the stoichiometric compositions with increase in Te concentration, more and more As_2Se_3 structural units will be replaced by As_2Te_3 structural units. Since Se and Te are isovalent, one can not expect any drastic variation in T_g by the replacement of Se by Te. However, with increase in Te concentration, the bond energy of the system on an average is reduced due to the replacement of As_2Se_3 structural units by As_2Te_3 structural units registering a gradual decrease in the glass transition temperature.

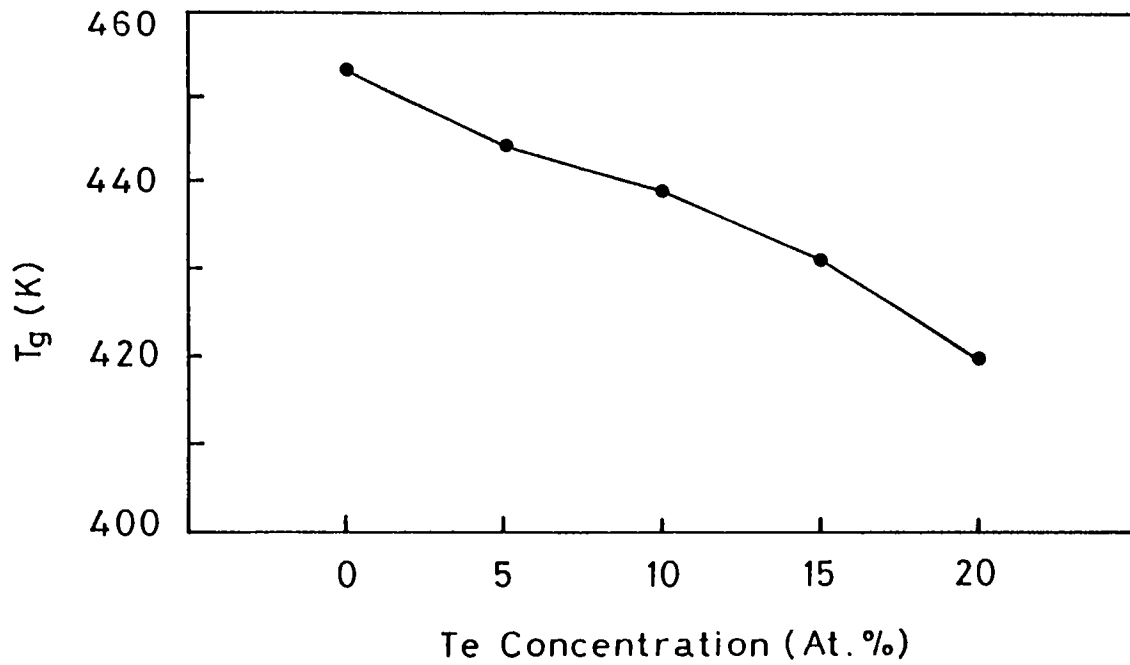


Fig.7.4 Variation of T_g with Te concentration for the stoichiometric compositions of the As-Te-Se glasses.

The variation of T_g with average coordination number $\langle r \rangle$ for $\text{Ge}_x\text{As}_{10}\text{Se}_{90-x}$ and $(\text{Ge}_{0.5}\text{As}_{0.5})_x\text{Se}_{100-x}$ glasses are shown in Fig.7.5. As the average coordination number $\langle r \rangle$ is increased T_g also increases gradually and shows a saturation behaviour beyond the average coordination number $\langle r \rangle = 2.67$. Another important feature observed is that the T_g values follow the same variation upto around $\langle r \rangle = 2.67$ and takes deviation showing a saturation behaviour beyond $\langle r \rangle = 2.67$. However, there is no anomaly near $\langle r \rangle = 2.4$.

The features exhibited by Ge-As-Se system suggests that the glass transition behaviour depend only on the average coordination number and shows that T_g is a universal function of $\langle r \rangle$ upto and somewhat beyond the percolation threshold. Based on the above observations it can be concluded that the changes in the network topology with $\langle r \rangle$ can be interpreted in the light of the formation and development of a layered structure in these glasses as predicted by Tanaka [9,10]. The present results also indicate that the mechanical threshold at $\langle r \rangle = 2.4$, predicted on the basis of short-range interactions [11,12] alone is not valid for these glasses.

7.4 Variation of C_p during glass transition in As-Te-Se and Ge-As-Se glasses

Heat capacity (C_p) measurements in the transition region have been made at a heating rate of $20^\circ\text{C}/\text{min}$ on all samples belonging to the As-Te-Se and Ge-As-Se systems covering a temperature range of 50°C to the region beyond the glass transition. Figs. 7.6 and 7.7 depicts the variation of specific heat with temperature near glass transition in $\text{As}_x\text{Te}_5\text{Se}_{95-x}$ and $\text{As}_x\text{Te}_{10}\text{Se}_{90-x}$ glasses. The variation of specific heat with

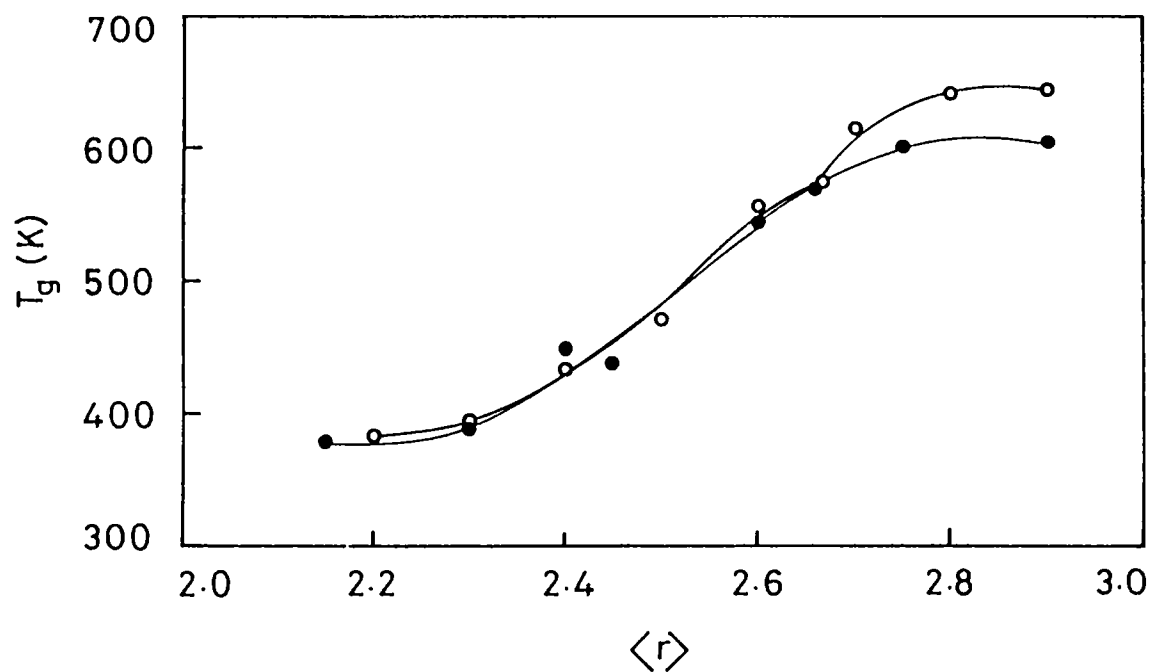


Fig.7.5 Variation of T_g with $\langle r \rangle$ of
 (O) $\text{Ge}_x\text{As}_{10}\text{Se}_{90-x}$,
 (●) $(\text{Ge}_{0.5}\text{As}_{0.5})_x\text{Se}_{100-x}$ glasses.

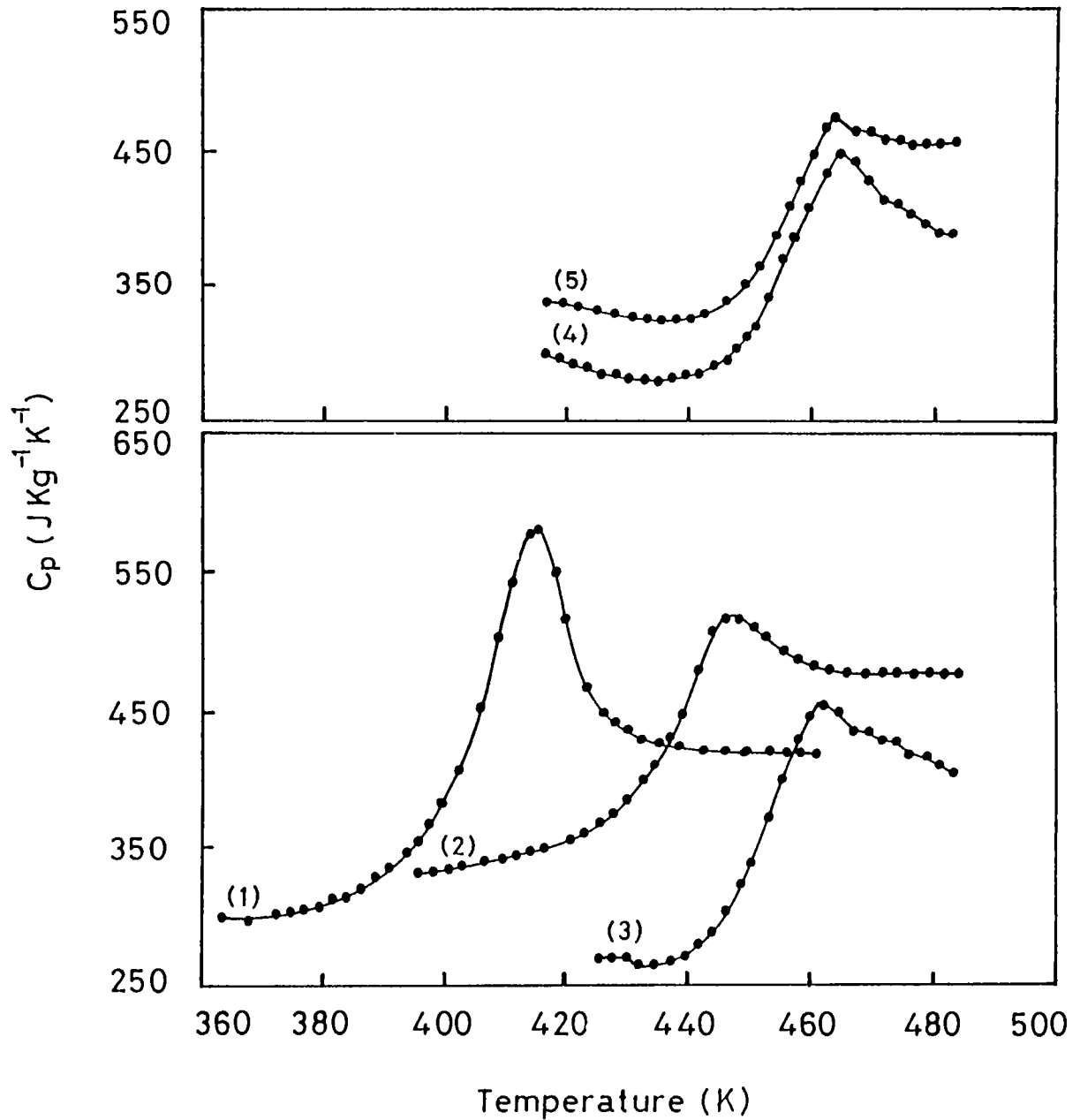


Fig.7.6 Variation of specific heat with temperature for $\text{As}_x\text{Te}_5\text{Se}_{95-x}$ glasses.
 (1) $\text{As}_{30}\text{Te}_5\text{Se}_{65}$, (2) $\text{As}_{35}\text{Te}_5\text{Se}_{60}$
 (3) $\text{As}_{40}\text{Te}_5\text{Se}_{55}$, (4) $\text{As}_{45}\text{Te}_5\text{Se}_{50}$
 (5) $\text{As}_{50}\text{Te}_5\text{Se}_{45}$

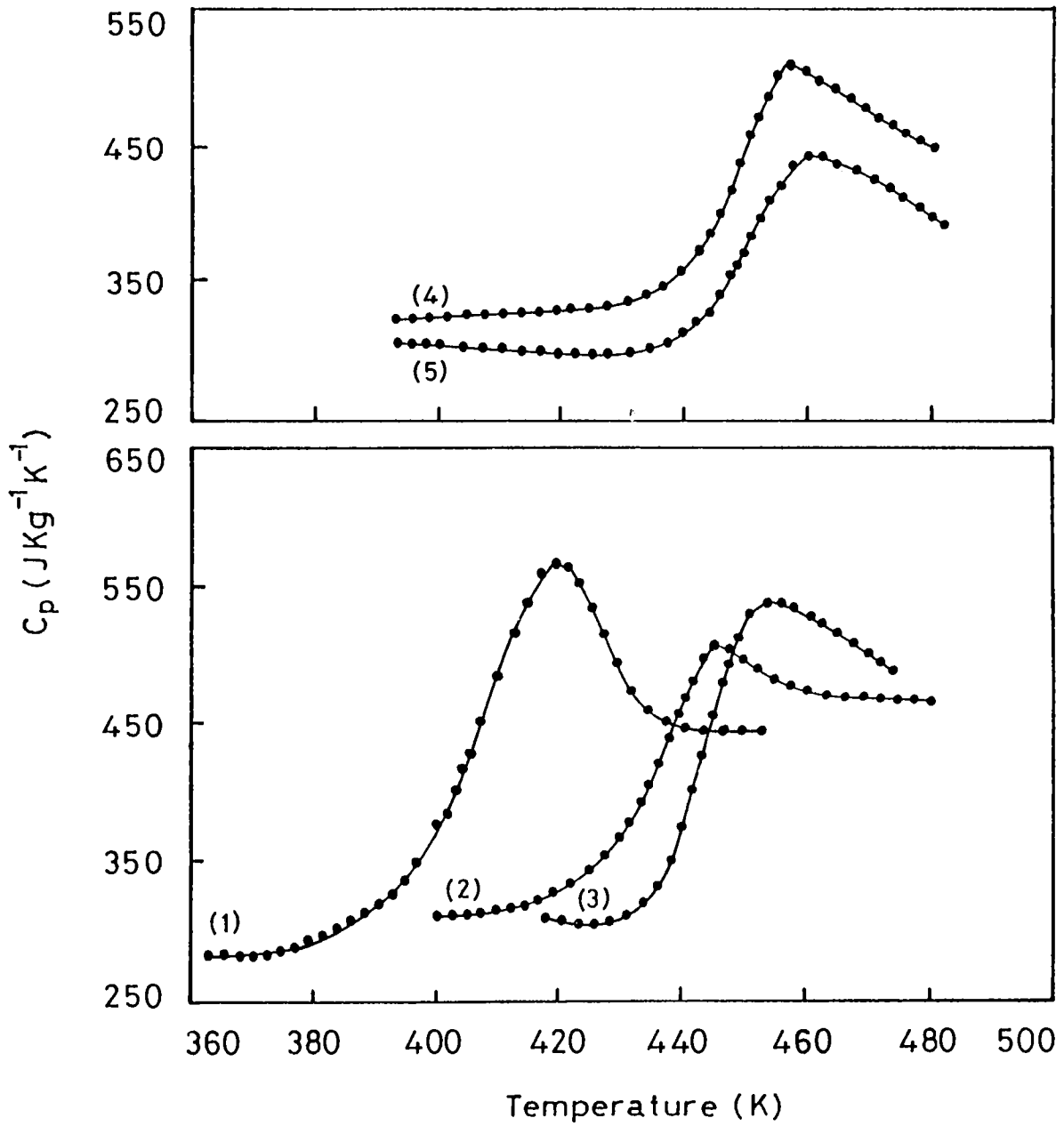


Fig.7.7 Variation of specific heat with temperature

for $As_xTe_{10}Se_{90-x}$ glasses.

(1) $As_{30}Te_{10}Se_{60}$, (2) $As_{35}Te_{10}Se_{55}$

(3) $As_{40}Te_{10}Se_{50}$, (4) $As_{45}Te_{10}Se_{45}$

(5) $As_{50}Te_{10}Se_{40}$

temperature for the $\text{Ge}_x\text{As}_{10}\text{Se}_{90-x}$ and $(\text{Ge}_{0.5}\text{As}_{0.5})_x\text{Se}_{100-x}$ glasses are shown in Fig. 7.8 to Fig. 7.13. In all the samples during glass transition a sharp increase in C_p is seen due to excess anharmonic contribution to the specific heat. The observed peak in C_p with temperatures in these systems occurs because the structural relaxation times are of the same order as the time scale of the experiment [13]. In keeping with the general behaviour of chalcogenide glasses [13-16], ΔC_p , the change in C_p during glass transition, is fairly large for the Se-rich glasses as can be seen from the figures.

The variation of ΔC_p with average coordination number for the $\text{As}_x\text{Te}_5\text{Se}_{95-x}$ and $\text{As}_x\text{Te}_{10}\text{Se}_{90-x}$ glasses is shown in Fig.7.14(a) and (b). In both systems the ΔC_p gradually decreases as the average coordination number is increased (As concentration is increased) from 2.3 to 2.5. In the As-Te system also, a decrease in ΔC_p is observed with increase in As concentration [17]. The present result in As-Te-Se systems indicates that the total number of structural configurations available for the molecules decreases with increasing As concentration.

The variation of ΔC_p with average coordination number $\langle r \rangle$ for $(\text{Ge}_{0.5}\text{As}_{0.5})_x\text{Se}_{100-x}$ and $\text{Ge}_x\text{As}_{10}\text{Se}_{90-x}$ glasses are shown in Fig.7.15(a) and (b) respectively. For both these systems the ΔC_p values decrease gradually and show a minimum around $\langle r \rangle = 2.4$, which corresponds to the mechanical threshold for these systems. The heat capacity "jump" at T_g in the vicinity of $\langle r \rangle = 2.4$ is very small and smeared out as the average coordination number is further increased. This implies a strong resistance to structural degradation in the liquid state and has been correlated to a minimum "fragility" (i.e., departure from Arrhenius viscosity behaviour) in the overall viscous liquid

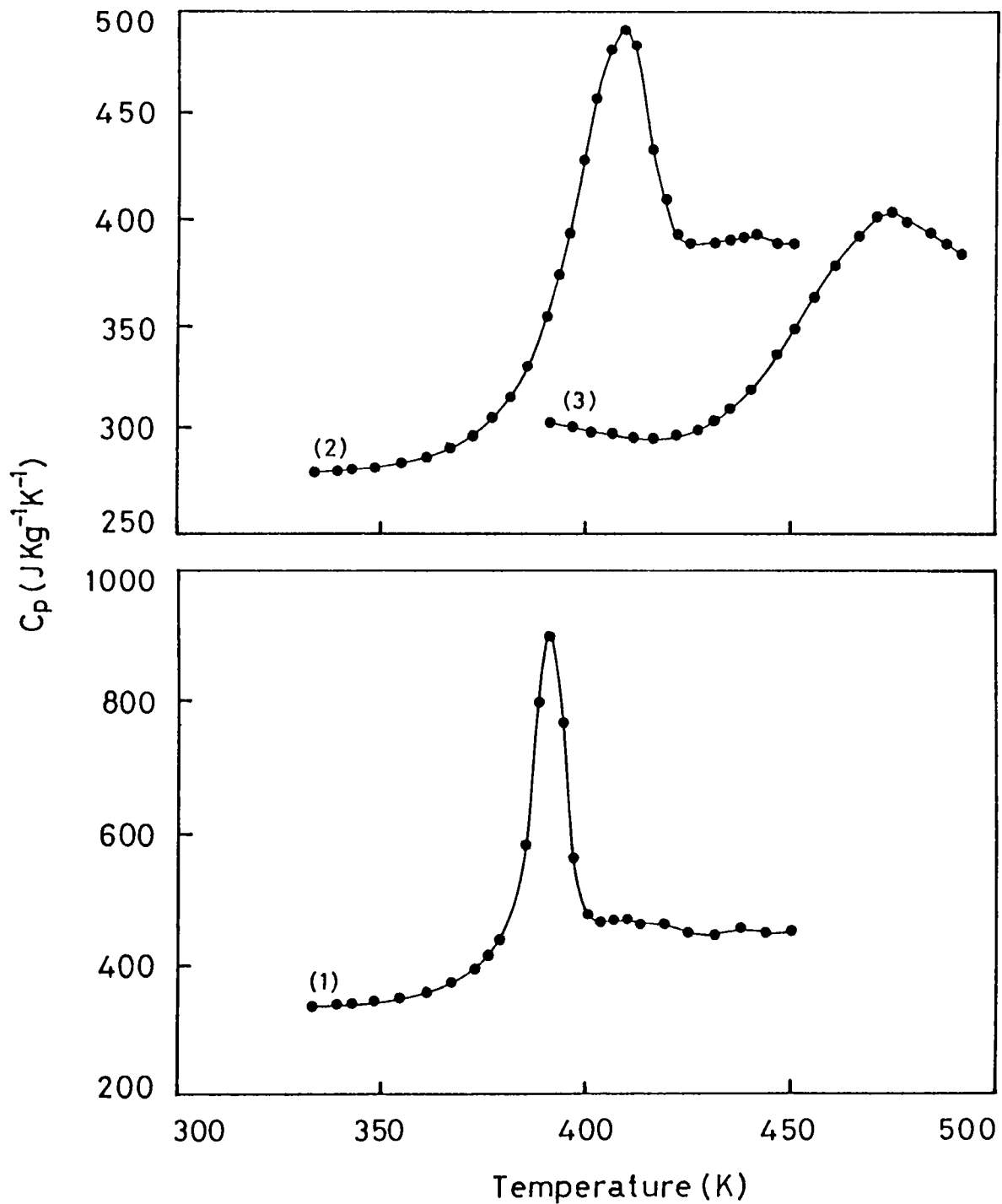


Fig.7.8 Variation of specific heat with temperature for
 (1) $\text{Ge}_5\text{As}_{10}\text{Se}_{85}$, (2) $\text{Ge}_{10}\text{As}_{10}\text{Se}_{80}$,
 (3) $\text{Ge}_{15}\text{As}_{10}\text{Se}_{75}$ glasses.

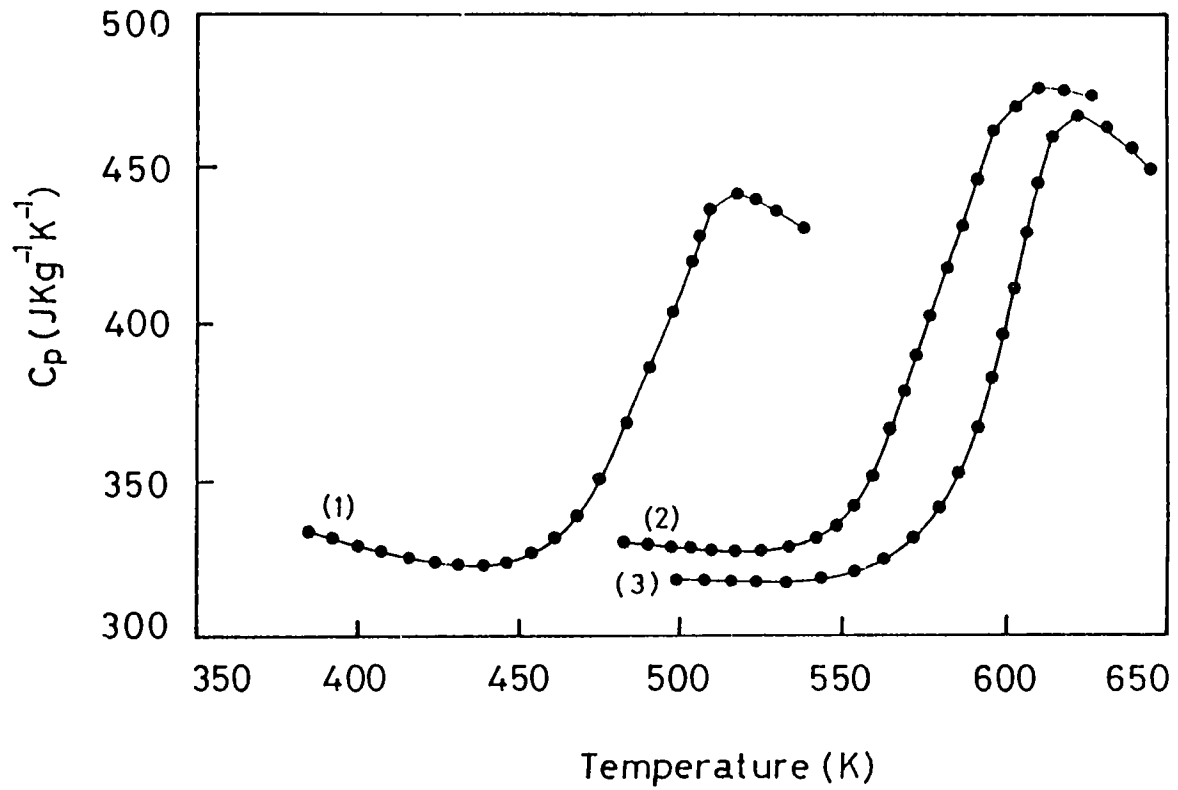


Fig.7.9 Variation of specific heat with temperature for
 (1) $\text{Ge}_{20}\text{As}_{10}\text{Se}_{70}$, (2) $\text{Ge}_{25}\text{As}_{10}\text{Se}_{65}$,
 (3) $\text{Ge}_{28.5}\text{As}_{10}\text{Se}_{71.5}$ glasses.

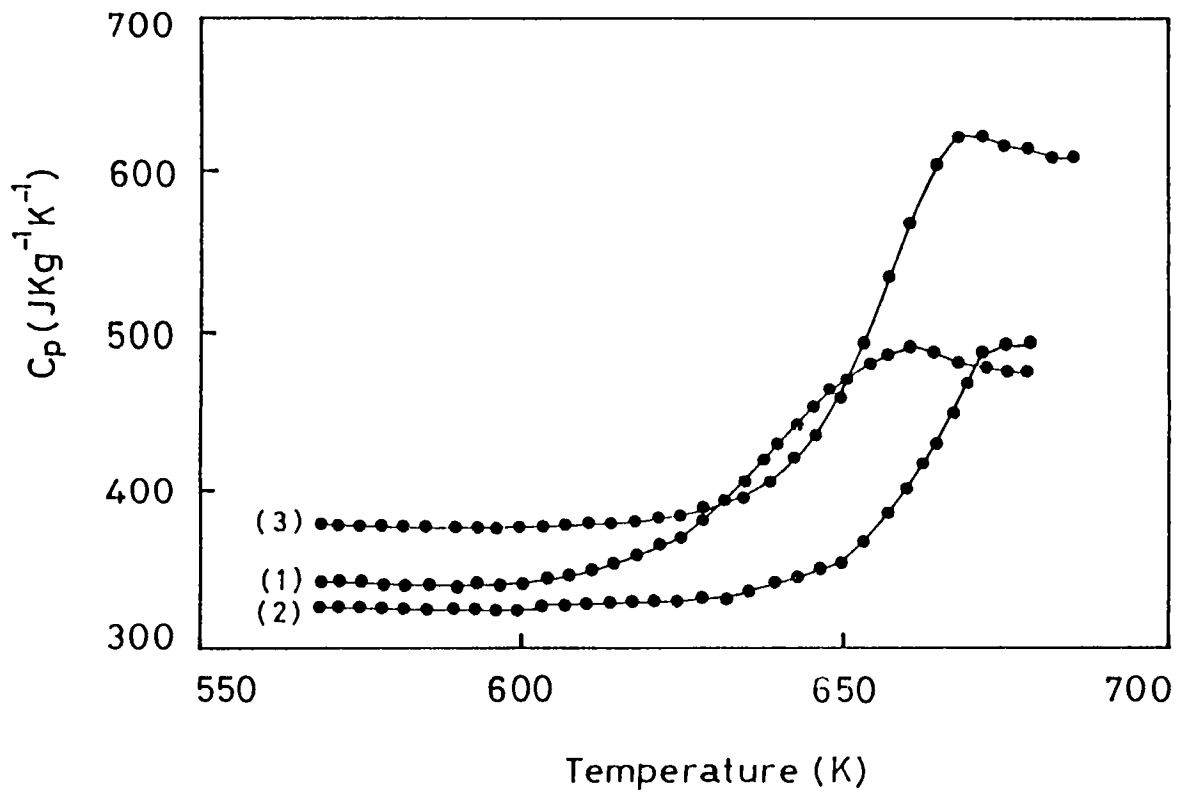


Fig.7.10 Variation of specific heat with temperature for
 (1) $\text{Ge}_{30}\text{As}_{10}\text{Se}_{60}$, (2) $\text{Ge}_{95}\text{As}_{10}\text{Se}_{55}$,
 (3) $\text{Ge}_{40}\text{As}_{10}\text{Se}_{50}$ glasses.

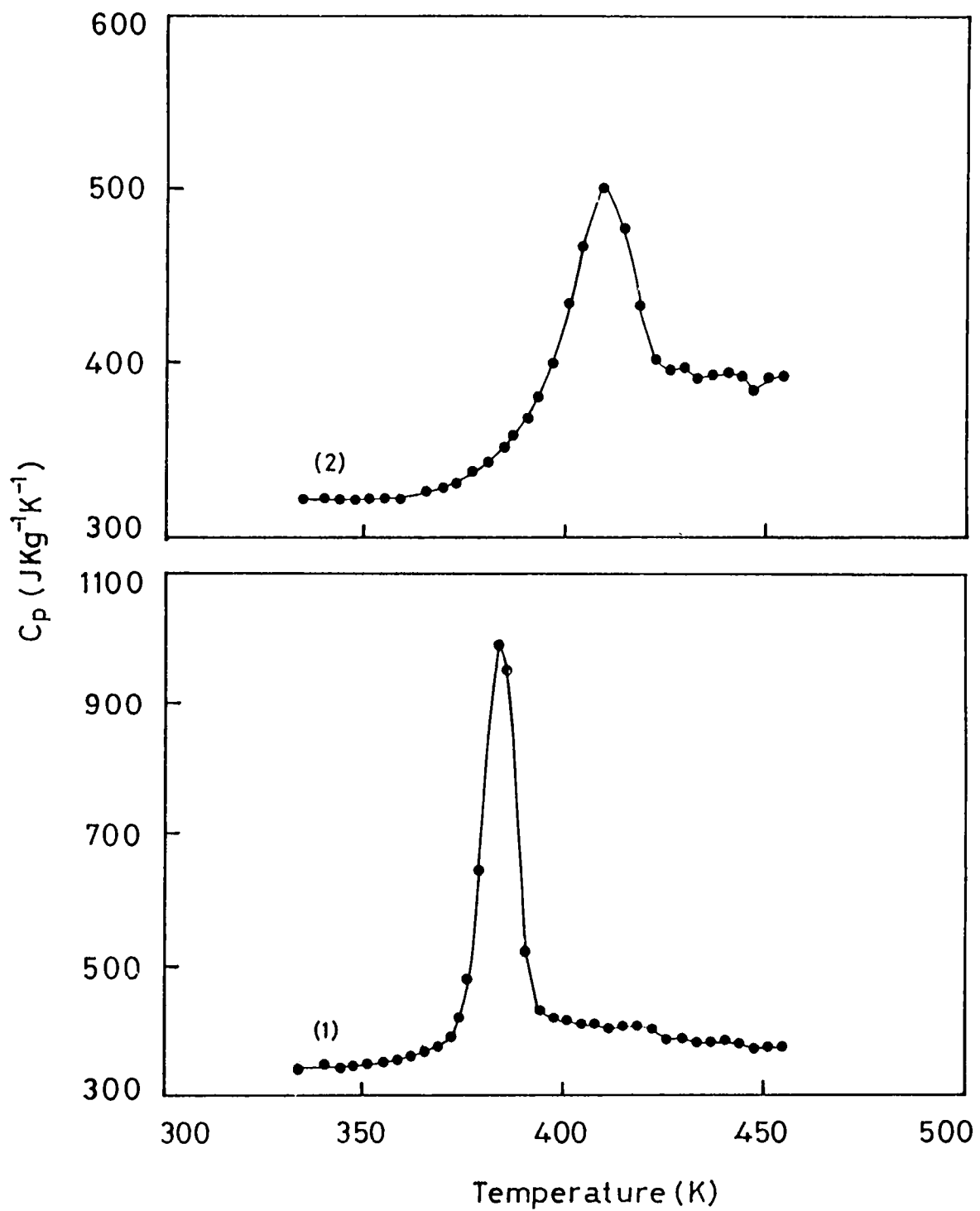


Fig.7.11 Variation of specific heat with temperature for (1) Ge₅As₅Se₉₀, (2)Ge₁₀As₁₀Se₈₀ glasses.

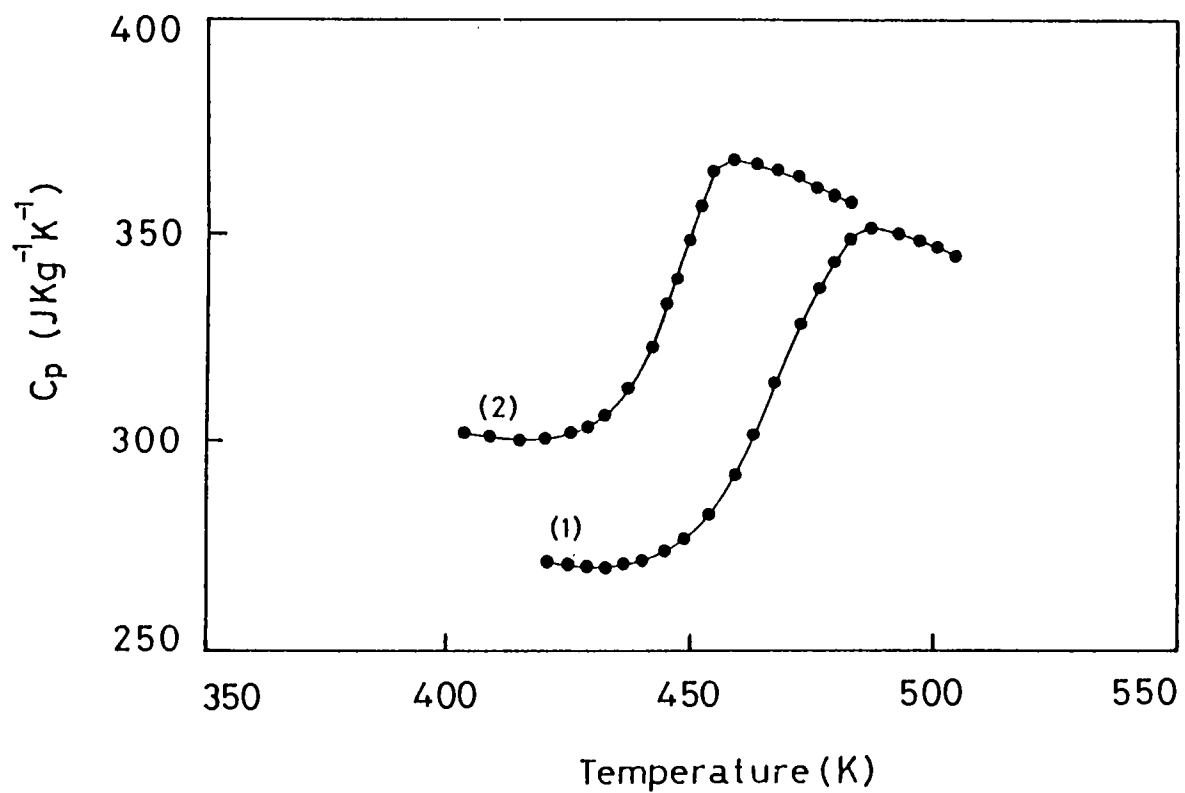


Fig.7.12 Variation of specific heat with temperature for
 (1) $\text{Ge}_{13.35}\text{As}_{13.35}\text{Se}_{73.3}$, (2) $\text{Ge}_{15}\text{As}_{15}\text{Se}_{70}$
 glasses.

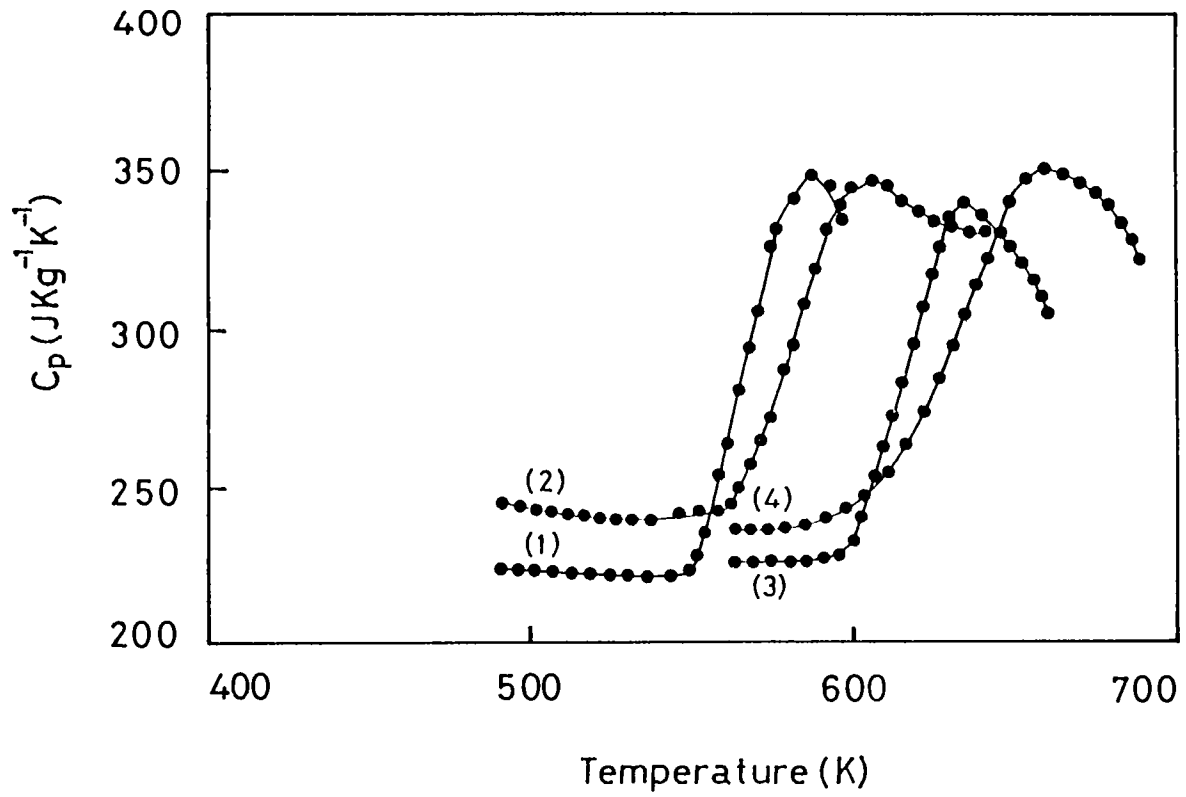


Fig.7.13 Variation of specific heat with temperature for
 (1) $\text{Ge}_{20}\text{As}_{20}\text{Se}_{60}$, (2) $\text{Ge}_{22}\text{As}_{22}\text{Se}_{56}$
 (3) $\text{Ge}_{25}\text{As}_{25}\text{Se}_{50}$, (4) $\text{Ge}_{30}\text{As}_{30}\text{Se}_{40}$ glasses.

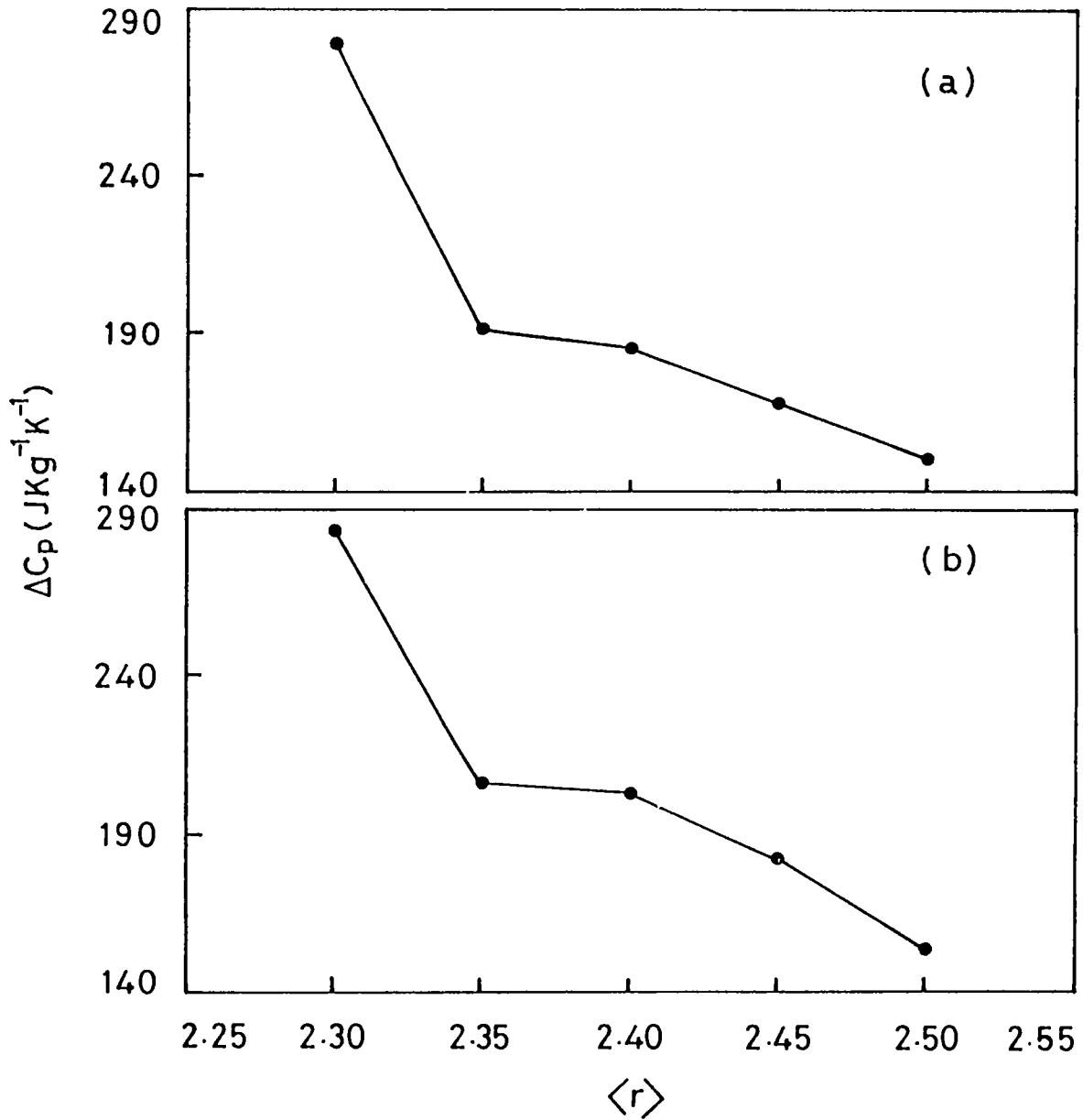


Fig.7.14 Variation of ΔC_p with average coordination number for
 (a) $\text{As}_x\text{Te}_5\text{Se}_{95-x}$, (b) $\text{As}_x\text{Te}_{10}\text{Se}_{90-x}$ glasses.

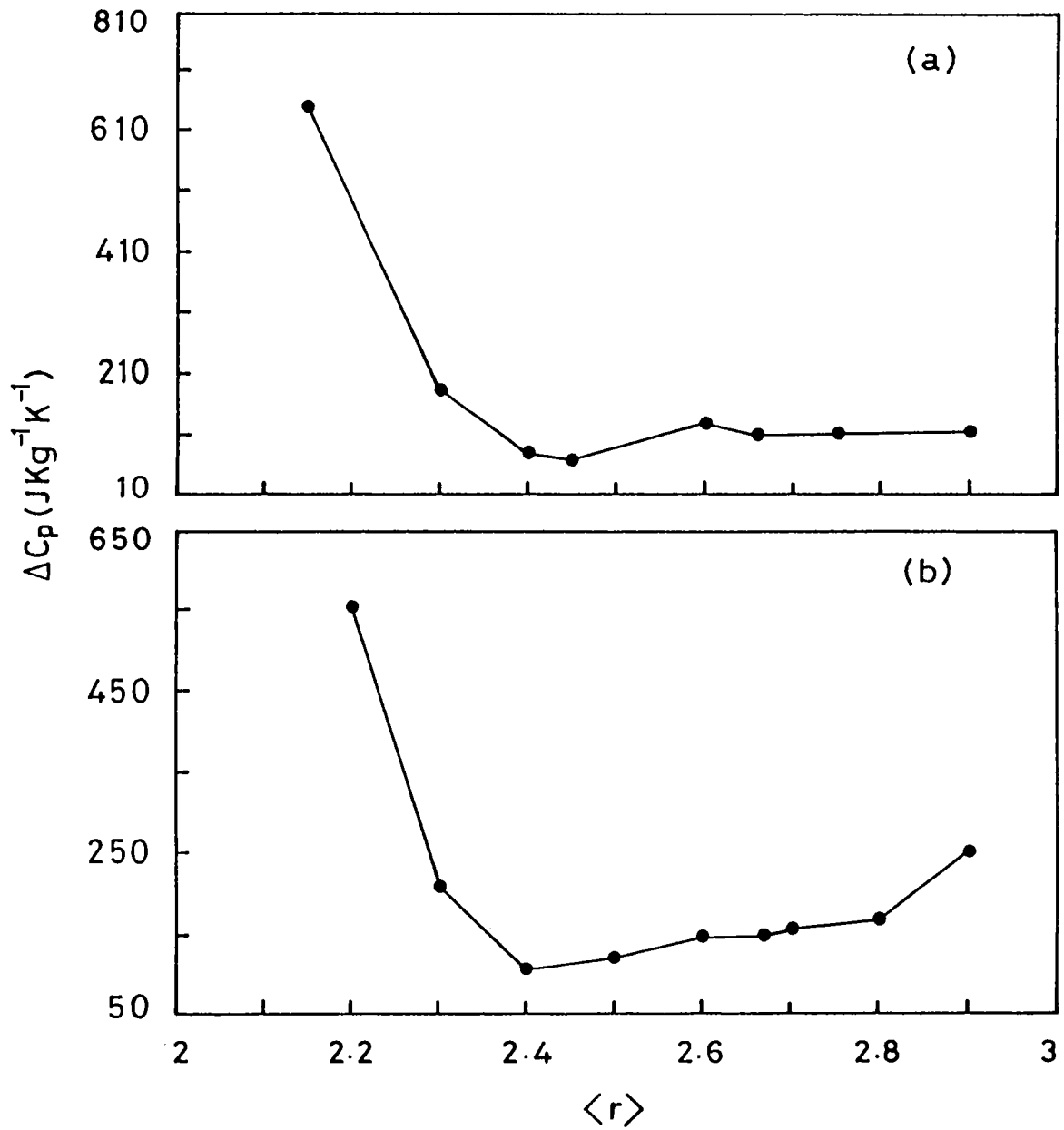


Fig.7.15 Variation of ΔC_p with average coordination number for
 (a) $\text{Ge}_x\text{As}_{10}\text{Se}_{90-x}$, (b) $(\text{Ge}_{0.5}\text{As}_{0.5})_x\text{Se}_{100-x}$
 glasses.

behaviour [18]. The source of ΔC_p at glass transition is generally taken to be "configurational" and the increase in the value of C_p above T_g is due to the addition of transitional and/or rotational modes becoming available by the breakage of bonds forming the glass network [14,19]. Though a quantitative explanation for the observed ΔC_p has not been possible, it is generally believed [16] that ΔC_p arises from thermal degradation of the glass network with increasing temperature.

Studies on several glass systems [20] indicate that "configurational" sources account, on an average, for about 55% of the value of ΔC_p obtained, the remainder being contributions from (i) changes in lattice frequencies with configurational states, (ii) changes in anharmonicity with configurational states and (iii) changes in the number of molecular groups that are able to engage in local motion, which is detectable as secondary relaxations below T_g . It has also been shown for polymeric glasses [21], that the total ΔC_p is made up of a configurational term arising from shape changes of molecules (about 50% of the total), a configuration term arising from the volume expansion (about 30% of the total) and a vibrational contribution arising from the change in the force constants or characteristic frequencies with temperature (20% of the total).

REFERENCES

1. Proc. 4th Int. Conf. on Amorphous and Liquid Semiconductors 1971, eds: M. H. Cohen and G. Lucovsky, J. Non-Cryst. Solids, 8-10, 1-1050 (1972); Amorphous Semiconductors, ed: M. H. Brodsky (Springer, New York, 1979)
2. D. Turnbull, Cont.Phys., 10, 473 (1969)
3. A. J. Kovacs, Adv. Polym. Sci., 3, 394 (1963)
4. R. O. Davies and G. O. Jones, Adv. Phys., 2, 370 (1953)
5. W. Kauzmann, Chem. Revs., 43, 43 (1948)
6. M. J. O'Neill, Anal.Chem., 38, 1331 (1966)
7. G. T. Furukawa, T. B. Douglas, R. E. McCoskey and D. C. Ginnings, J. Res. Nat. Bur. Std., 57, 67 (1956)
8. P. Boolchand, Phys. Rev. Lett., 57, 3233 (1986)
9. K. Tanaka, J. Non-Cryst. Solids, 103, 149 (1988)
10. K. Tanaka, Phys. Rev. B39, 1270 (1989)
11. J. C. Phillips, J. Non-Cryst. Solids, 34, 153 (1979)
12. M. F. Thorpe, J. Non-Cryst. Solids, 57, 355 (1983)
13. U. E. Schnaus, C. T. Moynihan, R. W. Gammon and P. B. Macedo, Phys. Chem. Glasses II, 213 (1970)

14. D. D. Thornburg and R. I. Johnson, J. Non-Cryst. Solids, 17, 2 (1975)
15. U. E. Schnaus and C. T. Moynihan, Mat. Sci. Eng., 7, 268 (1971)
16. U. E. Schnaus, A. Marshall and C. T. Moynihan, J. Am. Ceram. Soc., 55, 180 (1972)
17. J. Cornet and D. Rossier, J. Non-Cryst. Solids, 12, 61 (1973)
18. C. A. Angell, J. Non-Cryst. Solids, 73, 1 (1985)
19. G. O. Jones, in: Glass (Chapman and Hall, London, 1971)
20. M. Goldstein, Physics of Non-Crystalline Solids, Fourth Int. Conf., Zellerfeld, ed., G. H. Firschat (1976) p.391
21. E. A. DiMarzio and F. Dowell, J. Appl. Phys., 50, 6061 (1979)

CHAPTER VIII

SUMMARY AND CONCLUSIONS

The overall goal of this thesis work is to correlate the local atomic structure of selected ternary glasses belonging to the As-Sb-Se, As-Te-Se and Ge-As-Se systems with their physical properties, especially the optical and thermal properties. Two experimental techniques have been employed for the present investigations viz., the photoacoustic (PA) technique and differential scanning calorimetry (DSC). The PA technique is based on the detection of an acoustic signal generated in an enclosed volume when the sample is irradiated by intensity modulated radiation. The PA signal generated depends upon the optical properties of the sample and the thermal properties of the sample, backing material and surrounding gas. The PA technique has been effectively used to investigate the optical band gap E_g and thermal diffusivity α of the samples belonging to the above mentioned three families of glasses. This technique has also been used as a calorimetric technique to locate the glass transition temperature T_g of As-Sb-Se glasses. The DSC is a dynamic thermal analysis technique with which the thermal behaviour of samples can be investigated over a wide temperature range. This technique has been used to measure the glass transition temperature T_g and specific heat at constant pressure C_p of As-Te-Se and Ge-As-Se glasses.

For the studies reported in this thesis, an efficient PA spectrometer has been setup which consists of a high power Xenon lamp as the radiation source, a monochromator, a mechanical chopper, a PA cell with microphone and a lock-in

amplifier to analyse the signal. Two home made PA cells have been used; one for room temperature measurements and the other for measurements at high temperatures with which measurements can be made upto $\approx 300^\circ\text{C}$. Provisions have been given in both cells to change the volume of the sample chamber and to use different backing materials for the sample. The cells have been calibrated using highly absorbing carbon black sample.

The glasses belonging to the As-Sb-Se, As-Te-Se and Ge-As-Se systems have been prepared by the well established melt quenching technique. The compositions have been chosen such that they all fall in the glass forming regions of each system. The amorphous nature of all the samples has been confirmed by X-ray diffractometry. In the As-Sb-Se system, four groups have been prepared which can be represented as $\text{As}_x\text{Sb}_5\text{Se}_{95-x}$ (with $25 \leq x \leq 45$), $\text{As}_x\text{Sb}_{10}\text{Se}_{90-x}$ (with $20 \leq x \leq 40$), $\text{As}_x\text{Sb}_{15}\text{Se}_{85-x}$ (with $15 \leq x \leq 35$) and $\text{As}_x\text{Sb}_{20}\text{Se}_{80-x}$ (with $10 \leq x \leq 30$). In each group the compositions $(\text{As,Sb})_{40}\text{Se}_{60}$ fall along the stoichiometric compositions of the As-Sb-Se system. The compositions studied in As-Te-Se system can be categorized into three groups depending on the Te concentrations as $\text{As}_x\text{Te}_5\text{Se}_{95-x}$, $\text{As}_x\text{Te}_{10}\text{Se}_{90-x}$ (with $x = 30, 35, 40, 45$ and 50) and $\text{As}_{40}(\text{Te,Se})_{60}$ with Te content varying from 0 to 20 at.% and represent the stoichiometric compositions of the As-Te-Se system. In the Ge-As-Se system, two groups have been investigated which can be represented as $\text{Ge}_x\text{As}_{10}\text{Se}_{90-x}$ (with $x = 5, 10, 15, 20, 25, 28.5, 30, 35$ and 40) and $(\text{Ge}_{0.5}\text{As}_{0.5})_x\text{Se}_{100-x}$ (with $x = 10, 20, 26.7, 30, 40, 44, 50$ and 60).

The PA spectra of the samples of each family mentioned above have been recorded in the fundamental absorption edge region using the room temperature PA cell. These spectra give

information about the features of optical absorption viz., the power law absorption region, exponential absorption region and weak absorption region. The optical energy gap E_o of the samples have been determined from the PA spectra as the photon energy above which the spectra get saturated. The optical band gap of these samples has also been determined using UV-Vis-NIR spectrophotometer and found to be in good agreement with PA data. The composition dependence of optical band gap for all the groups of samples have been investigated. In the As-Sb-Se system, E_o decreases gradually with increase in As concentration but the rate of decrease is higher for compositions having As and Sb content together is less than 40 at.% than for those with As and Sb content together greater than 40 at.%. For stoichiometric compositions the optical band gap is found to decrease with increase in Sb concentration. In As-Te-Se systems, for a particular Te concentration, the optical band gap decreases gradually and shows a marked change in its rate of decrease at the stoichiometric composition at which the As content is 40 at.% corresponding to an average coordination number $\langle r \rangle = 2.4$. The rate of decrease is higher for compositions with As content less than 40 at.% than for those with As content larger than 40 at.%. The optical band gap of the stoichiometric compositions of the As-Te-Se system gradually decreases as the Te concentration is increased from 0 to 15 at.%. The composition dependence of optical band gap E_o of Ge-As-Se system shows a threshold maximum around the average coordination number $\langle r \rangle = 2.67$. The results of the composition dependence of optical band gap in As-Sb-Se, As-Te-Se and Ge-As-Se systems have been explained on the basis of chemical bonding and the change in the short range order taking place as the composition is varied.

The PA technique has been employed to measure the thermal diffusivity α of As-Sb-Se, As-Te-Se and Ge-As-Se glasses. The method involves the determination of the characteristic frequency f_c above which the sample is thermally thick, by measuring the variation of PA signal amplitude and phase as a function of the chopping frequency. The measurements have been performed on samples of appropriate thickness 'l' and thermal diffusivity is determined using the relation $\alpha = f_c l^2$. The composition dependence of α in As-Sb-Se systems shows a marked change in its rate of increase at the stoichiometric compositions corresponding to an average coordination number $\langle r \rangle = 2.4$. For the stoichiometric compositions of the As-Sb-Se system, with increase in Sb concentration, thermal diffusivity is found to decrease. The variation of α with As concentration in two sets of glasses of the As-Te-Se system shows a threshold maximum at the composition $x = 40$ which corresponds to an average coordination number $\langle r \rangle = 2.4$, whereas the thermal diffusivity α increases gradually with Te concentration for the stoichiometric compositions of the As-Te-Se system. The composition dependence of α in Ge-As-Se system show a threshold maximum around the average coordination number $\langle r \rangle = 2.67$.

An explanation for the observed variation of thermal diffusivity has been presented on the basis of constraints theory and the ideas of rigidity percolation in random networks. The As-Sb-Se and As-Te-Se systems behave as binary-like systems and for these systems the mechanical and chemical thresholds coincide. The variation of thermal diffusivity exhibited in these systems is attributed to the mechanical stiffening of the glass network at the critical composition as a result of the threshold percolation of rigidity. The thermal diffusivity studies on Ge-As-Se glasses do not show any significant anomaly

around $\langle r \rangle = 2.4$ but shows a threshold maximum around $\langle r \rangle = 2.67$. This suggests that the changes in the network topology with $\langle r \rangle$ can be interpreted in terms of the formation and development of layered structure in these glasses. Also, this result shows that the mechanical threshold at $\langle r \rangle = 2.4$, predicted on the basis of short-range interactions alone, is not valid for these glasses.

The PA technique has also been used to investigate glass transition temperature T_g of As-Sb-Se glasses by measuring the variation of PA amplitude and phase as a function of temperature. At T_g the PA signal amplitude shows a minimum and phase shows a critical maximum. The composition dependence of T_g in these glasses is almost similar to the variation of α with composition in these systems. The temperature dependence of α indicates that the critical coordination is fixed as the glass is formed at T_g and the network rigidity is kept intact at all temperatures below the glass transition.

The glass transition temperature T_g and heat capacity C_p of As-Te-Se and Ge-As-Se systems have been investigated using differential scanning calorimetry. For both $As_xTe_5Se_{95-x}$ and $As_xTe_{10}Se_{90-x}$ glasses, the glass transition temperature T_g gradually increases as As concentration is increased from 30 to 50 at.%. With the stoichiometric composition as reference, which corresponds to an average coordination number $\langle r \rangle = 2.4$, the rate of increase is higher for Se-rich glasses than for those with As-rich glasses. So as the average coordination number is increased, the system gradually undergoes a structural transition from a polymeric glassy state to a rigid network registering a gradual increase of T_g . For the stoichiometric compositions of the As-Te-Se system, as the Te concentration

increases, the T_g value registers a decrease, which could be attributed to the replacement of As_2Se_3 structural units by As_2Te_3 units and a corresponding decrease of the average bond energy of the system. The composition dependence of T_g in Ge-As-Se system do not show any anomaly around $\langle r \rangle = 2.4$. For both $Ge_xAs_{10-x}Se_{90-x}$ and $(Ge_{0.5}As_{0.5})_xSe_{100-x}$ glasses the T_g value increases gradually as the coordination number increases. The significant feature observed in this case is that the variation of T_g follows the same path till $\langle r \rangle \cong 2.67$ and beyond this the variation takes a different path. Moreover, the variation shows a saturation behaviour beyond $\langle r \rangle = 2.67$ for both groups of glasses in Ge-As-Se system. As the coordination number is increased layered structures will be formed gradually and around $\langle r \rangle = 2.67$ the stable layer structure will be fully developed in the system. This could be the reason for the observed variation of T_g with composition.

The specific heat C_p of the glasses belonging to the As-Te-Se and Ge-As-Se systems has been investigated using DSC. The ratio method has been employed for the determination of specific heat of each sample. For each sample the specific heat shows a sharp increase during transition. The observed peak in C_p with temperature occurs because the structural relaxation times become comparable with the time scale of the experiment. In As-Te-Se system, the variation of C_p during transition gradually decreases as the average coordination number is increased. This indicates that the total number of structural configurations available for the molecules is a decreasing function of the As concentration. For Ge-As-Se system, the variation of ΔC_p with average coordination number shows a minimum around $\langle r \rangle = 2.4$. Beyond $\langle r \rangle = 2.4$, the variation in ΔC_p is much less. The studies on Ge-As-Se system supports the

validity of Tanaka's ideas relating to the formation and development of layered structure in these network glasses. The minimum value of ΔC_p around $\langle r \rangle = 2.4$ and the small variation in ΔC_p beyond this value of $\langle r \rangle$ suggests that the system transforms to rigid structure as the average coordination number crosses the value of $\langle r \rangle = 2.4$ and the formation of stable layered structure begins gradually beyond this value of $\langle r \rangle$ and fully develops around $\langle r \rangle = 2.67$.

To conclude, an attempt has been made in this thesis to interpret the properties of the three ternary glass systems in terms of the average coordination number as against the general practice of interpreting these properties in terms of concentration. Our investigations support Phillips' idea, that $\langle r \rangle$ is an important parameter for interpreting the composition dependence of various physical properties of network glasses. Many of our results based on the investigations on As-Sb-Se, As-Te-Se and Ge-As-Se systems have been interpreted quite satisfactorily in terms of the average coordination number $\langle r \rangle$. Also, our investigations prove the potential applications of PA technique for the measurement of optical and thermal properties of bulk semiconducting glasses, apart from its use as a complementary technique to the conventional calorimetric techniques.

Eventhough many works have been carried out in chalcogenide systems, a lot more work is needed to clarify the way in which the chemical and mechanical thresholds get reflected in various physical properties and to elucidate the differences in the network topology of binary-like and ternary chalcogenide glasses. More work need to be carried out to provide an important link between key structural concepts of

glass science, the relaxation phenomena and the thermodynamic problems embodied in Kauzmann paradox. A recent report by A. Giridhar and S. Mahadevan on In-Ge-Se glasses suggest the occurrence of subtle features near $\langle r \rangle = 2.4$ and $\langle R \rangle = 2.63$, which is quite similar to the ones in Ge-As-S and Ge-Se glasses. This shows the possible occurrence of the mechanical threshold in III-IV-VI glasses at $\langle r \rangle = 2.63$ and supports the argument that the coordination of atoms may determine the type of medium range order in these glasses. So different experimental tools must be employed to confirm the influence of the individual coordination number of the elements on the network topology. Systems like Ga-Ge-Se, Ga-As-Se, Ga-Si-Se and In-Ge-Se form good candidates for further studies to analyse the existence of chemical and mechanical thresholds in ternary chalcogenide glasses.

Neutron scattering studies on these glasses can provide valuable information about the variation in the bonding structure of the glasses with average coordination number $\langle r \rangle$. Neutron scattering studies near glass transition temperature may probably throw much more light on the mechanism of glass transition and structural relaxation in network glasses. Microscopic probes such as extended X-ray absorption fine structure, scanning tunnelling microscopy, high resolution electron microscopy etc. may also be employed to provide information on the extent of order in network glasses. Eventhough there are many limitations to perform studies on network glasses using the above mentioned experimental tools, it is worth while to make an attempt since such investigations could improve our present understanding of the glassy state. It would also be interesting to carry out studies of elastic properties as well as application oriented investigations such as memory and switching properties of these materials.

